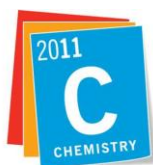


BULGARIAN CHEMICAL COMMUNICATIONS

2010 Volume 42 / Number 4

*Journal of the Chemical Institutes
of the Bulgarian Academy of Sciences
and of the Union of Chemists in Bulgaria*



International Year of **CHEMISTRY** 2011

Announcement

Seventh National Conference on Chemistry and 2nd International Conference on Green Technologies and Environmental Protection

INVITATION

The Union of Chemists in Bulgaria (UCB) extends a cordial invitation to all scientists in the field of chemistry to participate in the Seventh National Conference on Chemistry to be held at the University of Chemical Technology and Metallurgy in Sofia (Bulgaria) from 26 to 29 May 2011.

Parallely the 2nd International Conference on Green Technologies and Environmental Protection co-organized with the Chaudhary Charan Singh University, Meerut (India) and Devam Foundation – Bulgarian-Indian Art & Culture Centre will take place.

ORGANIZATION INSTITUTIONS

Union of Chemists in Bulgaria, Union of Scientists in Bulgaria, Bulgarian Academy of Sciences, Chaudhary Charan Singh University, Meerut (India), Devam Foundation, University of Chemical Technology and Metallurgy, Sofia, Prof. A. Zlatarov University of Burgas, Faculty of Chemistry at St. K. Ohridski University of Sofia, Faculty of Chemistry at P. Hilendarski, University of Plovdiv, Faculty of Chemistry at K. Preslavski University of Shumen, Faculty of Chemistry at N. Rilski Southwest University of Blagoevgrad, University of Food Technologies, Plovdiv.

SYMPOSIA TITLES AND CHAIRS

1. Physical chemistry and electrochemistry: R. Raichev, R. Jain

2. Organic chemistry: V. Dimitrov, P. K. Sharma

3. Inorganic chemistry: D. Todorovsky, R. K. Sharma

4. Analytical chemistry: D. Tsalev, R. K. Mahajan

5. Catalysis: S. Damyanova, R. D. Kaushik

6. Chemical engineering: V. Beshkov, M. A. Abdullaha

7. Chemistry and environmental protection: Y. Pelovsky, A. Mittal

8. Polymers (plastics, rubbers, chemical fibres, cellulose): N. Dishovsky, R. K. Soni

9. Chemical technologies: G. Vissokov, A. Muddoo

10. Oil processing, petrochemistry and organic synthesis: G. Cholakov, A. P. Gupta

11. Chemical education: B. Toshev, A. K. Halve

GENERAL SCOPE

The Seventh National Conference on Chemistry is organized within the International Year of Chemistry 2011 and together with an International Conference on Green Technologies and Environmental Protection. The main objective of the conference is to discuss all fields of chemistry related to innovative and current topics, with emphasis on the latest developments in chemistry and relation to everyday life and clean environment.

Multidisciplinary topics with related fields such as theoretical chemistry, chemical

engineering, physics, earth and life sciences will be strongly encouraged. High-level scientific contributions including basic research and industrial requirements will be particularly appreciated. Papers on the following topics are invited:

Agrochemistry: fertilisers and pesticides; Analytical chemistry; Biochemistry: biomaterials and biotechnology; Catalysis; Ceramics and silicate chemistry; Chemical engineering; Chemistry and technology of polymers; Computational chemistry and molecular modelling; Electrochemistry; Inorganic chemistry; Management in chemical industries;

Mineral processing; Natural products; New materials; Organic chemistry; Organometallics; Petrochemistry; Pharmaceuticals; Physical chemistry; Pulp and paper technology; Radiochemistry; Solid state chemistry; Supramolecular chemistry; Textile and leather chemistry.

SCIENTIFIC PROGRAMME

The programme of the conference will consist of plenary lectures (40 min), keynote lectures (30 min), oral presentations (15 min), and posters. All the presentations should be related to recent and innovative studies.

LANGUAGE

The official language of the conference is English.

CONTRIBUTIONS

The selection of the oral and poster presentations will be based on half-page abstracts.

New methods, approaches and applications will be encouraged. Contributions should comply with the scope of the conference. Submissions should be made online using the application form available at the web site: <http://7ncc.unionchem.org>. The reviewing process will be carried out online via the internet. After evaluation of the contributions the programme will be made available at the conference web site.

BOOK OF ABSTRACTS

A book of abstracts and a printed programme will be handed out to the participants upon registration at the conference site.

REGISTRATION FEE AND PAYMENT

Conference ticket for participants (EURO). This includes welcome reception drink, book of abstracts and conference programme, coffee, refreshments and sightseeing tour of Sofia:

- early payment -120
- payment after 31 January 2011-130
- payment at conference site – 140.

Payments should be made only by bank transfer to the following account:

Union of Chemists in Bulgaria

IBAN: BG68UNCR96601018407500

BIC: UNCRBGSF

UniCredit Bulbank, 1 Ivan Vazov St., 1000 Sofia, Bulgaria

ACCOMMODATION

A very wide range of accommodation from 5 star hotels to student hostels will be available during the conference. Please contact the conference organizer at the web site of the conference: <http://7ncc.unionchem.org>.

KEY DATES

15 January 2011: Submission of abstracts

31 January 2011: Early payment

1 May 2011: Final programme at the web site

26 May 2011: Welcome to 7NCC

CONTACT US

Prof. V. Beschkov, DSc

Chairman of the Organizing Committee
Institute of Chemical Engineering,
Bulgarian Academy of Sciences
Acad. G. Bonchev St., Bldg. 103, 1113
Sofia, Bulgaria
tel: +359-2-8702088, fax: +359-2-8707523
e-mail: bioreac@bas.bg

Assoc. Prof. Ch. Bonev, PhD

Scientific Secretary
Institute of Catalysis, Bulgarian Academy
of Sciences
Acad. G. Bonchev St., Bldg. 11, 1113 Sofia,
Bulgaria
tel: +359-2-9792591, fax: +359-2-9712967
e-mail: bonev@ic.bas.bg

Assoc. Prof. L. Fachikov, PhD

Secretary

University of Chemical Technology and
Metallurgy

8 St. K. Ohridski Blvd., 1756 Sofia,
Bulgaria

tel: +359-2-8681120, +359-2-8163251, fax:
+359-2-8685488

e-mail: fachikov@uctm.edu

Mr. N. Naydenov, Dipl. Eng.

Secretary

Union of Chemists in Bulgaria

108 Rakovski St., 1000 Sofia, Bulgaria

tel/fax: +359-2-9875812

e-mail: chem@fnts-bg.org

A rapid, sensitive, and direct quantification of tamosulosin in human plasma through LC-ESI-MS/MS for the purposes of a bioequivalence study

M. L. Kundlik¹, B. H. Zaware² S. R. Kuchekar^{1*}

¹Padmashri Vikhe Patil College, Pravaranagar, Loni Kurd, Pin-413713, Dis-Ahmednagar, Maharashtra State, India

²New Arts, Commerce and Science College of Ahmednagar-414 001, Maharashtra State, India.

Received August 26, 2010, accepted September 9, 2010

A high-throughput bioanalytical method based on a solid phase extraction (SPE) and rapid liquid chromatography-tandem mass spectrometry (LC-MS/MS) analysis has been developed and validated for the quantification of tamosulosin in heparinized human plasma. Plasma samples, without a drying and reconstitution step, were extracted by a simple SPE. The analytes and tamosulosin D4 isotope (internal standard, IS) were chromatographed on a Betabasic-8 column. The total chromatographic run time was 1.8 min per sample. The response was a linear function of concentration in the range of 0.075–50.0 ng/ml, with correlation coefficient ≥ 0.9992 . The assay has excellent characteristics and was successfully applied to bioequivalence study samples for estimation of tamosulosin in healthy human subjects.

Key words: human plasma; LC-MS/MS; tamosulosin; positive ion electrospray.

INTRODUCTION

The symptoms, associated with benign prostatic hyperplasia (BPH), are related to the bladder outlet obstruction, which is comprised of two underlying components: static and dynamic. The static component is related to the increase in the prostate size, caused partly by a proliferation of smooth muscle cells in the prostatic stroma. However, the severity of BPH symptoms and the degree of the urethral obstruction do not correlate well with the size of the prostate [1, 2]. The dynamic component is a function of increase in the smooth muscle tone in the prostate and bladder neck, leading to constriction of the bladder outlet. Smooth muscle tone is mediated by the sympathetic nervous stimulation of the alpha 1 adrenoceptors, which are abundant in the prostate, prostate capsule, prostatic urethra, and bladder neck. Blockage of these adrenoceptors can lead to smooth muscles in the bladder neck and relaxation in the prostate which results in improvement of the urine flow rate and reduction in the BPH symptoms [1, 2].

Several chromatographic methods, including LC-fluorescence detector [3] and LC-MS/MS [4-9], have been developed to measure tamosulosin in the

biological fluids. LC-fluorescence detector [4] and LC-MS/MS [4-6] methods are inadequate because of the low sensitivity (LLOQ > 0.2 ng/ml), high injection volume (> 10 μ l), long chromatographic run time (> 2.5 min) and large volume of plasma (> 0.5 ml), required for the analysis. Hence, these methods allow for limited numbers of sample analysis in a day, which is not enough for day to day analysis and commercial utilization in the pharmacokinetics studies. The reported LC-MS and LC-MS/MS methods [7-9] are sensitive enough but all these technique require laborious extraction procedure such as the liquid-liquid extraction (LLE), involving time-consuming and error-prone solvent evaporation and reconstitution steps, high injection volume, and large volume of plasma for the analysis. Therefore, it was necessary to develop a simple, rapid and sensitive analytical method with minimum plasma requirement for extraction and short run time method to quantify the tamosulosin in the human plasma.

We report a new validated LC-MS/MS method for quantitation of tamosulosin in the human plasma that includes a simple SPE technique without drying and following reconstitution steps. Proposed method reduces sample preparation and analysis time relative to other commonly employed techniques with an improved limit of quantitation (LOQ) 0.075 mg/ml. Present method has run time of 1.8 min per

*To whom all correspondence should be sent:
E-mail: shashi17@gmail.com.

Table 1a. Experimental condition for liquid chromatography

Sr. No.	Chromatographic parameters	Optimized parameters
1	Mobile Phase Delivery	Isocratic mode
2	Mobile Phase	80:10:10 (v/v/v) methanol: acetonitrile: 3mM ammonium acetate, pH adjusted to 3.0 with formic acid.
3	Analytical column	Betabasic-8, 50 mm X 4.6 mm, 3.0 μ m
4	Mobile phase flow rate	0.45 ml/min
5	Autosampler tray temperature	20°C
6	Column temperature	45°C
7	Injection volume	5 μ l
8	Autosampler rinsing volume	500 μ l before and after injection
9	Analytical run time	1.8 min

Table 1b. Experimental condition for mass spectrometric detection.

Sr. No.	ESI source optimized parameter						
1	Spray voltage	: 3500V					
2	Sheath gas	: 40 (arbitrary units)					
3	Auxiliary gas	: 20 (arbitrary units)					
4	Capillary temperature	: 350°C					
5	Collision gas pressure (Argon)	: 1.5 m Torr					
6	Scan type	: Selected Reaction Monitoring (SRM)					
7	Polarity for analytes	: Positive ion polarity					
Scan parameter for analyte	Parent (m/z)	Product (m/z)	Scan Time (sec.)	CE (V)	Q1 PW Resolution	Q3 PW Resolution	Tube lens (V)
Tamosulosin	409.18	228.18	0.2	32	0.7	0.7	89
IS	413.28	228.21	0.2	34	0.7	0.7	96

sample; 300 μ l of plasma needed for the analysis, and the injection volume required is 5.0 μ l, which helps to increase the electrospray ionization (ESI) source life and reduces the column backpressure during the analysis of the clinical sample. Tamosulosin D4 isotope was used as an internal standard.

EXPERIMENTAL

Chemicals, Reagents, Standards

Pharmaceutical grade of tamosulosin was kindly supplied by CIPLA (Mumbai, Maharashtra, India) and IS was procured from MEDICAL ISOTOPES INC (Pelham, New Hampshire, USA). Both analytes were certified to contain more than 98.00%, and were used without further purification. Organic solvents used were of gradient grade and were obtained from Ranbaxy (Delhi, India). Water was

obtained from the Milli-Q Gradient water purification system (Millipore, Bedford, Massachusetts, USA). Formic acid was of suprapur grade and was obtained from Merck (Darmstadt, Germany). Ammonium acetate used for mobile phase preparation was of molecular biology-tested grade from Sigma-Aldrich (Steinheim, Germany). *O*-phosphoric acid was of suprapur grade and was obtained from Merck (Darmstadt, Germany). Oasis SPE cartridges were obtained from Waters (Massachusetts, Ireland). Control human plasma was obtained from Green Cross Laboratory and was stored below -70°C prior to use.

Stock solutions of tamosulosin and IS were prepared in methanol at free base concentration of 1 mg/ml, respectively. Secondary and working standard solutions were prepared from stock solutions by dilution in water. These diluted working standard solutions were used to prepare the

calibration curve and quality control samples in human plasma.

Sample Preparation

A 0.3 ml aliquot of human plasma was mixed with 25 μ l of IS working solution (30 ng/ml of IS). Then 500 μ l of 2% (v/v) *O*-phosphoric acid in water was added by stirring. The sample mixture was loaded into an Oasis HLB (1 cm³/30mg), equipped with an extraction cartridge that was pre-conditioned with 1.0 ml of methanol, and consequently with 1.0 ml water. The extraction cartridge was washed with 2 ml water, followed by washing with 1.0 ml 20% methanol. Tamosulosin and IS were eluted with 0.5 ml of methanol, and 5.0 μ l of the eluate was injected into LC-MS/MS system.

LC-MS/MS

High-performance liquid chromatography was performed with a Prominence pump, autosampler, autoinjector, and column oven Shimadzu (Kyoto, Japan) made. Mass spectrometry was performed

with a TSQ Quantum triple-quadrupole mass spectrometer by Thermo Finnigan (Thermo Electron, San Jose, CA, USA). All LC and MS/MS conditions were controlled by LCQuan software, version 2.5.6.

Compounds were separated on Betabasic-8 reversed-phase column (Thermo Electron Corporation, 50 mm \times 4.6 mm, 3.0- μ m particles). The column temperature was 45°C and the autosampler tray temperature was 10°C. The mobile phase was (80:10:10, v/v/v) acetonitrile: methanol: 3 mM ammonium acetate, pH adjusted to 3.0 with formic acid, at a flow rate of 0.45 ml/min. The chromatographic condition and mass spectrometric parameter are presented in Table No.1a and 1b.

The LCQuan software provided a standard method for calculations for quantitative analysis. Peak-area ratios of the calibrators were used in linear regression analysis with a weighting factor of $1/x^2$. The response curve was used to calculate the concentration of the calibrators, QC, and stability samples.

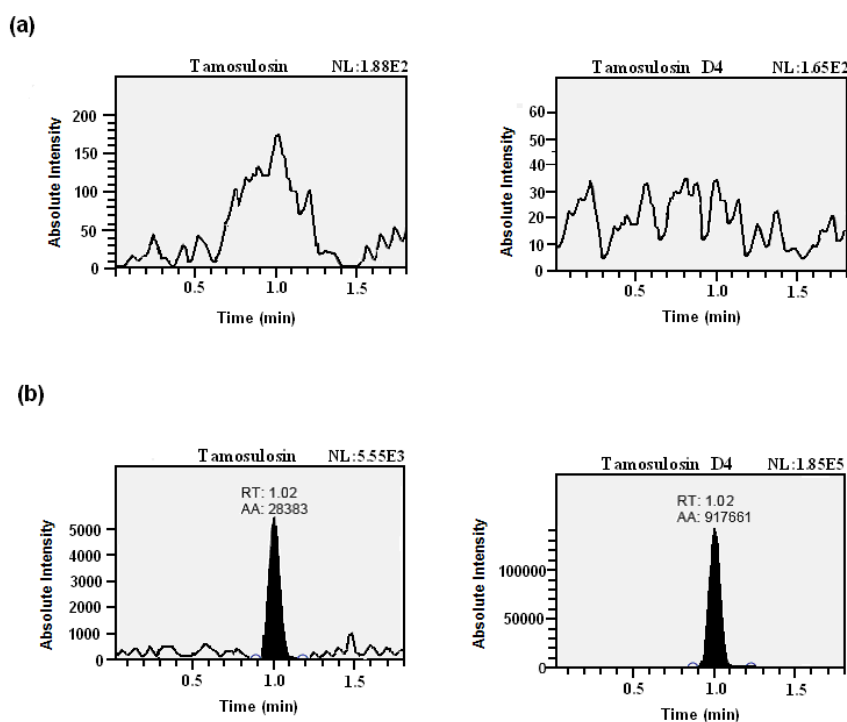


Fig. 1. Representative chromatograms for tamosulosin: (a) extracted blank plasma; (b) extracted tamosulosin LLOQ (0.075 ng/ml).

RESULTS AND DISCUSSION

Method Development

The objective of this method was to develop and validate [10] a rapid, sensitive and simple assay method for the extraction and quantification

of tamosulosin. During method development different detection, chromatographic, and sample-extraction condition were evaluated to achieve maximum response and good peak shape. Initially, tuning of the MS conditions in both, positive and negative modes, was performed for tamosulosin and IS, and the response was found to

be much higher in positive-ionization mode. Use of Betabasic-8 (50 mm x 4.6 mm i.d., 3.0 μ) column enabled usage of 0.45 ml/min flow rate, which resulted in run time as low as 1.8 min with better peak symmetry and signal of analytes. The optimum column oven temperature was 45°C, which resulted in symmetrical peaks.

In order to achieve cleanliness in the extract, the solid-phase extraction was optimized for extraction of analytes from plasma. Tamosulosin and IS showed good retention when eluted with methanol. In order to eliminate time-consuming and error-prone solvent evaporation and the reconstitution steps for concentration of samples after elution with methanol, the elution volume of methanol was reduced to 0.5 ml to concentrate the sample in the eluate. The optimized extraction condition was enabled to reduce processing and

analysis time. The sample volume of 5.0 μ l, avoided column backpressure and ESI source contamination during sample analysis in the clinical studies.

Method Validation

Specificity and selectivity

The specificity of the method was investigated by comparing chromatograms obtained from six different sources of plasma. The limit of detection (LOD) was 6 pg/ml. The selected reaction monitoring (SRM) transitions, 409.18→228.18 and 413.28→228.21, were chosen for quantification of tamosulosin and IS, respectively. The area observed at the tamosulosin retention time was much less than 20 % than that of the LLOQ (ng/ml) area (Fig. 1a and Fig.1b).

Table 2. Intra and Inter accuracy and precision for tamosulosin

Quality control samples	Intra assay precision and accuracy					Inter assay precision and accuracy			
	Conc. added (ng/ml)	Mean conc. found (ng/ml) (a)	SD	Precision % CV	Accuracy (%)	Mean conc. found (ng/ml) (b)	SD	Precision % CV	Accuracy (%)
LLOQ	0.075	0.069	0.006	8.44	92.00	0.073	0.007	9.57	97.33
LQC	0.225	0.243	0.013	5.44	108.00	0.235	0.030	12.64	104.44
MQC	15.0	15.789	2.058	6.96	105.26	15.354	1.571	10.23	102.36
HQC	37.0	36.250	3.108	3.94	97.97	34.726	3.219	9.27	93.85

(a) = mean of six replicates; (b) = mean of thirty replicates; Conc. = Concentration

Linearity

Five linearity curves, containing nine non-zero concentrations, were analyzed. The calibration curves appeared linear and were well described by least square lines. A weighting factor of 1/concentration i.e. $1/x^2$ was chosen to achieve homogeneity of the variance for tamosulosin. The correlation coefficient was ≥ 0.9992 (n=5) for tamosulosin.

Sensitivity

The LLOQ is defined as the lowest concentration of the calibration standard yielding accuracy $\pm 20\%$ RE and precision of $\leq 20\%$ RSD. The intra-run precision of LLOQ plasma samples, containing tamosulosin, was 8.84%. The mean intra-run accuracy of LLOQ plasma, containing tamosulosin, was 92.44%.

Recovery

Recovery of tamosulosin was calculated by comparing the peak area of the analyte from extracted plasma standard with that obtained from unextracted standard at the same concentration for the QC samples, containing 0.225, 15 and 37 ng/ml. The percentage mean recovery for tamosulosin was observed to be 74.12 %. The mean recovery of IS was 76.50% at concentration of 30 ng/ml.

Accuracy and precision

The intra-assay precision and accuracy were calculated in six replicate analyses for tamosulosin at four concentration levels viz. LLOQ (0.075 ng/ml), low quality control, (0.225 ng/ml), medium quality control, (15 ng/ml) and high quality control (37 ng/ml), each on the same analytical run. Inter-assay precision and accuracy was calculated after repeated analysis in three different analytical runs. The results are given in Table 2.

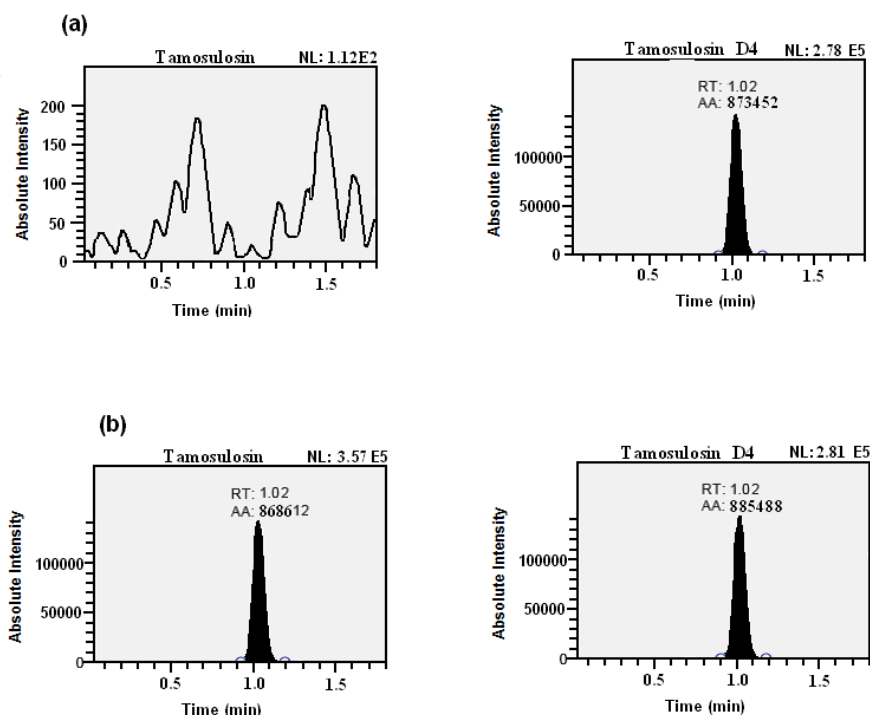


Fig. 2 Representative chromatograms for tamosulosin (a) extracted pre-dose sample from volunteer; (b) extracted volunteer sample for tamosulosin presence after 5.0 h.

Matrix effects

Matrix effects were investigated for six different samples of plasma which comprise four lots of normal control heparinized plasma, one lot of lipemic plasma, and one lot of haemolyzed plasma. Three samples, each at low and high quality control levels, were prepared from different lots of plasma (i.e. a total of 36 QC samples) and checked for accuracy to see whether the matrix affected the back-calculated value of the nominal concentrations for these different plasma samples. The results obtained were well within the acceptable limit of $\pm 15\%$.

Stability

Exhaustive experiments were performed to assess the stability of tamosulosin in stock solution and in plasma samples under different conditions, simulating the conditions which occurred during study analysis. The stock solutions of tamosulosin and IS were stable at a room temperature for 20 h and at 2–8°C for 28 days. Tamosulosin, in control human plasma, were stable for 14 h at a room temperature. Both analytes in the extracted plasma samples were stable for 54 h in an autosampler at 10°C. The tamosulosin was found to be stable at least for four freeze–thaw cycles. Tamosulosin spiked plasma samples, stored at –70°C to test long-term stability, were stable for at least 58 days.

The design of the study comprised an open randomized, two period, two sequence, replicate, crossover, comparative evaluation of the relative bioavailability of tamosulosin test formulation with reference in 12 healthy adult human subjects under fasting condition. Plasma samples were collected in 0.00, 0.50, 1.00, 1.50, 2.00, 2.50, 3.00, 3.50, 4.00, 4.50, 5.00, 5.50, 6.00, 6.50, 7.00, 8.00, 10.00, 12.00, 14.00, 16.00, 20.00, 24.00 and 48.00 h after the administration of a single oral dose of a 0.4 mg tamosulosin capsule to 12 male volunteers in each phase.

APPLICATIONS

The proposed validated method was successfully applied, for the assay of tamosulosin, to 12 healthy adult male human volunteer samples who received 0.4 mg of tamosulosin capsule under fasting condition. Current method is applicable for a large number of pharmacokinetics sample analysis because of its rapid sample preparation technology and short chromatographic run time. Tamosulosin presence in the volunteer's blood circulation was noticed in about 5.0 h after dose administration (Fig. 2).

CONCLUSION

The objective of this work was to develop a simple, specific, rugged and a high throughput method for estimation of tamosulosin in the

human plasma. The advantages of the SPE technique used in the present work are:

- (i) minimized sample extraction time;
- (ii) only 300 µL of human plasma were used, hence, reduced amount of blood withdrawn from the volunteers during the study;
- (iii) significantly less labor consuming (compared to the labor commonly associated with the LLE technique) in terms of the flash freezing of the aqueous part.

REFERENCES

1. Physicians Desk Reference (PDR), (2007). Medicines Economics Inc., 61th Edn. Montvale, NJ. www.PDR.net.
2. Flomax Drug Information, Flomax® Tamosulosin hydrochloride.(2010). www.rxlist.com/flomax-drugs.htm/.
3. J. Macek, P. Ptacek, J. Klima, J. Chromatogr. B., **809**, 307 (2004).
4. S. Agarwal, K.V. Gowda, A.K. Sarkar, D. Ghosh, U. Bhaumik, T.K. Chattaraj, T.K. Pal, Chromatographia., **67**, 893 (2008).
5. L. Ding, L. Li, P. Tao, J. Yang, Z. Zhang, J. Chromatogr. B., **767**, 75 (2002).
6. H. Matsushima, K.I. Takanuki, H. Kamimura, T. Watanabe, S. Higuchi, J. Chromatogr. Biomed. Sci. Appl., **695**, 317 (1997).
7. P. Keski-Rahkonen, O. Phrsson, E. Leppanen, T. Mauriala, M. Lehtonen, S. Auriola, J. Pharmaceuticals and Biomedical analysis, **43**, 606 (2007).
8. M. Qi, P. Wang, L. Liu, J. Chromatogr. B., **805**, 7 (2004).
9. N.V.S. Ramakrishna, K.N. Vishwottam, S. Manoj, M. Koteswara, S. Wishu, D. P. Verma, Biomedical Chromatogr., **19**, 709 (2005).
10. Guidance for Industry, Bioanalytical Method Validation, U.S. Department of Health and Human Services, Food Drug administration Center for Drug Evaluation and Research (CDER), Centre for veterinary Medicines (CVM), (2001).

БЪРЗО, ЧУВСТВИТЕЛНО И ПРЯКО КОЛИЧЕСТВЕНО ОПРЕДЕЛЯНЕ НА ТАМУЛОЗИН В ЧОВЕШКА ПЛАЗМА ЧРЕЗ LC-ESI-MS/MS ПРИ ИЗСЛЕДВАНЕТО НА БИОЕКВИВАЛЕНТНОСТ

М.Л. Кундлик¹, Б.Х. Зауаре², С.Р. Кучекар^{1*}

¹Колеж Падмашири Вике Патил, Праваранагар, Лони Кърд, Пин-413713, Дис-Ахмеднагар, Махарасастра, Индия

²Колеж за нови изкуства, търговия и наука в Ахмеданагар -414 001,

Постъпила на 26 август, 2010, приета на 9 септември, 2010

(Резюме)

Разработен е експресен биоаналитичен метод, основан на твърдо-течна екстракция (ТТЕ) и бърза течна хроматография, съчетана с мас-спектрометрия (LC-MS/MS). Методът е изпитан и утвърден за количественото определяне на тамулозин в хепаринизирана човешка плазма. Пробите от плазма, без сушене и повторно разтваряне, се екстрахират чрез ТТЕ. Пробите и вътрешният стандарт от тамулозин (изотоп D4) се подлагат на течна хроматография на колона Betabasic-8. Цялото време за хроматографското определяне е 1.8 мин. за проба. Отговорът е линейна функция на концентрацията при концентрации в интервала 0.075–50.0 ng/ml, с корелационен коефициент ≥ 0.9992 . Методът има отлични характеристики и е използван успешно за изследвания на биоеквивалентност на проби от плазма от здрави хора за наличие на тамулозин.

Synthesis and antibacterial activity of some new azopyrazoles

B.P.Patel*, H.S.Patel and P.J.Shah

Department of Chemistry, Sardar Patel University, Vallabh Vidyanagar-388120(India).

Received December 7, 2009; revised March 29, 2010

Mannich Reaction of benzotriazole (1), ethyl-4-amino benzoate (2) and formaldehyde in ethanol afford 4-(1H)-benzotriazolyl methyl amino benzoate (3), which on treatment with hydrazine hydrate in the presence of ethanol results in 4-(1H)-benzotriazolyl methyl amino benzoyl hydrazide (4). This compound was produced by condensation with pre-prepared various ethyl-2-substituted phenyl hydrazono-3-oxobutyrates (6a-h), and yielded 1-(4-((1H)-benzotriazolyl methyl amino benzoyl)-3-methyl-4-(2-substituted phenyl hydrazono)-1H-pyrazolin-5(4H)-one (7a-h). All the compounds (7a-h) were characterized by IR and NMR spectral studies. The compounds showed significant antimicrobial activity against various bacteria and fungi.

Key words: 5-pyrazolinone; benzotriazole; antimicrobial activity; Mannich reaction; spectral study.

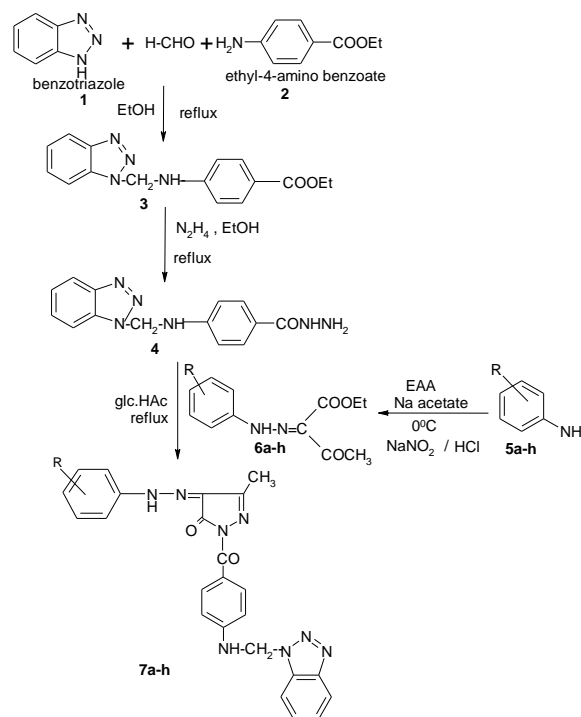
INTRODUCTION

The arylazopyrazoles are generally prepared by combination of aryl-azo-ethyl acetoacetate derivatives and hydrazine derivatives [1-6]. Another heterocyclic compound, say benzotriazole, is found to be important. Its prime application is in the composition of the corrosion inhibitors for copper or copper alloys [7, 8]. Ciba Geigy has introduced benzotriazole derivative under the trade name of Trinvin-P [9]. It is applied as an UV light absorber for stabilizing plastics and other organic materials against discoloration determination. It is employed as photographic emulsion stabilizer [10]. In the peptide synthesis it acts in the form of an active ester [11]. The area of application where the merged molecule like arylazopyrazole-benzotriazole has not been developed despite of their good biological properties. Hence this paper examines the synthesis and characterization of arylazopyrazole-benzotriazole derivatives, shown in Scheme 1.

EXPERIMENTAL

Materials

All chemicals used were of laboratory grade. Benzocain (i.e. ethyl-4-amino benzoate) and Benzotriazole were prepared by the reported method. [6]



R= (a) 4-H; (b) 2-CH₃; (c) 4-Cl; (d) 4-Br;
(e) 4-Nitro; (f) 2,4-Dinitro; (g) 2,4-Dichloro-6-Nitro;
(h) 2,4,6-tribromo.

Measurement

Melting points were determined in open capillary tubes and were uncorrected. IR spectra were recorded in KBr pellets on a Nicolet 760D spectrometer, and ¹H NMR and ¹³C NMR spectra

* To whom all correspondence should be sent:
E-mail: E-mail: purvesh23184@gmail.com

Table 1. Physical and analytical data of the synthesized (6a-h) compounds.

Compound No.	R	Molecular Formula	M.P. °C	Yield %	Elemental Analysis						Additional ¹ H-NMR Signals (δ, ppm)
					C%		H%		N%		
					Found	Calcd.	Found	Calcd.	Found	Calcd.	
6a	H	C ₁₁ H ₁₃ N ₃ O ₃	112	76	63.13	63.15	6.12	6.14	17.79	17.87	6.46-7.02 (s,5H,ArH) 2.36 (s,3H,CH ₃)
6b	2-Me	C ₁₂ H ₁₅ N ₃ O ₃	110	63	64.44	64.46	6.60	6.61	16.59	16.86	6.34-6.83 (s,4H,ArH)
6c	4-Cl	C ₁₁ H ₁₂ N ₃ O ₃ Cl	124	74	53.61	53.63	4.81	4.84	18.79	19.00	6.4-7.03 (s,4H,ArH)
6d	4-Br	C ₁₁ H ₁₂ N ₃ O ₃ Br	114	82	45.97	46.00	4.13	4.15	13.25	13.37	6.35-7.20 (s,4H,ArH)
6e	4-NO ₂	C ₁₁ H ₁₂ N ₄ O ₅	118	66	51.59	51.61	4.63	4.65	19.97	20.00	6.71-7.94 (s,4H,ArH)
6f	2,4-Dinitro	C ₁₁ H ₁₄ N ₅ O ₇	124	59	44.42	44.44	3.67	3.70	21.45	21.73	6.98-8.38 (s,3H,ArH)
6g	2,4-Dichloro-6-Nitro	C ₁₁ H ₁₀ N ₄ O ₅ Cl ₂	126	77	41.35	41.37	3.14	3.16	16.01	16.09	7.42-7.36 (s,2H,ArH)
6h	2,4,6-Tribromo	C ₁₁ H ₁₀ N ₃ O ₃ Br ₃	122	84	30.54	30.57	2.31	2.33	8.78	8.89	7.30 (s,2H,ArH)

were recorded in DMSO with TMS as internal standard on a Bruker spectrometer at 400 MHz and 100 MHz, respectively. LC-MS of selected samples were taken on LC-MSD-Trap-SL_01046. The compound purity was checked by TLC on silica gel plates, and the spots were visualized by exposure to iodine vapours.

Synthesis of 4-(1H)-benzotriazolyl methyl amino benzoate (3)

A mixture of 1H- Benzotriazole (1) (0.02mole), formaldehyde (0.02mole) and benzocain (2) (0.02mole) in ethanol (50ml) was heated under reflux for 4 hrs. Subsequently, the ethanol was distilled off and the obtained pasty mass obtained was triturated with petroleum ether (40-60°C). The solid compound 3 (see Scheme 1) was isolated, and dried. The yield was 62%, M.P.146–47°C (uncorrected). (Found 64.60 %, H 5.25 %, N 18.75 %; Calcd. C 64.85 %, H 5.44 %, N 18.91 %).

IR spectra: 3030-3088 cm⁻¹ (C-H of Ar.),1620-1489 cm⁻¹ (C-C of Ar.) 2960,1380 cm⁻¹ (-CH₃, -CH₂),1705–1765(C=O), 3450–3550 cm⁻¹ (-NH-), 1375–1350 cm⁻¹ (-CN),1196-1154 cm⁻¹ (C-O);¹H-NMR (400MHz, DMSO - d₆, δ / ppm) : 5.6 (s,2H, CH₂),6.56–7.87(s,8H,Ar-H),4.28(q,2H,-O-CH₂-CH₃),1.32(t,3H,-CH₂-CH₃);¹³C-NMR(100MHz, DMSO,δ/ppm):111.2-152.5(Ar-C),60.3(CH₂), 166.8(CO),61.4(O-CH₂),14.1 (CH₃) .

Synthesis of 4-(1H)-benzotriazolyl methyl amino benzoyl hydrazide (4)

4-(1H)-benzotriazolyl methyl amino benzoate (3) (0.05mole) was refluxed with hydrazine (0.05mole)

in absolute ethanol for 10 to 12 hours. It was cooled and kept overnight. The solid so obtained was filtered and recrystallized from ethanol. M.P.152–3°C, yield 46%. (Found : C 56.57 %, H 4.60 %, N 32.84 %; Calcd. C 56.75 %, H 4.76 %, N 33.09 %).

IR spectra: 3030-3090 cm⁻¹(C-H of Ar.),1640-1489cm⁻¹(C-C of Ar.),1705–1778(CONH),3450-3550cm⁻¹ (-NH-,NH₂)1375–1350 cm⁻¹ (-CN);¹H-NMR(400MHz,DMSO-d₆,δ/ppm)5.6(s,2H, CH₂),6.56-7.96(s,8H,Ar-H),3.95(2H,s,NH₂),9.65 (1H,s,CONH);¹³CNMR(100MHz,DMSO,δ/ppm) :111.2–153.4(Ar-C),60.3(CH₂),166.6(CO).

Synthesis of Ethyl-2-substituted phenyl hydrazono-3-oxobutyrate (6a-h)

Substituted aniline (5a-h) (0.01mole) was dissolved in HCl (8ml) and water (6ml) mixture. It was cooled to 0°C in ice bath. A cold aqueous solution of sodium nitrate (0.03mole) was added. The diazonium salt solution was filtered into a cooled solution of ethyl acetate (0.01mole) and sodium acetate (0.12mole), dissolved in ethanol (50ml). The resulting solid was washed with water and recrystallized from EtOH/MeOH. Yields, melting points and other compound characterization data are given in Table 1.

Synthesis of 1-(4-((1H)-benzotriazolyl methyl amino benzoyl)-3-methyl-4-(2-substituted phenyl hydrazono)-1H-pyrazoline-5(4H)-one (7a-h).

A solution of 4-(1H)-benzotriazolyl methyl amino benzoyl hydrazide (0.002mole) in 25 ml of glacial acetic acid was added to Ethyl-2-substituted phenyl hydrazono-3-oxobutyrate (6a-h) (0.002 mole), dissolved in glacial acetic acid (20ml), and

Table 2. Physical and analytical data of the synthesized (7a-h) compounds.

Compound No.	R	Molecular Formula	M.P. °C	Yield %	Elemental Analysis						Additional ¹ HNMR Signals (δ, ppm)
					C%		H%		N%		
					Found	Calcd.	Found	Calcd.	Found	Calcd.	
7a	H	C ₂₄ H ₂₀ N ₈ O ₂	208	48	63.68	63.71	4.40	4.42	24.68	24.77	6.48-7.02(s,5H,ArH) 0.9(s,3H,CH ₃)
7b	2-Me	C ₂₅ H ₂₂ N ₈ O ₂	210	53	64.34	64.37	4.69	4.72	23.97	24.03	6.47-7.02(s,4H,ArH)
7c	4-Cl	C ₂₄ H ₁₉ N ₈ O ₂ Cl	228	46	59.22	59.25	3.87	3.90	22.98	23.04	6.42-7.03(s,4H,ArH)
7d	4-Br	C ₂₄ H ₁₉ N ₈ O ₂ Br	248	59	54.20	54.23	3.55	3.57	21.02	21.09	6.48-7.02(s,4H,ArH)
7e	4-NO ₂	C ₂₄ H ₁₉ N ₉ O ₄	196	41	47.26	47.29	3.08	3.11	20.59	20.68	6.72-7.96(s,4H,ArH)
7f	2,4-Dinitro	C ₂₄ H ₁₈ N ₁₀ O ₄	214	42	56.45	56.47	3.49	3.52	27.36	27.45	6.98-8.89(s,3H,ArH)
7g	2,4-Dichloro-6-Nitro	C ₂₄ H ₁₇ N ₁₁ O ₄ Cl ₂	192	43	48.53	48.56	2.84	2.86	25.82	25.96	7.22-7.75(s,2H,ArH)
7h	2,4,6-Tribromo	C ₂₄ H ₁₇ N ₈ O ₂ Br ₃	252	54	41.78	41.79	2.44	2.46	15.22	16.25	7.14(s,2H,ArH)

this mixture was refluxed for 10–12 hrs. It was then cooled and allowed to stand overnight. The resulting solid was filtered off, dried, and crystallized from methanol. Yields, melting points, and other compound characterization data are given in Table 2.

BIOLOGICAL SCREENING

Antibacterial activities

The antibacterial activities of all compounds in 50 µg/ml concentration were studied against gram-positive bacteria (*Bacillus subtilis* and *Staphylococcus aureus*) and gram-negative Bacteria (*E. coil*, *Salmonella typhi* and *Klebsiella promioe*) using the agar cup plate method. This method uses a methanol system for control. We carried out a control experiment under similar conditions, using tetracycline as a standard for a comparison. The area of zone inhibition was measured in mm. An examination of the data reveals that all compounds showed good antibacterial activity. The results are presented in Table 3.

Antifungal activity

The fungicidal activity of all synthesized compounds was studied at 1000 ppm concentration in vitro of plant pathogenic organisms, listed in Table 4. The antifungal activities of all the samples were measured by cup plate method [12–14]. Each

of the plant pathogenic strains in potato dextrose agar (PDA) medium. Such a PDA medium contained 200 g of potato, 20g of dextrose, 20 g of

Table 3. Antibacterial activity of the (7a-h) compounds.

Compound No.	Zone of Inhibition				
	Gram-positive		Gram-negative		
	<i>Bacillus subtilis</i>	<i>Staphylococcus aureus</i>	<i>Klebsiella promioe</i>	<i>Salmonella typhi</i>	<i>E.coil</i>
7a	54	57	46	44	63
7b	43	65	57	54	67
7c	72	79	83	76	57
7d	82	69	70	67	83
7e	43	63	67	42	87
7f	64	59	44	64	37
7g	65	53	71	67	56
7h	82	65	58	76	71
Tetracycline	79	55	84	73	72

Table 4. Antifungal activity of the (7a-h) compounds.

Compo und No.	Zone of Inhibition at 1000 ppm (%)				
	<i>Penicillium expansum</i>	<i>Botrydepla dia thiobromine</i>	<i>Nigros spora sp.</i>	<i>Trichothe sium sp.</i>	<i>Rhizopus nigricans</i>
	7a	74	62	70	53
7b	62	73	64	54	67
7c	71	73	78	67	63
7d	67	69	68	79	71
7e	54	57	74	62	69
7f	51	64	58	73	58
7g	61	73	62	58	51
7h	73	78	62	74	67

agar, and 1 litre of water; 5 day old cultures were employed. The compounds to be tested were suspended (1000 ppm) in a PDA medium and autoclaved at 120° C for 15 min at 15 atm pressure.

These medium were poured into sterile Petri plate, and the organisms were inoculated after cooling the Petri plate. The percentage inhabitation for fungi was calculated after 5 days using the formula given below:

$$\text{PERCENTAGE OF INHIBITION} = 100 (X-Y)/X$$

Where, X: Area of colony in the control plate

Y: Area of colony in the test plate

The fungicidal activity of all compounds is shown in Table 4.

RESULTS AND DISCUSSIONS

The synthesis of (6a-h) has been performed based on the method reported. Only (6 b-d) has been reported [1]. The 4-(1H) - benzotriazolyl methyl amino benzoyl hydrazide (4) compound has been synthesized successfully as Mannich reaction, as reported previously [2]. It was observed that ethyl-2-substituted phenyl hydrazono-3-oxobutyrates (6a-h) condensation with 4-(1H) - benzotriazolyl methyl amino benzoyl hydrazide (4) gives 1-(4-((1H)-benzotriazolyl methyl amino benzoyl)-3-methyl-4-(2-substituted phenyl hydrazono)-1H-pyrazoline-5(4H)-one (7a-h).

The structures of (6a-h) were confirmed by elemental analysis and IR spectra, showing an absorption band at 3030–3080 cm^{-1} (C-H of Ar.), 3320–3250 (NH), 2825–2910 (CH aliphatic), 1295–1100 (C-O), 1610–1570 (C=N), 2950, 1370 cm^{-1} (-CH₃, CH₂), 1720–1660 (C=O).

¹H-NMR (400MHz, DMSO - d₆, δ / ppm): 1.29(3H,t,CH₃), 2.25 (3H,s,COCH₃), 4.25 (2H,q,COCH₂), 11.62 (1H,s,NH); (2a): 6.46–7.02 (s,5H,ArH); (2b): 2.36 (s,3H,CH₃), 6.34–6.83 (s,4H,ArH); (2c): 6.4–7.03 (s,4H,ArH); (2d): 6.35–7.20 (s,4H,ArH); (2e): 6.71–7.94 (s,4H,ArH); (2f): 6.98–8.38 (s,3H,ArH); (2g): 7.42–7.36 (s,2H,ArH); (2h): 7.30–7.32 (s,2H,ArH) (s,2H,ArH).

¹³C-NMR(100MHz,DMSO, δ /ppm):14.2(CH₃), 62.6(OCH₂),27.1(CH₃), 163.5–196.4 (-CO), 126.9 (C=N); (2a): 114.6–143.7 (Ar-C); (2b): 17.9 (CH₃), 113.4–142.1 (Ar-C); (2c): 118.2–130.4(Ar-C); (2d): 116.9–142.5(Ar-C),(2e)113.7–149.5(Ar-C);(2f) 116.9–139.1(Ar-C); (2g) 125.1–140.8(Ar-C);(2h) 109.8 -152.7(Ar-C). The C, H, N analysis data of all compounds are given in Table 1.

The IR spectra of all (7a-h) compounds show prominent spectral band due to 3270–3220 (NH),2825–2910(CH aliphatic),1770–1640 (C=O, Amide C=O),1610–1570(C=NNH),3030–3088 cm^{-1} (C-H of Ar.).

¹H-NMR (400MHz, DMSO - d₆, δ / ppm): 2.42(3H,s,CH₃), 5.6 (1H,s,CH₂),9.4–11.56 (2H,s, NH), 6.87–8.04 (complex,m,8H,ArH); (4a): 6.48–7.02(s,5H,ArH); (4b):0.9(s,3H,CH₃)6.47–7.02 (s, 4H, ArH); (4c): 6.42–7.03 (s,4H, ArH); (4d): 6.48–7.02 (s,4H,ArH); (4e): 6.72–7.96 (s,4H,ArH); (4f): 6.98–8.89 (s,3H,ArH); (4g): 7.22–7.75 (s,2H,ArH); (4h): 7.14 (s,2H,ArH).

¹³C-NMR(100MHz,DMSO, δ /ppm):11.6 (CH₃), 60.2–61.4 (CH₂), 163.7–172.4 (CO), 129.4–149.5 (C=N); (4a): 112.2–149.7 (Ar-C); (4b): 17.5 (CH₃), 112.2–149.6 (Ar-C); (4c): 112.9–149.4 (Ar-C); (4d): 112.9–149.5(Ar-C), (4e) 112.4–149.9 (Ar-C); (4f)112.1–149.2(Ar-C);(4g)112.3–149.8(Ar-C);(4h)110.7–149.4(Ar-C).The C, H, N analysis data of all compounds are given in Table 2.

The examination of data reveals that the elemental content is in consistence with the predicted structure, shown in Scheme-1. The IR and NMR spectral data also direct for assignment of the predicted structure. The LC- MS of one sample, i.e.7a, shows the peak of M⁺ ion at 451.5, which is consistent of molecular weight of 7a, i.e. 448.5. All these facts confirm the (7a-h) structures.

The examination of antibacterial activity data reveals that the compounds 7c, 7e and 7h are found to be more active against gram-positive and gram-negative bacteria.

CONCLUSION

In this paper, we report on the synthesis, the elemental analysis, the spectral studies, and the evaluation of antimicrobial activity of 1-(4-((1H)-benzotriazolyl methyl amino benzoyl)-3-methyl-4-(2-substituted phenyl hydrazono)-1H-pyrazoline-5(4H)-one (7a –h). The antimicrobial activity of these novel compounds was carried out against some strain bacteria. The results show that the synthesized compounds were toxic against the bacteria and fungus. The comparison between the antibacterial and antifungal activity of these compounds and the standard drugs shows that the presence of halogen groups in the phenyl ring increases the antimicrobial activity. In conclusion, we report herein, a simple and convenient route for the synthesis of some new heterocyclic compounds, based on pyrazolinone, which are of antimicrobial action.

REFERENCE

- 1 M. Amir, A. A. Siddiqui and S. Rizwan; *Oriental J Chem.*, **19(3)**, 629(2003).
- 2 A. K. Bhatt, P. R Shah, H. G. Karadiyya and H. D. Patel, *Oriental J Chem.*, **19(3)**, 643(2003).

- 3 K. V. Patel and A. Singh, *E-Journal of Chem.*, **6(1)**, 281(2009).
- 4 A. R. Kartritzky, S. Rachwal, *B. J. Chem. Soc., Perkin Trans.*, **1**, 805 (1987).
- 5 A. R. Kartritzky, K. Manju, S. K Singh and N. K. Meher, *Tetrahedron*, **61**, 2555 (2005).
- 6 A. I. Vogel, *A Text Book of Practical Organic Chemistry, 5th edn.*, 701, 1162 (1978).
- 7 J. W. Long, L. V. Vecek, *Sherwin-Williams Co U S*, 4663914 (1982).
- 8 F. Hageolom and W. Evertz, *Bayer U S*, 4424360 (1984).
- 9 N. J. Ratway, *The Merk Index 11th Ed.*, Merk & Co. (1981).
- 10 Ullman's Encyclopedia of Industrial Chemistry, *Willey Veh.*, 26, 614 (1984).
- 11 D.Hadson, R.C.River, G.E.Marshell, *Peptides: Chem. & Biology* (1990).
- 12 W. R. Baily and E.G.Scott, *Diagnostic Microbiology*, The C. V. Moshy Co. St. Lovis, 257 (1966).
- 13 A. L., Banty, *The Antimicrobial Susceptibility Test; The Principal and Practice*, edited by Illuslea and Febiger, (Philadephia, Pa USA), 180 (1976).
- 14 F.Simoncini, R. Rangone and C. Calani, *Farmaco. Ed. Prat*, **23(10)**, 559 (1968).

СИНТЕЗА И АНТИ-БАКТЕРИАЛНА АКТИВНОСТ НА НЯКОИ НОВИ АЗО-ПИРАЗОЛИ

Б.П. Пател, Х.С. Пател, П.Дж. Шах

Департамент по химия, Университет Сардар Пател, Валабх Видянагар – 388120, Индия

Постъпила на 7 декември, 2009 г.; преработена на 29 март, 2010 г.

(Резюме)

Установено е, че реакцията на Маних на бензо-триазол (1), етил-4-амино бензоат (2) и формалдехид в етанол позволява получаването на 4-(1H)-бензотриазоил-метил-амино-бензоат (3), който при третирането с хидразин-хидрат в присъствие на етанол дава 4-(1H)-бензотриазоил-метил-амино-бензоил хидразид (4). Това съединение е получено чрез кондензация на различни предварително приготвени етил-2-субституирани фенил-хидразоно-3-оксо-бутирати (6a-h) и дава 1-4-(1H)-бензотриазоил-метил-амино-бензоил)-3-метил-4-(заместен фенилхидразоно)-2-пирозолин-5-он (7a-h). Всички съединения (7a-h) са охарактеризирани с IR and NMR спектроскопия. Тези съединения показват значителна анти-микробна активност срещу различни бактерии и гъбички.

Synthesis and characterizations of charge-transfer complexes of 1,8-naphthalimides with different acceptors

M.S. Refat^{a,b*}, H. Al Didamony^c, Kh.M. Abou El-Nour^d, I. Grabchev^e, L. El-Zayat^a

^aDepartment of Chemistry, Faculty of Science, Port Said 42111, Port Said University, Egypt

^bDepartment of Chemistry, Faculty of Science, Taif University, 888 Taif, Kingdom Saudi Arabia

^cDepartment of Chemistry, Faculty of Science, Zagazig, Zagazig University, Egypt

^dDepartment of Chemistry, Faculty of Science, Ismailia, Suez Canal University, Egypt

^eUniversity of Sofia "St. Kliment Ohridski", Faculty of Medicine, 1407, 1 Koziak str, Sofia, Bulgaria

Received April 24, 2010; revised July 7, 2010

Five new Charge-Transfer (CT) complexes, formed from the of 4-substituted-N-allyl-1,8-naphthalimide derivatives as donors and σ -acceptor (iodine or π -acceptors) have been investigated. The data obtained indicate the formation of CT-complexes with the general formula of [(donors)(acceptor)_n], where n= 1 in the case of [(donors)]I₂, [(donors)(DDQ)], [(donors)(CLA)], [(donors)(PA)] complexes and [(donors)(TCNQ)] except for [(4MAN)(TCNQ)₂], and [(4PAN)(TCNQ)₂] where n = 2.

Keywords: Charge-transfer; spectroscopic studies; acceptors; 1,8-naphthalimide.

INTRODUCTION

1,8-Naphthalimides and their 4-substituted derivatives are the subject of many scientific investigations, including laser active media [1,2], potential photosensitive biologically active units [3], fluorescent markers in biology [4], analgetics in medicine [5,6], collectors in solar energy [7]. Recently, they have been examined as fluorescent dichroic dyes in liquid crystals for utilization in electro-optical devices [8–10].

In the recent years, the charge-transfer complexes of organic species are intensively studied due to their special type of interaction, accompanied by transferring of an electron from the donor to the acceptor [11–15].

We undertook this work following our studies of the charge transfer complexes [16–24], in order to investigate spectrophotometrically the CT complexes formed from the 4-substituted-N-allyl-1,8-naphthalimide (4-butylamino-N-allyl-1,8-naphthalimide (4BAAN), 4-morpholino-N-allyl-1,8-naphthalimide (4MAN), 4-piperdino-N-allyl-1,8-naphthalimide (4PAN), 4-Methylamino-N-allyl-1,8-naphthalimide (4MAAN), and 4-

propyloxy-N-allyl-1,8-naphthalimide (4POAN)), as donors with σ -acceptors as iodine, and some π -acceptors (2,3-dichloro-5,6-dicyano-1,4-benzoquinone (DDQ), 7,7', 8,8'-tetracyanoquinodimethane (TCNQ), chloranilic acid (CLA) and picric acid (PA))

EXPERIMENTAL

Materials and Methods

All chemicals used in this study are Analar or extra pure grade.

Preparation of 1,8-naphthalimide derivatives

The syntheses of 4-substituted-N-allyl-1,8-naphthalimides presented in Fig. 1 have been described recently [25].

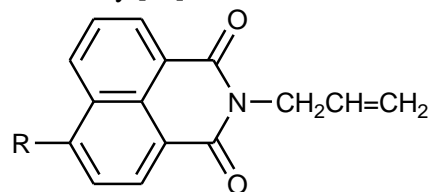


Fig. 1: General chemical structure of 1,8-naphthalimide derivatives, R = NHCH₂CH₂CH₂CH₃ (4-BAAN), Morpholino (4-MAN), Piperdino (4-PAN), NHCH₃ (4-MAAN) and OCH₂CH₂CH₃ (4-POAN).

* To whom all correspondence should be sent:
E-mail: msrefat@yahoo.com

Preparation of 1.8-naphthalimide charge-transfer complexes

Charge-transfer (CT) complexes, formed from the reactions between 4-substituted-N-allyl-1.8-naphthalimides and respective σ -acceptors, were synthesized as follows:

[4-Butylamino-N-allyl-1.8-naphthalimide]-I₂, DDQ, TCNQ, CLA and PA complexes

The charge-transfer complexes, [(4-BAAN)(Iodine)] (brown), [(4-BAAN)(DDQ)] (red), [(4-BAAN)(TCNQ)] (yellow crystal), [(4-BAAN)(CLA)] (yellow crystal), and [(4-BAAN)(PA)] (yellow crystal), were prepared by mixing 1 mmol of the donor in chloroform (10 ml) with 1 mmol of each of the acceptors, I₂, DDQ, TCNQ, CLA, and PA, in 10 ml of the same solvent with constant stirring for about 10 min. The solutions were allowed to evaporate slowly at a room temperature, the solids filtered and washed several times with little amounts of solvent, and dried under vacuum over anhydrous calcium chloride.

[4-Morpholino-N-allyl-1.8-naphthalimide]-I₂, DDQ, TCNQ, CLA and PA complexes:

The charge-transfer complexes, [(4-MAN)(Iodine)] (brown), [(4-MAN)(DDQ)] (red), [(4-MAN)(TCNQ)₂] (green), [(4-MAN)(CLA)] (red), and [(4-MAN)(PA)] (yellow), were prepared by mixing 1 mmol of the donor in chloroform (10 ml) with 1 mmol of each of the acceptors, I₂, DDQ, TCNQ, CLA, and PA, in 10 ml of the same solvent with constant stirring for about 10 min. The precipitate, formed in each of the cases, was filtered off immediately and washed several times with minimum amounts of chloroform, and dried under vacuum over P₂O₅.

[4-Piperdino-N-allyl-1.8-naphthalimide]-I₂, DDQ, TCNQ, CLA, and PA complexes

The charge-transfer complexes, [(4-PAN)(Iodine)] (brown), [(4-PAN)(DDQ)] (red), [(4-PAN)(TCNQ)₂] (yellow), [(4-PAN)(CLA)] (red), and [(4-PAN)(PA)] (yellow), were prepared by mixing 1 mmol of the donor in chloroform (10 ml) with 1 mmol of each of the f acceptors, I₂, DDQ, TCNQ, CLA, and PA, in 10 ml of the same solvent with constant stirring for about 10 min. The precipitate, formed in each of the cases, was filtered off immediately and washed several times with minimum amounts of chloroform, and dried under vacuum over P₂O₅.

[4-Methylamino-N-allyl-1.8-naphthalimide]-I₂, DDQ, TCNQ, CLA, and PA complexes

The charge-transfer complexes, [(4-MAAN)(Iodine)] (brown), [(4-MAAN)(DDQ)] (red), [(4-MAAN)(TCNQ)] (yellow), [(4-MAAN)(CLA)] (yellow), and [(4-MAAN)(PA)] (red), were prepared by mixing 1 mmol of the donor in chloroform (10 ml) with 1 mmol of each of the acceptors, I₂, DDQ, TCNQ, CLA, and PA, in 10 ml of the same solvent with constant stirring for about 10 min. The precipitate, formed in each of the cases, was filtered off immediately and washed several times with minimum amounts of chloroform, and dried under vacuum over P₂O₅.

[4-Propyloxy-N-allyl-1.8-naphthalimide]-I₂, DDQ, TCNQ, CLA, and PA complexes

The charge-transfer complexes, [(4-POAN)(Iodine)] (brown), [(4-POAN)(DDQ)] (red), [(4-POAN)(TCNQ)] (blue), [(4-POAN)(CLA)] (yellow), and [(4-POAN)(PA)] (yellow), were prepared by mixing 1 mmol of the donor in chloroform (10 ml) with 1 mmol of each of the acceptors, I₂, DDQ, TCNQ, CLA, and PA, in 10 ml of the same solvent with constant stirring for about 10 min. The precipitate, formed in each of the cases, was filtered off immediately and washed several times with minimum amounts of chloroform, and dried under vacuum over P₂O₅.

Instrumentation and physical measurements

The electronic spectra of donors, acceptors, and the respective CT complexes were recorded in the spectral region of 200-800 nm using a Jenway 6405 Spectrophotometer with quartz cells, 1.0 cm path in length. Photometric titration was performed at 25 °C for the reactions of the donors with the acceptors in chloroform, as follows: the concentration of the donors in the reaction mixtures was kept fixed at 5.0x10⁻⁴ M, while the concentration of the acceptors was changed over a wide range between Xx10⁻⁴ and Yx10⁻⁴ M. These produced solutions with donor/acceptor molar ratios, varying from 1: 0.25 to 1: 4.00.

FTIR measurements (KBr discs) of the donors, acceptor and CT complexes were carried out on a Bruker FT-IR spectrophotometer (400-4000 cm⁻¹). ¹HNMR spectra were obtained on Varian Gemini 200 MHz spectrometer. ¹HNMR data are expressed in parts per million (ppm), referenced internally to the residual proton impurity in DMSO (dimethylsulfoxide, d₆) as a solvent, and reported as chemical shift (m = multiplet and s = singlet; br =

broad). The complex compositions were confirmed by the mass spectra at 70 eV using AEI MS 30 mass spectrometer. We carried out the thermal analysis (TGA & DTG) out under nitrogen atmosphere at heating rate of 10 C/min using a Shimadzu TGA-50H thermal analyzers.

RESULTS AND DISCUSSION

The results of the elemental analysis for all CT complexes are listed in Table 1. The data shows that those values are in good agreement with the calculated ones, and the composition of the CT complexes is matched with the molar ratios, exhibited through the photometric titration, occurring between donors and acceptors (σ - and π -acceptors).

Table 1. Elemental analysis CHN and physical parameters data of the CT-complexes, formed from the reaction of the 4BAAN, 4MAN, 4PAN, 4MAAN, and 4POAN with iodine, DDQ, TCNQ, CLA, and PA.

Complexes (FW)	Mwt	C%		H%		N%		Physical data	
		Found	Calc.	Found	Calc.	Found	Calc.	Color	mp ($^{\circ}$ C)
[(4BAAN)]I ₂	562	40.32	40.57	3.50	3.56	4.88	4.98	Brown	95
[(4BAAN)(DDQ)]	535	60.23	60.56	3.56	3.73	8.87	8.97	Red	209
[(4BAAN)(TCNQ)]	512	72.19	72.61	4.56	4.68	16.25	16.40	Yellow	213
[(4BAAN)(CLA)]	517	57.85	58.02	4.18	4.25	5.39	5.41	Yellow	198
[(4BAAN)(PA)]	537	55.46	55.86	4.11	4.28	12.66	13.03	Yellow	168
[(4MAN)]I ₂	576	39.28	39.59	2.98	3.12	4.78	4.86	Brown	67
[(4MAN)(DDQ)]	549	58.94	59.01	3.19	3.46	10.09	10.20	Red	236
[(4MAN)(TCNQ) ₂]	731	70.19	70.63	3.48	3.56	18.98	19.16	Green	223
[(4MAN)(CLA)]	531	56.31	56.49	3.68	3.76	5.09	5.27	Red	216
[(4MAN)(PA)]	551	54.12	54.44	3.77	3.81	12.56	12.70	Yellow	184
[(4PAN)]I ₂	574	41.76	41.81	3.29	3.48	4.78	4.88	Brown	97
[(4PAN)(DDQ)]	547	61.11	61.42	3.78	3.84	10.11	10.23	Red	165
[(4PAN)(TCNQ) ₂]	729	72.32	72.47	3.65	3.84	18.98	19.21	Yellow	221
[(4-PAN)(CLA)]	529	58.73	58.98	4.08	4.16	5.09	5.29	Red	199
[(4PAN)(PA)]	549	56.28	56.83	4.13	4.19	12.69	12.75	Yellow	175
[(4MAAN)]I ₂	520	36.88	36.93	2.60	2.69	5.29	5.38	Brown	102
[(4MAAN)(DDQ)]	493	58.32	58.41	2.78	2.84	11.23	11.36	Red	196
[(4MAAN)(TCNQ)]	470	71.39	71.49	3.99	4.04	17.75	17.87	Yellow	187
[(4MAAN)(CLA)]	475	55.09	55.58	3.29	3.37	5.75	5.89	Yellow	149
[(4MAAN)(PA)]	495	53.25	53.33	3.37	3.43	13.95	14.14	Red	166
[(4POAN)]I ₂	549	39.11	39.36	2.89	3.09	2.51	2.55	Brown	85
[(4POAN)(DDQ)]	522	59.38	59.77	3.16	3.25	7.95	8.04	Red	239
[(4POAN)(TCNQ)]	499	72.08	72.14	4.15	4.21	13.85	14.03	Blue	211
[(4POAN)(CLA)]	504	57.03	57.14	3.62	3.77	2.56	2.78	Yellow	166
[(4POAN)(PA)]	524	54.66	54.96	3.76	3.81	10.65	10.68	Yellow	163

Electronic absorption spectra

The absorption UV/Vis spectra of the 1,8-naphthalimide/iodine complexes were measured in CHCl₃. The complexes are formed with donors (4BAAN, 4MAN, 4PAN, 4MAAN and 4POAN) by adding X ml of 5.0×10⁻⁴ M (I₂) (X = 0.25, 0.50, 0.75, 1.00, 1.50, 2.00, 2.50 and 3.00 ml) to 1.00 ml of 5.0×10⁻⁴ M of each donor. The volume of the

mixtures in each case was adjusted to 10 ml in each donor. The donor concentration in the reaction mixtures was kept fixed at 0.5×10⁻⁴ M, while the iodine concentration varied in the range between 0.125×10⁻⁴ M and 1.50×10⁻⁴ M. These concentrations produced base to I₂ ratios within the range between 1:0.25 and 1:3.00. The electronic absorption spectra of the reactants of I₂ and 4BAAN, 4MAN, 4PAN, 4MAAN, and 4POAN

mixed with CHCl_3 in a volumetric ratio of 1:1 are shown in Figures (2A-E), respectively. The spectra

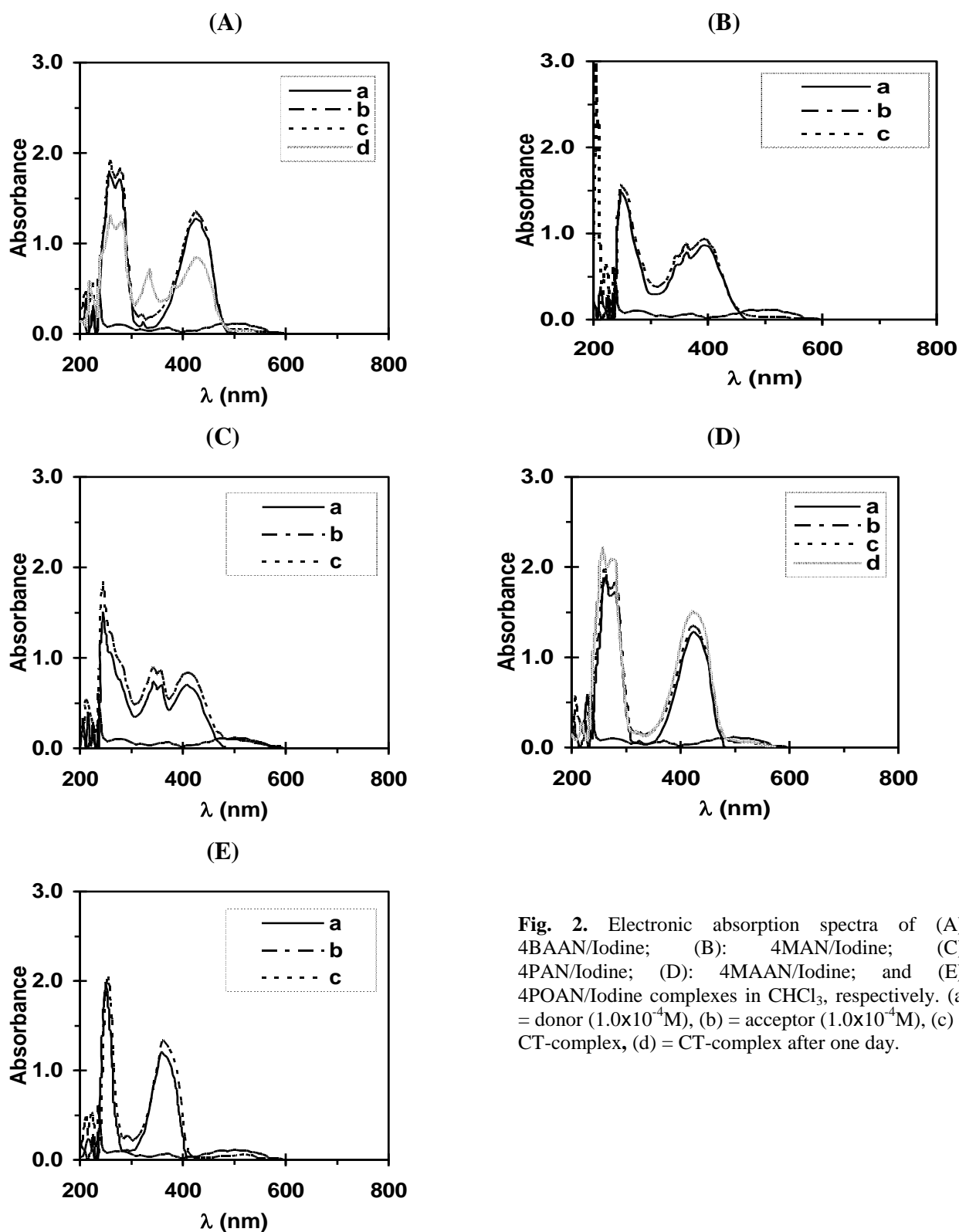


Fig. 2. Electronic absorption spectra of (A): 4BAAN/Iodine; (B): 4MAN/Iodine; (C): 4PAN/Iodine; (D): 4MAAN/Iodine; and (E): 4POAN/Iodine complexes in CHCl_3 , respectively. (a) = donor ($1.0 \times 10^{-4} \text{M}$), (b) = acceptor ($1.0 \times 10^{-4} \text{M}$), (c) = CT-complex, (d) = CT-complex after one day.

show detected absorption bands. These bands are assigned at (335, 385 and 505 nm), (390 and 505 nm), (410 and 510 nm), (425 and 500 nm), and at (360 and 500 nm) due to the CT complex, formed in the reaction of 4BAAN, 4MAN, 4PAN,

4MAAN, and 4POAN with I_2 in solvent chloroform, respectively. The photometric titration curves were obtained adhering to the molar ratio method [27], by plotting of the absorbance against the volume of the iodine σ -acceptor added. The

equivalence points, shown on these curves, clearly indicate that the CT-complex, formed between the donor (4BAAN, 4MAN, 4PAN, 4MAAN and 4POAN) and the iodine, is in a 1:1 ratio. The formation of 1:1 complex was strongly supported by elemental analysis, photometric titrations and far infrared spectra. The spectrophotometric data are employed to calculate the equilibrium constant (K_{CT}) and the molar absorbance (ϵ_{CT}) for donor- I_2 complexes in chloroform using the 1:1 modified Benesi-Hildebrand equation [28]. This equation is based on the assumptions of 1:1 (Acceptor-Donor) complex formation. Calculations are based on the data obtained for, C_D^0 of (4BAAN, 4MAN, 4PAN, 4MAAN and 4POAN), C_A^0 of I_2 , $C_A^0 + C_D^0$ and $C_A^0 \times C_D^0 / A$ in $CHCl_3$. When the $C_A^0 \times C_D^0 / A$ values for each donor are plotted against the corresponding $C_A^0 + C_D^0$ values, the straight lines are obtained with a slope of $1/\epsilon$ and intercept of $1/K\epsilon$ for the reactions in $CHCl_3$. Both, the equilibrium constant (K) and the molar absorbance (ϵ) for all CT complexes, are given in Table 2. The value trend in this table reveals high values of both, the equilibrium constant (K) and the molar absorbance (ϵ). This high value of (K) reflects the high stability of the iodine complexes because of the expected high donation of the 4-butylamino for (4BAAN), the 4-morpholino for (4MAN), the 4-piperidino for (4PAN), the 4-methylamino for (4MAAN), and the 4-propyloxy for (4POAN) N-allyl derivatives of 1.8-naphthalimide (donor).

The CT transition energies of CT-complexes are used to estimate the ionization potential of (4BAAN, 4MAN, 4PAN, 4MAAN and 4POAN) using the empirical equations, derived by Aloisi and Pignataro [29]. The values obtained are listed in Table 2.

The electronic absorption spectra of the free donors, 4BAAN, 4MAN, 4PAN, 4MAAN and 4POAN with DDQ in chloroform along with those of the formed 1:1 CT complexes, are shown on Figures (3 A-E), respectively. The spectra demonstrate that the formed CT-complexes show new absorption bands which do not exist in the spectra of the reactants. These bands are attributed to charge-transfer complexes formation and can be assigned as follows: 360 and 430 nm for 4BAAN/DDQ, 360 and 390 nm for 4MAN/DDQ, 357 and 410 nm for 4PAN/DDQ, 355 and 425 nm for 4MAAN, and (355 and 410 nm) for 4POAN/DDQ, respectively. In the measurements the concentration of the donors (4BAAN, 4MAN, 4PAN) was kept fixed at 0.25×10^{-4} M while the concentration of the acceptor varied in the range of

0.0625×10^{-4} M to 0.75×10^{-4} M. The concentration of the other donors (4MAAN and 4POAN) was kept fixed at 0.50×10^{-4} M while the concentration of the acceptor varied in the range of 0.125×10^{-4} M to 1.50×10^{-4} M. Accordingly, the CT-complexes, formed upon the reaction of 4BAAN, 4MAN, 4PAN, 4MAAN and 4POAN as donors with π -acceptor DDQ under investigation, have the general formula of [(donor)(acceptor)]. The 1:1 modified Benesi-Hildebrand equation [28] was used as shown in the previous sections in the calculation of the values of the equilibrium constant, K , and the molar absorbance, ϵ . While plotting the $C_A^0 \cdot C_D^0 / A$ values against the $C_A^0 + C_D^0$ values for the donors/DDQ, straight lines were obtained with a slope of $1/\epsilon$ and an intercept of $1/K\epsilon$. The obtained values of both K and ϵ , associated with these complexes, are given in Table 3.

Figures 4 (A-E) show the electronic absorption spectra of the reactant donors, 4BAAN, 4MAN, 4PAN, 4MAAN and 4POAN, with TCNQ in chloroform along with the 1:1 molar ratio of donor: acceptor with 4BAAN, 4MAAN, and 4POAN, while the molar ratio for donor: acceptor is 1:2 for the donors of 4PAN and 4MAAN. The spectra demonstrate that the formed CT complexes show new absorption bands at 410 and 455 nm for the 4BAAN/TCNQ, 410 nm for the 4MAN/TCNQ, 405 nm for the 4PAN/TCNQ, 405 and 450 nm for the 4MAAN/TCNQ, and (355 and 405 nm) for the 4POAN/TCNQ, respectively. The concentration of donors (4BAAN and 4MAN) in these measurements was kept fixed at 0.50×10^{-4} M while the concentration of the TCNQ varied in the range of 0.125×10^{-4} M to 1.50×10^{-4} M. The concentration of 4PAN donor was kept fixed at 0.125×10^{-4} M while the concentration of the TCNQ varied in the range of 0.031×10^{-4} M to 0.50×10^{-4} M. In the case of the donors (4MAAN and 4POAN) the concentration was kept fixed at 0.25×10^{-4} M while the concentration of the TCNQ varied in the range of 0.0625×10^{-4} M to 0.75×10^{-4} M. Accordingly, the CT complexes, formed upon the reaction of 4BAAN, 4MAN, 4PAN, 4MAAN and 4POAN, being the donors with TCNQ under investigation, have the formula of [(4BAAN)(TCNQ)], [(4MAN)(TCNQ)₂], [(4PAN)(TCNQ)₂], [(4MAAN)(TCNQ)] and [(4POAN)(TCNQ)] CT complexes. The 1:1 modified Benesi-Hildebrand equation [28] was used to calculate the values of the equilibrium constant, K ($l \text{ mol}^{-1}$), and the molar absorptivity, ϵ ($l \text{ mol}^{-1} \text{ cm}^{-1}$), for the [(4BAAN)(TCNQ)], the [(4MAAN)(TCNQ)] and

the [(4POAN)(TCNQ)] CT complexes. The corresponding spectral parameters for the complexes of [(4MAN)(TCNQ)₂] and [(4PAN)(TCNQ)₂], were calculated using the known El-Kourashy equation [30] for 1:2 complexes.

Here, C_A^0 and C_D^0 are the initial concentration of the TCNQ and the donors, respectively, while A is the absorbance at the mentioned CT bands. Straight lines are obtained with a slope of $1/\epsilon$ and intercept of $1/K\epsilon$ when plotting the values of $C_A^0 C_D^0 / A$ against the $(C_A^0 + C_D^0)$ values, and the

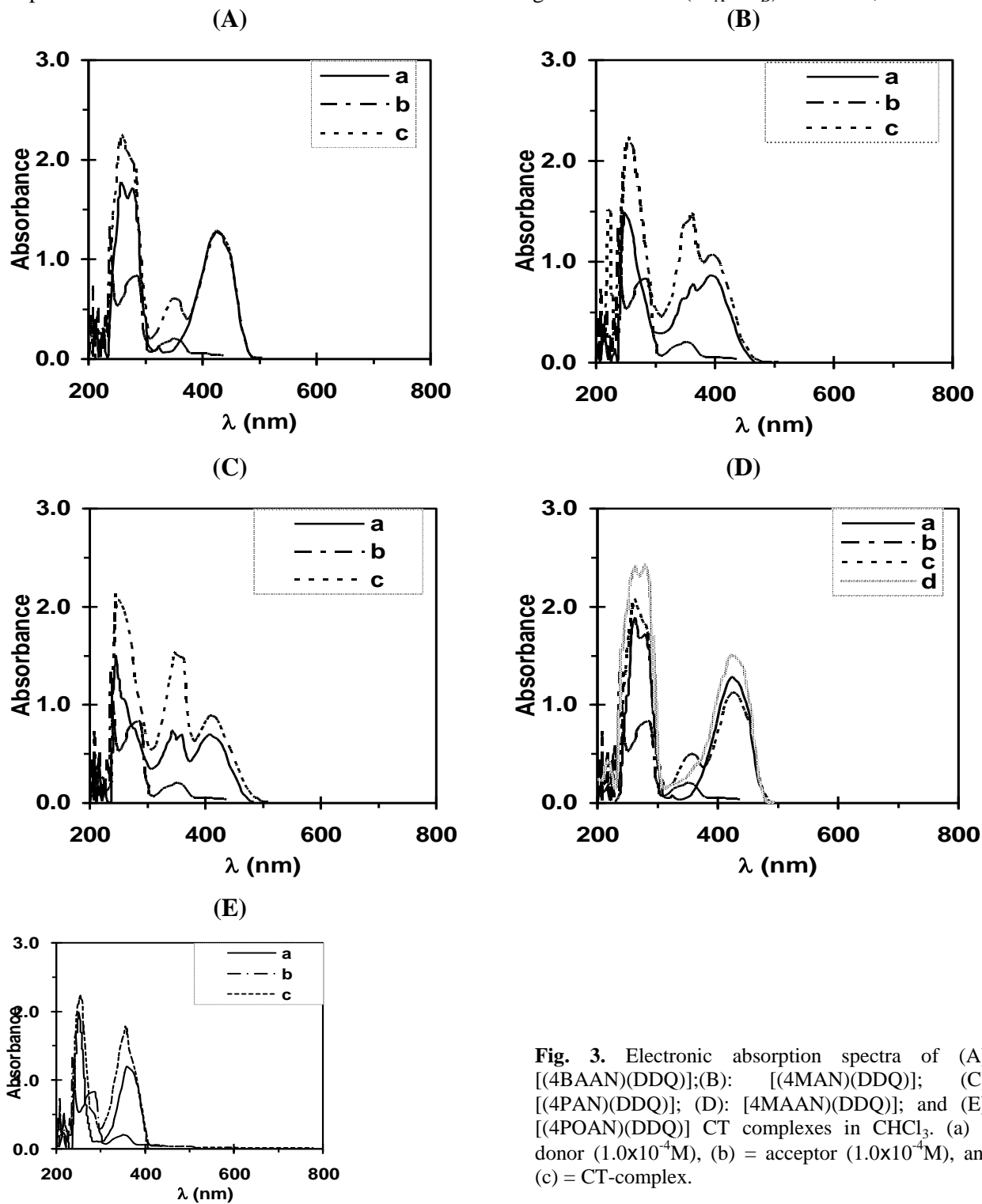


Fig. 3. Electronic absorption spectra of (A): [(4BAAN)(DDQ)]; (B): [(4MAN)(DDQ)]; (C): [(4PAN)(DDQ)]; (D): [4MAAN)(DDQ)]; and (E): [(4POAN)(DDQ)] CT complexes in CHCl₃. (a) = donor (1.0×10^{-4} M), (b) = acceptor (1.0×10^{-4} M), and (c) = CT-complex.

values of $(C_A^0)^2 C_D^0 / A$ versus the $C_A^0 (C_A^0 + 4C_D^0)$ values. Table 4 shows the calculated values of the

spectroscopic data, containing the ϵ , K and I_p .

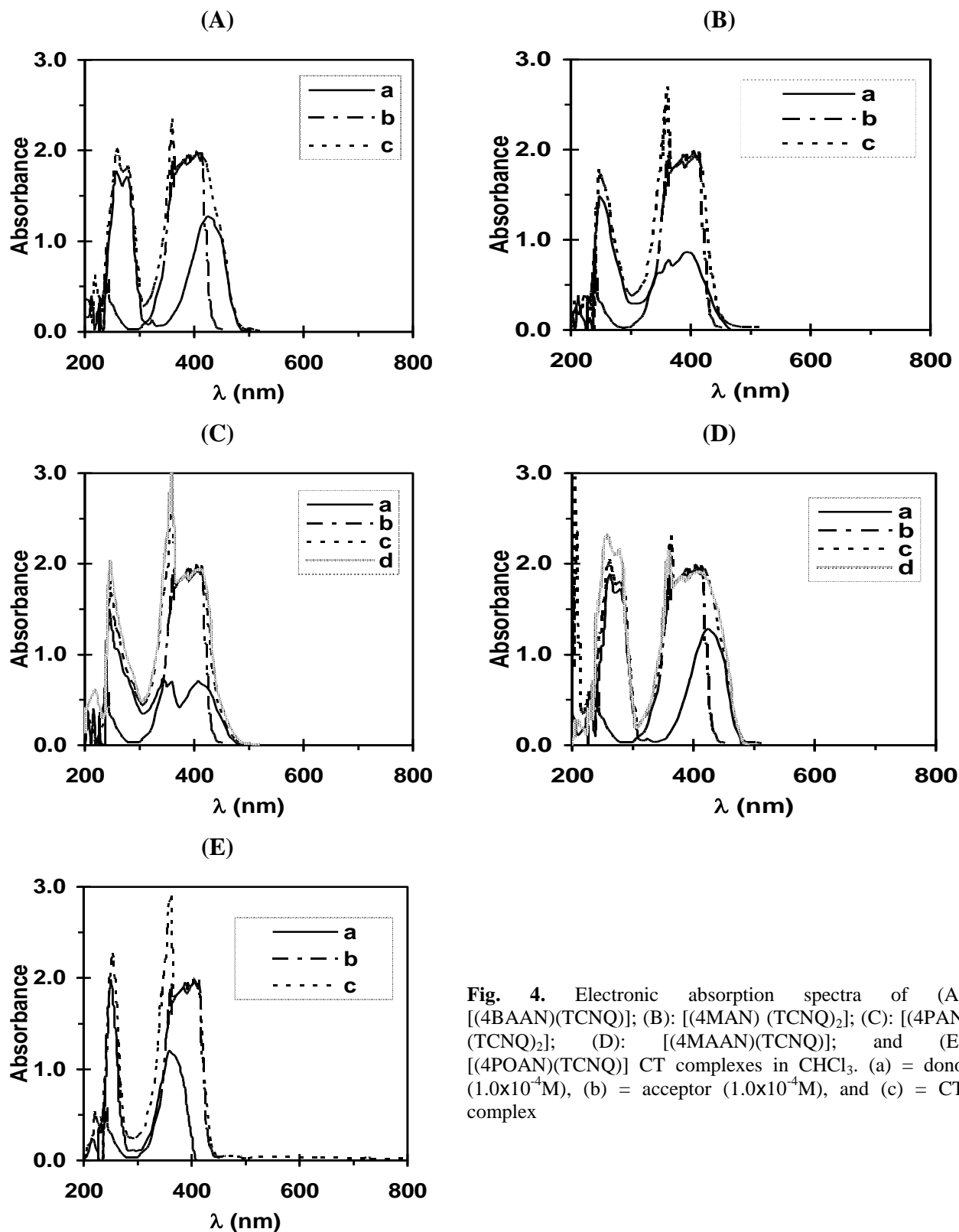


Fig. 4. Electronic absorption spectra of (A): [(4BAAN)(TCNQ)]; (B): [(4MAN)(TCNQ)₂]; (C): [(4PAN)(TCNQ)₂]; (D): [(4MAAN)(TCNQ)]; and (E): [(4POAN)(TCNQ)] CT complexes in CHCl₃. (a) = donor (1.0×10⁻⁴M), (b) = acceptor (1.0×10⁻⁴M), and (c) = CT-complex

The electronic absorption spectra of the reactant donors of 4BAAN, 4MAN, 4PAN, 4MAAN, and 4POAN with CLA in CH₃OH along with those of the formed 1:1 CT complexes are shown on Figure 5. The

spectra demonstrate that the formed CT complexes show new absorption bands as follows: at 320 and 525 nm for the 4BAAN/CLA, 310 and 520 nm for the 4MAN/CLA, 315 and 535 nm for the 4PAN/CLA,

general formula of [(donor)(acceptor)]. The 1:1 modified Benesi-Hildebrand equation was used as shown in the previous sections for the calculation of the values of the equilibrium constant, K , and the molar absorptivity, ϵ . Straight lines are obtained with

a slope of $1/\epsilon$ and an intercept of $1/K\epsilon$. Table 5 shows the obtained values of both, K and ϵ , associated with these complexes.

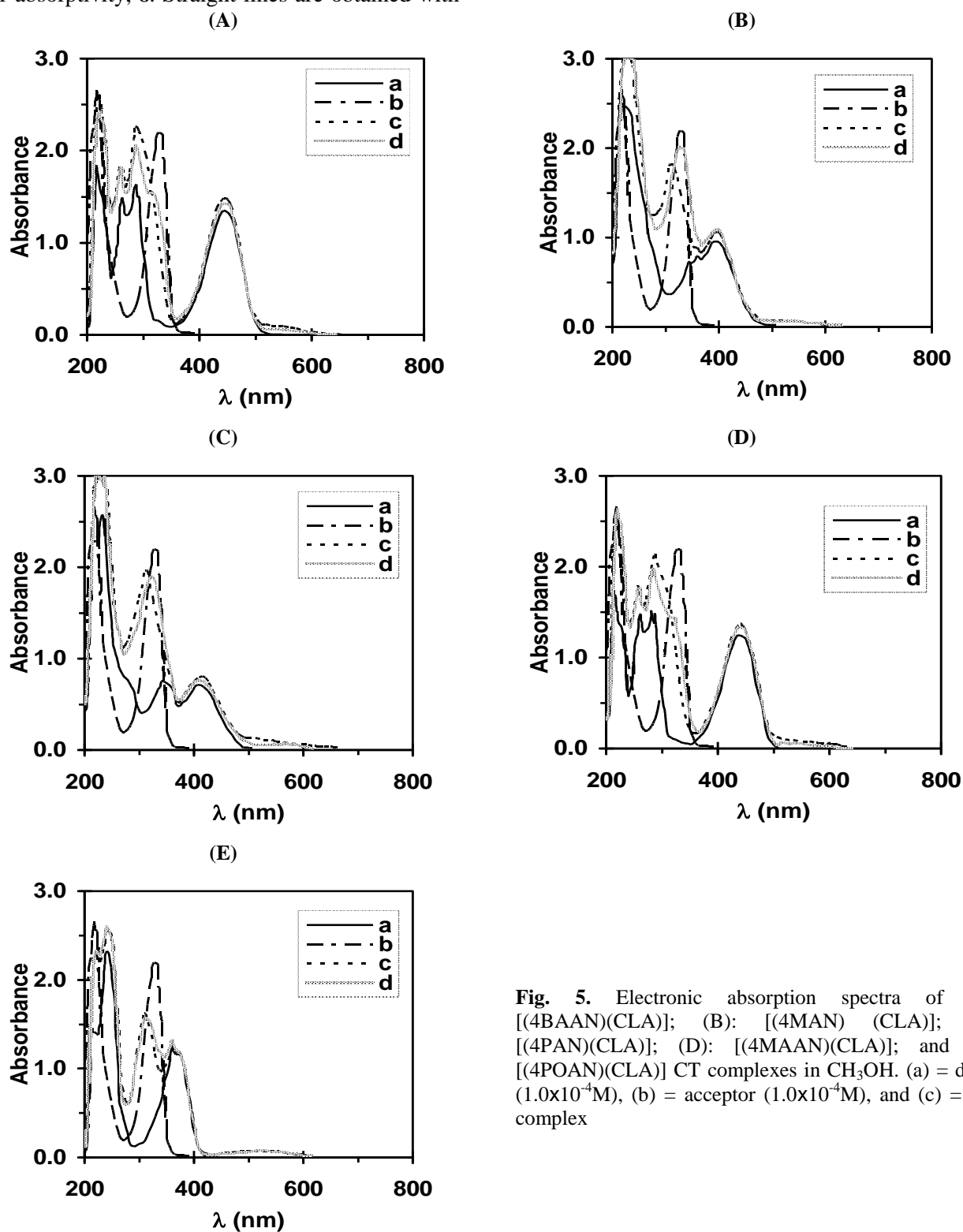


Fig. 5. Electronic absorption spectra of (A): [(4BAAN)(CLA)]; (B): [(4MAN)(CLA)]; (C): [(4PAN)(CLA)]; (D): [(4MAAN)(CLA)]; and (E): [(4POAN)(CLA)] CT complexes in CH_3OH . (a) = donor ($1.0 \times 10^{-4}\text{M}$), (b) = acceptor ($1.0 \times 10^{-4}\text{M}$), and (c) = CT-complex

Table 2: Spectrophotometric results for (A): 4BAAN/iodine; (B): 4MAN/iodine; (C): 4PAN/iodine; (D): 4MAAN/iodine; and (E): 4POAN/iodine CT complexes.

CT-complexes	λ_{\max} (nm)	E_{CT} (eV)	K ($l.mol^{-1}$)	ϵ_{\max} ($l.mol^{-1}.cm^{-1}$)	I_p
A	385	3.23	2.06×10^4	2.36×10^4	7.37
B	390	3.19	2.22×10^4	2.85×10^4	7.35
C	410	3.03	2.19×10^4	2.06×10^4	7.23
D	425	2.93	2.12×10^4	2.74×10^4	7.16
E	360	3.45	2.07×10^4	4.96×10^4	7.53

Table 3: Spectrophotometric results for (A): [(4BAAN)(DDQ)]; (B): [(4MAN)(DDQ)]; (C): [(4PAN)(DDQ)]; (D): [(4MAAN)(DDQ)]; and (E): [(4POAN)(DDQ)] CT complexes.

CT complexes	λ_{\max} (nm)	E_{CT} (eV)	K ($l.mol^{-1}$)	ϵ_{\max} ($l.mol^{-1}.cm^{-1}$)	I_p
A	430	2.89	4.30×10^4	3.34×10^4	7.14
B	390	3.18	4.15×10^4	4.97×10^4	7.34
C	410	3.03	4.08×10^4	4.97×10^4	7.23
D	425	2.93	2.35×10^4	3.26×10^4	7.16
E	410	3.03	2.49×10^4	0.816×10^4	7.23

Table 4: Spectrophotometric results for (A): [(4BAAN)(TCNQ)]; (B): [(4MAN)(TCNQ)₂]; (C): [(4PAN)(TCNQ)₂]; (D): [4MAAN)(TCNQ)]; and (E): [(4POAN)(TCNQ)] CT complexes.

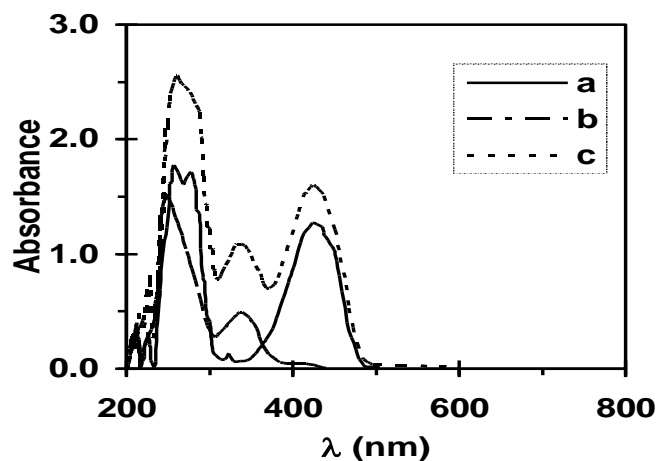
CT complexes	λ_{\max} (nm)	E_{CT} (eV)	K ($l.mol^{-1}$)	ϵ_{\max} ($l.mol^{-1}.cm^{-1}$)	I_p
A	455	2.73	2.21×10^4	1.61×10^4	7.02
B	410	3.03	1.68×10^8	9.47×10^4	7.23
C	405	3.07	34.99×10^8	3.93×10^5	7.26
D	450	2.76	4.87×10^4	2.51×10^4	7.04
E	405	3.07	7.84×10^4	11.28×10^4	7.26

Table 5: Spectrophotometric results for (A): [(4BAAN)(CLA)]; (B): [(4MAN)(CLA)]; (C): [(4PAN)(CLA)]; (D): [4MAAN)(CLA)]; and (E): [(4POAN)(CLA)] CT complexes.

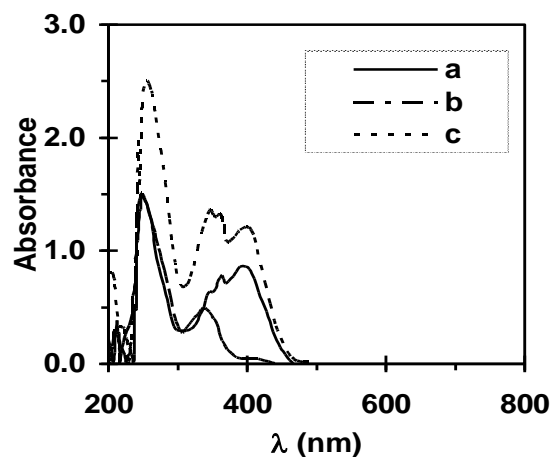
CT complexes	λ_{\max} (nm)	E_{CT} (eV)	K ($l.mol^{-1}$)	ϵ_{\max} ($l.mol^{-1}.cm^{-1}$)	I_p
A	525	2.73	10.61×10^4	0.996×10^4	7.02
B	520	2.39	10.88×10^4	0.389×10^4	6.79
C	535	2.32	3.15×10^4	0.901×10^4	6.74
D	530	2.34	7.83×10^4	0.470×10^4	6.75
E	520	2.39	21.36×10^4	0.692×10^4	6.79

The electronic absorption spectra of the donors, 4BAAN, 4MAN, 4PAN, 4MAAN and 4POAN with PA in $CHCl_3$ along with those of the formed 1:1 CT complexes are shown on Figure 6. The spectra demonstrate that the formed CT complexes show new absorption bands as follows: 335 and 425 nm for the 4BAAN/PA, 340 and 400 nm for

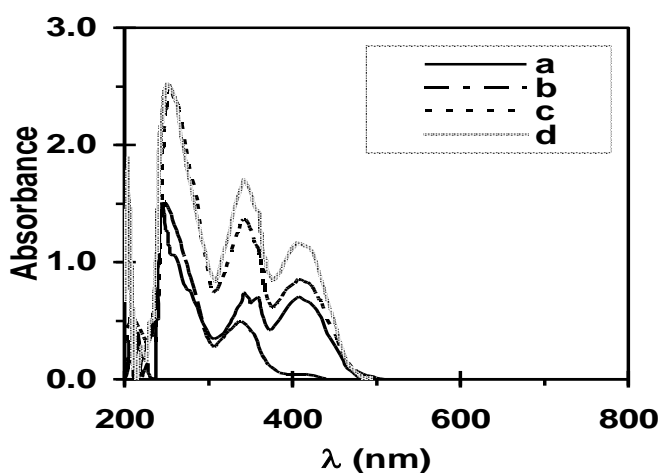
the 4MAN/PA, 330 and 410 nm for the 4PAN/PA, 335 and 425 nm for the 4MAAN/PA, and 360 and 430 nm for the 4POAN/PA. In these measurements the concentration of the donors (4BAAN, 4MAN, 4PAN, 4MAAN and 4POAN) was kept fixed at 0.25×10^{-4} M while the concentration of the PA was in the range of 0.0625×10^{-4} M to 0.75×10^{-4} M.



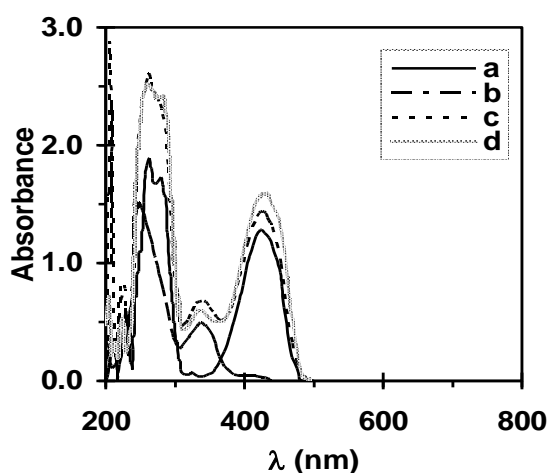
(A)



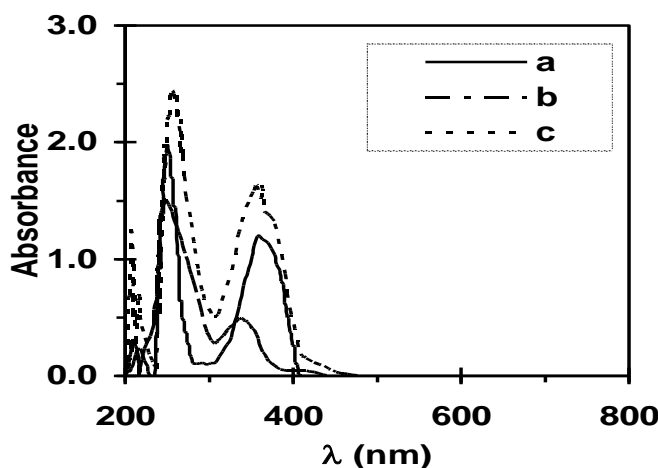
(B)



(C)



(D)



(E)

Fig. 6: Electronic absorption spectra of (A): [(4BAAN)(PA)]; (B): [(4MAN)(PA)]; (C): [(4PAN)(PA)]; (D): [(4MAAN)(PA)]; and (E): [(4POAN)(PA)] CT complexes in CHCl_3 . (a) = donor ($1.0 \times 10^{-4} \text{M}$), (b) = acceptor ($1.0 \times 10^{-4} \text{M}$), and (c) = CT-complex

Accordingly, the CT-complexes, formed upon the reaction of 4BAAN, 4MAN, 4PAN, 4MAAN and 4POAN, being the donors with PA under investigation, have the general formula of [(donor)(acceptor)]. The 1:1 modified Benesi-Hildebrand equation was used in the calculation of the values of the equilibrium constant, K , and the

molar absorptivity, ϵ . The values C_a^0 and C_d^0 are the initial concentrations of the PA and the donors of 4BAAN, 4MAN, 4PAN, 4MAAN and 4POAN, respectively, while A is the absorbance at the CT bands. A straight line with a slope of $1/\epsilon$ and intercept of $1/K\epsilon$ is obtained when plotting the

values of the $C_a^o \cdot C_d^o/A$ against the $C_a^o + C_d^o$ values for each donor. The obtained values of both, K and ϵ , associated with these complexes, are given in Table 6. These complexes show high values of both the

formation constants (K) and the molar absorptivity (ϵ). These high values of K confirm the expected high stabilities of the formed CT complexes.

Table 6: Spectrophotometric results for (A): [(4BAAN)(PA)]; (B): [(4MAN)(PA)]; (C): [(4PAN)(PA)]; (D): [(4MAAN)(PA)]; and (E): [(4POAN)(PA)] CT complexes.

CT complexes	λ_{\max} (nm)	E_{CT} (eV)	K (l.mol^{-1})	ϵ_{\max} ($\text{l.mol}^{-1} \cdot \text{cm}^{-1}$)	I_p
A	425	2.93	4.32×10^4	3.75×10^4	7.16
B	400	3.11	4.21×10^4	4.73×10^4	7.29
C	410	3.03	4.50×10^4	4.21×10^4	7.23
D	425	2.93	4.44×10^4	3.98×10^4	7.16
E	430	2.90	5.35×10^4	2.27×10^4	7.14

Infrared spectra

The FTIR spectra of 4BAAN, 4MAN, 4PAN, 4MAAN and 4POAN and the respective CT complexes of [(4BAAN)]₂, [(4MAN)]₂, [(4PAN)]₂, [(4MAAN)]₂ and [(4POAN)]₂ were recorded at KBr and data are listed in Table 7. As expected, the band characteristics for the 4BAAN, 4MAN, 4PAN, 4MAAN and 4POAN units in [(donor)]₂ CT-complexes are shown with small changes in band intensities and frequency values, indicating the formation of the charge-transfer complexes.

The far infrared spectra of [(4BAAN)]₂, [(4MAAN)]₂ and [(4POAN)]₂ CT complexes were recorded from Nujol mulls, dispersed on polyethylene windows in the region of 50-300 cm^{-1} . The absence of the bands, characteristic for I_3^- in the spectra show the formation of the [(donor)]₂ CT-complexes.

The infrared characteristic bands of the CT complexes, formed from the interaction of the 1,8-naphthalimide with (acceptor = DDQ, TCNQ, CLA and PA), are assignments and are given in Tables (8 to 11). These assignments are based on the comparison between the spectra of CT complexes and the spectra of the reactants, the donors and the acceptors. The spectra of the reaction products contain the main bands for both reactants, and this strongly supports the formation of the CT-complexes. However, the bands of the acceptors and the donor in the spectra of 1,8-naphthalimide CT complexes show some changes in the intensities and in some cases show small shifts in the frequency values, compared to those of the free acceptors and the donor. This could be understood based on the symmetry and the

electronic structure changes in both, the acceptors and the donors in the formed CT-complexes, compared to those of the free molecules.

The comparison between the important IR spectral bands of the free donors of N-allyl derivatives of 1,8-naphthalimide and the π -acceptor DDQ and the corresponding bands, appearing in the IR spectra of the prepared CT complexes, shows strong patterns due to the corresponding radical anions, DDQ \cdot^- . Essentially, the vibration frequencies of the C \equiv N groups for DDQ, observed at 2250 and 2231 cm^{-1} , are shifted to lower wavenumbers of 2213-2237 cm^{-1} in the corresponding IR spectra of its CT complexes with 1,8-naphthalimide (4BAAN, 4MAN, 4PAN, 4MAAN, and 4POAN). Also, the stretching vibration frequencies of the C=O groups, appearing at 1673 cm^{-1} in the IR spectrum of free DDQ, is displayed at 1635-1655 cm^{-1} and 1678-1698 cm^{-1} in their complexes. Furthermore, the bands belonging to the C-Cl vibrations which appeared at 800 and 720 cm^{-1} in the IR spectra of the free DDQ, exhibit a high shift in the corresponding IR spectra of the CT complexes (at 894-885 and 744-783 cm^{-1}). Accordingly, these interpretation led to the deduction that the CT complexation occurs as π - π^* (aromatic ring of donor to aromatic ring of acceptor), see Scheme 1. The IR spectral bands of the [(4BAAN)(TCNQ)], [(4MAN)(TCNQ)]₂, [(4PAN)(TCNQ)]₂, [(4MAAN)(TCNQ)] and the [(4POAN)(TCNQ)] solid CT complexes are given in Table 9. The structures of the 1,8-naphthalimide/TCNQ CT complexes,

Table 7: Infrared frequencies^(a) (cm⁻¹) and tentative assignments for (A): 4BAAN; (B): 4MAN; (C): 4PAN; (D): 4MAAN; (E): 4POAN; (F): 4BAAN/iodine; (G): 4MAN/iodine; (H): 4PAN/iodine; (I): 4MAAN/iodine; and (J): 4POAN/iodine complexes in CHCl₃, respectively.

A	B	C	D	E	[(Donors)]I ₂					Assignments ^(b)
					F	G	H	I	J	
3382 s	--	--	3391 vs	3424 w,br	3391 w 3336 w	--	--	3389 s 3321 w	3424 br	v(O-H); H ₂ O of KBr v(N-H)
3075 w	3072 w	3071 w 3010 w	3085 vw	3078 w	3079 vw	--	3076 w	3058 vw	3078 w	v _{as} (C-H); aromatic v(C-H); CH ₂ +CH ₃
2955 ms	2952 m	2934 ms	2989 vw	2964 ms	2923 m	2925 vs	2925ms	2929 m	2962 ms	v _s (C-H)
2867 m	2895 w 2846ms	2850 m 2812 m	2930 w 2851vw	2938 w 2876 mw	2856 w	2854 s	2853 m		2928 ms 2874 w	v _{as} (C-H)
1682 s	1690 s	1697 s	1681 s	1697 s	1673 s	1741 s	1698 ms	1682 s	1696 s	v(C=O)
1642 vs	1656 vs	1652 vs	1637 s	1659 vs	1608 ms	1699 s 1627 vs	1656 s	1635 s	1658 vs	
1612 vw	1588 s	1590 s 1512 m	1577 vs 1549 s	1590 s 1514 ms	1580 vs	1582ms 1515 m	1582 s 1514 m	1579 vs 1548 s 1528 w	1590 s 1590 s 1522 ms	v(C=C); aromatic
1577 vs	1512 m	1447 vw	1446 m	1461 ms	1550 ms	1458 ms	1459 m	1478 w	1460 ms	δ(CH); CH def.
1544 vs	1448 m	1452 mw	1418 m	1380 s	1523 s	1375 ms	1423 w	1451 w	1422 m	δ(CH); aromatic
1470 m	1380 s	1381 ms	1380 s		1470 ms 1376 m		1375 s 1340 m	1380 s	1379 s	
1335 s	1342 ms	1235 ms 1235 s	1355 ms 1299 ms	1327 vw 1269 s	1345 ms 1279 w	1340 w 1235 ms	1234 ms 1156vw	1353 s 1299 w	1267 s 1233 s	v(C-C) v(C-N)
1247 s	1238 s	1178 m	1245 ms	1234 s	1248 s	1161 m	1130 w	1276 w	1182 w	v(C-O)
1187 w	1179	1134 m	1155 ms	1185 m	1191 w	1117 m	1078 w	1246 ms	1137 m	CH, in-plane bend
1143 s	ms	1080 mw	1090 w	1136 m	1165 s			1166 ms	1099 w	
1097 m	1118 s 1078 m		1060 vw	1100 ms 1076 ms	1044 w			1056 m	1076 m	
1023 w	1021 w	1019 w	1023 vw	1026 m	977 ms	1031 w	982 w	976 ms	1026 vw	δ _{rock} ; NH
979 m	983 ms	975 mw	946 vw	995 ms	891 w	983 w	931 w	947 w	995 m	CH-deformation
940 w	942 w	952 vw	819 w	927 ms	854 w	927 w	855 m	893 vw	927 m	
916 w	883 m	851 m	770 s	832 ms	823 w	857 w	773 vs	815 w	830 ms	
827 w	844 ms	780 s	695 vw	780 s	766 ms	772 vs		769 s	779 s	
779 s	785 s 757 ms	717 vw	656 vw	756 m				694 w		
673 vw	677 w	691 vw		668 m	655 w	673 vw	607 vw	583 m	668 m	Skeletal vibration
584 m	629 w 562 w 501 w	625 vw 564 vw	581 m 522 m	630 w 581 w	585 m	599 vw	564 w 492 w	531 m 498 w	615 w 577 w	CH bend
507 m	417 ms	464 vw	467 vw	496 w	501 m	417 m	464 w	466 w	494 w	CH out of plane
467 w		419 m	420 w	457 w 410 m	438 vw		422 m	420 w	460 w 415 w	bend Skeletal vibration CNC def.

(a): s = strong, w = weak, m = medium, sh = shoulder, v = very, br = broad.

(b): v, stretching; δ, bending.

are strongly supported by the observed main infrared bands for the reactants. However, the bands of 1,8-naphthalimide derivatives and TCNQ in the spectra of the [(4BAAN)(TCNQ)], [(4MAN)(TCNQ)₂], [(4PAN)(TCNQ)₂], [(4MAAN)(TCNQ)], and [(4POAN)(TCNQ)] complexes show small

shifts in the frequency values as well as some changes in their intensities in comparison to those of the free donors and the TCNQ. This could be attributed to the expected symmetry and electronic structure changes in the formation of the CT complexes. In the case of the In the case of the [(4MAN)(TCNQ)₂] and

Table 8: Infrared frequencies^(a) (cm⁻¹) and tentative assignments for (A): [(4BAAN)(DDQ)]; (B): [(4MAN)(DDQ)]; (C): [(4PAN)(DDQ)]; (D): [(4MAAN)(DDQ)]; and (E): [(4POAN)(DDQ)] CT complexes.

A	B	C	D	E	Assignments ^(b)
3248 s, br	3421 w, br 3227 w, br	3226 vs, br	3388 ms 3236 ms, br	3423 ms, br 3240 w, br	v(O-H); and H ₂ O of KBr v(N-H)
2978 vw 2945 vw	2982 w	2932 ms	2925 vw	2966 ms	v _{as} (C-H); CH ₂ +CH ₃ v(C-H); aromatic
2838 vw	2951 mw 2845 m	2854 w	2849 vw	2879 w	v _s (C-H) + v _{as} (C-H)
2251 s	2213 s	2251 ms	2237 ms	2231 ms	v(C≡N); DDQ
1680 w 1635 ms	1691 s 1655 vs	1698 s 1655 vs	1678 ms 1637 s	1694 s 1652 vs	v(C=O); DDQ + donors
1576 s	1584 vs	1581 vs 1514 w	1577 vs 1549 w	1587 s 1517 m	v(C=C); aromatic
1452 vs	1450 ms 1380 s	1452 vs 1376 s	1451 s 1421 w 1379 ms	1454 ms 1382 s	δ(CH); CH _{def.} δ(CH); aromatic
1359 m 1274 s 1246 vw 1191 s 1074 ms	1339 m 1237 s 1180 m 1116 ms 1077 m	1340 ms 1274 ms 1235 ms 1190 s 1076 ms	1337 m 1275 ms 1275 ms 1189 ms 1117 w 1079 w	1346 w 1271 s 1237 s 1181 w 1102 m 1079 m	v(C-C) + v(C-N) CH, in-plane bend
997 vw 889 s 775 ms 744 ms	1021 w 983 ms 943 w 885 ms 846 w 783 s 756 ms	1022 w 993 vw 931 vw 890 s 780 s 748 w	994 vw 939 vw 891 s 824 vw 774 s 751 vw 691 m 615 w	1025 w 997 m 939 m 894 m 818 m 781 s 757 w	δ _{rock} ; NH CH-deformation v(C-Cl); DDQ
691 w 621 ms 525 w	676 w 598 mw 564 vw 501 vw	691 mw 620 m 525 vw	579 w 502 m	667 w 608 w	skeletal vibration CH bend
430 ms	423 w	422 m	426 m	494 w 418 m	CH out of plane bend Skeletal vibration CNC def.

(a): s = strong, w = weak, m = medium, sh = shoulder, v = very, br = broad.

(b): v, stretching; δ, bending.

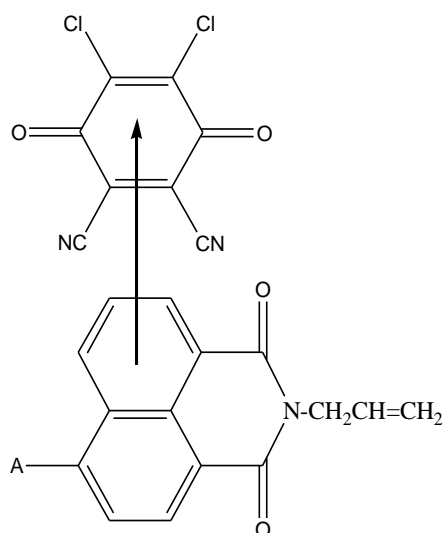
[(4PAN)(TCNQ)₂] CT complexes, the powerful electron withdrawal by CN groups in conjugation with the aromatic ring, cause a high delocalization and a great increase in the TCNQ affinity to the electron. Due to this fact, the 4MAN and 4PAN donors, which have rich donating sites (two aromatic rings, morpholine, and piperidino cyclic), are easy to be sandwiched between two TCNQ moieties to display the 1:2 stoichiometry of such CT complexes (Scheme 2). Tables 10 and 11 show the characteristic bands of CLA and

PA CT complexes. The comparison between the infrared spectral bands of the free donors and the acceptors (CLA and PA) and the corresponding bands that appear in the IR spectra of the CT complexes show the following:

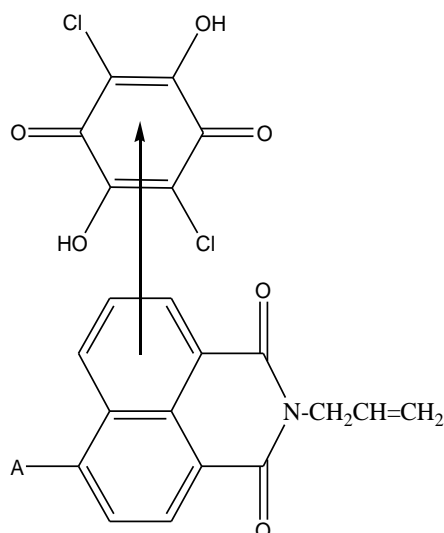
- The vibration frequency of the O-H group for the CLA and PA at 3235 cm⁻¹ and (3416 and 3103 cm⁻¹) is slightly affected in the IR spectra of the CT complexes, which means that the hydroxyl group is not involved in the CT complexation.
- The C=O group stretching vibrations, appearing at (1664 and 1630 cm⁻¹) in the case of the CLA CT complexes, are slightly shifted to

(1678 and 1637 cm^{-1}), (1632 and 1610 cm^{-1}), (1656 and 1631 cm^{-1}), (1662 and 1631 cm^{-1}) and (1630 cm^{-1}) for the 4MAN, 4PAN, 4MAAN and 4POAN, respectively. On the other hand, in the case of the picric acid, the stretching vibrations of the CT complexes of the C=O group, appearing at (1861 and 1632 cm^{-1}) are slightly shifted to (1682 and 1637 cm^{-1}), (1632 and 1610 cm^{-1}), (1699 and 1654 cm^{-1}), (1688 and 1637 cm^{-1}) and (1695, 1657 and 1632 cm^{-1}) for 4MAN, 4PAN, 4MAAN and 4POAN, respectively

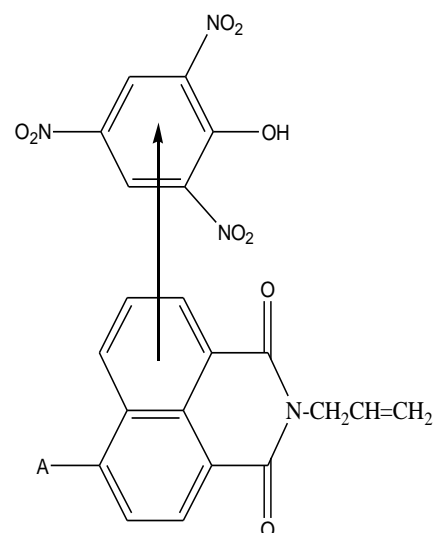
iii) The group of bands, in terms with the C-Cl vibration, which appeared at 752 and 690 cm^{-1} , exhibit a shift to a higher and a lower wavenumber in the corresponding CT complexes:



Scheme 1: The charge transfer interaction between 1,8-naphthalimide derivatives and the π -acceptor, DDQ (where A= 4-morpholino for (4MAN), 4-piperdino for (4PAN), 4-methylamino for (4MAAN), and 4-propyloxy for (4POAN)).



Scheme 2: The [(4MAN)(TCNQ)₂] and [(4PAN)(TCNQ)₂] CT complexes (where A= 4-morpholino for (4MAN) and 4-piperdino for (4PAN)).



Scheme 3: The charge transfer interaction between 1,8-naphthalimide and the π -acceptor, CLA and PA (where A= 4-morpholino for (4MAN), 4-piperdino for (4PAN), 4-methylamino for (4MAAN) and 4-propyloxy for (4POAN)).

Mass Spectra

The mass spectrum of [(4MAAN)]₂ complex proves the complexation between 4MAAN and iodine. This becomes obvious the presence of the main fragment peaks of the donor (4MAAN), and the iodine at $m/z(\%) = 266(37\%)$ and $251(100\%)$, respectively. On the other hand, the TLC diagram, accompanying the mass spectrum, gives one sharp peak. This gives an idea about the purity of the resulted complex.

The mass spectra of the 4BAAN/TCNQ, 4MAN/TCNQ, 4PAN/TCNQ, 4MAAN/TCNQ, 4POAN/CLA, 4MAN/CLA, and 4MAAN/PA CT complexes displayed molecular ion peaks, M^+ , at

(772 and 693 cm^{-1}), (732 and 704 cm^{-1}), (754 and 690 cm^{-1}), (755 and 688 cm^{-1}) and (756 and 695 cm^{-1}) for 4MAN, 4PAN, 4MAAN and 4POAN, respectively.

iv) The characteristic bands of the free donor, such as the stretching vibrations of the C=C, $\delta(\text{CH})$; aromatic ring, $\nu(\text{C-C})$, $\nu(\text{C-N})$, and the CH-deformation, are largely affected, demonstrated by their intensities. The CT complexation of N-allyl derivatives of 1,8-naphthalimide and the chloranilic acid (CLA) and picric acid (PA) occurs through π - π^* transition (from the aromatic ring of the donor to the aromatic ring of the acceptors), Scheme 3.

$m/z(\%)$: (308(44%) and 204(24%)) for 4BAAN and TCNQ, at (322(9%) and 204(100%)) for 4MAN and TCNQ, at (320(46%) and 204(100%)) for 4PAN and TCNQ, at (266(46%) and 204(7%)) for 4MAAN and TCNQ, at (295(37%) and 209(9%)) for 4POAN and CLA, at (322(84%) and 209(14%)) for 4MAN and CLA, and at (266(44%) and 227(2%)) for 4MAAN and PA, respectively. The intensity of these peaks gives an idea about the stability of these fragments. The presence of the molecular ion peaks of both, donor and acceptor, strongly supports the association of the charge transfer complexes of the donor and the acceptor.

Table 9. Infrared frequencies^(a) (cm^{-1}) and tentative assignments for (A): [(4BAAN)(TCNQ)]; (B): [(4MAN)(TCNQ)₂]; (C): [(4PAN)(TCNQ)₂]; (D): [(4MAAN)(TCNQ)]; and (E): [(4POAN)(TCNQ)] CT complexes.

A	B	C	D	E	Assignments ^(b)
3366 s, br 3137 w	3425 ms,br 3137 w	3425 ms, br 3136 w	3390 vs 3136 vw	3567 vw 3424 w,br 3136 vw	v(O-H); and H ₂ O of KBr v(N-H)
3050 ms	3050 ms	3050 ms	3050 ms	3050 ms	v _{as} (C-H); CH ₂ +CH ₃ v(C-H); aromatic
2957 ms 2930 ms 2866 w	2952 m 2918 vw 2847 m	2933 ms 2850 m 2810 w	2932 w 2851 vw	2964 ms 2933 w	v _s (C-H) + v _{as} (C-H)
2220 s	2221 ms	2220 s	2221 ms	2219 ms	v(C≡N); TCNQ
1683 s 1641 s	1690 s 1655 vs	1697 s 1652 vs	1680 s 1635 s	1696 s 1659 vs	v(C=O); donors
1579 vs 1542 vs	1588 s 1541 s 1512 vw	1589 ms 1541 ms 1513 vw	1576 vs 1545 vs	1589 s 1541 m 1514 mw	v(C=C); aromatic
1440 w 1421 vw 1376 s	1446 m 1379 s	1448 vw 1420 w 1381 ms	1446 m 1418 m 1380 vs	1461 ms 1380 s	δ(CH); CH _{def.} δ(CH); aromatic
1374 s 1335 s 1294 w 1246 s 1187 vw 1129 m 1100 m	1352 s 1238 s 1179 m 1152 vw 1118 s 1078 m 1021 w	1347 ms 1234 s 1177 m 1130 m 1080 m	1354 s 1298 ms 1245 ms 1154 ms 1122 vw 1089 vw 1060 vw	1328 vw 1269 s 1234 s 1183 w 1134 w 1100 ms 1077 w	v(C-C) + v(C-N) CH, in-plane bend
993 vw 934 vw 860 s 817 vw 770 ms	983 m 958 vw 917 vw 883 vw 860 s 784 ms 757 m	1020 vw 974 mw 926 vw 860 s 808 vw 780ms	1022 vw 974 vw 949 vw 861 s 814 w 771 s 655 w 652 w	1026 w 995 ms 928 ms 860 ms 833 vw 781 s 756 w	δ _{rock} ; NH CH-deformation
695 vw 662 vw	673 m 624 w 591 w 562 w	692 vw 622 mw 566 vw	581 m 521 w	668 w 625 w 551 w	skeletal vibration CH bend
474 s	498 w 474 ms	474 ms 417 m	473 ms 420 m	472 ms 410 m	CH out of plane bend Skeletal vibration CNC def.

(a): s = strong, w = weak, m = medium, sh = shoulder, v = very, br = broad.

(b): v, stretching; δ, bending.

¹HNMR Spectra

¹HNMR spectra of the 4POAN/DDQ, 4POAN/TCNQ, 4BAAN/CLA, 4PAN/CLA, 4MAAN/CLA, and 4POAN/CLA CT-complexes in DMSO were measured. It is obvious that the results from the elemental analysis, the infrared spectra, and the photometric titrations agree well with each other in the same point of ¹HNMR

spectra to interpret the mode of interaction between the donor and the acceptor. The chemical shifts (δ ppm) of the proton NMR spectra within the range of 6.5 to 8.5 peaks, assigned to the proton of the aromatic rings, were intensively affected at low intensities due to the π-π* transition.

Table 10. Infrared frequencies^(a) (cm⁻¹) and tentative assignments for (A): [(4BAAN)(CLA)]; (B): [(4MAN)(CLA)]; (C): [(4PAN)(CLA)]; (D): [(4MAAN)(CLA)]; and (E): [(4POAN)(CLA)] CT-complexes.

A	B	C	D	E	Assignments ^(b)
3508 w br 3372 s 3236 ms	3423 w br 3298 s	3510 m 3400 vw,br 3236 s	3513 ms 3390 s 3236 ms	3507 vw 3235 s	$\nu(\text{O-H})$; CLA and H ₂ O of KBr $\square(\text{N-H})$
--	3104 ms	3125 vw	3109 vw	3115 vw, sh	$\nu_{\text{as}}(\text{C-H})$; CH ₂ +CH ₃ $\nu(\text{C-H})$; aromatic
2957 ms 2867 w	2957 ms 2867 w	2935 m 2850 w 2815 vw	2935 vw	2966 ms 2880 w	$\nu_{\text{s}}(\text{C-H}) + \square \square_{\text{as}}(\text{C-H})$
1678 s 1637 vs	1632 s 1610 ms	1697 m 1656 vs 1631 vs	1662 w 1631 vs	1630 vs	$\nu(\text{C=O})$; CLA $\square \square \square$ donors
1580 vs 1549 s	1532 s	1592 vw 1541 w	1577 ms 1547 ms	1591 s 1543 vw 1517 m	$\nu(\text{C=C})$; aromatic
1462 w 1375 s	1430 ms	1458 w 1420 vw 1371 s	1446 w 1379 vs	1461 m 1422 vw 1380 s	$\delta(\text{CH})$; CH _{def.} $\delta(\text{CH})$; aromatic
1338 ms 1290 w 1247 s 1186 w 1141 m 1101 m	1342 vs 1271 ms 1153 ms 1087 ms	1269 vs 1178 vw 1135 vw 1081 vw	1288 vs 1156 m 1090 vw	1272 vs 1242 vs 1170 ms 1097 ms	$\nu(\text{C-C}) + \square(\text{C-N})$ CH, in-plane bend
980 s 939 w 846 ms 772 ms 693 ms	919 ms 784 m 732 ms 704 ms	1019 vw 983 s 930 vw 848 s 780 ms 754 ms 690 ms	987 s 852 s 772 ms 755 m 688 ms	1027 w 978 s 927 vw 841 ms 785 s 756 ms 695 m	δ_{rock} ; NH CH-deformation \square $\nu(\text{C-Cl})$; CLA
572 ms 542 vw	541 w	571 s	574 ms	669 vw 569 ms	skeletal vibration CH bend
417 w	-----	420 w	422 w	462 w 410 m	CH out of plane bend Skeletal vibration CNC def.

(a): s = strong, w = weak, m = medium, sh = shoulder, v = very, br = broad.

(b): ν , stretching; δ , bending.

Thermal Investigation

The thermal stability domains, the melting points, the decomposition phenomena and their assignments for the N-allyl derivatives of the 1.8-naphthalimide such as 4-Butylamino-N-allyl-1.8-naphthalimide (4BAAN), 4-Morpholino-N-allyl-1.8-naphthalimide (4MAN), 4-Piperdino-N-allyl-1.8-naphthalimide (4PAN), 4-Methylamino-N-allyl-1.8-naphthalimide (4MAAN), and 4-Propyloxy-N-allyl-1.8-naphthalimide (4POAN) CT-complexes are summarized in Table 12. The simultaneous TG/DTG curves for the 4BAAN/DDQ, 4MAN/DDQ, 4PAN/DDQ, 4MAAN/DDQ, 4POAN/TCNQ, and 4MAN/PA

(1:1) charge-transfer complexes at heating rate of 10 °C/min in static nitrogen atmosphere are given in Figure 7 (A-F).

The overall mass loss from the TG curves is 49.22% for the 4BAAN/DDQ, 63.77% for the 4MAN/DDQ, 58.08% for the 4PAN/DDQ, 41.38% for the 4MAAN/DDQ, 45.59% for the 4POAN/TCNQ, and 95.47% for the 4MAN/PA complexes, respectively. The complexes have from one to four maximal peak mass losses. The analysis of thermal curves for the CT complexes clearly indicates that the first maximum peaks are at 268, 274, 248, 150, 226, and 223°C, respectively.

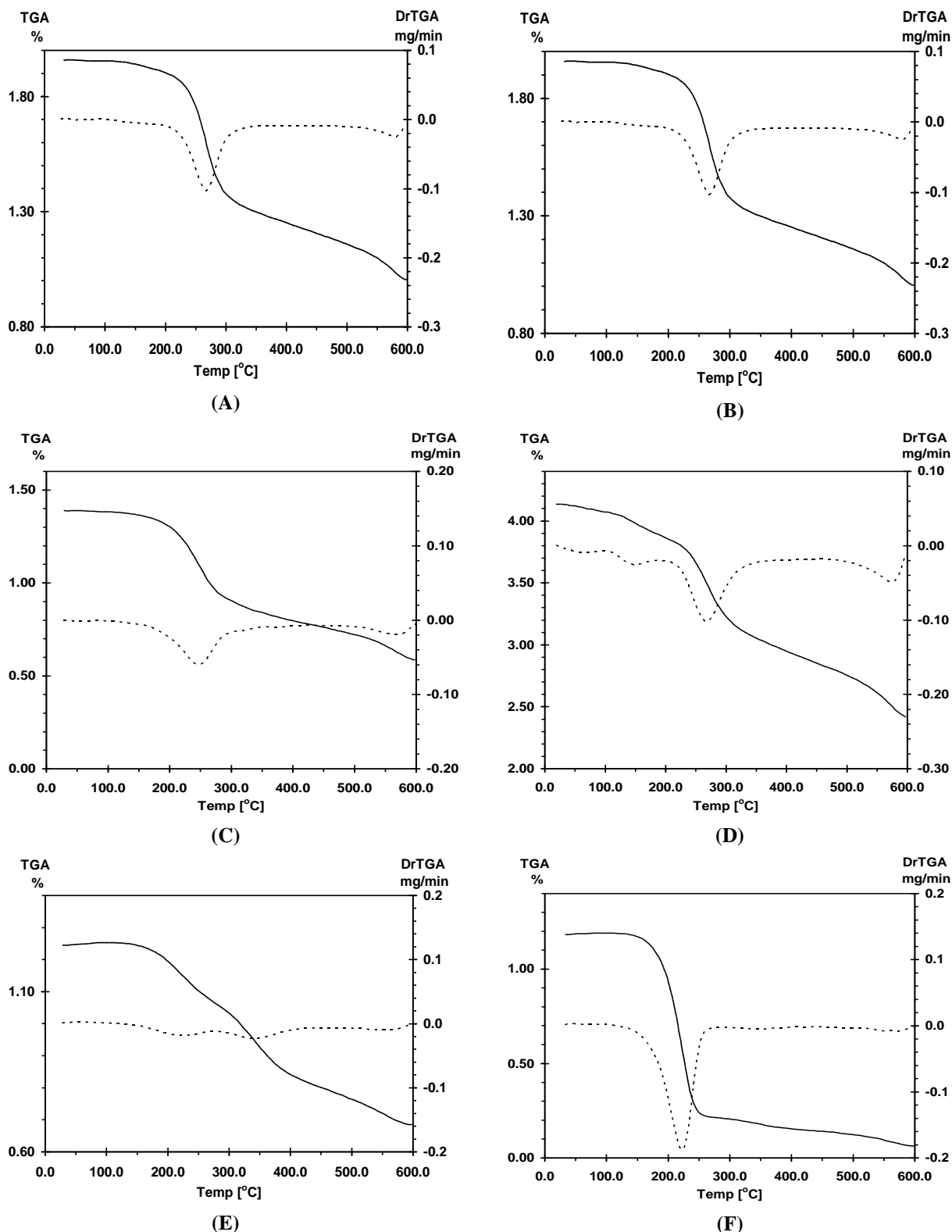


Fig. 7. TGA/DTG curves for (A): 4BAAN/DDQ; (B): 4MAN/DDQ; (C): 4PAN/DDQ; (D): 4MAAN/DDQ; (E): 4POAN/TCNQ; and (F): 4MAN/PA CT complexes.

4BAAN/DDQ CT Complex

The [(4BAAN)(DDQ)] melts at 209 °C with a simultaneous decomposition occurring. The main degradation peak is observed at 268 °C in the thermogravimetric analysis (TG) profile. Figure 7A shows the TG profile of the [(4BAAN)(DDQ)]

CT complex. It appears from the TG curve that the sample decomposes in two sharp stages in a wide temperature range of 130-600 °C. The decomposition occurs with a mass loss of 49.22%, and its calculated value is 50.65%.

Table 11. Infrared frequencies^(a) (cm⁻¹) and tentative assignments for (A): [(4BAAN)(PA)]; (B): [(4MAN)(PA)]; (C): [(4PAN)(PA)]; (D): [(4MAAN)(PA)]; and (E): [(4POAN)(PA)] CT complexes.

A	B	C	D	E	Assignments ^(b)
3365 s	3423 w,br 3297 w	3423 vw,br 3297 vw	3437 vs	3424 w,br 3299 vw	v (O-H); PA and H ₂ O of KBr v (N-H)
3102 ms	3104 ms	3102 ms	3089 ms	3102 ms	v _{as} (C-H); CH ₂ +CH ₃ v(C-H); aromatic
2956 ms 2930 m s 2868 w		2934 m 2850 vw 2813 vw	2923 vw	2967 m 2938 w 2879 w	v _s (C-H) + □ v _{as} (C-H) □
1682 s 1637 vs	1632 s 1610 ms	1699 s 1654 s	1688 s 1637 vs	1695 s 1657 vs 1632 m	v (C=O); donors
1610 mw	1532 s	1608 ms 1541 s	1576 vs 1547 vs	1596 s 1543 s	v(C=C); aromatic v _{as} (NO ₂); PA
1580 s 1545 s 1424 ms	1430 ms	1427 ms	1423 ms 1382 s	1464 w 1425 ms 1381 w	δ(CH); CH _{def.} δ(CH); aromatic
1368 w 1340 vs 1247 s 1147 ms 1087 ms	1342 vs 1315 vw 1270 ms 1152 ms 1087 ms	1342 vs 1271 m 1235 s 1154 ms 1084 ms	1341 s 1304 ms 1242 s 1153 s 1086 ms 1060 vw	1343 s 1270 s 1237 s 1180 w 1153 m 1084 ms	v (C-C) + □ (C-N) CH, in-plane bend v _s (NO ₂); PA
991 w 919 ms 821 w 771 ms 732 ms 704 ms	919 ms 784 m 732 ms 704 ms	1019 vw 975 w 918 s 851 w 781 s 731 ms	977 m 937 w 914 ms 834 w 779 ms 729 m 702 m 658 w	1025 m 994 m 919 ms 834 ms 783 s 757 w 732 m	δ _{rock} ; NH CH-deformation □
580 m 522m	541 w	705 ms 541 vw	589 w 543 m	668 w 581 w 544 w	skeletal vibration CH bend
418 w	424 vw	476 vw 417 m	423 m	462 w 410m	CH out of plane bend Skeletal vibration CNC def. δ(ONO); PA

(a): s = strong, w = weak, m = medium, sh = shoulder, v = very, br = broad.

(b): v, stretching; δ, bending.

4MAN/DDQ CT Complex

The thermal analysis curves for the 4MAN/DDQ CT complex show that decomposition takes place in a single stage in a temperature range between 150 and 600 °C at maximum differential thermogravimetric analysis (DTG_{max}) of 274 °C (Figure 7 B). The single endothermic decomposition stage corresponds to the decomposition of both, the donor and the acceptor (DDQ). The TG curve of the [(4MAN)(DDQ)] complex shows a weight loss

(Found 63.77, Calcd. 65.03%) corresponding to the loss of organic moiety, C₁₁H₁₈N₄O₅Cl₂). The final product, formed at 600 °C, consists of limited 16C with insufficient oxygen atoms.

4PAN/DDQ CT Complex

The thermal degradation of the [(4PAN)(DDQ)] CT-complex proceeds in two main stages (Figure 7C). These two stages relate to the decomposition of the 4-Piperdino-N-allyl-1.8naphthalimide (4PAN) and the DDQ as an acceptor; (Found 58.08%; Calcd. 58.32%), in

Table 12: Thermal data of: (A): 4BAAN/DDQ; (B): 4MAN/DDQ; (C): 4PAN/DDQ; (D): 4MAAN/DDQ; (E): 4POAN/TCNQ; and (F): 4MAN/PA CT complexes.

Complexes	Steps	Temp/range (°C)	DTG _{max}	TG		Assignments
				Total weight loss (%)		
				Found	Calc.	
A	1 st	130-475	268	49.22	50.65	C ₅ H ₂₀ N ₄ O ₄ Cl ₂ 22C Residue
	2 nd	475-600	581			
B	1 st	150-600	274	63.77	65.03	C ₁₁ H ₁₈ N ₄ O ₅ Cl ₂ 16C Residue
C	1 st	70-325	248	58.08	58.32	C ₉ H ₂₀ N ₄ O ₄ Cl ₂ 19C Residue
	2 nd	325-600	570			
D	1 st	25-80	61	41.38	41.58	H ₁₄ N ₄ O ₄ Cl ₂ 24C Residue
	2 nd	80-200	150			
	3 rd	200-350	269			
	4 th	350-600	576			
E	1 st	150-250	226	45.59	47.09	C ₈ H ₂₁ N ₅ O ₃ 22C Residue
	2 nd	250-400	343			
	3 rd	400-600	560			
F	1 st	130-280	223	95.47	95.64	C ₂₃ H ₂₁ N ₅ O ₁₃ 2C Residue
	2 nd	280-400	352			
	3 rd	400-600	561			

temperature ranges of 70-600 °C by giving an endothermic effect (DTG_{max}: 248 and 570 °C).

4MAAN/DDQ CT Complex

The TG diagrams of the [(4MAAN)(DDQ)] CT complex reveal mass loss in the temperature range of 25-600°C, corresponding to the formation of residual carbon atoms due to a limited supply of oxygen. The four endothermic peaks are observed in the DTG analysis (Figure 7D). The maxima of these peaks are found to be (DTG_{max}: 61, 150, 269, and 576°C). The first peak is referring to the melting point of the CT complex. This step occurred without mass loss and it can be assigned any organic moiety. The mass losses at 150, 269, and 579°C DTG_{max}, respectively, are endothermic decompositions and correspond to the loss of the H₁₄N₄O₄Cl₂ organic rest. The overall weight loss (Found 41.38%, calcd. 41.58%) agrees well with the proposed structure.

4POAN/TCNQ CT Complex

The TG of the [(4POAN)(TCNQ)] CT complex: three steps are shown in the pyrolysis curve at 226, 343 and 560 °C. The first step corresponds to the eliminated C₃H₆O molecule (Calcd.: 11.62%, Found: 12.26%). The remaining two, the TCNQ and the 1.8naphthalimide molecules, decompose in the second and the third steps with the formation of 22C as the final residue.

4MAN/PA CT Complexes

The 4MAN/PA CT complex consists of three decomposition steps at 223, 352, and 561 °C. The

first step, which is in the 130-280°C temperature range, corresponds to the decomposition of both, the donor (4MAN) and the acceptor (PA) (C₂₃H₂₁N₅O₁₃, organic moiety), in the presence of oxygen atoms, gave 83.16% weight loss. The second and the third steps (DTG_{max}: 352 and 561°C) seems to be consistent with the evolution of the CO (Calcd.: 5.08%, Found: 4.61%), and the CO₂ (Calcd.: 7.98%, Found: 7.70%) molecules, respectively.

Kinetic Studies

The kinetic data of the first and the second decomposition steps of the 4BAAN/DDQ, 4MAN/DDQ, 4PAN/DDQ, 4MAAN/DDQ, 4POAN/TCNQ, and 4MAN/PA CT complexes was presented using the Coats-Readfern and Horowitz-Metzger methods [31,32]. The kinetic parameters, E, A, ΔS, ΔH, ΔG, and r, is calculated and the data are listed in Table 13.

The activation energies of the formation of 1.8-naphthalimide derivatives with DDQ in the case of the first degradation step are in the following order:



The comparison between 4POAN/TCNQ and 4MAN/PA found that the activation energy in the TCNQ complex is higher five times than in the PA charge-transfer complex due to the strong powerful TCNQ acceptor, which contains four cyano groups.



Table 13: Kinetic parameters, obtained through the Coats–Redfern (CR) and Horowitz–Metzger (HM) methods for (A): 4BAAN/DDQ; (B): 4MAN/DDQ; (C): 4PAN/DDQ; (D): 4MAAN/DDQ; (E): 4POAN/TCNQ; and (F): 4MAN/PA CT complexes.

complex	stage	method	parameter					r
			E (Jol ⁻¹)	A (s ⁻¹)	ΔS (J mol ⁻¹ K ⁻¹)	ΔH (J mol ⁻¹)	ΔG (J mol ⁻¹)	
A	1 st	CR	1.11×10 ⁵	4.06 ×10 ⁸	-8.49 ×10 ¹	1.06×10 ⁵	1.52 ×10 ⁵	0.9989
		HM	1.19×10 ⁵	5.57 ×10 ⁹	-6.32 ×10 ¹	1.14×10 ⁵	1.48 ×10 ⁵	0.9978
		average	1.15×10 ⁵	2.31 ×10 ⁸	-7.41 ×10 ¹	1.10×10 ⁵	1.5 ×10 ⁵	
	2 nd	CR	3.49×10 ⁵	3.91 ×10 ¹⁹	1.21 ×10 ²	3.42×10 ⁵	2.38 ×10 ⁵	0.9961
		HM	3.69×10 ⁵	5.54 ×10 ²⁰	1.43 ×10 ²	3.61×10 ⁵	2.39 ×10 ⁵	0.9988
		average	3.59×10 ⁵	2.232×10 ¹⁹	1.32 ×10 ²	3.51×10 ⁵	2.39 ×10 ⁵	
B	1 st	CR	7.7 ×10 ⁴	1.49 ×10 ⁵	-1.51 ×10 ²	7.24×10 ⁴	1.55 ×10 ⁵	0.9977
		HM	8.59×10 ⁴	1.32 ×10 ⁵	-1.33 ×10 ²	8.13×10 ⁴	1.54 ×10 ⁵	0.9984
		average	8.15×10 ⁴	1.41 ×10 ⁵	-1.42 ×10 ²	7.68×10 ⁴	1.55 ×10 ⁵	
C	1 st	CR	6.4 ×10 ⁴	1.30 ×10 ⁴	-1.71 ×10 ²	5.97×10 ⁴	1.49 ×10 ⁵	0.9996
		HM	7.18×10 ⁴	1.16 ×10 ⁴	-1.53 ×10 ²	6.74×10 ⁴	1.47 ×10 ⁵	0.9981
		average	6.79×10 ⁴	1.23 ×10 ⁴	-1.62 ×10 ²	6.36×10 ⁴	1.48 ×10 ⁵	
	2 nd	CR	2.33×10 ⁵	3.21 ×10 ¹²	-1.41 ×10 ¹	2.26×10 ⁵	2.38 ×10 ⁵	0.9999
		HM	2.31×10 ⁵	2.12 ×10 ¹²	-1.76 ×10 ¹	2.24×10 ⁵	2.39 ×10 ⁵	0.9996
		average	2.32×10 ⁵	2.67 ×10 ¹²	-1.58 ×10 ¹	2.25×10 ⁵	2.39 ×10 ⁵	
D	1 st	CR	4.73×10 ⁴	1.4 ×10 ⁵	-1.47 ×10 ²	4.46×10 ⁴	9.36 ×10 ⁴	0.9936
		HM	5.17×10 ⁴	1.82 ×10 ⁶	-1.26 ×10 ²	4.9 ×10 ⁴	9.1 ×10 ⁴	0.9973
		average	4.95×10 ⁴	0.791 ×10 ⁵	-1.37 ×10 ²	4.68×10 ⁴	9.23 ×10 ⁴	
	2 nd	CR	5.04×10 ⁴	4.98 ×10 ³	-1.77 ×10 ²	4.68×10 ⁴	1.22 ×10 ⁵	0.9998
		HM	5.84×10 ⁴	1.56 ×10 ⁵	-1.48 ×10 ²	5.48×10 ⁴	1.18 ×10 ⁵	0.9981
		average	5.44×10 ⁴	2.49 ×10 ³	-1.63 ×10 ²	5.08×10 ⁴	1.2 ×10 ⁵	
E	1 st	CR	5.71×10 ⁴	5.01 ×10 ³	-1.78 ×10 ²	5.3 ×10 ⁴	1.42 ×10 ⁵	0.9893
		HM	6.23×10 ⁴	2.6 ×10 ⁴	-1.65 ×10 ²	5.82×10 ⁴	1.4 ×10 ⁵	0.9997
		average	5.97×10 ⁴	2.64 ×10 ³	-1.72 ×10 ²	5.56×10 ⁴	1.41 ×10 ⁵	
	2 nd	CR	7.9 ×10 ⁴	2.16 ×10 ⁴	-1.68 ×10 ²	7.4 ×10 ⁴	1.77 ×10 ⁵	0.9854
		HM	8.75×10 ⁴	1.98 ×10 ⁵	-1.5 ×10 ²	8.24×10 ⁴	1.74 ×10 ⁵	0.9992
		average	8.33×10 ⁴	2.07 ×10 ⁴	-1.59 ×10 ²	4.82×10 ⁴	1.76 ×10 ⁵	
F	1 st	CR	1.01×10 ⁵	6.18×10 ⁸	-8.09×10 ¹	9.74×10 ⁴	1.38×10 ⁵	0.9988
		HM	1.11×10 ⁵	5.45×10 ⁹	-6.28×10 ¹	1.07×10 ⁵	1.38×10 ⁵	0.9999
		average	1.06×10 ⁵	30.3×10 ⁸	7.19×10 ¹	10.2×10 ⁴	1.38×10 ⁵	
	2 nd	CR	1.16×10 ⁵	3.64×10 ⁷	-1.06×10 ²	1.11×10 ⁵	1.77×10 ⁵	0.9985
		HM	1.29×10 ⁵	6.60×10 ⁸	-8.22×10 ¹	1.24×10 ⁵	1.75×10 ⁵	0.9983
		average	1.23×10 ⁵	34.8×10 ⁷	-9.41×10 ¹	1.18×10 ⁵	1.76×10 ⁵	

REFERENCES

- E. Martin, R. Weigand, A.Pardo, *J. Lumines.*, **68**, 157 (1996).
- V. Gruzinskii, A. Kukhta, G. Shakkah, *J. Appl. Spectr.*, **65**, 444 (1998).
- Z-F. Tao, X. Qian, *Dyes and Pigments*, **43**, 139 (1999).
- K. Dubey, R. Singh, K. Mizra, *Indian J. Chem.*, **34B**, 876 (1995).
- M. M. de Souza, R. Correa, V. Cechinel Filho, I. Grabchev, V. Bojinov, *Pharmazie*, **56**, 75 (2002).
- A. D. Andricopulo, R.A. Yunes, V. Cechinel Filho, R. Correa, A.W. Filho, A.R. Santos, R.J. Nunes, *Acta Farm. Bonaerens.*, **17**, 219 (1998).
- X. Qian, K. Zhu, K. Chen, *Dyes and Pigments*, **11**, 13 (1989).
- E. Wolarz, H. Moryson, D. Bauman, *Displays*, **13**, 171 (1992).
- E. Mykowska, K. Jazwanska, W. Grupa, D. Bauman, *Proc SPIE* **3318**, 378 (1998).
- I. Grabchev, I. Moneva, E. Wolarz, D. Bauman, *Z Naturforsch.*, **51a**, 1185 (1996).
- S. K. Das, G. Krishnamoorthy and S. K. Dofra, *Can. J. Chem.*, **78**, 191 (2000).
- G. Jones, J. A. C. Jimenez, *Tetrahedron Lett.*, **40**, 8551(1999).
- G. Smith, R. C. Bott, A. D. Rae, A. C. Willis, *Aust. J. Chem.*, **53**, 531 (2000).
- G. Smith, D. E. Lynch, R. C. Bott, *Aust. J. Chem.*, **51**, 159 (1998).
- G. Smith, D. E. Lynch, K. A. Byriel, C. H. L. Kennard, *J. Chem. Crystallogr.*, **27**, 307 (1997).
- M.S. Refat, S. A. Sadeek, H.M. Khater, *Spectrochim. Acta Part A*, **64(3)**, 778 (2006).
- M.S. Refat, A.M. El-Didamony, *Spectrochim. Acta Part A*, **65(3-4)**, 732 (2006).

18. M.S. Refat, I. Grabchev, J.-M. Chovelon, G. Ivanova, *Spectrochim. Acta Part A*, **64(2)**, 435 (2006).
19. M.S. Refat, H. Al-Didamony Ahmed, L.A. El-Zayat, *Can. J. Anal. Sci. Spec.*, **51(3)**, 147 (2006).
20. M.S. Refat, H.M.A. Killa, I. Grabchev, M.Y. El-Sayed, *Spectrochim. Acta Part A*, **68(1)**, 123 (2007).
21. M.S. Refat, L.A. El-Zayat, Okan Zafer Yeşilel, *Polyhedron*, **27(2)**, 475 (2008).
22. M.S. Refat, H.A. Ahmed, I. Grabchev, L.A. El-Zayat, *Spectrochim. Acta*, **70(4)**, 907 (2008).
23. M.S. Refat, L.A. El-Zayat, Okan Zafer Yeşilel, *Spectrochimica Acta Part A*, **75**, 745 (2010).
24. M.S. Refat, Hamdy Al. Didamony, Khlood M. Abou El-Nour, I. Grabchev, Lamia El-Zayat, *Arab. J. Chem.*, in press.
25. 25 (a) I. Grabchev, Ch. Petkov, and V. Bojinov, *Dyes and Pigments*, **48**, 239 (2001); (b) T Konstantinova, P. Meallier, I. Grabchev, *Dyes and Pigments*, **22**, 191 (1993); (c) I. Grabchev, T Konstantinova, P. Meallier, M. Popova, *Dyes and Pigments*, **28**, 41 (1995).
26. F. M. Abou Attia, *Farmaco*, **55**, 659 (2000).
27. D. A. Skoog, *Principle of Instrumental Analysis*, 3rd edn., Saunders College Publishing, New York, USA, 1985, Ch. 7.
28. R. Abu-Eittah, F. Al-Sugeir, *Can. J. Chem.*, **54**, 3705 (1976).
29. G. G. Aloisi, S. Pignataro, *J. Chem. Soc., Faraday Trans.*, **69**, 534 (1973).
30. A. El-Kourashy, *Spectrochim. Acta.*, **37A**, 399 (1981).
31. A.W. Coats, J.P. Redfern, *Nature*, **201**, 68 (1964).
32. H.W. Horowitz, G. Metzger, *Anal. Chem.*, **35**, 1464 (1963).

СИНТЕЗИ И ХАРАКТЕРИЗИРАНЕ НА КОМПЛЕКСИ С ПРЕНОС НА ЗАРЯДА НА 1,8-НАФТАЛИМИДИ С РАЗЛИЧНИ АКЦЕПТОРИ

М.С. Рефат^{a,b}, Х.А. Дидамони^c, Х.М. Абу Ел-Нур^d,
И. Грабчев^e, Л. Ел-Заят^a

^aДепартамент по химия, Факултет за наука, Университет в Порт Сауд, Порт Сауд 42111, Египет

^bДепартамент по химия Факултет за наука, Университет в Тауф, 888 Тауф, Кралство Саудитска Арабия

^cДепартамент по химия Факултет за наука, Университет в Загазиг, Загазиг, Египет

^dДепартамент по химия Факултет за наука, Университет "Суецки канал", Исмаилия, Египет

^eФакултет по медицина, Софийски университет "Св. Климент Охридски" ул. Козяк 1, 1407 София, България

Постъпила на 24 април, 2010 г.; преработена на 7 юли, 2010 г.

(Резюме)

При взаимодействието на донори (4-заместени-N-алил-1,8-нафталиמידни производни), и σ -акцептори (йод или π -акцептори) са получени пет нови комплекса с пренос на заряда (КПЗ) и детайлно са изследвани функционалните им характеристиките. Показано е, че се образуват комплекси с пренос на заряда с общи формули: [(донор)(акцептор)_n], при n= 1 в случая на комплексите [(донори)I₂], [(донори)(DDQ)], [(донори)(CLA)], [(донори)(PA)] и [(донори)(TCNQ)] докато при n = 2 комплексите са [(4MAN)(TCNQ)₂], и [(4PAN)(TCNQ)₂].

Preparation of aluminium tungstate $\text{Al}_2(\text{WO}_4)_3$ using sol-gel modified Pechini method

I. I. Koseva*, V. S. Nikolov

Institute of General and Inorganic Chemistry, Bulgarian Academy of Sciences, 1113 Sofia, Bulgaria

Received February 16, 2010; revised May 13, 2010

Aluminium tungstate $\text{Al}_2(\text{WO}_4)_3$ pure phase with nanosized particles was prepared using modified Pechini method. Citric acid was used as chelating agent and ethylene glycol was used for sterification. Dried resin was treated at different temperatures and different heating time. The pure phase $\text{Al}_2(\text{WO}_4)_3$ appears after treatment at 830 °C for 36 h. Increasing the heating temperature to higher than 830 °C leads to obtaining of the pure $\text{Al}_2(\text{WO}_4)_3$ phase for a shorter time. The TEM bright field micrographics of the samples show that the size varies between 50 and 200 nm, and strongly depends on the time and the treating temperature. Heating of the polymeric resin in oxygen flow leads to obtaining of the pure $\text{Al}_2(\text{WO}_4)_3$ phase at significant lower temperature and significant shorter treating time.

Keywords: ceramics; tungstates; sol-gel processes; nanostructured materials; transmission electron microscopy; X-ray diffraction.

INTRODUCTION

In the recent years several compounds of the $\text{M}_2\text{W}_3\text{O}_{12}$ family, where M is a trivalent cation (Al, Sc, Zr, Y, Cr, etc.), have been investigated due to their interesting physical and chemical properties. One of them is the temperature-induced ferroelastic phase transition from orthorhombic (D14 2h, Pnca) to monoclinic (C5 2h, P21/a) structure [1, 2, 3]. The orthorhombic phase shows thermal expansion, strongly depending on the chemical substitution in the basic phase [2, 4, 5, 6]. Some reports demonstrated production of ceramics in this way with negative, positive or zero thermal expansion coefficients [5, 6]. Another feature of these materials is the unusual anisotropic high trivalent ion conduction [7, 8, 9]. A pressure-induced amorphization phenomena (PIA) were reported recently also [3, 10, 11]. Due to the acentric site symmetry of the Cr^{3+} laser ions, in place for M^{3+} into the $\text{M}_2\text{W}_3\text{O}_{12}$, these compounds exhibit strong absorption and emission cross sections in the 10^{-19}cm^2 range and therefore belong to the class of high-gain Cr materials with potential application as tunable laser active media [12]. All these features make these compounds suitable for a wide variety of applications in fuel cell electrolytes, gas sensors, and lasers.

Aluminium tungstate $\text{Al}_2(\text{WO}_4)_3$ which is a member of this family (being with orthorhombic

symmetry, point group Pnca), shows all above mentioned properties and perspective applications [2, 6, 11, 13, 14, 15, 16].

Most of the $\text{Al}_2(\text{WO}_4)_3$ properties reported in the literature have been measured on polycrystalline samples, prepared using the conventional solid-state reaction. Mainly XRD-control of the phase has been used [7, 8, 10, 15].

Some optical and ion conductivity measurements have been made on single crystal samples, obtained via Czochralski or Bridgman methods [12, 13, 14, 16, 17, 18, 19, 20, 21, 22]. However, the crystal growth process, involving these methods, is strongly limited due to the WO_3 evaporation. Flux growth process is demonstrated also [23]. In this case the process takes a long period of time and the crystal dimensions are small. In addition, high anisotropy of single crystal growth velocity is detected.

In the last years more attention has been paid to the nanosized transparent ceramics [24, 25, 26, 27]. The samples hold the same chemical composition, but they are isotropic in the different crystallographic directions. Nanosized ceramics are the main key for the improvement of the material physical properties. Therefore, the transparent ceramics can be used in place for single crystal elements in the fields of optics and electronics to improve the optical homogeneity, the high threshold of the materials, as well as to obtain elements of specific size and shape.

One of the main requirements for obtaining transparent ceramics is to control the powder grain

* To whom all correspondence should be sent:
E-mail: E-mail: ikosseva@svr.igic.bas.bg

size. Obtaining powders by a conventional solid state synthesis does not allow grain size control. Generally the size of the particles depends on the sintering temperature and the process duration. Synthesis of $KRE(WO_4)_2$ samples, where RE is rare-earth element, with controlled grain size, obtained via sol-gel method (the so called modified Pechini method), has been reported [28]. The particle size here depends on the correlation between the compound components, the chelating agent, and the sterification agent, as well as on the chelating agent nature. [24]. Citric acid has been used as chelating agent for obtaining aluminium molybdates [27]. Citric acid and EDTA have been used as chelating agent for obtaining potassium gadolinium tungstate. [26]. Ethylene glycol has been used for sterification.

Taking into consideration the above papers we report on the preparation of aluminium tungstate for a first time ever, using modified Pechini method.

EXPERIMENTAL PART

Powders of $Al(OH)_3$ (p.a.), and H_2WO_4 (p.a.) were used as starting materials. Citric acid (p.a.) was used as a chelating agent, and ethylene glycol (pure) for sterification.

$Al(OH)_3$ was dissolved at a room temperature in concentrated citric acid solution in metal ions to citric acid molar ratio of 1:2.

H_2WO_4 was dissolved at a room temperature in 25% NH_3 , and than was added to the metal solution under stirring.

Ethylene glycol was added after to citric acid and ethylene glycol in 1:1 molar ratio.

The formation of resin occurs at 80°C, and the resin transforms to gel. Afterwards, the resin was dried at 90 °C for 5 days.

The resultant product was heated at 300 °C for 30 minutes to obtain a brown powder, than the temperature was increased to 600 °C by a 150 °C/h step. The powder becomes of light brown color during the last procedure.

The light brown powder was hold at different temperatures in the range between 620 and 900 °C, and at different heating time to obtain a pure phase. The final sintering product was of white or pale yellow colour, depending on the thermal conditions.

Structural characterization was carried out by powder X-ray diffraction (XRD) using a Bruker D8 Advance powder diffractometer with Cu Ka radiation and SolX detector. XRD spectra were recorded at room temperature. Data were collected in the 2θ range within 10 to 80 deg. with a step of

0.04 deg. and 1s/step counting time. XRD spectra were identified using Diffractplus EVA program. The presence of the $Al_2(WO_4)_3$ phase in the different specimens was estimated by a comparison with JCPDS card N 24-1101 for pure $Al_2(WO_4)_3$.

The particle size and morphology were performed using TEM JEOL 2100 at 200 kV. For this purpose, the specimens were prepared by grinding the samples in agate mortar and dispersing in methanol via ultrasonic treatment for 6 minutes. A droplet of suspension was dispersed on holey carbon films placed over Cu grids.

RESULTS AND DISCUSSIONS

The X-ray diffraction patterns of the samples, treated at different temperatures and constant heating time, are shown on Fig. 1. The lines of the additional phases are marked by stars. As can be seen, pure $Al_2(WO_4)_3$ phase appears after heating at 860°C. The amount of the additional phases decreases with temperature increase.

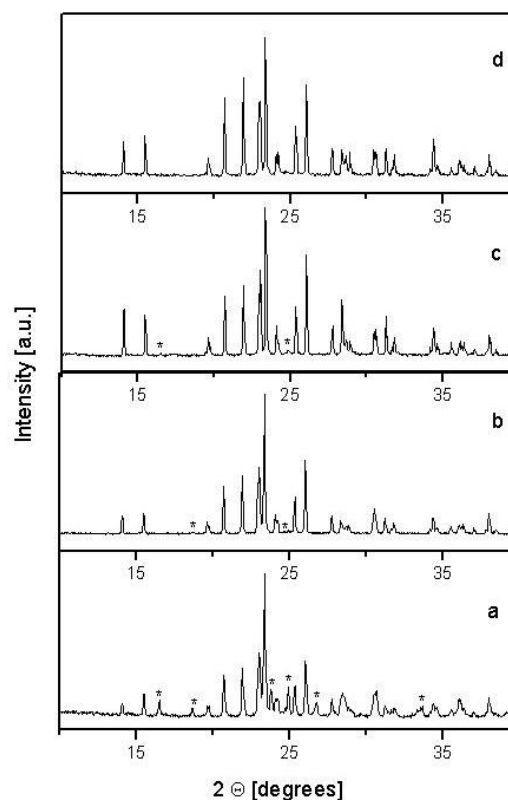


Fig. 1. X-ray diffraction patterns of the samples, treated at different temperatures, and at 12 h constant heating time: a) at 620 °C, b) at 800 °C, c) at 830 °C, and d) at 860 °C.

Taking into account our final aim, i.e. to prepare a transparent ceramic, it was important to find out what the conditions are for obtaining $Al_2(WO_4)_3$ powder with smaller particle size. For this reason,

the second series of experiments was done where the samples were treated at different temperature and different heating time.

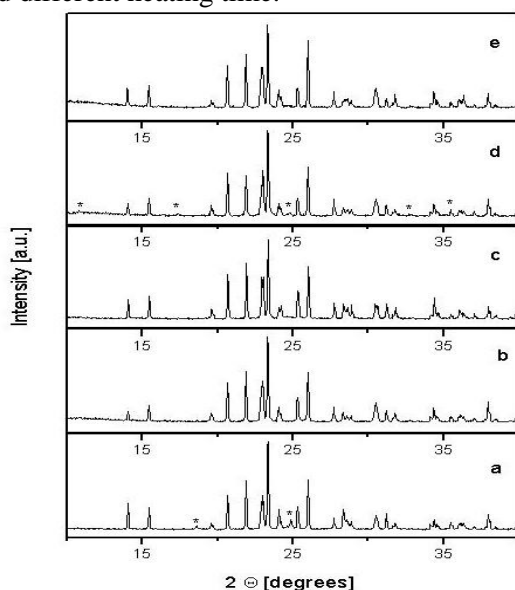


Fig. 2. X-ray diffraction patterns of the samples, treated at different temperatures, and at different heating time: a) at 760 °C for 72 h, b) at 830 °C for 36 h, c) at 860 °C for 12 h, d) at 900 °C for 2 h, and e) at 900 °C for 6 h.

Fig. 2 includes the X-ray sample patterns of this series. Heating the samples for a time period longer than 12 h at below 830 °C does not lead to obtaining of pure $Al_2(WO_4)_3$ phase. Increasing the heating temperature to higher than 830 °C leads to obtaining of pure $Al_2(WO_4)_3$ phase for a shorter time (for 36 h at 830 °C, for 12 h at 860 °C, and for 6 h at 900 °C).

An important result was obtained when the polymeric resin was treated in oxygen flow for 5 h at 620 °C. As can be seen on Fig. 3, pure $Al_2(WO_4)_3$ phase was received in oxygen atmosphere at significant lower temperature and significant shorter treating time.

Thermal treatment conditions of the dried resin for the preparation of $Al_2(WO_4)_3$, and the results of the X-Ray phase analyses are summarized in Table 1. The quantity of the additional phases (marked by stars on the X-Ray diffraction pattern figures) was roughly evaluated as a correlation between the intensity of the highest pick of $Al_2(WO_4)_3$ ($2\theta = 23.27$) and the highest pick of the additional phases ($2\theta = 24.88$). The nature of the additional phases were not determined taking into account the JCPDS data for aluminium and tungstate phases.

The TEM bright field micrographics of the samples, treated at 620°C for 12 hours and at 830 °C for 36 hours, are shown on Fig. 4. The particle

size at the lower temperature is distributed in the narrow region from 50 to 80 nm without clear defined habit, while that at the higher temperature is distributed in a wide region from 50 to 200 nm

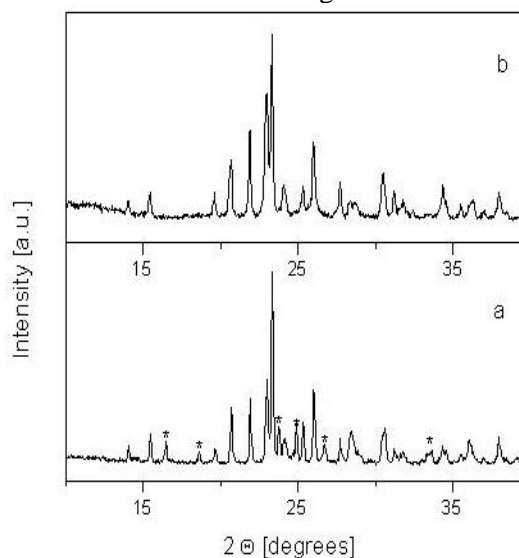


Fig. 3. X-ray diffraction patterns of the samples treated in air and in oxygen flow: a) in air at 620 °C for 12 h, and b) in oxygen flow at 620 °C for 5 h.

with a clear defined habit according to the orthorhombic structure.

Thermal treatment conditions of the dried resin for the preparation of $Al_2(WO_4)_3$, and the results of the X-Ray phase analyses are summarized in Table 1. The quantity of the additional phases (marked by stars on the X-Ray diffraction pattern figures) was roughly evaluated as a correlation between the samples, treated at 620 °C for 12 hours and at 830 °C for 36 hours, are shown on Fig. 4.

The particle size at the lower temperature is distributed in the narrow region from 50 to 80 nm without clear defined habit, while that at the higher temperature is distributed in a wide region from 50 to 200 nm with clear defined habit according to the orthorhombic structure. TEM analysis shows that heating time decrease while temperature increase does not lead to a smaller particle size. Thus, the final and optimal result from the described experiments is pure $Al_2(WO_4)_3$ phase with particle size within 50 to 200 nm when the resin is treated at 830 °C for 36 h.

The TEM bright field micrographics of the oxygen treated specimen show well separated particles with dimensions within 70 and 100 nm. The particle size is a little bigger than that of the air treated specimen (Fig. 5).

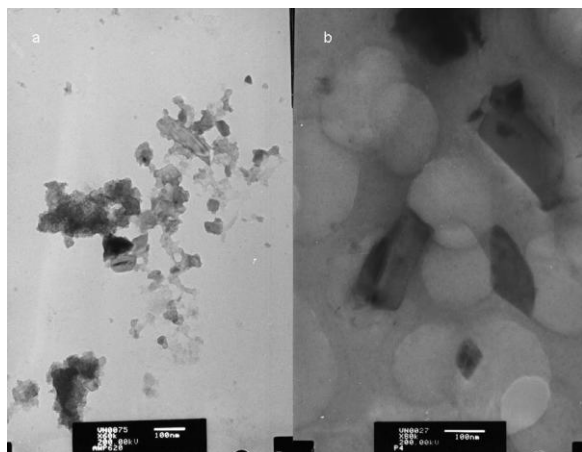


Fig. 4. TEM bright field micrographics of the samples, treated: a) at 620 °C for 12 hours, and b) at 830 °C for 36 hours

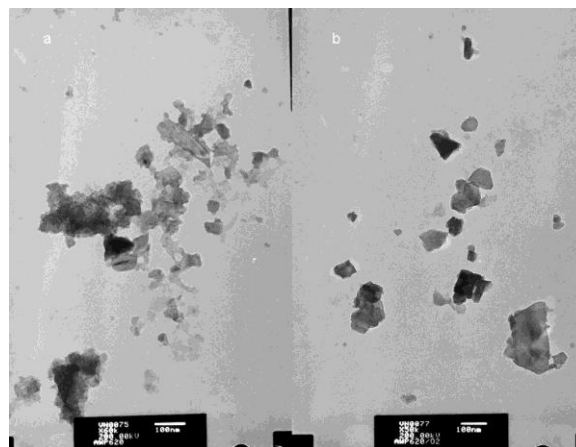


Fig. 5. TEM bright field micrographics of the samples, treated: a) in air at 620 °C for 12 h, and b) in oxygen flow at 620 °C for 5 h

Table 1. Thermal treatment conditions of the dried resin for the preparation of $Al_2(WO_4)_3$ and X-ray phase analyses results.

Sample	Heating temperature [°C]	Heating time [hours]	Atmosphere	X-Ray results
1	620	12	Air	$Al_2(WO_4)_3$ + about 21% additional phases
2	800	12	Air	$Al_2(WO_4)_3$ + about 2% additional phases
3	830	12	Air	$Al_2(WO_4)_3$ + about 2% additional phases
4	860	12	Air	$Al_2(WO_4)_3$ Pure phase
5	760	72	Air	$Al_2(WO_4)_3$ + about 14% additional phases
6	830	36	Air	$Al_2(WO_4)_3$ Pure phase
7	900	2	Air	$Al_2(WO_4)_3$ + about 2% additional phases
8	900	6	Air	$Al_2(WO_4)_3$ Pure phase
9	620	5	Oxygen	$Al_2(WO_4)_3$ Pure phase

CONCLUSIONS

This study shows that the $Al_2(WO_4)_3$ pure phase with nanosized particles could be obtained by modified Pechini method.

The particle size and the morphology strongly depend on the time and treatment temperature. The size varies between 50 nm at 620 °C for 12 h and 200 nm at 830 °C for 36 h.

The treatment of the polymeric resin in oxygen flow leads to pure $Al_2(WO_4)_3$ phase at a significant lower temperature and a significant shorter treatment time but the particle size remains approximately the same.

Obtaining $Al_2(WO_4)_3$ pure phase via modified Pechini method with a particle size less than 50 nm seems to be problematic because of the formation of additional phases. The decomposition of these phases needs high temperature and long treatment time.

Acknowledgements: This work was supported by the National Science Foundation of Bulgaria (Grant DO-02-216 'Nanostructured Transparent Ceramics as a New Tunable Laser Media').

REFERENCES

- 1 J. Hanuza, M. Maczka, K. Hermanowicz, M. Andruszkiewicz, A. Pietraszko, W. Strek, P. Deren, *J. Sol. State Chem.* **105**, 49 (1993).
- 2 J.S.O. Evans, T.A. Mary, A.W. Sleight, *J. Solid State Chem.* **133**, 580 (1997).
- 3 M. Maczka, W. Paraguassu, A.G. Souza Filho, P.T.C. Freire, J. Mendes Filho, F.E.A. Melo, J. Hanuza, *J. Solid State Chem.* **177**, 2002 (2004).
- 4 J.S.O. Evans, T.A. Mary, *Int. J. Inorg. Mater.* **2**, 143 (2000).
- 5 W. Paraguassu, M. Maczka, A.G. Souza Filho, P.T.C. Freire, F.E.A. Melo, J. Mendes Filho, J. Hanuza, *Vibrational Spectroscopy* **44**, 69 (2007).
- 6 J.S.O. Evans, T.A. Mary, A.W. Sleight, *Physica B* **241-243**, 311 (1998).
- 7 T. Kulikova, A. Neiman, A. Kartavtseva, D. Edwards, S. Adams, *Solid State Ionics* **178**, 1714 (2008).
- 8 J. Kohler, N. Imanaka, G. Adachi, *J. Mater. Chem.* **9**, 1357 (1999)
- 9 N. Imanaka, Y. Kobayashi, S. Tamura, G. Adachi, *Solid State Ionics* **136-137**, 319 (2000).
- 10 N. Garga, V. Panchal, A.K. Tyagi, Surinder M. Sharma, *J. Solid State Chem.* **178**, 998 (2005).

- 11 G.D. Mukherjee, S.N. Achary, A.K. Tyagi, S.N. Vaidya, *J. Phys. and Chem. Solids* **64**, 611 (2003).
- 12 K. Petermann, P. Mitzscherlich, *IEEE Journal of Quantum Electronics* **23**, 1122 (1987).
- 13 N. Imanaka, M. Hiraiwa, G. Adachi, H. Dabkowska, A. Dabkowski, *J. Cryst. Growth* **220**, 176 (2000).
- 14 A. Dabkowski, H.A. Dabkowska, J.E. Greedan, G. Adachi, Y. Kobayashi, S. Tamura, M. Hirakawa, N. Imanaka, *J. Cryst. Growth* **197**, 879 (1999).
- 15 Y. Kobayashi, S. Tamura, N. Imanaka, G. Adachi, *International Conference on Solid State Ionics N°11, Honolulu, Hawaii , ETATS-UNIS (16/11/1997)* **113-115**, 545 (1998).
- 16 N. Imanaka, M. Hirakawa, S. Tamura, G. Adachi, H. Dabkowska, A. Dabkowski, *J. Mater. Sci.* **37**, 3483 (2002).
- 17 N. Imanaka, M. Hiraiwa, S. Tamura, G. Adachi, H. Dabkowska, A. Dabkowski, *Materials Letters* **55**, 93 (2002).
- 18 M. Hiraiwa, S. Tamura, N. Imanaka, G. Adachi, H. Dabkowska, A. Dabkowski, *Solid State Ionics* **136-137**, 427 (2000).
- 19 N. Imanaka, M. Hiraiwa, S. Tamura, G. Adachi, H. Dabkowska, A. Dabkowski, *J. Cryst. Growth* **200**, 169 (1999).
- 20 N. Imanaka, M. Hiraiwa, S. Tamura, G. Adachi, H. Dabkowska, A. Dabkowski, *J. Cryst. Growth* **208**, 466 (2000).
- 21 N. Imanaka, M. Hiraiwa, S. Tamura, G.Y. Adachi, H. Dabkowska, A. Dabkowski, *J. Cryst. Growth* **209**, 217 (2000).
- 22 E. Gallucci, s. Ermeneux, C. Goutaudier, M. Th. Cohen-Adad, *Optical Materials* **16**, 193 (2001).
- 23 D. Ivanova, V. Nikolov, R. Todorov, *J. Cryst. Growth* **311**, 3428 (2009).
- 24 M. Galceran, M.C. Pijol, M. Aguilo, F. Diaz, *J.Sol-Gel Sci. Techn.* **42**, 79 (2007).
- 25 M. Galceran, M.C. Pujol, M. Aguilo, F. Diaz, *Materials Science and Engineering B* **146**, 7 (2008).
- 26 L. Macalik, P.E. Tomaszewski, R. Lisiecki, J. Hanuza, *J. Solid State Chem.*, 181 (2008) 259.1
- 27 M. Maczka, K. Hermanowicz, P.E. Tomaszewski, M. Zawadzki, J. Hanuza, *Opt. Mater.* **31** (2008) 167.
- 28 M.P. Pechini, US Patent No. 3231328, 25 January 1966.

ПОЛУЧАВАНЕ НА АЛУМИНИЕВ ВОЛФРАМАТ $Al_2(WO_4)_3$ ПО МОДИФИЦИРАНИЯ ЗОЛ-ГЕЛ МЕТОД НА ПЕЧИНИ

Й.И. Косева*, В.С. Николов

Институт по обща и неорганична химия, Българска академия на науките, 1113 София, България

Постъпила на 16 февруари, 2010 г.; преработена на 13 май, 2010 г.

(Резюме)

Получена е чиста фаза от алуминиев волфрамат $Al_2(WO_4)_3$ с наноразмерни частици по модифицирания метод на Печини. Като комплексобразуващи агенти са използвани лимонена киселина и етиленгликол. Полученият сух гел е нагриван при различни температури и различна продължителност. Установено е, че чистата фаза от $Al_2(WO_4)_3$ се получава след нагриване при 830 °C в продължение на 36 часа. Повишаването на температурата над 830 °C води до получаването на чист $Al_2(WO_4)_3$ за по-кратко време. Микрофотографии от ТЕМ на различни образци показват, че размерът на частиците варира между 50 и 200 nm и силно зависи от температурата и продължителността на нагриването. При нагриването на гела в поток от кислород се получава чиста фаза от $Al_2(WO_4)_3$ при значително по-ниски температури и по-кратко време на третиране.

Kinetics and equilibrium of ion exchange of Ag^+ on Na-clinoptilolite

N. Lihareva*, L. Dimova, O. Petrov, Y. Tzvetanova

Central Laboratory of Mineralogy and Crystallography, Bulgarian Academy of Sciences, Acad. G. Bonchev St, Bl. 107, 1113 Sofia, Bulgaria

Received December 16, 2009; Revised April 21, 2010

This study investigates silver sorption by Na-clinoptilolite. Bath sorption procedure is applied in order to study the kinetics and equilibrium of Ag^+ uptake. Kinetic sorption data are analyzed using a pseudo-first- and pseudo-second-order model. It is found that pseudo-second-order model provides the most appropriate description of data for both studied 50 and 517 mg/L initial concentrations. The respective apparent pseudo-second-order rate constants k_2 are calculated to be 5.12 and 1.07 g/(meq min). The equilibrium data fit well to the Langmuir isotherms model from which the maximum uptake of Ag^+ is estimated to be $q_{m,calc} = 234.28$ meq/g. The Freundlich model is found to be less appropriate. The total exchange capacity (TEC) is calculated from the chemical composition of the sample and the maximum exchange level (MEL) is obtained experimentally. The obtained results are compared with data on kinetics and equilibrium of Ag^+ sorption by clinoptilolite and other zeolites found in the literature, and discussed appropriately.

Keywords: Na-clinoptilolite; Ag^+ sorption; kinetics; equilibrium isotherms; ion exchange capacity.

1. INTRODUCTION

Natural zeolites are hydrated aluminosilicates of alkaline and alkaline earth metals, forming a group of minerals with microporous structure built up of spatial interaction of apex, sharing SiO_4 and AlO_4 tetrahedrons [1].

The channels in the structure are formed by sequences of tetrahedral rings, and they contain sub-lattices of cation positions and water molecules. This specificity of the zeolite structure is a basis for useful properties such as ion exchange, selective sorption, dehydration/rehydration alteration, catalytic activity, etc [2].

Since a long time zeolites are subject of interest and of increasing investigation activity in order to use them for removal of metal cations from polluted industrial waters, municipal sewage, and radionuclide wastes [3–5].

Among the studied elements, silver is the one of special interest [6]. It is released in industrial waters during the production of a number of non-ferrous metals. Due to its toxicity, it is harmful for living organisms and should be removed. On the other hand, silver can be used as a bactericide in the inactivation and suppression of microorganisms in water disinfection. Silver supported zeolites and other materials are used in various technical and biomedical applications. [3,7,8].

Despite of the interesting potential applications, there is not much data on the interaction between the zeolites and silver in terms of kinetics and equilibrium of the sorption processes. A study of the Ag^+ exchange equilibrium of natural and Na-modified Turkish clinoptilolite, with respect to its application in removing ions from polluted industrial waters and as a bactericide, is performed in [9,10]. IR spectra and equilibrium isotherms of Ag^+ sorption on various clinoptilolite samples are presented in [11,12]. Ag^+ exchange kinetics of two synthetic tobermorites and their subsequent bactericide action are reported by Coleman et al. [8] as well.

This study reports the results of the research on exchange properties of Na-clinoptilolite from Eastern Rhodopes (Bulgaria) towards Ag^+ ions. Data on the kinetics of uptake and equilibrium state of the processes are presented and discussed.

2. MATERIALS AND METHODS

2.1. Materials and characterization

The sample of natural clinoptilolite, used in the study, was collected from the Beli Plast deposit (Eastern Rhodopes, Bulgaria). After grinding and sieving, the fraction below 75 μm (200 mesh) was separated for further use.

The chemical composition of the tested zeolite sample is (wt%): $\text{SiO}_2 - 66.47$; $\text{Al}_2\text{O}_3 - 10.75$; $\text{Fe}_2\text{O}_3 - 0.77$; $\text{K}_2\text{O} - 2.94$; $\text{Na}_2\text{O} - 0.44$; $\text{CaO} - 4.78$; MgO

* To whom all correspondence should be sent:
E-mail: nlhareva@abv.bg

– 1.50; TiO₂ – 0.11; MnO – 0.12; loss of ignition – 11.61; total 99.49%.

The X-ray powder diffraction (XRD) showed that the main mineral in the sample is clinoptilolite, 70%, the associated minerals are dolomite, 15%, and opal-cristobalite, 10%. The sample also contains traces of feldspar, ~3%, and mica, about 2%.

2. 2. Theoretical models

2.2.1. Kinetic models

Simplified kinetic models, including pseudo-first- and pseudo-second-order rate laws, were applied. These pseudo rate models are based on the assumption that the adsorption rate, dq_t/dt , is proportional to the number of sample available sorption sites.

The pseudo-first-order rate expression in integrated form for the boundary conditions, $q_t=0$ and $q_t = q_t$ at $t=0$ to $t = t$ [13], is linear:

$$\log(q_e - q_t) = \log q_e - (k_1/2.303) t \quad (1),$$

where k_1 is the apparent pseudo-first order rate constant for the adsorption (in min^{-1}), and q_e and q_t (in meq/g) are the amounts of metal ion, adsorbed at equilibrium and time t (min), respectively.

The pseudo-second order rate model describes the adsorption processes, in which the reaction rate is proportional to the square of the available sorption site number, and is expressed as:

$$t/q_t = 1/(k_2 q_e^2) + (1/q_e) t \quad (2),$$

where k_2 (g/meq min) is the rate constant for the sorption, q_e and q_t (meq/g) are the amounts of metal ions, sorbed at equilibrium and time t [14,15].

This mathematical description of the sorption is developed on the basis of the following assumptions [15]: the sorbed ions form a monolayer on the surface, the sorption is independent of the surface coverage, and there are no interactions between the sorbed ions.

The chemical equilibrium results from the mechanism of sorption which includes a mass transfer and chemical reactions. The ion transport includes surface diffusion and intraparticle diffusion depending on the diffusivity of sorbate within the particle. The chemical phenomena include hydrolysis, ion exchange or chemisorption, and precipitation. The apparent rate constant results from the adsorption and desorption rate constants. The simple kinetic models do not describe the real mechanism and the rate constants because the steps,

determining the process, are experimentally uncertain.

The rate of these processes depends on the temperature, the initial metal concentrations, the pH, the used amount of adsorbent, the type of adsorbent and metal cations. The simple kinetic models are concerned only with the effect of these parameters on the overall reaction rate. In spite of these restrictions, this analysis of adsorption rates is sufficient for practical applications as a tool for prediction and comparison.

2. 2. 2. Adsorption isotherm models and MEL

The adsorption equilibrium is usually characterized by the ion exchange capacity of the material and by the equilibrium isotherms.

The adsorption equilibrium depends on the temperature and the parameters of the sorption system such as the pH, the solution composition, and the initial metal concentration, as well as on the mineral and chemical characteristics of the sorbing material. Usually, the equilibrium of the adsorption process is described in terms of adsorption isotherms. Several mathematical models, namely Langmuir, Freundlich, IAST, and Sips, have been applied to express the relationship between the sorbed amount and the equilibrium metal concentration [16], the Langmuir and Freundlich being the most frequently used.

In thermodynamic terms, the original Langmuir adsorption model for monolayer chemisorption of gases on homogenous solid surfaces is based on the assumption that the adsorption enthalpy is constant and independent on the degree of surface coverage [17]. Applied to the sorption of metal ions from solutions, this means that the binding energy per adsorbed ion remains the same during the whole adsorption process and that there is no interaction between the sorbed ions. The mathematical expression of the Langmuir model for a single metal ion uptake is:

$$C_e/q_e = 1/bq_m + C_e/q_m \quad (3),$$

where C_e (meq/L) and q_e (meq/g) are respectively the equilibrium Ag concentration in the aqueous phase and in the solid phase. The Langmuir parameter q_m (meq/g) represents the maximum sorbed amount and the parameter b (L/meq) is the site energy factor.

The Freundlich isotherm model is of an empirical nature and is applied to interpret the sorption on surfaces with sites of varying bonding strength. In this model, the ions occupy predominantly sites with a stronger sorption

affinity, thus provoking a decrease in the binding strength with increasing the extent of surface occupation. The linear form of Freundlich model, used to fit the Ag sorption data, is:

$$\log q_e = \log K_F + N \log C_e, \quad (4)$$

where K_F (meq/g)/(meq/L)^N and N (dimensionless) are Freundlich parameters.

Another equilibrium parameter is the ion exchange capacity [18]. The ion exchange properties of zeolites are based on the negative charge (-1), caused by each aluminum atom in the tetrahedral structure of the clinoptilolite, balanced by the exchangeable cations. These sites determine the total exchange capacity (TEC), expressed as a number of ionogenic groups, in equivalents, per fixed amount of sorbent [19, 20].

The cation exchange capacity (meq/g) of homoionic Na-form of the zeolite is derived from the sample analysis as equal to the mmol/g of (Al+Fe) minus meq/g of (K⁺+Ca²⁺+Mg²⁺) for a pure material. Alternatively, TEC is equal to meq Na/g. When negligible mineral impurities are present in the sample, this capacity presents the total amounts of zeolite exchangeable groups and is named "ideal exchange capacity" (IEC) [18]. However, the natural samples usually contain other mineral phases. In addition, the exchangeable cations can be situated at inaccessible sites of the framework. The size of channel characteristic of each zeolite determines the incoming ions which can diffuse in the sample (ion-sieving phenomenon). For these reasons, the calculated TEC may be overestimated.

More important for practical purposes is the maximum exchange level (MEL) (expressed in meq/g) [18, 20], representing the part of the TEC which is actually available for ion exchange. MEL is determined experimentally by the "cross-exchange method" column [21] or by repeated batch experiments of ion exchange [20, 22–24]. Its value depends on the experimental conditions and on the sorbent nature and sorbed ions.

3. EXPERIMENTAL

3.1 Preparation of Na-exchanged clinoptilolite

The sodium-loaded, homoionic clinoptilolite was prepared by stirring 50 g of the natural sample and 500 ml of 1 M NaCl solution at 500 rpm. The treatment was performed in a closed bottle placed in an oven and heated at 60 °C. The NaCl solution was replaced every day by a fresh one and then analyzed. This procedure was repeated 12 times. Finally, the clinoptilolite sample was washed with

distilled water in order to remove completely the occluded salt. The washing lasted until was reached a negative reaction of the Cl⁻ with the silver ions. Then the sample was dried in oven at 60 °C.

The kinetic experiments were carried out in a bath sorption mode, using screw capped polypropylene bottles for various fixed contact times. We added 20 ml of 50 mg/L and 517 mg/L Ag⁺ solution with initial pH = 4 to series of samples, 0.1g Na-clinoptilolite each. The suspension was shaken at 20°C on a horizontal shaker (amplitude of 20 mm and 150 oscillation.min⁻¹) and then centrifuged for 15 min at 4000 rpm. The silver concentration in the separated solutions was measured by AAS using a Perkin-Elmer 30–30 apparatus.

Cation exchange isotherms were obtained by treating 0.1 g of samples in centrifugal tubes with 20 ml of Ag⁺ aqueous solution with concentrations of 10, 25, 50, 100, 200, 300, 500, and 5000 mg/L at pH_{initial} = 4.0. The reaction time was fixed equal to 90 min at 20 °C. Further, we proceeded as described above.

The maximum exchange level of Na-clinoptilolite with Ag⁺ ions was measured using bath procedure. 20 ml of Ag⁺ solution with initial concentration 5mM and pH 4.0 were added to 0.1 g of sample. The mixture was separated every 2 days by centrifugation and decantation. A new fresh portion of Ag⁺ solution was added to a solid residue, and the treatment was repeated. The solution was analyzed for the content of Ag⁺ cations. The procedure was repeated until the concentration of Ag⁺ in the solutions from two consecutive treatments becomes the same and the deviation from the initial concentration becomes less than 4%. Totally, five treatments and 10 days were necessary in our case.

4. RESULTS AND DISCUSSION

4.1. Material characterisation

The chemical composition of Na-exchanged clinoptilolite sample is: (wt%): SiO₂ – 63.41; Al₂O₃ – 10.97; Fe₂O₃ – 0.77; K₂O – 1.26; ; Na₂O – 5.32; CaO – 1.97; MgO – 1.27; TiO₂ - 0.11; MnO - 0.12; loss of ignition – 14.78; total 99.99. The percentages of exchanged elements of natural clinoptilolite are: K – 57.14%, Ca – 58.77%, Mg – 14.4%, i.e. more than half of Ca²⁺ and K⁺ ions in the clinoptilolite are readily exchanged for Na⁺ ions. The content of Na in the exchanged form increases more than 10 times. The remaining Ca²⁺, K⁺ and

Mg²⁺ ions should not be available for reaction with Ag⁺ under the selected experimental conditions.

4.2. Kinetics

Figure 1 shows the effectiveness of Ag⁺ ions uptake by Na-clinoptilolite as a function of contact time. The effectiveness ($E\%$) was calculated by the formula:

$$E\% = 100m_s/(VC_0),$$

where m_s is the mass of sorbed metal (mg), C_0 is the initial Ag⁺ concentration (in mg/L), and V (L) is the volume of solution from which the sorption occurs.

At initial concentration of 50 mg/L, the sorbed Ag⁺ amount increases rapidly and reaches an equilibrium value with 94% effectiveness after 15 min. For the higher initial concentration of 517 mg/L, the effectiveness of Ag⁺ uptake is lower, being after 60, 90, and 360 min equal to about 87.5%, 84.4%, and 83.5%, respectively. Akgul et al. report on 45 min equilibrium adsorption time for the Ag⁺ uptake by clinoptilolite [9]. Top and Ülkü [10] have fixed a two-day duration of the adsorption in a study on the antibacterial activity of Ag⁺ loaded clinoptilolite.

The initial metal ion concentrations exert influence on the contact time, necessary to reach an equilibrium. The adsorption was very fast for the 50 mg/L concentration, and high effectiveness of sorption was reached in the first 15 min. The time to reach equilibrium was about 90 min for the higher 517 mg/L concentration.

The initial pH=4.0 increases with the increase of the contact time, changing between 6.5 and 8.6, and between 7.4 and 7.7 for both studied initial concentrations of 50 mg/L and 517 mg/L, respectively.

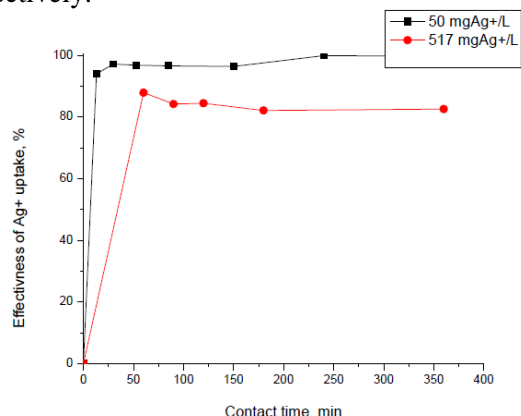


Fig. 1 Uptake of Ag⁺ ions by Na-clinoptilolite as a function of the contact time (0.1000 g Na-clinoptilolite, 20 ml Ag⁺ solution of 50 mg/L and 517 mg/L, pH_{init} = 4.0, t=20 °C).

The experimental data for the Ag⁺ uptake by Na-clinoptilolite were fitted to the pseudo-first- and pseudo-second-order kinetic models by least square regression analysis to check their applicability to the process. The pseudo-first-order model was shown to be non-representative because the correlation coefficient is low, whereas a good correlation between experimental data and the pseudo-second-order reaction model was proved. The parameters of the pseudo-second-order reaction model: integrated rate equations, squares of the correlation coefficients (R^2), apparent rate constants, and experimental and calculated uptake amounts are listed in Table 1. The calculated values of Ag⁺ uptake, obtained from the model ($q_{e,calc}$), are in good agreement with the experimental data (the differences are 2.1 and 0.4 %). Hence, the sorption of Ag⁺ ions onto Na-clinoptilolite could be a pseudo-second-order process. The determined values of k_2 rate constant increased from 1.074 to 5.162 when the initial silver concentration decreased from 517 to 50 mg/L, as reported also by other authors [15].

Table 1. Kinetic parameters for the Ag⁺ uptake by Na-clinoptilolite, pseudo-second-order rate model.

Ag (mg/L)	Integrated rate equation	R^2	k_2 (g/(meq min))	$q_{e,exp}$ (meq/g)	$q_{e,calc}$ (meq/g)
50	$t/q_t = 10.77t + 22.42$	0.9998	5.16	0.091 (± 0.002)	0.093
517	$t/q_t = 1.25t + 1.46$	0.9995	1.07	0.801 (± 0.012)	0.798

During the last 20 years, numerous sorption systems have been investigated, and particularly for application of simple kinetic model to describe the process [25]. However, in the studies, concerning Ag⁺ sorption by diverse materials, the kinetics of the processes has almost not been examined. To date, no studies for the application of kinetic models for description of Ag⁺ uptake by natural and modified clinoptilolite and other zeolites were found. Data on the uptake of Ag⁺ conforming to the pseudo-second-order kinetic model with $k_2 = 0.033$ g/mmol min has been reported in the investigations on the use of the chitosan, the Ag⁺ loaded biosorbent, as a bactericide [26], and in the study for the uptake of Ag⁺ ions by two tobermorites - k_2 is 0.067 and 0.079 g/(mmol min), respectively [8]. The pseudo-second-order rate constant for the uptake of Ag⁺ by Na-clinoptilolite at initial concentration 517 mgAg⁺/L (~ 5mM), determined in the present study, is about 16 times greater than the silver uptake in the above cited investigations [8] and 32 times faster than the sorption on modified

chitosan [26]. The rate constant for initial concentration 50 mgAg⁺/L is almost five times greater than for 517 mg/L. These results suppose that the rate limiting step depends not only on the concentration of sorbed ions, but on the concentration of active sites and the bonding mechanism - especially on the transfer phenomena and accessibility of the active sites.

4.2. Adsorption isotherms

The silver sorption isotherms for the initial Ag⁺ concentrations 10 to 5000 mgAg⁺/L are presented in Figure 2.

The applicability of the Langmuir and Freundlich models to silver sorption by Na-clinoptilolite was tested by fitting the experimental data to the theoretical models by least squares regression analysis. The obtained equations, experimental and calculated values of maximum uptake, the constants and the corresponding squares of correlation coefficients (*R*²) are listed in Table 2. The experimental equilibrium data correlate well with the Langmuir isotherm model for the interval

of concentrations 10 to 500 and 10 to 5000 mgAg⁺/L. The Freundlich model was found to be comparatively less appropriate for both studied intervals of concentrations.

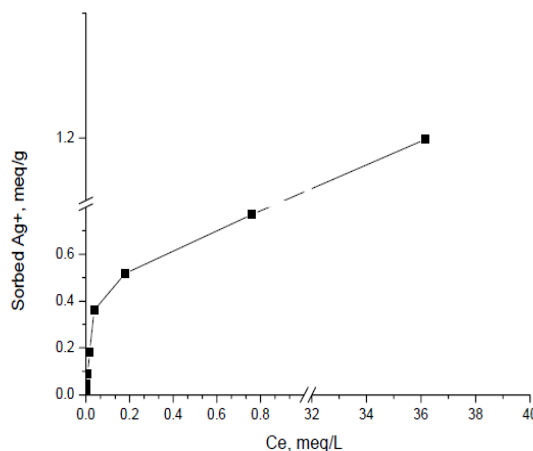


Fig. 2. Sorption isotherm of Ag⁺ ions uptake by Na-clinoptilolite (0.1 g of zeolite, 20 ml Ag⁺ solution, pH_{init} = 4.0, t = 20°C).

Table 2. Langmuir and Freundlich sorption equations and parameters for Ag sorption by Na-clinoptilolite

Langmuir model equation	Initial concentrations range (mg/L)	<i>R</i> ²	<i>b</i> (L/meq)	<i>q</i> _{m,calc} (meq/g)	<i>q</i> _{m,calc} (mg/g)
$C_e/q_e = 1.229C_e + 0.067$	10 - 500	0.9925	18.234	0.813	87.76
$C_e/q_e = 0.831C_e + 0.124$	10-5000	0.9999	6.703	1.204	129.86
Freundlich model equation		<i>R</i> ²	<i>K</i> _F (meq/g)/(meq/L) ^N	<i>N</i>	
$\log q_e = 0.533 \log C_e + 0.060$	10 - 500	0.9776	1.149	0.533	
$\log q_e = 0.487 \log C_e - 0.037$	10 -5000	0.9610	0.632	0.386	

To date only a small number of studies on the equilibrium of Ag⁺ uptake by clinoptilolite could be found in the literature. In [9] the sorption isotherm of Ag⁺ by clinoptilolite is presented and a good correlation with both Langmuir and Freundlich models is reported. The maximum adsorption capacity, calculated according to the Langmuir model is 38.91 mgAg⁺/g for experimental conditions: 0.05 g of sample, 25 ml of solution, and highest initial concentration 150 mg Ag⁺/L. The amounts of Ag⁺ sorbed by a composite material containing clinoptilolite [12] have been determined as 4.36, 27.85, and 183.78 mg/g, for initial AgNO₃ concentrations of 50, 500, and 5000 mg/L, respectively, solid to liquid ratio 1:100 (w/v) and 24 h of treatment. The experimental data for the sorption isotherm have showed a better fitting with the Freundlich model. The capacities of a series of clinoptilolites of different origin for silver are within the range 59.75 – 85.32 mgAg⁺/g [11], and the capacities of two tobermorites are 0.958 and 0.993 meq/g [8]. In a recent study [26] using

modified chitosan for Ag⁺ sorption a good correlation with the Langmuir model has been reported with high maximum adsorption capacity 2.1 meqAg⁺/g. The result for the maximal Ag⁺ uptake of 87.76 mg/g and 129.8 mg/g by Na - clinoptilolite in our work are in the range of the reported values, although it is difficult to compare these values, because they are obtained at very different conditions.

4.3. Cation exchange capacity

The sample of natural clinoptilolite, used in this study, is not pure - it contains some amounts of other minerals, mainly dolomite. That is why it is not appropriate to calculate the total cation exchange capacity (TEC) of Na-clinoptilolite from the contents of framework and extra-framework cations, as described in Section 2.2. The value, obtained on the basis of Na content (in meq/g) is 1.72.

The maximum exchange level for Ag⁺ sorption by Na-clinoptilolite, measured by repeated bath

ion-exchange experiments is 1.43 meq/g or 83.1% from the calculated TEC, due to failure of complete replacement of Na⁺ for Ag⁺. During these treatments the initial pH 4.0 changed in the interval 8.7 – 7.5 with a trend to decrease with the number of treatments.

The maximum uptake calculated from the Langmuir isotherms model represents 84.2% of the measured maximum exchange level. This discrepancy is due to different extent of replacement of exchangeable extra-framework cations and can be explained by the difference in experimental conditions. MEL is determined under conditions of repeated refreshing of high concentrated sorbate solution after each equilibrium state. Moreover, during the intense and long shaking, typical mechanical and structural changes in the sorbent could take place and influence the ions uptake.

The results, obtained from the kinetics and equilibrium studies in the investigation of sorption systems are useful for comparison of sorption properties of sorbents, the cations uptake effectiveness, and estimation of performance, although the theoretical base of modeling and the real process mechanisms are disputable.

5. CONCLUSION

Sodium exchanged form of natural clinoptilolite from Beli plast deposit was studied for Ag⁺ sorption. Batch studies show that a simple model of pseudo-second-order kinetic equation can adequately describe the Ag⁺ uptake with the rate constant k_2 being more faster than the ones reported in the literature for other materials. The isotherm equilibrium data fit well to the Langmuir and Freundlich models. The calculated maximum uptake values are 87.76 and 234.28 mgAg⁺/g at initial concentrations up to 500 and 5000 mgAg⁺/L. The calculated value of TEC is found to be 1.72 meq/g and the measured MEL is 1.43 meq/g. The obtained results show that Na-exchanged clinoptilolite has excellent adsorptive characteristics represented by a high sorption capacity and fast sorption process and is very effective for the sorption of Ag⁺ from aqueous solutions.

REFERENCES

1. K. Koyama, Y. Takeuchi, *Zeits. Krist.*, **145**, 216 (1977).
2. S. Ouki, M. Kavannah, *Waste manage Res.*, **15**, 383 (1997).
3. F. A. Mumpton, in: *Natural Zeolites for the Third Millennium*, C. Colella and F. A. Mumpton (Eds.), De Frede, 2000, p. 19.
4. M. J. Zamzow, J. E. Murphy, *Sep. Sci. Technol.*, **27**, 1969 (1992).
5. G. Blanchard, M. Maunaye, G. Martin, *Water Res.*, **18**, 1501 (1984).
6. E. Czarán, J. Papp, A. Meszaros-Kis, E. Domokos, *Acta Chimica Hungarica*, **126**, 673 (1989).
7. M. Rivera –Garza, M. T. Olguin, I. Garcia-Sosa, D. Alcantara, G. Rodriguez-Fuentes, *Micropor. Mesopor. Mater.*, **39**, 431 (2000).
8. N. J. Coleman, A. H. Bishop, S. E. Booth, J. W. Nicholson, *J. Eur. Ceram. Soc.*, **29**, 1109 (2009).
9. M. Akgül, A. Karabakan, O. Acar, Y. Yürüm, *Micropor. Mesopor. Mater.*, **94**, 99 (2006).
10. A. Top, S. Ülkü, *Appl. Clay Sci.*, **27**, 13 (2004).
11. W. Mozgawa, T. Bajda, *J. Mol. Struct.*, **792–793**, 170 (2006).
12. H. Pehlivan, D. Balköse, S. Ülkü, F. Tihminlioglu, *Compos. Sci. Technol.*, **65**, 2049 (2005).
13. Y. S. Ho and G. McKay, *Wat. Res.*, **33**, 578 (1999).
14. F-C. Wu, R-L. Tseng, R.-S. Juang, *Wat. Res.*, **35**, 61 (2001).
15. Y. S. Ho and G. McKay, *Water Res.*, **34**, 735 (2000).
16. S. K. Papageorgiou, F. K. Katsaros, E.P. Kouvelos, N. K. Kanellopoulos, *J. Hazard. Mater.*, **162**, 1347 (2009).
17. W. Stumm and J. Morgan, *Aquatic Chemistry*, Wiley Interscience, New York; 1996, p.1022.
18. V. J. Inglezakis, *J. Colloid Interface Sci.*, **281**, 68 (2005).
19. R. T. Pabalan, *Geochim. Cosmochim. Acta*, **58**, 4573 (1994).
20. A. Langella, M. Pansini, P. Cappeleti, B. de Gennaro, M. de Gennaro, C. Colella, *Micropor. Mesopor. Mater.*, **37**, 337 (2000).
21. M. Pansini, C. Colella, D. Caputo, M. de' Gennaro, A. Langella, *Micropor. Mater.*, **5**, 357 (1996).
22. V. J. Inglezakis, M. M. Loizidou, H. P. Grigoropoulou, *Water Res.*, **36**, 2784 (2002).
23. M. Loizidou, R. P. Townsend, *Zeolites*, **7**, 153 (1987).
24. S. H. Abdel-Halim, A. M. A. Shehata, M. F. El-Shahat, *Water Res.*, **37**, 1678 (2003).
25. Y. S. Ho, G. McKay, *Process Biochem.*, **34**, 451 (1999)
26. A. M. Donia, A. A. Atia, K. Z. Elwakeel, **87**, 197 (2007).

КИНЕТИКА И РАВНОВЕСИЕ НА ЙОННИЯ ОБМЕН НА Ag^+ ВЪРХУ КЛИНОПТИОЛИТ

Н. Лихарева*, Л. Димова, О. Петров, Я. Цветанова

Централна лаборатория по минералогия и кристалография, Българска академия на науките, ул. „Акад. Г. Бончев”, Бл. 107, 1113 София, България

Постъпила на 16 декември, 2010 г.; в окончателен вид на 21 април, 2010 г.

(Резюме)

Изследвана е сорбцията на сребро от Na-клиноптилолит. Експериментите за изучаване на кинетиката и равновесието на извличането на сребро от разтвора са извършени в статични условия. Данните от изследване на кинетиката са анализирани чрез прилагане на модела на реакции от псевдо-първи и псевдо-втори порядък. Намерено е, че моделът на реакции от псевдо-втори порядък дава по-добро описание на данните за двете изследвани изходни концентрации на сребро – 50 и 517 mg/L със скоростни константи k_2 съответно 5.12 и 1.07 g/(meq min). Данните за равновесието на сорбцията се описват по-добре с модела на изотермите на Langmuir, откъдето е намерено максималното извличане на сребро $q_{m,calc} = 234.28$ meq/g. Общият обменен капацитет (ТЭС) е изчислен на базата на химическия състав на изходния клиноптилолит. Максималното обменено количество за изследвания йон Ag^+ (MEL) е намерено експериментално. Получените резултати са сравнени с данните за кинетиката и равновесието на сорбцията на Ag^+ от клиноптилолит и други зеолити, намерени в литературата и са съответно дискутирани.

EFFICIENCY OF FORMATION OF NANOPOROUS ALUMINA FILMS IN FLUORIDE ION-CONTAINING ELECTROLYTE

Chr. A. Girginov*, M. S. Bojinov

*Department of Physical Chemistry, University of Chemical Technology and Metallurgy,
8 Kliment Ohridski Blvd., 1756 Sofia, Bulgaria*

Received July 15, 2010, Revised September 27, 2010

The formation of porous anodic films on Al was carried out in electrolytes based on 0.5 M (NH₄)₂SO₄ with the addition of NH₄F. The anodization was performed in two stages. In the first stage the formation voltage is reached at a scan rate of 50 mV s⁻¹. In the second stage, the anodization was continued tensiostatically for up to 1 hour. Current density / formation voltage (first stage) and current density / time curves (second stage) were found to be in agreement with previous results of other authors. The current efficiency of film formation has been estimated by determining the concentration of Al, dissolved in electrolyte during anodization by inductively coupled plasma optical emission spectrometry (ICP-OES). Assuming that all the Al ions that migrate through the film are ejected in the solution, the transference number for Al³⁺ is also estimated. The obtained estimates allowed the determination of the total porosity of the alumina templates by re-anodization in 1 M AS/DMF (ammonium salicylate in dimethyl formamide) electrolyte. The obtained porosity values decreased with the increased voltage in the tensiodynamic stage and slightly increased with the time during the tensiostatic stage, in general agreement with the results, reported during porous anodization of Al in acidic electrolytes.

Key words: alumina films; sulphate-fluoride electrolyte; anodic films; oxides, nanoporous templates.

INTRODUCTION

Nanoporous oxide templates are formed during the anodic polarization of aluminum in suitable electrolytes. These self-organised structures grow as comparatively thick layers with very large surface area. The structures are well reproducible and their properties (pore diameter, distribution and length) are easily controlled by the parameters of the anodization process. Subsequent incorporation of a range of substances in the form of nanorods, nanodots, and nanotubes, results in the formation of a wide series of functional nanomaterials, characterized by unique magnetic, photocatalytic, semiconducting, and electrical properties [1]. Such materials find increasing application as high density storage media, functional nanomaterials exhibiting quantum size effect, highly selective chemical sensors [2], nano electronic devices [3], and functional bio-chemical membranes [4]. Active centres can be created in the porous templates via incorporation of suitable compounds, resulting in effective catalyst materials [5]. Besides classical

electrolytes for porous anodization of Al (sulphuric, oxalic, phosphoric and chromic acids) [6], a range of organic acids have been also successfully employed (sulfamic acid [7], malonic acid [8, 9], tartaric acid [9], etc.).

It has been reported recently that acidic and neutral electrolytes, containing fluoride ions are also suitable for the formation of self-organized alumina templates on Al [10, 11]. Such electrolytes are widely used for porous anodization of several valve metals such as Ti [12], Nb [13] and W [14]. It has been proposed that during anodic oxidation in the presence of fluoride, nucleation of ordered pores takes place with subsequent formation of self-organized nanotube arrays. In order to be able to propose a mechanism for such pore nucleation and growth processes, data on the relative importance of the processes of film growth and metal dissolution through the film are needed. In that respect, the present paper aims at estimating the charge density efficiency for porous alumina formation on Al in a neutral fluoride-containing electrolyte by electrochemical methods.

EXPERIMENTAL

*To whom all correspondence should be sent:
E-mail: christian.girginov@gmail.com.

Sheets of high purity (99.999%) and technical purity (99.5%) aluminum were electropolished in a phosphoric acid-chromic acid electrolyte at 343 K. The electropolished samples were then anodized in an electrolyte based on 0.5 M $(\text{NH}_4)_2\text{SO}_4$ with the addition of 0.075 M NH_4F at 293 K. A two-electrode cell with a platinum mesh counter electrode, situated symmetrically around the working electrode, was used. The anodization was performed in two stages. In the first stage, a range of voltages were reached at a scan rate of 50 mV s^{-1} . In the second stage, the anodization was continued tensiostatically ($U = \text{const}$) for up to 1 h. The anodization was carried out using a high voltage potentiostat/galvanostat (600 V, 0.5 A), precision multimeters (Mastech MS 8050), and a PC-based data acquisition system were employed. The amount of dissolved Al in the forming electrolytes has been estimated by ICP-OES (Prodigy, Teledyne Leeman Labs). Pore-filling of the alumina templates, formed under different conditions, was achieved via re-anodization in 1 M AS/DMF (ammonium salicylate in dimethyl formamide), current density being of 1 mA cm^{-2} at 293 K.

RESULTS AND DISCUSSION

Influence of the Al purity on porous anodization

Preliminary investigations have shown that the current densities during porous anodization are influenced to a certain extent by the purity of the metal substrate. It turned out that the current density of tensiodynamic anodization of pure (99.999%) Al in all cases is larger compared to that of the technically pure (99.5%) Al. This trend is illustrated on Fig. 1, where the current vs. voltage curves during the first stage of anodization of the two types of Al substrates are superimposed. A tentative explanation of that phenomenon is the slower rate of oxidation of secondary phases, most probably present at the surface of the electropolished technically pure Al, although further investigations are planned to get a deeper insight into that experimental fact.

Kinetics of porous film formation

The formation of porous anodic films was carried out in an electrolyte (0.5 M $(\text{NH}_4)_2\text{SO}_4$) with added NH_4F (0.075 M). A formation voltage $U = 20 \text{ V}$ is reached at a scan rate of 50 mV s^{-1} in the first stage. The respective current density vs. voltage curves were recorded. Subsequently, the anodization was continued tensiostatically ($U = 20 \text{ V}$) with different durations (up to 1 h). The current density vs. time curves was recorded. Representative examples of the

dependences obtained in stage 1 and 2 are shown on Fig. 2.

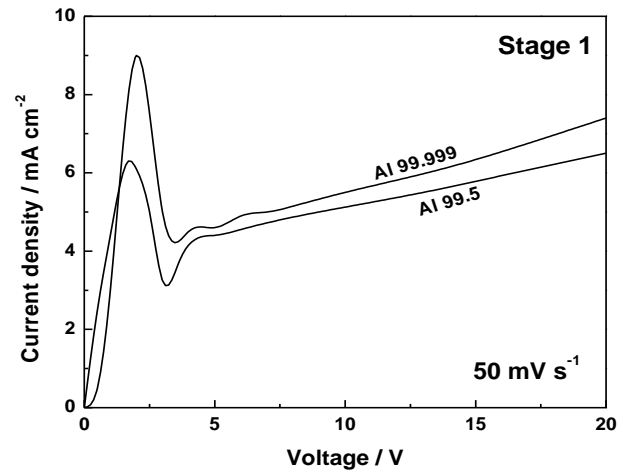


Fig. 1. Current density vs. voltage during tensiodynamic anodization of Al with different purity in (0.5 M $(\text{NH}_4)_2\text{SO}_4$ + 0.075 M NH_4F) at 293 K.

Charge density efficiency

Numerical integration of $J(t)$ -curves, resulted in estimates of the total charge density (Q_{total}), passed during the two stages of anodization:

$$Q_{\text{total}} = \int_0^t (Jt) dt \quad (\text{C cm}^{-2}). \quad (1)$$

The amount of dissolved aluminum (m_{Al}) was estimated by determining the concentration of Al, dissolved in the electrolyte during anodization by ICP-OES. The dependence of m_{Al} on total charge density (Q_{total}) during anodization in 0.5 M $(\text{NH}_4)_2\text{SO}_4$ + 0.075 M NH_4F is presented on Fig.3.

Starting from the estimated amount of dissolved Al, the quantity of charge for dissolution of Al ($Q_{\text{dissolving}}$) was easily calculated using Faraday's law

$$Q_{\text{dissolving}} = \frac{m_{\text{Al}}}{A_{\text{Al}}} zF \quad (\text{C cm}^{-2}), \quad (2)$$

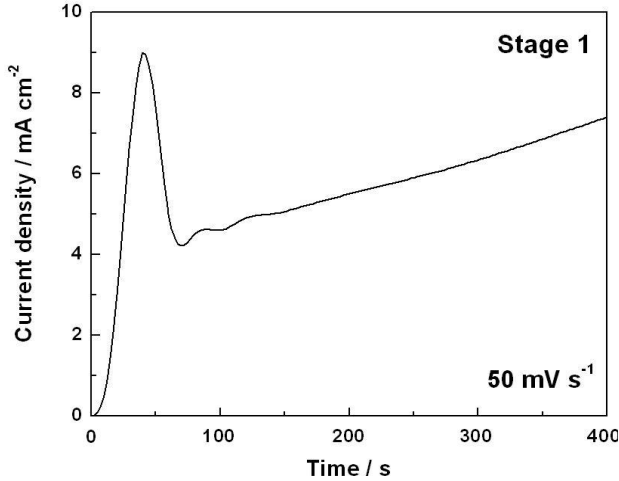
where A_{Al} is the atomic weight of Al, F is the Faraday constant, and $z = 3$.

In turn, the charge density efficiency for film formation was determined as follows:

$$\Lambda = 100 \frac{Q_{\text{total}} - Q_{\text{dissolving}}}{Q_{\text{total}}} \quad (\%). \quad (3)$$

The Λ -(Q_{total}) -dependence is shown on Fig.4. During Stage 1, the anodization efficiency increases with applied voltage. In the second stage ($U = \text{const}$), however, it was found that the efficiency slightly decreases with time (or

equivalently, with the thickness of the porous oxide



layer).

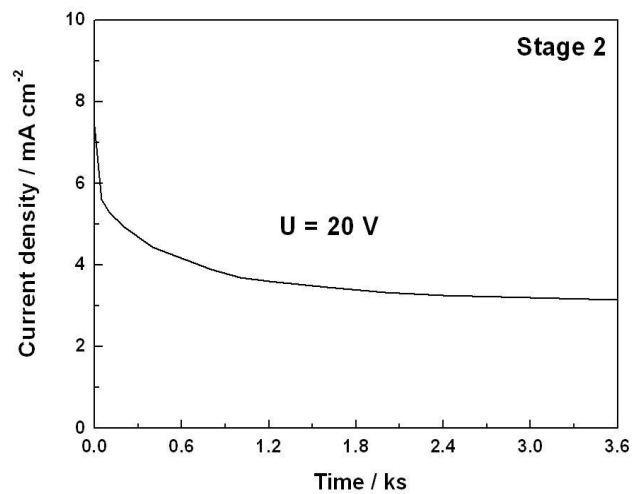


Fig.2 Current density vs. time during the first and second stages of anodization of pure Al in $(0.5 \text{ M } (\text{NH}_4)_2\text{SO}_4 + 0.075 \text{ M } \text{NH}_4\text{F})$ at 293 K.

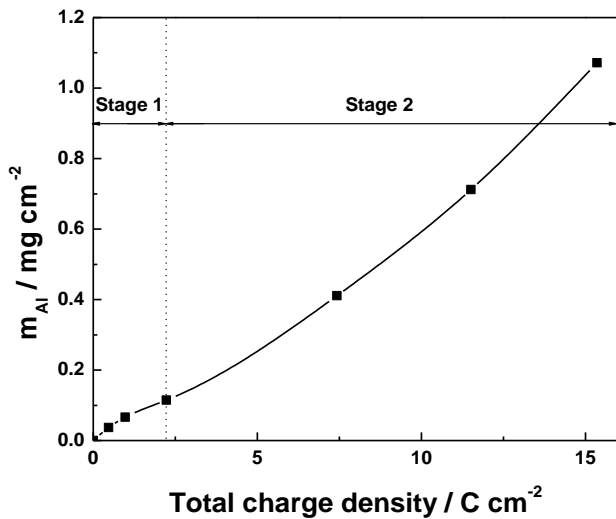


Fig. 3. Amount of dissolved Al vs. total charge density during anodization

Porosity of alumina templates

The total porosity (α), i.e. the ratio of pore volume to the total oxide volume, is an important characteristic of the anodic alumina templates. As the mean pore radius does not change significantly in-depth, porosity can be also expressed as the ratio of the area of pores to the total sample area.

It is well known that porous anodic films on Al can be re-anodized in a non-dissolving electrolyte. The current during re-anodization is transferred through the barrier oxide via Al^{3+} and O^{2-} electromigration, as a result of which new oxide is formed both at the metal/film and the film/electrolyte interfaces [15, 16]. The pores are gradually filled and as a result of ionic migration, the thickness of the barrier oxide increases with re-anodization time. The increase of the formation voltage in galvanostatic conditions is a measure of barrier film growth, which gives a

possibility to estimate α via analysis of kinetic $U(t)$ -curves. Takahashi and Nagayama [16] have analyzed the kinetics of pore-filling during re-anodization. In galvanostatic conditions, the formation voltage (U) increases linearly with time (t), the slope of the straight line changing from

$m_I = \left(\frac{\partial U}{\partial t}\right)_I$, when anodization takes place in the

pores, to $m_{II} = \left(\frac{\partial U}{\partial t}\right)_{II}$, when the pores are totally filled. At the moment of total pore-filling, the area of the barrier sublayer/electrolyte interface increases sharply, i.e. the apparent “porosity” assumes a value of 1. This explains the smaller rate of increase of the barrier film thickness after pore-filling, which is expected to be equal to that during direct anodization in non-dissolving electrolytes. As a result of this analysis, the total porosity of the alumina template is expressed as [16]:

$$\alpha = \frac{t_{\text{Al}^{3+}} m_{II} / m_I}{1 - \left[(1 - t_{\text{Al}^{3+}}) m_{II} / m_I \right]}, \quad (4)$$

where $t_{\text{Al}^{3+}}$ is the transference number of Al^{3+} in the barrier oxide.

Using this method, α can be estimated from experimental kinetic data, received from the ratio of the two slopes (m_I and m_{II}), if the transference number $t_{\text{Al}^{3+}}$ is known.

Several authors [17, 18] have proposed that the growth of the oxide in porous anodization is due to the migration of oxygen ions alone, i.e. they grow at

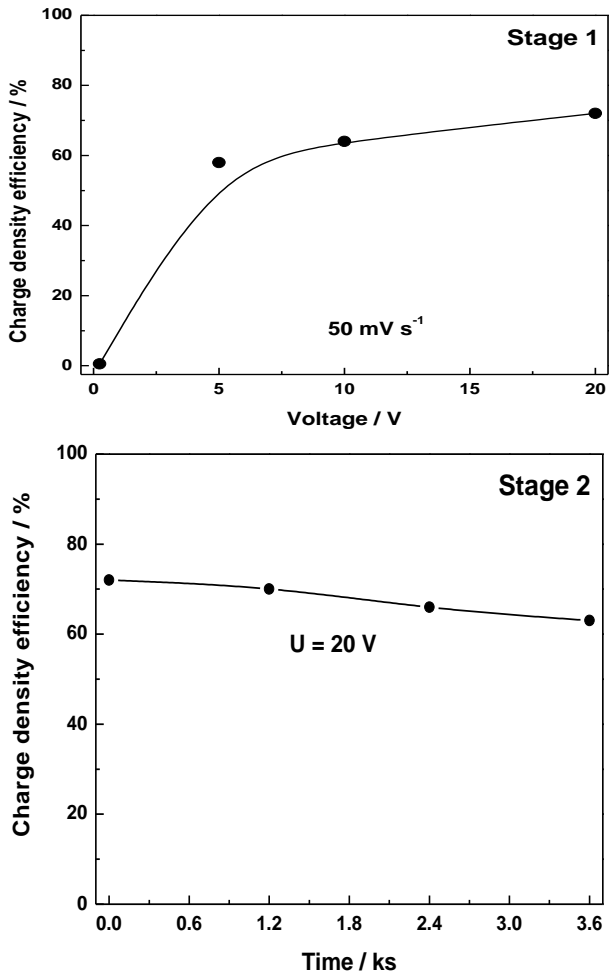


Fig. 4. Charge density efficiency vs. formation voltage (stage 1) and vs. time (stage 2) during anodization in 0.5 M $(\text{NH}_4)_2\text{SO}_4 + 0.075 \text{ M NH}_4\text{F}$.

the metal/film interface. This means that all the Al^{3+} that migrate through the oxide are ejected in the electrolyte. Following this assumption, the transference number $t_{\text{Al}^{3+}}$ was estimated as:

$$t_{\text{Al}^{3+}} = \frac{100 - \Lambda}{100} \quad (5)$$

for templates in both stages of anodization. The oxide films, formed in different conditions, were re-anodized in 1 M AS/DMF (ammonium salicylate in dimethylformamide). The kinetic $U(t)$ -curves were recorded and the porosity of the obtained templates was estimated from the m_I and m_{II} using the calculated values of $t_{\text{Al}^{3+}}$. The results are presented on Fig.5. During the first stage of anodization, porosity decreases with increasing voltage, reaching the value of ca. 0.1 at 20 V, and then slightly increases during the second stage of anodization. The obtained values and trends are in good agreement with the results of Ono et al.[19, 20], obtained by re-anodization of alumina templates, formed in sulphuric and oxalic acids at 293 K, as

well as those of Sulka and Parkola [21],

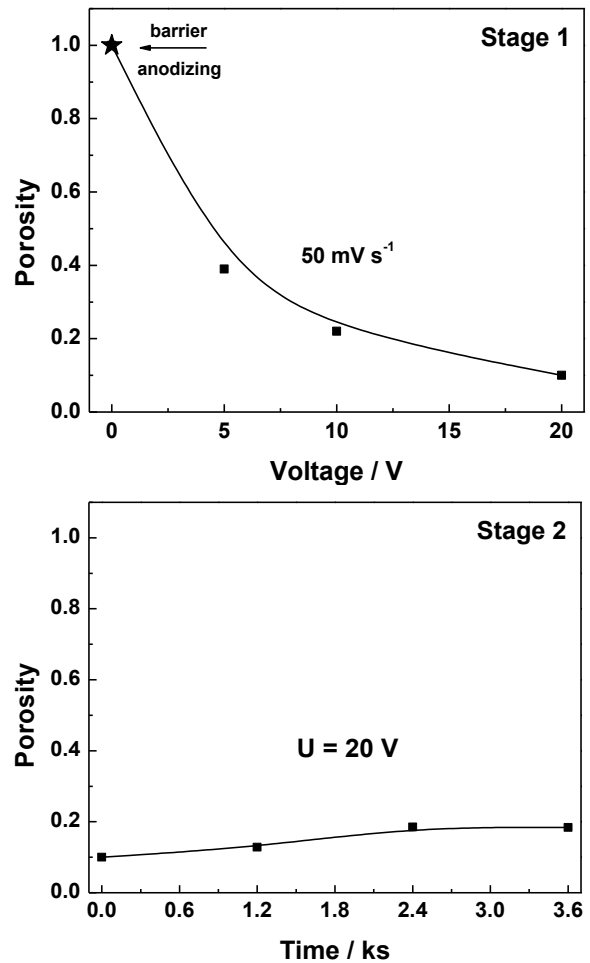


Fig. 5. Porosity vs. formation voltage (stage 1) and vs. time (stage 2) during anodization in 0.5 M $(\text{NH}_4)_2\text{SO}_4 + 0.075 \text{ M NH}_4\text{F}$ at 293 K.

estimated from post-processing of scanning electron micrographs of nanoporous alumina, formed in sulphuric acid at 274 K.

CONCLUSION

Well reproducible alumina templates are obtained during anodization of Al at room temperature in neutral sulphate electrolytes with the addition of fluoride. To assess the charge density efficiency during the two stages of film formation (tensiodynamic and tensiostatic), the amount of dissolved Al was quantified using ICP-OES. During Stage 1, the anodization efficiency increases with applied voltage. In the second stage ($U = \text{const}$), however, it was found that the efficiency slightly decreases with time (or equivalently with the thickness of the porous oxide layer). Assuming that entire Al that migrates through the forming oxide is ejected into the solution, the transference number of Al^{3+} was estimated from the amount of dissolved Al and the charge density efficiency. Using pore-filling via re-anodization, the total porosity of the

templates, depending on the formation voltage (in tensiodynamic anodization) and anodization time (in tensiostatic anodization), is determined. The porosity decreases with increasing voltage in tensiodynamic anodization and slightly increases in the tensiostatic stage, in general agreement with the results from the porous anodization of Al in acidic electrolytes. Further investigations, aiming at elucidating the effect of fluoride concentration, formation voltage, and tensiostatic stage duration on the main characteristics of the alumina templates, are in progress and will be reported in the near future.

Acknowledgements: The authors are obliged to the National Scientific Research Fund, Ministry of Education, for the funding this work under contract BYX-307/2007.

REFERENCES

1. R.K. Jha, M.R. Rao, *Int. J. Heat Mass Transfer*, **10**, 395 (1967).
2. C.E. Kalb, J.D. Seader, *Int. J. Heat and Mass Transfer*, **15**, 801 (1972).
3. L.-S. Yao, S.A. Berger, *J. Fluid Mech.*, **88** (2), 339 (1978).
4. G. Havas, A. Deak, J. Sawinsky, *The Chem. Eng. J.*, **35**, 61 (1987).
5. T. Lemenand, H. Peerhossaini, *Appl. Therm. Eng.*, **22**, 1717 (2002).
6. J.A.W. Gut, R. Fernandes, P.M. Jose, C.C. Tadini, *Chem. Eng. Sci.*, **59**, 4591 (2004).
7. R.R. Hemamalini, P. Partheeban, J. S.C. Babu, S. Sundaram, *Int. J. Heat Mass Transfer*, **48**, 2911 (2005).
8. R.K. Shah, *Heat Transfer Engineering*, **27**, 3 (2006).
9. N. Paisarn, S. Jamnean, *Int. J. Heat Mass Transfer*, **50**, 444 (2007).
10. A. Marchitto, F. Devia, M. Fossa, G. Guglielmini, C. Schenone, *Int. J. Multiphase Flow*, **34**, 128 (2008).
11. R.H. Perry, D.W. Green, J.O. Maloney, *Perry's Chemical Engineers' Handbook*, Seventh Edition, McGraw-Hill, New York, 1998, pp. 11, 55.
12. C.L. Yaws, *Chemical Properties Handbook*, McGraw-Hill Inc., New York, 1999.

ЕФЕКТИВНОСТ НА ОБРАЗУВАНЕ НА НАНО-ПОРЪОЗНИ ФИЛМИ ОТ ДВУАЛУМИНИЕВ ТРИОКСИД В ЕЛЕКТРОЛИТ, СЪДЪРЖАЩ ФЛУОРИДНИ ЙОНИ

Кр. А. Гиргинов*, М. С. Божинов

Катедра „Физикохимия“, Химикотехнологичен и металургичен университет, бул. „Климент Охридски“ № 8, 1756 София

Постъпила на 15 юли, 2010 г., преработена на 27 септември, 2010 г.

(Резюме)

Формирани са порести анодни филми върху алуминий в електролит 0.5 М $(\text{NH}_4)_2\text{SO}_4$ с добавка на 0.075 М NH_4F . Анодирането е проведено в два стадия. В първия стадий определено напрежение се достига с постоянна скорост (50 mV s^{-1}) на нарастване на потенциала. Във втория стадий формирането продължава при постоянно напрежение (20 V) с различна продължителност (до 1 час). Определена е токовата ефективност на анодирането чрез аналитично определяне на количеството разтворен алуминий в електролита. Определени са стойностите на преносното число ($t_{\text{Al}^{3+}}$) на алуминиевите йони. Формираните алуминиеви оксидни матрици са повторно анодирани (ре-анодирани) в неразтварящ филма електролит. Чрез анализ на кинетичните криви на ре-анодирание и получените стойности за $t_{\text{Al}^{3+}}$ е изчислена пористостта на филмите в двата стадия на тяхното формиране. Пористостта намалява с повишаване на напрежението (в първия стадий) и слабо се променя с нарастване дебелината на филмите (във втория стадий) на анодирането.

Influence of the D(+)-glucose on the electrochemical deposition of Ag-Bi alloy from a cyanide electrolyte

T. Valkova^{1*}, I. Krastev¹, A. Zielonka²

¹ Institute of Physical Chemistry, Bulgarian Academy of Sciences, 1113 Sofia, Bulgaria

² Forschungsinstitut für Edelmetalle und Metallchemie, 73525 Schwäbisch Gmünd, Germany

Received July 9, 2010, Revised September 24, 2010

The influence of D(+)-glucose on the electrochemical processes of deposition and dissolution of silver, bismuth and silver-bismuth alloy from a cyanide electrolyte are studied by means of cyclic voltammetry.

The addition of D(+)-glucose has no significant influence on the deposition of silver and relatively weak influence on the deposition of bismuth, but a strong negative effect on the stability of the electrolyte. The excess of free cyanide improves the electrolyte stability, the silver deposition is polarized, and the bismuth becomes a more positive element in the system. The addition of the D(+)-glucose and the increase of its concentration leads to a slight decrease in the bismuth percentage in the coatings.

Dull coatings with high bismuth content can be deposited from the investigated electrolyte. Depending on the free cyanide concentration, the deposition of coatings with bismuth content in the whole range from 0 up to 100 wt. % is possible.

Under certain conditions instabilities in the electrochemical system and resulting potential oscillations could be observed.

Key words: electrodeposition; silver-bismuth alloys; oscillations, D(+)-glucose.

INTRODUCTION

Silver-bismuth alloy finds application in electronics, radiotechnics and in the production of coatings, exposed to severe conditions, e.g., friction under high pressure [1,2]. The deposition of this alloy is performed mainly from alkaline electrolytes. The deposition potentials of both metals are relatively close to each other, thus making the alloy deposition not so difficult. The composition of the coatings can be changed depending on the cyanide content in the electrolyte. At a low cyanide concentration, the deposition potential of silver is much more positive than that of bismuth. At a sufficiently high concentration, the deposition potential of silver is strongly shifted in the negative direction, and bismuth becomes the more readily depositing metal. Bismuth deposition is prevailing at the lower current densities [3, 4].

The influence of the electrolyte components and electrolysis conditions on the composition and structure of the alloy have been extensively studied [3- 6]. The properties of single or multi-layered coatings have been described in previous papers [7, 8]. It is known that bismuth and bismuth modified

platinum and palladium electrodes have a strong catalytic effect on the processes of oxidation of various organic substances [9-14]. Particularly appropriate is the use of bismuth in the study of electrochemical oxidation of glucose [12,14,15]. By potentiostatic investigations it has been shown that bismuth can be bonded in complex with glucose or some of its derivatives [12]. Also, well known is the variety of degradation products of glucose in highly alkaline medium [16]. Glucose itself is a desirable additive component in the deposition of some metals and alloys, eg. indium and silver-indium alloys, where its derivatives participate in the formation of complex compounds in alkaline medium, which greatly improves the stability of the electrolytes used [17].

The aim of this work is to study the influence of D(+)-glucose on the electrochemical deposition of Ag-Bi alloys.

EXPERIMENTAL

The composition of the electrolyte for deposition of Ag-Bi alloy coatings is given in Table 1.

Distilled water and *pro analysi* grade reagents were used. The experiments were performed in a

*To whom all correspondence should be sent:
E-mail: tvalkova@ipc.bas.bg

Table 1. Electrolyte composition

Components	Concentration, mol dm ⁻³
Ag as KAg(CN) ₂	0-0.3
Bi as BiNO ₃	0.1
NaOH	0.64
KNaC ₄ H ₄ ·4H ₂ O	0.42
KCN	0-0.1
D(+)-Glucose	0-0.4

glass cell of 100 cm³ at room temperature (298 K) without stirring of the electrolyte. The working electrode (1 cm²) and the two counter electrodes were made of platinum. A reference electrode Ag/AgCl with $E_{\text{Ag/AgCl}} = -0.197$ V against the hydrogen electrode was used. During the experiments, the reference electrode was placed in a separate cell, filled with KCl solution (3 M). It was connected to the electrolysis cell by a Haber-Luggin capillary through a salt bridge, containing KCl solution of the same concentration. All potentials in the present study are given against this reference electrode.

The cyclic voltammetric investigations were performed by means of a computerized potentiostat/galvanostat, PAR 263A (Princeton Applied Research), using the SoftCorr II software for the electrochemical corrosion studies.

The sweep rate of the potential was varied in the range of 0.005 — 1.000 V s⁻¹. The alloy coatings, *ca.*, 10 μm thick, were deposited in an electrolysis cell of 100 cm³. The silver content in the coatings as well as their thickness were determined using a Fischerscope XRAY XDVM-W apparatus for X-ray fluorescence.

RESULTS AND DISCUSSION

It was shown in a previous paper [4] that the deposition potentials of silver and bismuth are close to each other, thus making the deposition of alloy coatings possible. By means of appropriate complex forming agents, the deposition potential of silver can be strongly shifted in the negative direction, so that bismuth deposition becomes predominant. By changing the electrolyte composition and the conditions of the electrolysis, coatings of any desired composition can be obtained. Figure 1 shows the cyclic voltammetric (CVA) curve in absence of KCN in the alloy deposition electrolyte.

In this case, pure silver coatings are deposited at low current densities. Three cathodic reactions are

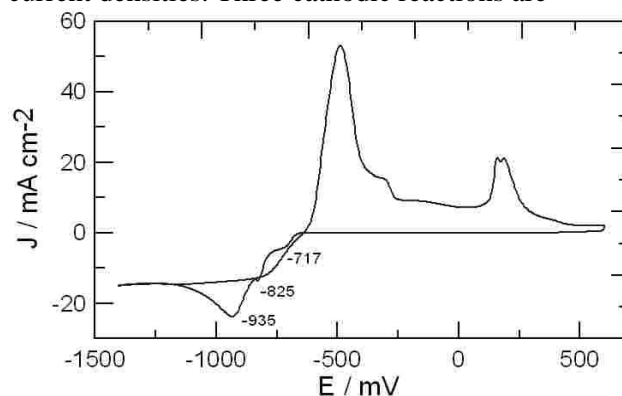


Fig. 1. CVA curves in absence of free cyanide in the electrolyte; $v = 25$ mV s⁻¹, $C_{\text{Ag}} = 0.075$ M; $C_{\text{Bi}} = 0.1$ M; $C_{\text{KCN}} = 0$ M.

observed corresponding to deposition of silver (-717 mV), and deposition of bismuth (-825 mV) and (-935 mV), respectively. The first anodic reaction corresponds to the dissolution of bismuth and the second one to the dissolution of silver. In most cases additional humps to the anodic peaks appear due to incomplete dissolution of the coating and the formation of passive layers, which are dissolved in more positive potentials.

According to the phase diagram of the Ag-Bi alloy [3, 18], the silver crystal lattice could accept up to about 3 wt. % Bi under formation of a solid solution. When the quantity of the co-deposited bismuth exceeds this limit, coatings appear heterogeneous and contain a solid solution of bismuth in silver and pure bismuth [3,5,4]. In many cases, the deposition of phase heterogeneous coatings is related to the onset of instabilities in the electrochemical systems and observation of current or potential oscillations [17, 19, and 20].

Figure 2 presents cathodic current changes with time under potentiostatic conditions at potentials, corresponding to different points of the cyclic voltammetric (CVA) curve. At potentials more positive than -717 mV, the coatings consist of pure silver. With increasing potential in the negative direction, the system reaches the limiting current density for silver, and then the registered currents rapidly increase due to the bismuth co-deposition. On the surface of the electrode the deposition of heterogeneous coating, consisting of darker and lighter areas, is visually observed. The steady state polarization curve, constructed on the basis of the potentiostatic curves, shows different regions, corresponding to different coatings composition (pure silver and Ag-Bi electrolytes). Figure 2 indicates that at potentials, corresponding to the

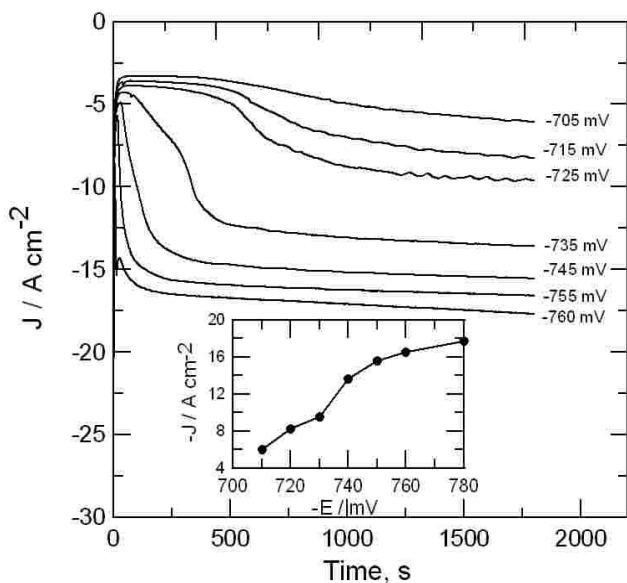


Fig. 2. Cathodic current density during deposition under potentiostatic conditions; (inset stationary polarization curve on the basis of the current transients) $v = 25 \text{ mV s}^{-1}$ $C_{\text{Ag}} = 0.075 \text{ M}$; $C_{\text{Bi}} = 0.1 \text{ M}$; $C_{\text{KCN}} = 0 \text{ M}$

transition from pure silver to alloy deposition (-725 mV), instabilities in the system and oscillations of the cathodic current with time could be observed.

It was shown that, depending on the electrolyte composition and the KCN concentration, the deposition potential of silver could be strongly shifted in the negative direction which results in the preferred bismuth deposition at low current densities [3, 4]. This means that, depending on the concentration of the complex forming agent for silver in the electrolyte, deposition of alloy coatings with bismuth content in a quite broad range is possible. Considering the instability constants for the hydroxide (3.8×10^{-13}) and the mixed hydroxide-tartrate (1×10^{-31}) complexes [21], as well as the high hydroxide content in the electrolyte, it could be presumed that the bismuth deposition process is implemented mainly by the hydroxide and mixed hydroxide-tartrate complexes. The latter are extremely stable, so that the use of other additional complexing agents will not change significantly the deposition potential of bismuth, but may affect the appearance and the structure of the resulting coatings. As such, D(+)-glucose was chosen as substance in these studies.

XPS investigations of bismuth modified platinum electrodes show that Bi species are partially complexed by glucose or its reaction products [12]. Otherwise bismuth electrodes are completely inactive for glucose oxidation, but noble metal catalysts modified with Bi show much better selectivity and activity during the glucose oxidation [12].

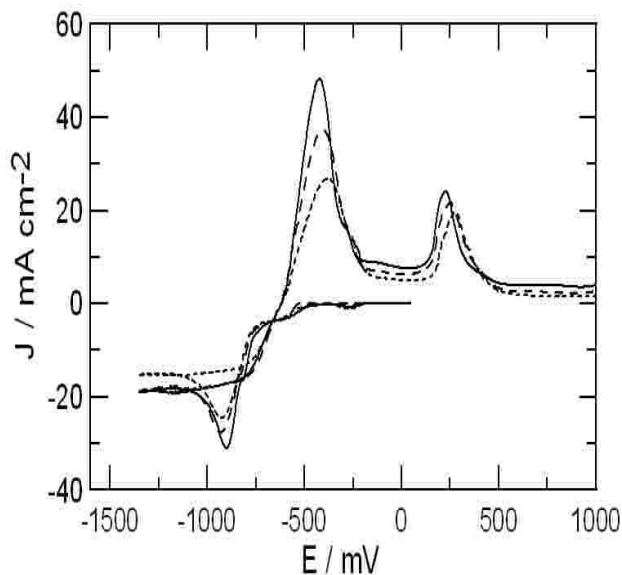


Fig. 3. Effect of $C_{\text{D}(+)\text{-Glucose}}$ in the absence of free cyanide in the electrolyte; $v = 25 \text{ mV s}^{-1}$; $C_{\text{Ag}} = 0.075 \text{ M}$; $C_{\text{Bi}} = 0.1 \text{ M}$; $C_{\text{KCN}} = 0 \text{ M}$; $C_{\text{D}(+)\text{-Glucose}} = \text{---} 0 \text{ M}$; $\text{----} 0.1 \text{ M}$; $\text{.....} 0.3 \text{ M}$

Figure 3 shows the cyclic voltammetric (CVA) curves at different D(+)-glucose concentrations in absence of free cyanide ions in the alloy deposition electrolyte. The increase of the D(+)-glucose concentration leads to a slight polarization and inhibition of the cathodic reactions. A similar conclusion can be made on the basis of the anodic reaction rate at different D(+)-glucose concentrations in the electrolyte. It is obvious that the influence of D(+)-glucose on the deposition of bismuth is not so strong. Probably it is different in a fresh prepared electrolyte compared with a worked electrolyte where the effect of the D(+)-glucose could be stronger. Unfortunately, the addition of D(+)-glucose in absence of free cyanide in the electrolyte lowers its stability and precipitation of silver is observed. The electrolyte becomes dark during one day exploitation. Its stability can be enhanced using appropriate quantities of free KCN as an additional complexing agent for the silver.

The presence of 1 M KCN in the electrolyte leads to additional polarization of the silver deposition with approximately 0.6 V, both in presence or absence of D(+)-glucose. As a result, the silver is deposited at more negative potential than the bismuth, and is dissolved at potentials near to the dissolution potential of the bismuth (Figure 4).

The effect of the D(+)-glucose on the deposition and dissolution processes of silver in the bismuth-free alloy electrolyte in presence of free cyanide is not substantial.

In the silver-free cyanide electrolyte for alloy deposition, the D(+)-glucose exerts some

depolarizing effect and inhibits the cathodic reaction with increasing concentration (Figure 5). This inhi-

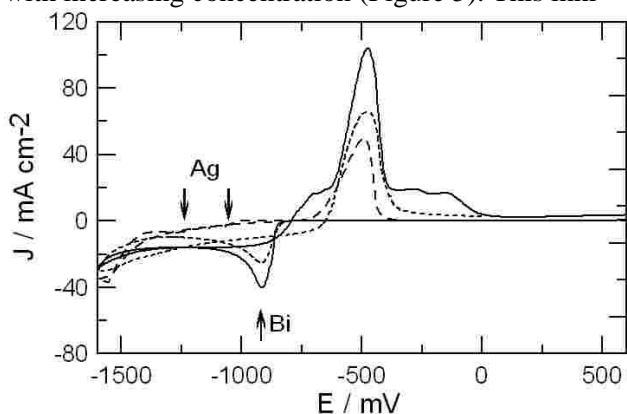


Fig. 4. CVA curves in presence of free cyanide in the electrolyte. $v = 25 \text{ mV s}^{-1}$; $C_{\text{KCN}} = 1 \text{ M}$; $C_{\text{Ag}} = \text{---} 0.075 \text{ M}$ (in absence of Bi); $C_{\text{Bi}} = \text{---} 0.1 \text{ M}$ (in absence of Ag); In the alloy deposition electrolyte $C_{\text{AgBi}} = \text{---} 0.075 / 0.1 \text{ M}$.

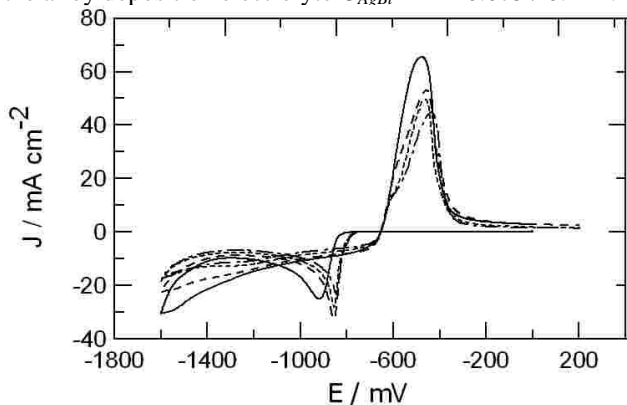


Fig. 5. Influence of $C_{\text{D(+)-Glucose}}$ on the deposition of bismuth in the presence of free cyanide in the electrolyte; $v = 25 \text{ mV s}^{-1}$; $C_{\text{Ag}} = 0.075 \text{ M}$; $C_{\text{Bi}} = 0.1 \text{ M}$; $C_{\text{KCN}} = 1 \text{ M}$; $C_{\text{D(+)-Glucose}} = \text{---} 0 \text{ M}$; $\text{---} 0.1 \text{ M}$; $\text{---} 0.2 \text{ M}$; $\text{---} 0.3 \text{ M}$.

bition results in lower deposition rate of bismuth, which is confirmed by comparing the anodic maxima.

In the presence of 1 M KCN, pure bismuth is deposited at low current densities from the alloy deposition electrolyte (Figure 6). The silver content in the coating increases with the increase in the current density. The effect of D(+)-glucose on the deposition of the alloy is similar to its effect on pure bismuth deposition. On the basis of cyclic voltammetric investigations no conclusions could be drawn about the influence of the D(+)-glucose on the deposition of silver from the alloy electrolyte. The first anodic maximum corresponds to the dissolution of silver. Independently of the presence of silver in the electrolyte, the effect of D(+)-glucose on the anodic process is expressed by the dissolution of smaller quantities of electrodeposited bismuth with increased D(+)-glucose concentration and by the disappearance of the more positive peaks, corresponding to the dissolution of passive bismuth

layers. The dissolution of bismuth is easier and more complete with sufficient amounts of D(+)-glucose in

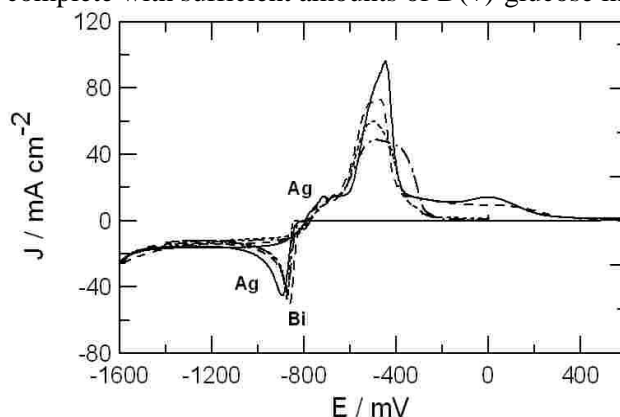


Fig. 6. Influence of $C_{\text{D(+)-Glucose}}$ on the deposition of alloy in the presence of free cyanide in the electrolyte; $v = 25 \text{ mV s}^{-1}$; $C_{\text{Ag}} = 0.075 \text{ M}$; $C_{\text{Bi}} = 0.1 \text{ M}$; $C_{\text{KCN}} = 1 \text{ M}$; $C_{\text{D(+)-Glucose}} = \text{---} 0 \text{ M}$; $\text{---} 0.1 \text{ M}$; $\text{---} 0.2 \text{ M}$; $\text{---} 0.3 \text{ M}$

the electrolyte. It can be concluded that glucose and /or its derivatives affect more strongly the electrochemical processes of deposition and dissolution of bismuth than these of the silver. Possibly, the effect of D(+)-glucose on the alloy deposition corresponds to the case of pure bismuth deposition due to the formation of heterogeneous coatings of solid solution of bismuth in silver and pure bismuth [5].

Independently of the presence of D(+)-glucose in absence of free cyanide in the electrolyte, the deposition system is regular according to Brenner [22]. In the presence of free cyanide with increased concentration of D(+)-glucose, the bismuth content of the coatings slightly decrease, as shown in the cyclic voltammetry experiments. Compact coatings can be deposited in the current densities range from 0.2 to 1 A dm^{-2} with bismuth content between 100 and 50 wt. % (Figure 7).

Higher current densities could be applied when higher metal concentrations in the electrolyte are used. Using a silver concentration of 32 g dm^{-3} in the electrolyte, the deposition of coatings with almost constant composition in a broad range of current densities is possible [5].

The observed structures on the heterogeneous coating surface [5] show the possible existence of some instabilities in the electrochemical system, resulting in current (s. Figure 2) or potential oscillations. The oscillations appear under diffusion controlled deposition of the more positive element in simultaneous deposition of a bismuth richer phase. In general, the galvanostatic potential oscillations are not quite regular (Figure 8), which is an indirect indication that the phases form a pattern of spots and chaotic fronts but not periodic waves on the

electrode surface as is the case of the periodic current oscillations during the potentiostatic deposition of Ag-Sb alloy [19, 20].

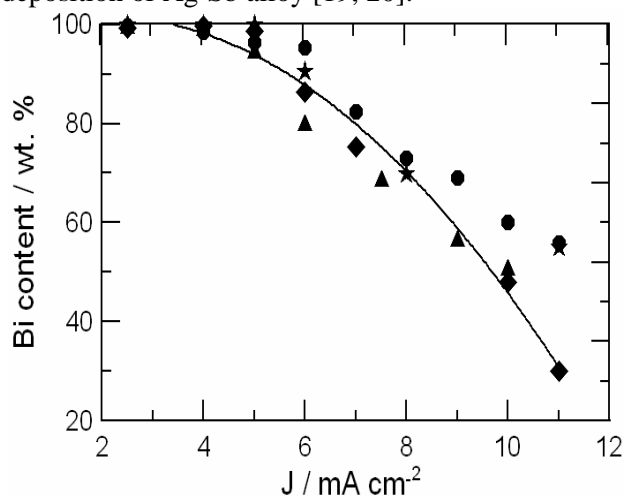


Fig. 7. Influence of the current density and $C_{D(+)-Glucose}$ on the bismuth content in the alloy; $C_{Ag} = 0.075$ M; $C_{Bi} = 0.1$ M; $C_{KCN} = 1$ M; (●) - $C_{D(+)-Glucose} = 0$ M; (★) - $C_{D(+)-Glucose} = 0.025$ M; (◆) - $C_{D(+)-Glucose} = 0.1$ M; (▲) - $C_{D(+)-Glucose} = 0.2$ M.

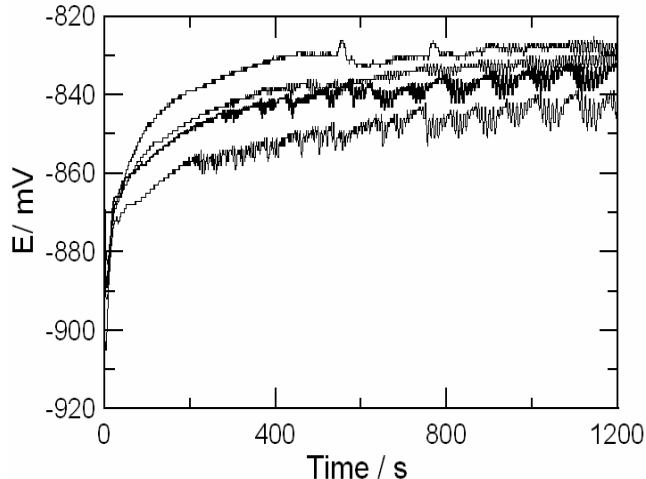


Fig. 8. Potential oscillations during the deposition of the alloy under galvanostatic conditions.; $C_{Ag} = 0.3$ M; $C_{Bi} = 0.1$ M; $C_{KCN} = 1$ M; $C_{D(+)-Glucose} = 0.1$ M

The investigations allow to conclude that the addition of D(+)-glucose to the alkaline electrolyte for deposition of Ag-Bi alloys has no significant influence on the deposition of silver and has relatively weak influence on the deposition of bismuth, with a strong negative effect on the stability of the electrolyte. The excess of free cyanide improves the electrolyte stability, the silver deposition is polarized, a strong depolarization of its dissolution is observed, and the bismuth becomes the more positive element in the system. The addition of the D(+)-glucose and the increase of its concentration leads to a slight decrease in the bismuth percentage in the coatings.

Dull coatings with high bismuth content can be deposited from such an electrolyte. Depending on the free cyanide concentration the deposition of coatings with bismuth content in the whole range from 0 up to 100 wt. % is possible. Under certain conditions instabilities in the electrochemical system and resulting potential oscillations could be observed, which could be of interest for further investigations.

Acknowledgements: The authors would like to thank to the Deutsche Forschungsgemeinschaft (DFG) and the National Science Fund of Republic of Bulgaria for the support (Project 436 Bul 113/97/0-4) and (Project BG051P0001/07/33-02/40).

REFERENCES

1. P.M. Vjacheslavov, S.J. Griliches, G.K. Burkat, E.G.Kruglova, *Galvanotekhnika blagorodnih i redkih metallov*, Mashinostroenie, Leningrad, 1 Ed.,(1970), 5 (in Russian).
2. P.M. Vjacheslavov, *Novie elektrokhimicheskie pokritija*, Lenizdat, Leningrad, I Ed.,(1972), 1 (in Russian).
3. E. Raub, A.E ngel, *Z Metallkunde*, **41** (1950) 485.
4. I. Krastev, T. Valkova, A. Zielonka, *J Appl Electrochem*, **33** 12 (2003) 1199.
5. I. Krastev, T. Valkova, A. Zielonka, *J Appl Electrochem*, **34** 1 (2004) 79.
6. T. Valkova, I. Krastev, *Trans Inst Metal Finish*, **80** 1 (2002) 21.
7. I. Krastev, T. Valkova, A. Zielonka, *Galvanoteknik*, **8** (2005) 1790.
8. I. Krastev, T. Valkova, A. Zielonka, *J Appl Electrochem*, **35** 6 (2005) 539.
9. J. Lee, P. Strasser, M. Eiswirth, G. Ertl, *Electrochim Acta*, **47** 3 (2001) 501.
10. J. Lee, J.Christoph, M. Eiswirth, G. Ertl, *J Chem.Physics*, **115** 3 (2001) 1485.
11. J. Lee, J.Christoph, M. Eiswirth, G. Ertl, *Z Phys Chemie*, **216** 4 (2007) 479.
12. G. Wittstock, A. Stroking, R. Szargan, G. Werne, *J Electroanal Chem.*, **444** (1998) 61.
13. S. Karski, I. Witoska, *J Molecular Catalysis A*, **191** 1 (2003) 87.
14. M. Wenkina, P. Ruizb, B. Delmonb, M. Devillers, *J Molecular Catalysis A*: **180** 1-2 (2002) 141.
15. H.-W. Leia, B. Wua, Ch.-S. Chaa, H. Kitab, *J Electroanal Chem.*, **382** 1-2 (1995) 103.
16. U. Nef, in: D.Ivanov, *Organichna khimija*, Nauka i izkustvo, 6th Ed., Sofia, (1964), 291 (in Bulgarian).
17. Ts. Dobrovolska, I. Krastev, A. Zielonka, *J Appl Electrochem*, **35** (2005) 1245.
18. M. Hansen, K. Anderko, *Constitution of binary alloys*, McGraw-Hill Book Company, Inc., New York, 2nd Ed.,(1958), p. 10.
19. I. Krastev, M. Baumgärtner, Ch.J. Raub, *Metalloberfläche*, **46** 2 (1992) 63.

20. I. Krastev, M.E. Baumgärtner, Ch.J. Raub, *Metalloberfläche*, **46** 3 (1992) 115.
21. *Spravochnik Khimika*, Izdatelstvo Khimija, Moskva, Leningrad, 2nd Ed., Vol. 3, (1964), 119 (in Russian).
22. A. Brenner, *Electrodeposition of Alloys. Principles and Practice*, 2, Academic Press, New York and London, 1 Ed., Vol. 2, (1963), 589.

ВЛИЯНИЕ НА D (+)-ГЛЮКОЗАТА ВЪРХУ ЕЛЕКТРОХИМИЧНОТО ОТЛАГАНЕ НА СРЕБЪРНО-БИСМУТОВИ СПЛАВИ ОТ ЦИАНИДЕН ЕЛЕКТРОЛИТ

Т. Вълкова, Ив. Кръстев, А. Циелонка

¹ *Институт по физикохимия, Българска академия на науките, 1113 София*

² *Изследователски институт за благородни метали и металохимия, 73525 Швебиш Гмюнд, Германия*

Постъпила на 9 юли, 2010 г.; преработена на 24 септември, 2010 г.

(Резюме)

Изследвано е влиянието на D(+)-глюкозата върху електрохимичното отлагане на сребро, бисмут и сребърно-бисмутова сплав от цианиден електролит с помощта на циклична волтамперометрия.

Добавянето на D(+)-глюкоза няма значимо влияние върху отлагането на среброто. То оказва сравнително слабо влияние върху отлагането на бисмут, но има силно отрицателно въздействие върху стабилността на електролита. Излишъкът на свободен цианид подобрява стабилността на електролита, отлагането на сребро се поляризира, а бисмутът става по-положителният елемент в системата. Добавянето на D(+)-глюкоза и повишаването на концентрацията ѝ води до слабо понижение на концентрацията на бисмут в покритията.

От изследвания електролит се отлагат матови покрития с високо съдържание на бисмут. То зависи от концентрацията на свободния цианид в електролита и може да варира между 0 и 100 тегл. %.

В някои случаи се наблюдават неустойчивости в електрохимичната система водещи до осцилации на катодния потенциал.

Gas flow maldistribution in columns packed with HOLPACK packing

S. R. Darakchiev

Institute of Chemical Engineering, Bulgarian Academy of Sciences, Academic G. Bonchev St., Building 103, 1113 Sofia, Bulgaria

Received April 30, 2010; accepted May 25, 2010

HOLPACK packing is the type of horizontal structured packing and is already widely used in the industry. It has good heat and mass transfer characteristics, and good ability to distribute uniformly the flows over the column cross-section. This work reports on the examination of the gas distribution using the so called maldistribution factor, Mf . The uniformity limit and the depth of penetration are determined for the various packing types, differing by dimensions of the packing sheets as well as by distances between the sheets. In arrangement where sheets are distant from each other within the range between 10 and 50 mm, the uniformity limit is at $Mf = 0.19$ and $Mf = 0.18$, and if no distance $Mf = 0.23$.

Key words: packed-bed columns; HOLPACK packing; gas flow maldistribution; maldistribution factor; penetration depth; uniformity limit.

INTRODUCTION

The HOLPACK packing consists of expanded metal sheets, placed horizontally inside the column at a given distance [1, 2] (Fig. 1). To improve the uniform gas and liquid distribution over the column cross-section it is only necessary to alternate the direction of the slits from sheet to sheet, each sheet rotated in the same direction as the previous, to 90° . The packing has shown by far very good efficiency and low pressure drop, and thus it has found industrial application [3–5].

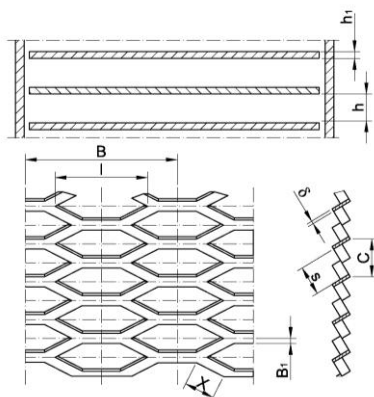


Fig.1. Scheme of the HOLPACK packing arrangement

It is known that a basic problem for the packed columns is the non-uniform flow distribution over the column cross section. This changes the flow velocity and the mass transfer intensity which

results in variable concentrations of the radial direction and reduction of the efficiency. There is a method for determination of the influence of the vapor phase radial maldistribution on the column efficiency in the rectification process [6, 7]. This method is based on data for the maldistribution factor which is an integral indicator that takes into account both the velocity value at a point of the column cross section and the area of the section it occupies. In order to apply this method in columns, using the HOLPACK packing, it is necessary to determine the maldistribution factor for the different heights of the packed layer, and to find its lower value – the so called uniformity limit.

EXPERIMENTAL

The first studies on gas distribution in HOLPACK packed columns are from 1984 [8], and they show the velocity profiles at different heights along the column. The examinations were made with two types of packings that differ by their dimensions and distances between the sheets. The geometric characteristics of the examined packings are given in Table 1, lines 1 to 4. Line 5 shows the characteristics of a packing, examined later.

The present experiments are carried out as gas flow velocity is measured above a packed layer with a given height at two mutually perpendicular diameters, along the axis of the gas inlet device and perpendicularly to it [8]. The velocity was measured by electrical anemometer without a counter current liquid flow. Gas was fed into the

* To whom all correspondence should be sent:
E-mail: s_darakchiev@abv.bg

column with two types of gas inlet devices. Table 1 shows initial distribution data for both types of inlet

Table 1. Geometric characteristics of the studied types of the HOLPACK packings.

Packing No	Hydraulic diameter of the orifices, d_h , mm	Distance between the sheets, h , mm	Thickness of the metal sheet, δ , mm	Thickness of the packing sheet, h_l , mm	Free volume, ϵ
1	6.5	10	0.8	3.0	0.87
2	6.5	50	0.8	3.0	0.87
3	20.8	10	4.0	17.5	0.85
4	20.8	50	4.0	17.5	0.85
5	20.8	0	4.0	17.5	0.85

devices along with the velocity profiles above the packing layers [8]. This gives an idea about the distribution ability of the HOLPACK packing layers. The data [8] show that the packing layers ‘smooth down’ the velocity profile to a uniformity of less than 25 %, having a very high value of the initial maldistribution.

Using the results of these experiments, data was collected to find the dependence of the maldistribution factor from the layer height. These data were processed in order to determine the value of the uniformity limit and the penetration depth.

More recently experiments were carried out with HOLPACK packing but having no distance between the metal sheets, i.e. at $h = 0$ (see line 5 in Table 1). However, measurements were done while changing the packing height.

RESULTS AND DISCUSSION

The packing layer heights at which a uniform distribution of the gas flow is achieved, or the so called penetration depth, are defined based on these experiments [8, 9].

The correlation between the maldistribution factor, Mf and the packing layer height, H , is a very important characteristic in practical terms [9]. Figure 2 shows this correlation for packing No 1 (see Table 1). We see a sharp improvement of the uniformity to a certain value, and then with increase of the layer height, it remains constant. This value of the Mf is called the uniformity limit, and the layer height at which it is obtained is the penetration depth. Thus, the uniformity limit is 0.19 and the penetration depth is 0.6 m for HOLPACK packing No 1.

The maldistribution factor, Mf , is defined as follows [10]:

$$M_f = \sqrt{\frac{1}{n} \sum_{i=1}^n \left(\frac{w_i - w_0}{w_0} \right)^2}, \quad (1)$$

where w is the local gas flow velocity, w_0 – the mean velocity over the column cross section, and n is the number of the experimental points.

The maldistribution is generally divided into two types: large-scale and small-scale [11]. Large-scale maldistribution is due to the initial phase distribution and the formation of local flows such as wall flow or bypass gas flows. Small-scale maldistribution is due to the packing discrete structure and cannot be eliminated. These two types of maldistribution can be easily distinguished on Fig. 2. The section of the curve from $H = 0$ to the depth of penetration is the maldistribution, caused by the gas inlet device, i.e. this is the large-scale maldistribution, and the uniformity limit characterizes the small-scale maldistribution.

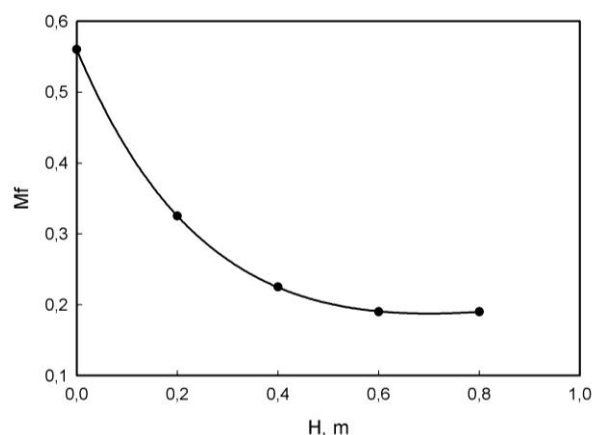


Fig.2. Dependence of the maldistribution factor Mf from the layer height for HOLPACK No 1 at gas velocity $w = 1.8$ m/s.

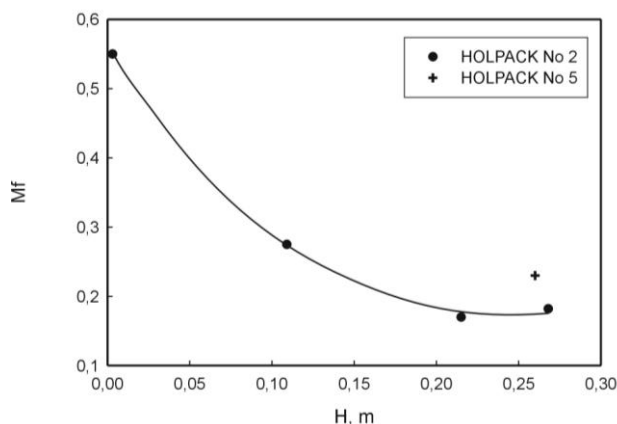


Fig.3. Dependence of the maldistribution factor, Mf , from the layer height for HOLPACK No 2 at gas velocity $w = 1.8$ m/s.

Fig. 3 shows the dependence of the maldistribution factor from the packing height, H , for HOLPACK

packing No 2. A value at which the uniformity remains constant also can be seen. This happens at $Mf = 0.18$, and the height at which it is reached, i.e. the penetration depth, is 0.25 m. The same figure shows as well the value of the maldistribution factor for packing No 5, i.e. with no distance between the sheets. It is $Mf = 0.23$ at $H = 0.26$ m, and it remains the same at $H = 0.63$ m. This gives us grounds to assume that this value remains constant. Obviously, the lack of distance between the sheets does not allow radial distribution as gas passes through the sheets.

As we said above, the minimal values of the maldistribution factor that can be reached are the uniformity limit [9, 12, 13]. They are limited by the small-scale maldistribution which is characterized by the discrete structure of each type of packing

The maldistribution factor values below and above the packing layer at different gas flow velocities [12] are interesting. Such data for packing No 5 are given on Fig. 4. We see the big difference in the Mf value below and above the packing layer. This is probably due to the aerodynamic resistance, spreading coefficient, and the packing type. Therefore, data for the pressure drop, Δp , of several types of the HOLPACK packing are given on next Figure 5.

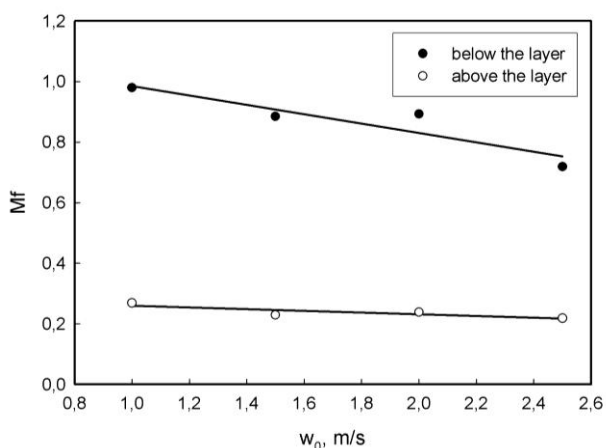


Fig.4. Dependence of the maldistribution factor, Mf , from the mean velocity w_0 at column cross section, measured below and above a layer of HOLPACK No 5 with height of 0.63 m.

Uniformity limit of packings No 3 and No 4 can be determined based on the aerodynamic picture of packings No 1 and No 2. They have the same distance between the packing sheets, similar geometry and similar pressure drop (Fig. 5). Therefore, we can assume that the uniformity limit of packings HOLPACK No 3 and No 4 is also 0.19 and 0.18, respectively.

For HOLPACK packing with distance between the sheets of 20 mm, which is often used in practice, the uniformity limit can be assumed at $Mf = 0.185$.

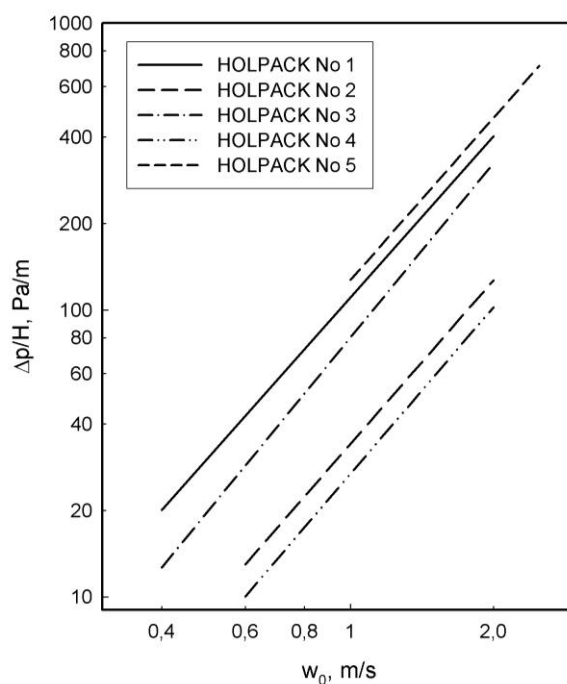


Fig.5. Dependence of the pressure drop at 1 m height of the HOLPACK layer from the gas velocity w_0 .

To determine the value of the Mf for an uniformity limit is not a goal of this paper in itself. It gives a possibility to determine the impact of the gas flow maldistribution on the mass transfer efficiency in a packed column. This can be done using the recently found stochastic model for quantitative evaluation of the influence of vapor phase small-scale maldistribution on the packing efficiency in rectification packed columns based on data for maldistribution factor [6, 7]. The obtained here data for the maldistribution factor at reaching the penetration depth does not change with the increase of the layer height. Therefore, it can be assumed that this lowest value of the Mf characterizes specifically the small-scale maldistribution, caused by the discrete packing structure. In the rectification of ethanol-water system in the range of high ethanol concentrations, the efficiency reduction of the HOLPACK packing is found to be 10 – 12 %. It should be noticed that under the same conditions the efficiency reduction of some modern random packings is between 14 and 38 %, although in general, they show higher mass transfer efficiency. Therefore, non-uniform distribution in gas (vapor) phase is significant in some cases and has to be taken into consideration. The above should be considered when choosing a

packing for a given particular process. The lesser efficiency reduction due to gas maldistribution is another important feature of the HOLPACK packing.

CONCLUSION

In conclusion we can say that the HOLPACK packing, apart from its good heat and mass transfer characteristics, has very good ability to equalize gas flow in packed columns. The packings with distance between the expanded metal sheets make it possible by equalization of velocity profile in radial direction in the space between the sheets. The packings with no distance between the sheets give less opportunity to the gas to spread in all directions. The uniformity limit is found to be 0.19 for packings No 1 and 3 (Table 1), and 0.18 for packings No 2 and No 4. A uniformity limit at $Mf = 0.185$ can be assumed for the HOLPACK packing with distance between the sheets of 20 mm (often used in practice). A uniformity limit is determined at $Mf = 0.23$ (for packing No 5 (Table 1)). These values lead to a comparatively small deterioration of the mass transfer processes, occurred in the columns, packed with HOLPACK packing, because of the gas flow maldistribution.

Acknowledgements This study has been carried out with the financial support received through the Grant Scheme № BG051PO001-3.3.04/30 /28.08.2009 under the Operational Program

“Human Resources Development” 2007–2013, co-financed by the European Social Fund of the European Community.

REFERENCES

1. N. Kolev, R. Darakchiev, Bulgarian Patent No. 16783 / 17.06.1971.
2. N. Kolev, R. Daraktschiev, *Verfahrenstechnik*, **7**, 214 (1973).
3. N. Kolev, R. Darakchiev, L. Kolev, *Теплоенергетика*, **6**, 91 (1975).
4. N. Kolev, R. Darakchiev, K. Semkov, *Water Research*, **30**, 1312 (1996).
5. N. Kolev, R. Darakchiev, K. Semkov, *Ind. Eng. Chem. Res.*, **36**, 238 (1997).
6. S. Darakchiev, PhD Thesis, IChE – BAS, Sofia, 2009.
7. K. Semkov, S. Darakchiev, *Bulg. Chem. Commun.*, **42**, 194 (2010).
8. R. Daraktschiev, *Chem. Eng. Process.*, **18**, 317 (1984).
9. R. Darakchiev, *Chem. Biochem. Eng. Q.*, **18**, 145 (2004).
10. T. Petrova, R. Darakchiev, K. Semkov, S. Darakchiev, *Chem. Eng. Technol.*, **31**, 1723 (2008).
11. P.J. Hoek, J.A. Wesselingh, F.J. Zuiderweg, *Chem. Eng. Res. Des.*, **64**, 431 (1986).
12. R. Darakchiev, Ch. Dodev, *Bulg. Chem. Commun.*, **33**, 237 (2001).
13. Ch. Dodev, R. Darakchiev, Scientific Works of the Higher Institute of Food and Flavor Industries, vol. XLIV (3), 51 (2000).

НЕРАВНОМЕРНОСТ НА ГАЗОВОТО ТЕЧЕНИЕ В КОЛОНИ С ПЪЛНЕЖ HOLPACK

С. Даракчиев

Институт по инженерна химия, Българска академия на науките, ул. “Акад. Г. Бончев” бл. 103, 1113 София

Постъпила на 30 април 2010 г.; приета на 25 май, 2010 г.

(Резюме)

Пълнежът HOLPACK е от типа на хоризонталните структурирани пълнежи и е намерил вече широко приложение в промишлеността. Той притежава добри топло- и масообменни характеристики както и добра способност да разпределя равномерно потоците по напречното сечение на колоната. В настоящата работа е изследвано разпределението на газа с помощта на фактора на неравномерност. Установени са лимита на равномерност и дълбочината на проникване на различните видове пълнежи, различаващи се както по размери на пълнежните листа, така също и по разстоянията между тях. За пълнежите с разстояние между листата 10 и 50 mm, лимита на равномерност е при $Mf = 0,19$ и $Mf = 0,18$, а при липса на разстояние $Mf = 0,23$.

Influence of acid solutes on the phase behaviour of aqueous two-phase systems, containing poly(ethylene glycol) and poly(ethylene imine)

D.S. Yankov*, V.N. Beschkov, R.P. Stateva

Institute of Chemical Engineering, Bulgarian Academy of Sciences, Sofia 1113, Bulgaria

Received March 10, 2010; Accepted July 24, 2010

This paper is part of a study on the possibility of using aqueous two-phase systems (ATPSs) for separation of low-molar-mass organic acids in the biotechnology industry. We present for the first time experimental data on the influence of titrating organic acids on the phase behaviour of the ATPSs, containing poly(ethyleneglycol) (PEG) and poly(ethyleneimine). The underlying hypothesis of the mechanism advanced is discussed from the point of view of the acid structure, and is validated by the observed ATPSs phase behaviour. Finally, we demonstrate the opposing influence of the lactic acid and titrating acids in these systems.

Key words: ATPS; poly(ethyleneglycol); poly(ethyleneimine); organic acid solutes; lactic acid.

1. INTRODUCTION

Aqueous two-phase systems (ATPSs), consisting of two structurally different polymers like poly(ethyleneimine) (PEI) and either poly(ethyleneglycol) (PEG) or hydroxyethylcellulose (HEC), are extensively employed for the bioseparation of low-molar-mass organic acids [1 – 4] since they provide the possibility to obtain high equilibrium concentration of the desired product in the PEI-rich phase through acid-base association.

In recent contributions [5, 6], devoted to a systematic study on ATPSs for the separation of lactic acid (LA), we have examined the phase behaviour of (PEG+PEI) ATPSs as a function of key variables such as temperature, pH and lactic acid concentration. Our work was motivated by the fact that PEI forms a two-phase system with a neutral (uncharged) polymer, such as PEG, only when strong bivalent or polyvalent counter-ions to the charges on the polycation are introduced [1,2,4]. To the best of our knowledge, our paper [6] was the first to illuminate in details the influence of anions such as phosphate and sulphate on the phase diagrams of (PEI + PEG) ATPSs and to propose a mechanism, explaining the experimentally observed phase behaviour.

The purpose of this work is to contribute further to the experimental evidence and expand the ideas, advocated in [6] by offering new insights on the influence of an acid solute on the phase behaviour

of (PEI+PEG) ATPSs.

To realize that, we will firstly focus on the experimental validation of the suggested mechanism by examining yet again how the nature of an inorganic acid solute, used in titrating the PEI, influences the phase formation of the (PEI+PEG) ATPSs. According to the assumptions of our hypothesis [6] which have been confirmed experimentally, a higher valency titrating acid expands the two-phase region, while mono-valent acids (such as HCl and HClO₄) do not form an ATPS with the neutral PEG at any concentrations (we have tried up to 30 mass percent of each polymer). To substantiate further these ideas by new experimental data we have chosen to examine the influence of boric acid because it is of uncertain valency in water solutions. Thus, by experimentally locating where the binodal of the boric acid titrated ATPS will be situated in the compositional phase space (relevant to the ATPSs of the other two acid solutes), we will test the viability of the phase-formation mechanism advocated.

Then we expand further the scope of the mechanism application by studying how an organic acid solute will influence the (PEG+PEI) ATPSs phase formation. The reasons behind that are three-fold: *i*) To obtain new experimental evidence. To the best of our knowledge, so far, organic acids have not been used as PEI titrating acids, and hence there are no data on how they might influence the phase behaviour of the (PEG+PEI) ATPSs; *ii*) From theoretical point of view it is important to investigate how solutes with different molecular structures, representatives of the very large variety

* To whom all correspondence should be sent:
E-mail: yanpe@bas.bg

of organic acids, will affect the ATPSs phase formation; *iii*) To expand the verification of the (PEG+PEI) ATPSs phase formation mechanism, applying the new experimental data obtained.

In the view of this, and by analogy with the inorganic acid solutes, we have chosen the following organic acids: citric, oxalic, succinic, malic, and tartaric ones (Figure 1). Thus, the influence of the nature of the organic solutes, manifested either by the acid chain length (i.e. molecular structure influence) or by the number of present OH groups (i.e. the ability to form additional H⁺ bonds), will be examined. In the first case, oxalic and succinic acids will be applied as titrating acids, while in the second – citric, succinic, malic, and tartaric acids will be studied.

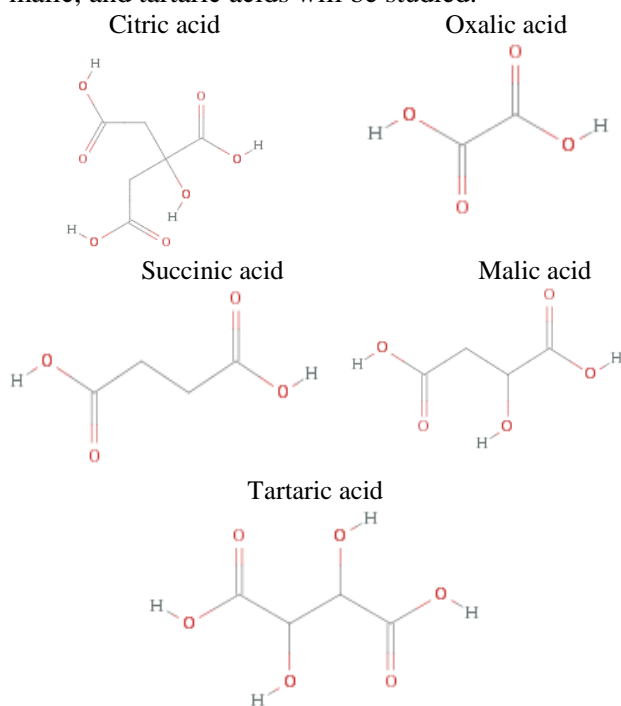


Figure 1. Structure of the organic acids, applied in this study.

Finally, the effect of addition of a second acid, lactic acid, on the phase behaviour will be examined and compared for the cases of H₂SO₄ and tartaric acid, used to titrate the PEI.

2. EXPERIMENTS

2.1. Materials and Methods

PEG 4000 was obtained from Fluka. It is a narrowly distributed technical product, with a polydispersity index of about 1.05 as determined in this study by gel permeation chromatography (GPC). PEI was obtained from Aldrich. According to the manufacturer, the number-average molar mass M_n of the PEI was approximately 10000

g·mol⁻¹ by GPC, and the mass-average molar mass M_w was approximately 25000 g·mol⁻¹ by light scattering; so the PEI sample was characterised by a polydispersity index of about 2.5.

Stock solutions of the polymers in distilled water were prepared gravimetrically on an analytical balance. For the PEG, the mass fraction (*w*) of the stock solution was 0.4, while for PEI a mass fraction of 0.2 was chosen. The PEI solutions were titrated with the inorganic acid solutes (H₂SO₄, H₃PO₄ and H₃BO₃), and with the organic acid solutes to pH = 7.5; in all cases with uncertainties of approximately ±0.05 pH units.

Since concentrated lactic acid solution contains high levels of dimers, it was first diluted tenfold and then boiled under reflux for 8 to 10 h to hydrolyse the dimers. The resulting solution, containing about 130 g·L⁻¹ lactic acid, was further diluted to obtain a stock solution of known concentration for use in the preparation of the quaternary ATPS.

All stock solutions were prepared gravimetrically on an analytical balance with ± 0.0001 g accuracy. The expanded uncertainty of all gravimetric measurements was ± 5.3·10⁻⁴ g with coverage factor of 2.

2.2. Experimental Procedure.

ATPS Preparation

All ATPSs were prepared gravimetrically by mixing appropriate quantities of the necessary stock solutions with distilled water in 50 ml beakers. For determination of the binodal curves, a glass vessel with a volume of 125 ml was used. It was provided with an external jacket through which water at a constant temperature of (36.0 ± 0.1) °C was circulated.

For the preparation of the quaternary ATPSs, stock solutions for PEG and PEI were made like the above but with the addition of either 4.3 or 8.6 g·L⁻¹ of lactic acid, when the PEI was titrated with H₂SO₄, or with addition of either 4.85 or 8.70 g·L⁻¹ of lactic acid when the PEI was titrated with tartaric acid. These particular concentrations were chosen to exemplify the concentration range in which the inhibitory effect of lactic acid was manifested.

Determination of the Binodal Curves

In our experiments, the binodal curve was approximated by the cloud-point curve, determined by dropwise addition of water to the well stirred ATPSs, prepared as described above, until turbidity

Table 1. The coefficients of equation (1) for the binodal curves of the (PEG+PEI) ATPSs in which PEI was titrated with different acids to pH = 7.5.

Titrating Acids	Coefficients		
	<i>a</i>	<i>b</i>	<i>c</i>
Phosphoric acid	16.5771	1.3533	$1.6446 \cdot 10^{-4}$
Sulphuric acid (no LA)	15.2028	0.6665	$7.5751 \cdot 10^{-4}$
$c_{\text{LA}} = 4.3 \text{ g}\cdot\text{L}^{-1}$	51.1574	0.9620	$7.0714 \cdot 10^{-4}$
$c_{\text{LA}} = 8.6 \text{ g}\cdot\text{L}^{-1}$	59.9603	0.8618	$9.7091 \cdot 10^{-4}$
Boric acid	50.3827	0.8100	$3.8722 \cdot 10^{-4}$
Tartaric acid (no LA)	15.2028	0.6665	$7.5751 \cdot 10^{-4}$
$c_{\text{LA}} = 4.85 \text{ g}\cdot\text{L}^{-1}$	40.2332	0.8226	$7.9867 \cdot 10^{-4}$
$c_{\text{LA}} = 8.7 \text{ g}\cdot\text{L}^{-1}$	36.0429	0.7231	$1.0540 \cdot 10^{-4}$
Oxalyc acid	17.0781	0.6581	$4.8062 \cdot 10^{-4}$
Succinic acid	22.6295	0.5867	$8.2416 \cdot 10^{-4}$
Malic acid	17.9718	0.6123	$1.2048 \cdot 10^{-4}$

disappeared and the solution became transparent, which indicated the transition from heterogeneous to homogeneous phase behaviour. All solutions were maintained at $(36.0 \pm 0.1)^\circ\text{C}$ in a temperature controlled glass vessel. The composition of the last point in the two-phase region and the composition of the first point in the homogeneous region were determined gravimetrically, and the mean value of the two was taken as a point on the binodal. This typically introduced an ambiguity not worse than $\pm 0.005 \cdot w_i$ in the binodal composition.

Then a polymer solution (either PEI or PEG) was added to the homogeneous phase in a drop wise manner until turbidity appeared. The system was allowed to rest until a complete separation was assured before water was added again to transfer it to the homogeneous region. The process was repeated until the binodal was determined. This mechanism of the binodal determination assures a clear-cut distinction of phase separation and excludes precipitation/aggregation.

The binodal curves of the quaternary ATPSs were determined in the same way. However, lactic acid stock solution was used throughout in place of pure water in order to maintain a constant lactic acid concentration, either $c_{\text{LA}} = 4.3$ or $8.6 \text{ g}\cdot\text{L}^{-1}$, when the PEI was titrated with H_2SO_4 , or $c_{\text{LA}} = 4.85, 8.70 \text{ g}\cdot\text{L}^{-1}$ when the PEI was titrated with tartaric acid.

All experiments and measurements were conducted at least in triplicates.

For the ATPSs, examined in this study, the binodal curves were correlated with the following equation [7]:

$$w_2 = a \exp(-bw_1^{0.5} - cw_1^3) \quad (1)$$

where w_1 and w_2 are the mass fractions of PEG and PEI, respectively, and a , b and c are coefficients.

The coefficients of Eq. 1 for the binodal curves of the ATPSs in which PEI was titrated with different acids at pH = 7.5, are given in Table 1.

3. RESULTS aND DISCUSSION

Influence of the PEI Titrating Acid

The assumptions of the mechanism, explaining the experimentally observed phase behaviour of (PEG+PEI) ATPSs [6], can be briefly summarized as follows: PEI is a strong polybase which behaves markedly different from the corresponding monomers and other polybases, even at high ionic strength, and its behaviour is accounted for by: (a) the branched structure of the polymer, containing three different types of amine group; (b) strong inter- and intra-molecular electrostatic and hydrogen-bonding interactions between the various amine groups; and (c) the pH-dependent structure of the polymer in aqueous solution [8]. At low pH values, mutual charge repulsion leads to expansion of the polyion, while in the higher pH range, the polymer contracts due to hydrogen bonding. Further protonation for $\text{pH} < 3$ is precluded by strong electrostatic repulsions between the charged groups, which, depending on the type of acid used, corresponds to approximately 70 % protonation [9]. These changes in the PEI molecule conformation

will influence the interaction between the charged polymer and the solvent (water) and the uncharged polymer (PEG), and consequently will expand or contract the two-phase region of the phase diagram.

We also advanced the hypothesis that the change in PEI molecular conformation alone is not sufficient to lead to two-phase formation and that there is another factor, most probably related to the nature of the titrating acid. Thus, we suggested that the addition of polyvalent anions, as part of the titrating acid, influences the ability of PEI molecules to form aggregates either by H-bonding or by cross-linking. Aggregation of PEI molecules would clearly enhance the incompatibility of the two polymers and would lead, in its turn, to an expansion of the two-phase region. Obviously, different titrating acids will stabilize (promote) to a different extent the aggregation process [6].

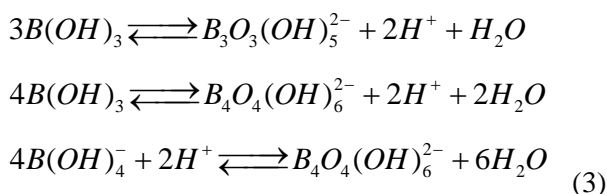
3.1. Inorganic Acid Solutes

We have shown experimentally that when phosphoric acid is used to titrate the PEI, the resulting ATPS has a larger two-phase region compared to the case when sulphuric acid is applied, because the aggregation of PEI molecules (via cross-linking) in the case of H₂SO₄ is less pronounced [6]. Thus, the question is how titrating the PEI with boric acid will influence the phase behaviour of the PEG+PEI ATPS.

It is well known that boric acid, H₃BO₃, (or better boron trihydroxide B(OH)₃) is a weak acid. It behaves more like a Lewis, than a Brønsted acid. In an aqueous solution boric acid does not dissociate but interacts with water molecules to form tetrahydroxyborate ion:



Monomeric species can exist under the limited conditions where the total concentration of boron is less than 0.025 M, while polymeric ions prevail at higher concentration and at high pH. Different polyborate ions can be formed, for example [10, 11]:



According to the above, in the conditions of our experiment (pH = 7.5 and high boric acid concentration), boric acid anions with valency of 1 and 2 are present in the solution. Hence, within the

light of the phase formation mechanism advocated, it is expected that the phase behaviour of the boric acid PEI titrated ATPS will be an intermediate one, namely between that of an HCl/HClO₄ titrated PEI (no two phase region) and H₂SO₄ titrated PEI. This is because the PEI cross linking will be even less pronounced than when H₂SO₄ is used, and therefore the two-phase region will be smaller. Our experiments confirmed that, the boric acid PEI titrated ATPS' binodal is situated in the concentration phase space to the right of the H₂SO₄ phase.

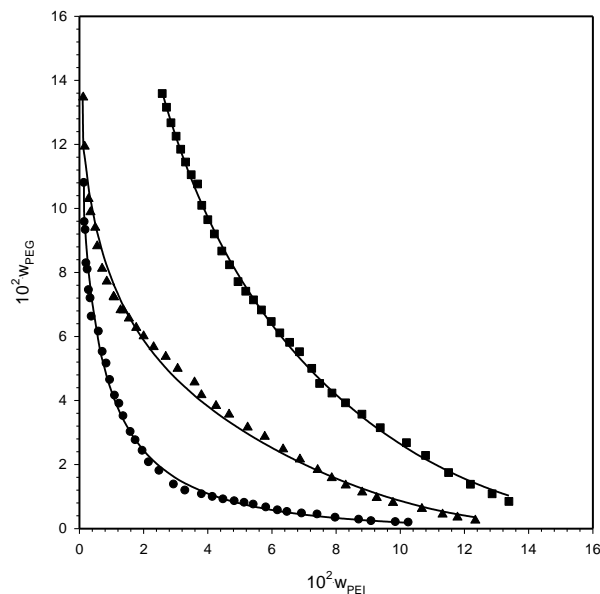


Fig. 2. Binodal curves for the (PEG + PEI) ATPSs at pH = 7.5 and $T = 36$ °C, experimental: (●) H₃PO₄; (▲) H₂SO₄; (■) H₃BO₃; (—) calculated binodals from Eq 1.

Figure 2 shows the influence of H₃PO₄, H₂SO₄ and boric acid as PEI titrating acids on the (PEG+PEI) ATPS phase formation.

3.2. Organic Acid Solutes

To examine how organic acid solutes influence the ATPSs formation we firstly chose tartaric and citric acids as analogues (same number of H, same valency of the anions) of H₂SO₄ and H₃PO₄. It should be noticed that we were not able to determine the ATPS binodal curve when citric acid was used to titrate the PEI. The reason behind this is the high concentration of the citric acid in the PEI solution (needed to obtain the required pH) when PEG was added. The resulting system was at least three phase (at this concentration citric acid forms ATPS with PEG). Applying the technique outlined above the binodal curve could not be determined.

When tartaric acid was used to titrate the PEI, the binodal curve of the resulting (PEG+PEI) ATPS was determined without any difficulty. Moreover, when compared with the binodal of the (PEG + H₂SO₄ PEI titrated) ATPS, the two-phase regions of the two ATPSs completely coincided (**Figure 3**). Although this fact might be unexpected at a first glance, still it does not contradict the assumptions of our mechanism contributing the phase formation in this particular case to the PEI cross-linking.

However, we believed that this line of behaviour

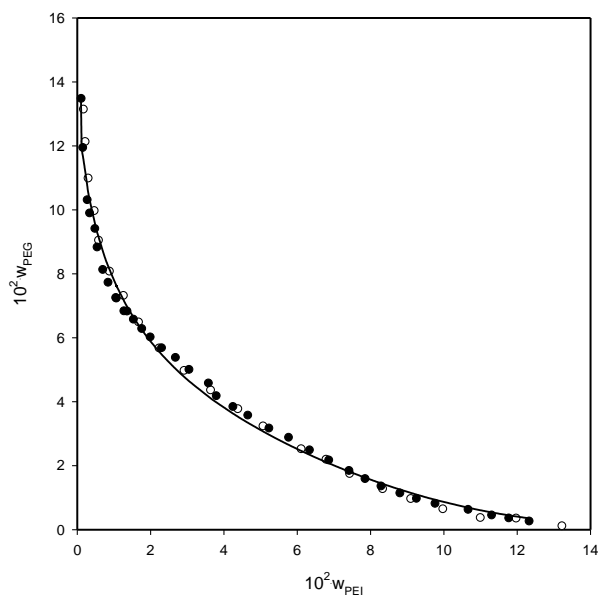


Fig. 3. Binodal curves for the (PEG + PEI) ATPSs at pH = 7.5 and $T = 36$ °C, experimental: (●) H₂SO₄; (○) tartaric acid; (—) calculated binodals from E. 1.

should be further examined in more details. In view of this, new series of experiments with other organic acids, used to titrate the PEI solution, were performed. The organic acid solutes were chosen in such a way that will represent a diversified selection of acids with either different chain length or different number of OH groups. We believe that those two factors play a dominant role in the ATPSs phase formation mechanism: the chain length represents the difference in the molecular configuration of the acid solutes, and has an important influence on the strength of the PEI aggregates (the latter are a result of a bridge formation between two polymer chains), while the number of the OH groups influence on the aggregation via H-bonding.

3.2.1. Influence of the Chain Length

We chose two acids, succinic and oxalic, for our study of the influence of chain length on the ATPS phase formation. Each of them has two carboxylic groups but different chain length (Figure 1). The

resulting binodals are presented on Figure 4. The oxalic acid PEI titrated ATPS has a larger two-phase region than the one with the succinic acid titrated PEI but smaller than the tartaric acid titrated PEI (Figure 4). The explanation within the light of the mechanism suggested is the following: the shorter the acid solute's chain, the more rigid is the polymer aggregate formed. Hence the two polymers become more incompatible which, in its turn, leads to an expansion of the two-phase region.

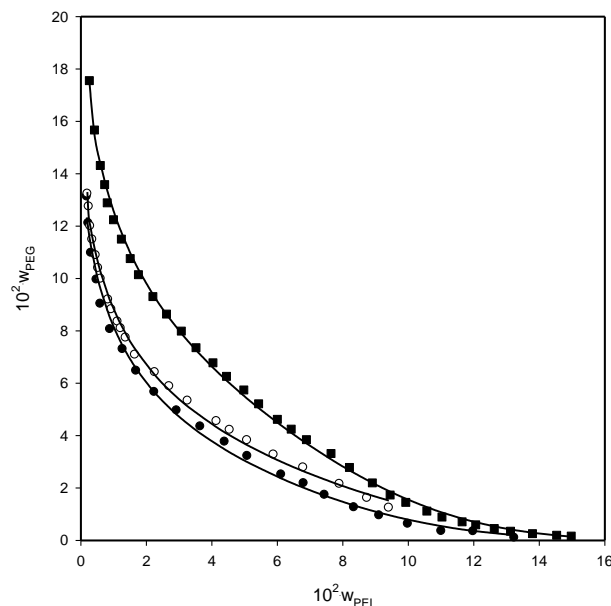


Fig. 4. Binodal curves for the (PEG + PEI) ATPSs at pH = 7.5 and $T = 36$ °C, experimental: (●) tartaric acid; (○) oxalic acid; (■) succinic acid; (—) calculated binodals from Eq 1.

However, the comparison of the two binodals against the tartaric acid PEI titrated ATPS binodal, points to the fact that the chain length is not the single factor influencing the phase formation. Both, succinic and tartaric acids, have four C atoms. Obviously, both the presence of OH groups and their number, influence the ability of PEI molecules to aggregate via H-bonding.

3.2.2. Influence of the Number of OH Groups Present

In view of the above, we examined tartaric, malic and succinic acids. These acids have the same number of C atoms but different number of OH groups. The largest two-phase region is formed when PEI is titrated with tartaric acid, and the smallest – with the succinic (the tartaric has two OH groups and the succinic - none). The results obtained are shown on **Figure 5** and they comply completely with the mechanism, advocated by us.

Namely, the possibility of PEI molecules to form aggregates via H-bonding is greater when the number of the OH groups, present in the acid solute, is bigger. The latter either increases the rigidity of the PEI aggregates or their molar mass, which in its turn leads to increasing the incompatibility between the neutral PEG and the charged PEI, and expands the two-phase region.

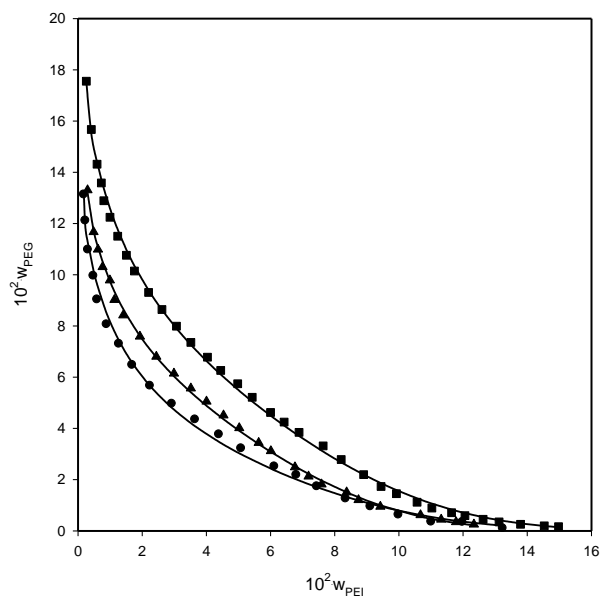


Fig. 5. Binodal curves for the (PEG + PEI) ATPSs at pH = 7.5 and $T = 36\text{ }^{\circ}\text{C}$, experimental: (●) tartaric acid; (▲) - malic acid; (■) succinic acid; (—) calculated binodals from Eq. 1.

3.3. Influence of the Lactic Acid

In our previous work [6] we demonstrated that the addition of Lactic Acid (LA) has a negative effect on the ATPS phase formation (the two-phase region contracts). This was attributed to the destabilization of the PEI polymer aggregates, probably as a consequence of displacement of the polyvalent acid

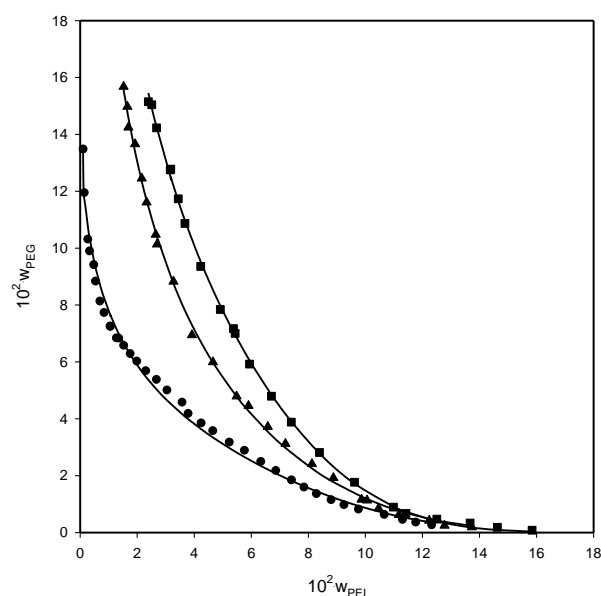


Fig. 7a. Binodal curves for the (PEG + PEI) ATPSs at pH = 7.5 and $T = 36\text{ }^{\circ}\text{C}$, experimental: (●) for the PEI titrated with H_2SO_4 , no lactic acid present; (▲) $c_{\text{LA}} = 4.3\text{ g}\cdot\text{L}^{-1}$; (■) $c_{\text{LA}} = 8.6\text{ g}\cdot\text{L}^{-1}$; (—) calculated binodals from Eq. 1.

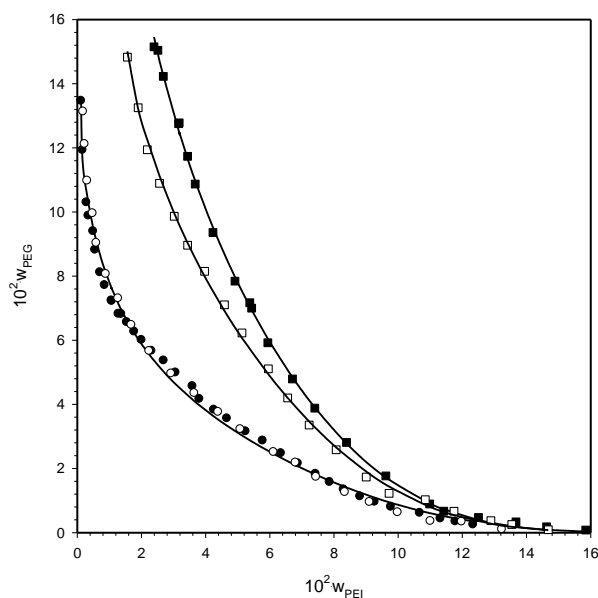


Fig. 6. Binodal curves for the (PEG + PEI) ATPSs at pH = 7.5 and $T = 36\text{ }^{\circ}\text{C}$, experimental: (●) for the PEI titrated with H_2SO_4 , no lactic acid present; (○) for the PEI titrated with tartaric acid, no lactic acid present; (■) for the PEI titrated with H_2SO_4 and $c_{\text{LA}} = 8.6\text{ g}\cdot\text{L}^{-1}$; (□) for the PEI titrated with tartaric acid and $c_{\text{LA}} = 8.7\text{ g}\cdot\text{L}^{-1}$; (—) calculated binodals from Eq. 1.

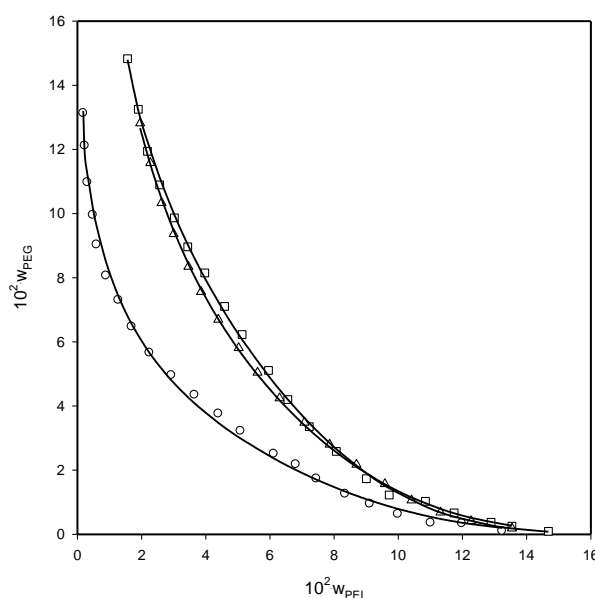


Fig. 7b. Binodal curves for the (PEG + PEI) ATPSs at pH = 7.5 and $T = 36\text{ }^{\circ}\text{C}$, experimental: (○) for the PEI titrated with tartaric acid, no lactic acid present; (Δ) $c_{\text{LA}} = 4.85\text{ g}\cdot\text{L}^{-1}$; (□) $c_{\text{LA}} = 8.7\text{ g}\cdot\text{L}^{-1}$; (—) calculated binodals from Eq. 1

anions. As a result, the aggregating and cross-linking is decreased. To further explore how the addition of a second acid solute influences the ATPS phase formation we have compared the addition of LA to ATPSs titrated either with H₂SO₄ or with tartaric acid. As shown above, the two-phase regions of the two ATPSs coincide when there is no LA present (Figures 6 and 7).

The influence of LA on the phase formation of the ATPSs where PEI is titrated with tartaric acid is less pronounced (Figure 6). The two-phase region contracts to a lesser extent than that of the H₂SO₄ PEI titrated ATPS. The explanation of this fact within the light of the mechanism suggested is that though LA destabilizes the polymer aggregates by destructing the bridges between two polymer chains, still the additional stabilizing effects, caused by the H-bonding (presence of OH groups), prevail as demonstrated in the case of tartaric acid titrated PEI ATPS.

To further confirm the H-bonding effect we have studied the influence of different lactic acid concentrations on the phase formation of H₂SO₄ PEI titrated ATPSs and tartaric acid PEI titrated ATPSs (Figures 7a and 7b). Unlike the H₂SO₄ PEI titrated ATPSs, when different concentrations of LA are added, the change in the two-phase regions of the tartaric acid titrated ATPSs is negligible. The latter indicates that the stabilizing effect of the OH groups is more important and prevails over the destabilizing of the PEI polymer aggregates, caused by the addition of lactic acid.

4. CONCLUSIONS

This study offers new experimental data on the influence of organic acid solutes on the phase behaviour of aqueous solutions, containing PEG and PEI. Also, a detailed and thorough analysis of the application of the phase formation mechanism, advocated previously, is performed, and the influence of the chain length and number of OH groups of the organic acids is demonstrated. Finally, the effect of the addition of a second acid, the lactic acid, on the ATPS phase formation is also briefly discussed.

Our future research will be focused on obtaining further experimental evidence for the viability of the hypothesis advocated. One possible option is to explore how the molar mass of PEI solutions changes when titrated with a range of acid solutes (both organic and inorganic) to different pH. The change in the molar mass will be calculated out from the changes in the viscosity of PEI solutions of different concentrations.

Acknowledgements: The authors would like to acknowledge with gratitude the financial support of the NSF-Bulgaria, Grant X-1416.

REFERENCES

1. U. Dissing, B. Mattiasson, Poly(ethyleneimine) as a phase-forming polymer in aqueous two-phase systems. *Biotechnol. Appl. Biochem.* 17 (1993) 15–21.
2. U. Dissing, B. Mattiasson, Cultivation of *Lactococcus lactis* in a polyelectrolyte–neutral polymer aqueous two-phase system, *Biotechnol. Lett.* 16 (1994) 333–338.
3. J. Planas, A. Kozlowski, J.M. Harris, F. Tjerneld, B. Hahn-Hägerdal, Novel polymer–polymer conjugates for recovery of lactic acid by aqueous two-phase extraction, *Biotechnol. Bioeng.* 66 (1999) 211–218.
4. J. Kwon, R. Kaul, B. Mattiasson, Extractive lactic acid fermentation in poly(ethyleneimine)-based aqueous two-phase system, *Biotechnol. Bioeng.* 50 (1996) 280–290.
5. D.S. Yankov, R.P. Stateva, J.P.M. Trusler, G.St. Cholakov, Liquid–Liquid Equilibria in Aqueous Two-phase Systems of Poly(ethylene glycol) and Poly(ethyleneimine). *Experimental Measurements and Correlation J. Chem. & Eng. Data* 51 (2006) 1056–1061.
6. D.S. Yankov, J.P.M. Trusler, R.P. Stateva, G.St. Cholakov, Influence of pH and Acid Solutes on the Phase Behaviour of Aqueous Solutions Containing Poly(ethylene glycol) and Poly(ethyleneimine), *Biochemical Engineering Journal* 48 (2009) 104–110.
7. J.C. Merchuk, B.A. Andrews, J.A. Asenjo, Aqueous two-phase systems for protein separation studies on phase inversion, *J. Chromatogr. B* 711 (1998) 285–293.
8. A. von Zelewsky, L. Barbosa, C. W. Schläpfer, Poly(ethylenimines) as Brønsted bases and as ligands for metal ions, *Coordination Chemistry Reviews*, 123 (1993) 229–246.
9. G.M. Lindquist, R.A. Stratton, The role of polyelectrolyte charge density and molecular weight on the absorption and flocculation of colloidal silica with polyethyleneimine, *J. Colloid and Interface Science* 55 (1974) 45–59.
10. R. E. Mesmer, C. F. Baes, F. H. Sweeton, Acidity Measurements at Elevated Temperatures. VI. Boric Acid Equilibria, *Inorganic Chemistry*, 11 (1972) 537–543.
11. N. Ingri, Equilibrium Studies of Polyanions 8. On the First Equilibrium Steps in the Hydrolysis of Boric Acid, a Comparison between Equilibria in 0.1 M and 3.0 M NaCl₄, *Acta Chemica Scandinavica*, 16 (1962) 439–448.

ВЛИЯНИЕ НА КИСЕЛИНИ ВЪРХУ ФАЗОВОТО ПОВЕДЕНИЕ НА ВОДНИ ДВУФАЗНИ СИСТЕМИ, СЪДЪРЖАЩИ ПОЛИЕТИЛЕН ГЛИКОЛ И ПОЛИЕТИЛЕН ИМИН.

Д. Янков, В. Бешков, Р. Статева

Институт по инженерна химия, Българска академия на науките, 1113 София, България

(Резюме)

Тази статия е част от изследвания, посветени на изучаване на възможността за използване на водни двуфазни системи (ВДС) за разделяне на органични киселини с ниска молекулна маса. За първи път са представени експериментални данни за влиянието на титруващата киселина върху фазовото поведение на ВДС, съдържащи полиетилен гликол и полиетилен имин. Основната хипотеза на предложения механизъм е дискутирана от гледна точка на структурата на киселините и е потвърдена от наблюдаваното фазово поведение на ВДС. Показано е противоположното въздействие на млечната киселина и титруващата киселина в тези системи.

On analyzing DNA sequences

Parisa Farhami and Ali Reza Ashrafi*

Institute for Nanoscience and Nanotechnology, University of Kashan, Kashan 87317-51167, I. R. of Iran

Received January 5, 2010; accepted May 21, 2010

A DNA sequence can be identified with a word over the alphabet $W = \{A, C, G, T\}$. He and Wang presented an algebraic method for analyzing the DNA sequences. We discuss in this paper the model of Randić, Vračko, Nandy and Basak to extend some results of He and Wang.

Keywords: DNA sequence ; DNA sequence matrix.

INTRODUCTION

The extremely long DNA molecule is actually made of a long string of chemical building blocks called “nucleotides.” There are four different nucleotides, which are labeled: adenine (A), thymine (T), guanine (G), and cytosine (C). A DNA sequence is a succession of the letters A, C, G, and T, representing these four nucleotide bases of the DNA strand.

DNA computing is a form of computing which uses DNA, biochemistry and molecular biology instead of the traditional silicon-based computer technologies. DNA computing is fundamentally similar to the parallel computing in that it takes advantage of many different molecules of the DNA to try many different possibilities at once. Generally, in DNA computing, the DNA sequences used for the computation should be critically designed in order to reduce error that could occur during computation.

Since 2000, Randić’s research group had proposed several visualization schemes for the DNA sequences [1–8]. In one of his methods, the four vertices, associated with a regular tetrahedron, are assigned to four nucleotides. The mapping between four nucleotides and the corresponding 3–D coordinates is shown below:

$$(1-1, -1) \rightarrow A, \quad (-1,1, -1) \rightarrow G, \quad (-1, -1,1) \rightarrow C, \\ (1,1,1) \rightarrow T.$$

For a positive integer n , the \mathcal{D}_n denotes the set of all DNA sequences of length n and $\mathcal{D} = \cup_{n \geq 1} \mathcal{D}_n$. Suppose $\Sigma = \{A, C, G, T\}$, $w = x_1x_2\dots x_n$ is a DNA sequence of length n and $L_i(w) = |\{j \mid 1 \leq j \leq i \ \& \ x_j = L\}|$, where $L \in \Sigma$. Our other notations are

standard and taken mainly from [9].

MAIN RESULTS AND DISCUSSION

He and Wang [10] considered the coordinates of a graphical representation of the DNA sequence, introduced by Zhang [11]. They presented an action of the symmetric group S_4 on Z -curves and the DNA matrices, and proved that the information entropy is invariant under the action of S_4 . In this section, we consider another model, presented by Randić and his group [8], and extend the results given by He and Wang, mentioned above. We name the model, presented by Randić et al, RVNB Model. We first consider the following matrix equations:

$$\begin{pmatrix} A_i \\ G_i \\ C_i \\ T_i \end{pmatrix} = \frac{i}{4} \begin{pmatrix} 1 \\ 1 \\ 1 \\ 1 \end{pmatrix} + \frac{1}{4} \begin{pmatrix} 1 & -1 & -1 \\ -1 & 1 & -1 \\ -1 & -1 & 1 \\ 1 & 1 & 1 \end{pmatrix} \begin{pmatrix} x_i \\ y_i \\ z_i \end{pmatrix} \quad (1)$$

By simplifying Eq. (1), one can see that:

$$\begin{cases} x_i = 2(T_i + A_i) - i \\ y_i = 2(T_i + G_i) - i \\ z_i = 2(T_i + C_i) - i \end{cases} \quad (2)$$

For a DNA sequence w , we define its DNA sequence matrix, $\Pi(w)$, to be defined as follows:

$$\Pi(w) = \begin{pmatrix} x_1 & x_2 & \dots & x_n \\ y_1 & y_2 & \dots & y_n \\ z_1 & z_2 & \dots & z_n \end{pmatrix}.$$

* To whom all correspondence should be sent:
E-mail: E-mail: : Ashrafi@kashanu.ac.ir

Let M_n denote the set of all DNA sequence matrix and $M = \bigcup_{n \geq 1} M_n$. Clearly, Π is defined as a one-to-one correspondence between \mathcal{D} and \mathcal{M} . For every $v \in \mathcal{D}_n$ and $w \in \mathcal{D}_m$, one can see that $vw \in \mathcal{D}_{m+n}$, where vw is a DNA sequence, constructed by v and w by juxtaposition. Suppose $A \in M_n$ and $B \in M_m$. Define:

$$\begin{cases} x'_i = x_i + x_A \\ y'_i = y_i + y_A \\ z'_i = z_i + z_A \end{cases} \quad (3)$$

and $A*B = (A,B')$, where (A,B') is defined by concatenating matrix A and matrix B' is obtained from B by applying Eq. (3). Here (x_i, y_i, z_i) and (x'_i, y'_i, z'_i) are the i th columns of the matrix B and B' , respectively, and (x_A, y_A, z_A) is the end column of A .

We are now ready to extend Proposition 2.1 of He and Wang [10] to Randić's et al. model [8].

Lemma 1. If $v, w \in \mathcal{D}$ then $\Pi(vw) = \Pi(v)*\Pi(w)$.

Proof. Suppose $|v| = n_1, |w| = n_2$. Then $|vw| = n_1 + n_2$ and we have:

$$\Pi(v) = \begin{pmatrix} \alpha_1(i) \\ \alpha_2(i) \\ \alpha_3(i) \end{pmatrix}_{1 \leq i \leq n_1}, \quad \Pi(w) = \begin{pmatrix} \beta_1(i) \\ \beta_2(i) \\ \beta_3(i) \end{pmatrix}_{1 \leq i \leq n_2},$$

$$\Pi(vw) = \begin{pmatrix} \gamma_1(i) \\ \gamma_2(i) \\ \gamma_3(i) \end{pmatrix}_{1 \leq i \leq n_1 + n_2}.$$

If $i \in [1, n_1]$ then

$\gamma_1(i) = 2((A_i(v) + T_i(v) - i) = \alpha_1(i)$ and if $i = n_1 + k \in [n_1 + 1, n_1 + n_2]$ then

$\gamma_1(i) = 2(T_i(vw) + A_i(vw)) - i = 2(T_{n_1}(v) + A_{n_1}(v)) + 2(T_k(vw) + A_k(vw)) - n_1 - k = \beta_1(i) + \alpha_1(n)$.

Therefore, we prove that:

$$\gamma_1(i) = \begin{cases} \alpha_1(i) & i \in [1, n_1] \\ \beta_1(k) + \alpha_1(n) & i \in [n_1 + 1, n_1 + n_2] \end{cases}.$$

In a similar way, one can prove:

$$\gamma_2(i) = \begin{cases} \alpha_2(i) & i \in [1, n_1] \\ \beta_2(k) + \alpha_2(n) & i \in [n_1 + 1, n_1 + n_2] \end{cases},$$

$$\gamma_3(i) = \begin{cases} \alpha_3(i) & i \in [1, n_1] \\ \beta_3(k) + \alpha_3(n) & i \in [n_1 + 1, n_1 + n_2] \end{cases}.$$

This completes our proof.

He and Wang [10] also presented an action of the symmetric group S_4 on the DNA sequences. We now present new generators for this group, compatible with the RVNB model. Clearly, $S_4 = \langle (G T), (A T), (C T) \rangle$. Suppose $O(3)$ denotes the set of all 3×3 orthogonal matrices on real numbers. Define:

$$\Phi(G T) = \begin{pmatrix} 0 & 0 & -1 \\ 0 & 1 & 0 \\ -1 & 0 & 0 \end{pmatrix},$$

$$\Phi(A T) = \begin{pmatrix} 1 & 0 & 0 \\ 0 & 0 & -1 \\ 0 & -1 & 0 \end{pmatrix},$$

$$\Phi(C T) = \begin{pmatrix} 0 & -1 & 0 \\ -1 & 0 & 0 \\ 0 & 0 & 1 \end{pmatrix}$$

Extend these values to an injective homomorphism $\Phi: S_4 \rightarrow O(3)$. We now define an action of the symmetric group S_4 on the set of all DNA sequence matrices by $A^\alpha = A\Phi(\alpha)$, where $\alpha \in S_4$ and $A \in \mathcal{M}$.

Lemma 2. Suppose $\alpha \in S_4$ and $P, Q \in \mathcal{M}$. Then:

$\Pi \alpha = \alpha \Pi$,

$\alpha (P * Q) = \alpha (P) * \alpha (Q)$.

Proof. (i) Since $\{(G T), (C T), (A T)\}$ is a generating set for S_4 , it is enough to investigate equation (i), for $\alpha = (G T), (C T)$ and $(A T)$. Suppose $v \in \mathcal{D}_n$. Then:

$$\Pi(v) = \begin{pmatrix} x_i \\ y_i \\ z_i \end{pmatrix} = \begin{pmatrix} 2(T_i + A_i) - i \\ 2(T_i + G_i) - i \\ 2(T_i + C_i) - i \end{pmatrix}.$$

Since $A_i + T_i + G_i + C_i = i$, we have:

$$\Phi(G T)\Pi(v) = \begin{pmatrix} -z_i \\ y_i \\ -x_i \end{pmatrix} = \begin{pmatrix} i - 2(T_i + C_i) \\ 2(T_i + G_i) - i \\ i - 2(T_i + A_i) \end{pmatrix} = \begin{pmatrix} 2(A_i + G_i) - i \\ 2(T_i + G_i) - i \\ 2(C_i + G_i) - i \end{pmatrix},$$

$$\Phi(A\ T)\Pi(v) = \begin{pmatrix} x_i \\ -z_i \\ -y_i \end{pmatrix} = \begin{pmatrix} 2(T_i + A_i) - i \\ i - 2(T_i + C_i) \\ i - 2(T_i + G_i) \end{pmatrix} = \begin{pmatrix} 2(T_i + A_i) - i \\ 2(G_i + A_i) - i \\ 2(C_i + A_i) - i \end{pmatrix},$$

$$\Phi(T\ C)\Pi(v) = \begin{pmatrix} -y_i \\ -x_i \\ z_i \end{pmatrix} = \begin{pmatrix} i - 2(T_i + G_i) \\ i - 2(T_i + A_i) \\ 2(T_i + C_i) - i \end{pmatrix} = \begin{pmatrix} 2(C_i + A_i) - i \\ 2(G_i + C_i) - i \\ 2(T_i + G_i) - i \end{pmatrix}.$$

Therefore,

$$\Phi(\alpha)\Pi(v) = \begin{pmatrix} 2(\alpha(T_i) + \alpha(A_i)) - i \\ 2(\alpha(T_i) + \alpha(G_i)) - i \\ 2(\alpha(T_i) + \alpha(C_i)) - i \end{pmatrix} = \Pi\alpha(v).$$

To prove (ii), we assume that $v, w \in \mathcal{D}$ such that $\Pi(v) = P$ and $\Pi(w) = Q$. Since $\alpha(vw) = \alpha(v)\alpha(w)$, $\Pi\alpha(vw) = \Pi(\alpha(v)\alpha(w)) = \Pi(\alpha(v))\Pi(\alpha(w)) =$

$\alpha\Pi(v) * \alpha\Pi(w) = \alpha(P) * \alpha(Q)$, which completes the proof.

REFERENCES

- 1 M. Randić, Chem. Phys. Lett. **317**, 29 (2000).
- 2 M. Randić, Chem. Phys. Lett. **386**, 468 (2004).
- 3 M. Randić and A. T. Balaban, J. Chem. Inf. Comput. Sci. **43**, 532 (2003).
- 4 M. Randić and S. C. Basak, J. Chem. Inf. Comput. Sci. **41**, 561 (2001).
- 5 M. Randić G. Krilov, Chem. Phys. Lett. **272**, 115 (1997).
- 6 M. Randić and M. Vracko, J. Chem. Inf. Comput. Sci. **40**, 599 (2000).
- 7 M. Randić, A. F. Kleiner and L. M. De Alba, J. Chem. Inf. Comput. Sci. **34**, 277 (1994).
- 8 M. Randić, M. Vračko, A. Nandy and S. C. Basak, J. Chem. Inf. Comput. Sci. **40**, 1235 (2000).
- 9 H.-H. Hsu, Advanced Data Mining Technologies in Informatics, Idea Group Inc., London, 2006.
- 10 P. He and J. Wang, J. Phys. A: Math. Gen. **37**, 7135 (2004).
- 11 R. Zhang and C. T. Zhang, J. Biomol. Struct. Dyn. **11**, 767 (1994).

ВЪРХУ АНАЛИЗА НА ДНК-СЕКВЕНЦИИ

Париса Фархами, Али Реза Ашрафи

Институт за нано-науки и нано-технологии, Университет в Кашан, Кашан 87317-51167,

Ислямска република Иран

Постъпила на 5 януари, 2010 г.; приета на 21 май, 2010 г.

(Резюме)

He и Wang са представили алгебричен метод за анализ на ДНК-секвенциите. ДНК-секвенциите могат да се идентифицират с буква от латиницата $W = \{A, C, G, T\}$. В настоящата работа се обсъжда развитието на модела на Randić, Vračko, Nandy and Basak за разширяване на резултатите на He и Wang.

Charge-related molecular index (CMI), a novel descriptor for quantitative structure/property relationship (QSPR) models. I. General considerations.

I. Bangov*, M. Moskovkina, A. Patleeva

'Episkop Konstantin Preslavski' University of Shumen, Department of Nature Sciences, 115 University St, Shumen 9712, Bulgaria

Received April 7, 2010; Revised June 7, 2010

The charge-related molecular index (CMI), developed by one of the authors (Bangov), and its use in chemoinformatics is discussed. A comparison is carried out between the Charge-related Topological Index (CTI) values and the Charge-related Geometrical Index (CGI) values, generated by using different quantum chemistry methods. It is shown that both indices can be successfully employed for isomorphic structure perception and for correlations with structure branching.

Key words: QSPR modelling; charge-related molecular index (CMI); charge-related topological index (CTI); charge-related geometrical index (CGI).

INTRODUCTION

A charge-related molecular index (CMI) was developed by one of us [1,2] in 1989. It has the following form:

$$CTI = \sum_i \sum_j \frac{L_i L_j}{D_{ij}} \quad (1)$$

Here D_{ij} is the inter-atomic distances and L_i is the local indices, characterizing the individual heavy (non-hydrogen) atoms i , expressed as follows:

$$L_i = L_o - N_H + q_i \quad (2)$$

L_o is the constant values for each atom for each hybridization state (they can be in some cases atom valences); N_H is the number of the hydrogen atoms, attached to a given heavy atom, and q_i is the corresponding charge densities. These are computed by either the topological empirical method of Gasteiger-Marsili [3] or by any of the sophisticated quantum chemistry methods on semi-empirical or non-empirical level. We used the Gasteiger-Marsili method for calculation of the atomic charges and the topological distance matrix inter-atomic distances when we take into consideration the 2D topology of the molecule. In this case we employ a Charge-related Topological Index (CTI). Vice versa, in case of using 3D molecular models, the distances and charge

densities are calculated out from the atom coordinates, and in this case the index is no more topological. Further, we shall call it Charge-related Geometrical Index (CGI).

The L_o values with the corresponding hybridization states and valences for some elements are presented in **Table 1**.

Table 1. Valences, atom codes, and L_o initial values for some elements and their hybridization states.

Element and hybridization state	Valence	Code	L_o
C			
sp^3	4	C	4
sp^2 (olefinic)	3	=C	11
sp^2 (aromatic)	3	:C	13
sp	2	#C	7
N			
sp^3	3	N	15
sp^2	2	=N	18
sp	1	#N	20
O			
sp^3	2	O	23
sp^2	1	=O	25
S	2	S	28
F	1	F	32
Cl	1	Cl	33
Br	1	Br	34
I	1	I	35

Initially, the CTI was developed for perception of isomorphic (equivalent) complete molecular structures and substructures (fragments) in the process of 2D structure generation.[1] Although, it cannot be strictly mathematically proved, our practice shows that this index manifests an extremely good discriminating power and appears

* To whom all correspondence should be sent:
E-mail: ivanbangov@shu-bg.net

to be practically an index of no degeneracy. Thus, equivalent (isomorphic) structures produce the same *CTI* values (within the computer word precision), and different (non equivalent) structures, i.e. different values. Hence, the reason that we use the L_o values, is to achieve better discrimination (clustering) between the L values of the different atom types and their hybridization states within the chemical structure whereas no overlapping of their L values is produced and better perception of the isomorphism and automorphism is achieved.

We found that this index can be further developed to feature 3D chemical structures. This can be achieved by using the electron charge densities in the L_i values and the real inter-atomic distances R_{ij} rather than the topological distance matrix D_{ij} values in Eqn. 1, both generated by using quantum chemistry methods either on semi- or non-empirical level. Further on we shall call the latter index Charge-related Geometrical Index (*CGI*). Accordingly, the purpose of this and the following papers is to study the use of the *CGI* in the various cheminformatics areas.

As seen from the relations (1) and (3), both *CTI* and *CGI* consists of two parts, numerator and denominator. Whereas the denominator accounts for the branching of the chemical structure in a way similar to that of the *Wiener* index [4], the numerator features the atomic type differences and their polarity. Furthermore, the charges (especially these produced from the Gasteiger - Marsili method using iteratively different atom environments) experience the influence of the electron density of the whole molecule on each separate atom. In this respect they algorithmically resemble the usual hashing procedures, used in chemistry. Accordingly, this combination of the two parts makes the index both very discriminative and a good descriptor for different types of quantitative structure/property relationships (QSPR), especially for the cases of interactions of polar moieties and media. Since it has the form of an electrostatic potential we can call it *molecular potential*.

EXPERIMENTAL.

Some of the *CTI* values are taken from a previous paper, written by Mr. Bangov [2], while other values are calculated together with the *CGI* values by using the *QSPR.exe* program which was written in Java by Bangov. The charges and the inter-atomic distances for the *CGI* calculations are generated by using quantum chemistry methods on a semi-empirical and non-empirical level from the

GAMESS package (USA). Thus, the *CGI* values are compared with the corresponding *CTI* values.

RESULTS AND DISCUSSIONS.

3.1. *CTI* Versus *CGI* Results.

The discriminating potential of our indices in comparison with the Wiener [4] and Randic [5] indices is illustrated on Fig. 1 for two couples of isomers. One can see that both the Wiener index in case *a* and the Randic index in case *b* produce degenerate (the same) values. In contrast, our *CTI* and *CGI* indices successfully discriminate the isomers.

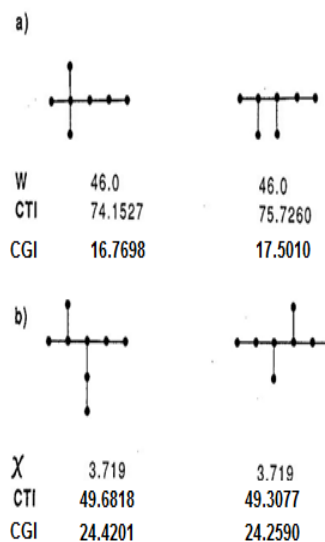


Fig. 1. a) Two isomers of different connectivity, providing the same Wiener index values W but different *CTI* and *CGI* values; b) two isomers of different connectivity, providing the same Randic index values χ but different *CTI* and *CGI* values.

It must be noticed here that the use of the *CGI* for perception of isomorphic (duplicated) structures depends on the precision of the SCF-procedure consistency and the conditions of the quantum chemistry calculations (parameterization, the basis set, geometry optimization, etc). The *CTI*, carried out with a fixed number of iterations of the Gasteiger-Marsili procedure (6 iterations in our case), is more suitable to this end on the one hand. On the other hand, it is much faster, hence it can be applied to large 2D structure datasets.

The L_i values were also used for perception of the constitutional molecular structure symmetry (automorphism). Thus, symmetric atoms have the same L_i values. [6]

First, it should be mentioned that both the *CTI* and the *CGI*, as well as the Wiener index, depend on the molecule size. This is illustrated in **Table 2**

with the *CGI* results of the first 8 alkanes, generated from quantum chemical methods on different levels (the semi-empirical *AM1*, and *ab initio* calculations with **3-21G** and **6-31G** basis sets).

Table 2. *CGI* values for the first 8 alkanes, ethene, propene, butane, and butadiene.

Compound	Wiener	CTI	CGI (AM1)	CGI (3-21G)	CGI (6-31G)
Ethane	1.0	1.0940	0.4141	0.1032	0.18006
Propane	6.0	5.5174	3.4466	2.8160	1.2720
Butane	16.0	12.4114	6.8630	5.1819	3.8126
Pentane	20.0	21.0965	9.8116	6.0120	8.5504
Hexane	35.0	30.9838	19.4892	16.7350	11.3400
Heptane	56.0	41.9989	20.4546	13.5525	16.1190
Octane	84.0	53.7756	26.5340	17.9132	20.8957
Ethene	1.0	23.0940	17.2461	16.0280	16.3992
Propene	6.0	27.5174	25.6882	22.1318	23.3331
1-Butene	16.0	34.4114	35.6854	30.5694	32.4841
Butadiene	16.0	56.4114	94.9199	89.7188	91.6864

Clearly, the *CGI* takes into account the chemical structure diversity, i.e., both different types of the atoms and the bonds, while the *Wiener* index does not distinguish them, hence structures such as butane, 1-butene, butadiene produce the same values. The *CGI* values of four compounds which have double bonds: ethene, propene, 1-butene and butadiene are also presented in **Table 2**. Naturally, their values are larger because of the L_o values of the double bonds, as given in **Table 1** (compare the *CGI* values for butane, 1-butene and butadiene there).

CGI values of different alcohols are provided in **Table 3** at two *ab initio* basis sets (**3-21G** and **6-31G**), and are compared with the *CTI* values from our previous paper [2]

Table 3. Charge-related topological index (*CTI*), calculated for a series of alcohols, and compared with the charge-related geometrical index (*CGI*), calculated by *ab initio* of different basis sets.

No	Compound	CTI	CGI (3-21G basis set)	CGI (6-31G basis set)
1.	Ethanol	56.3998	32.2479	35.8291
2.	Propane-3-ol	78.9698	47.4938	51.8761
3.	Propane-2-ol	92.9637	53.9825	59.1265
4.	Butane-4-ol	97.7223	59.0230	64.1728
5.	2-methylpropane-3-ol	103.9319	64.25757	69.2459
6.	Butane-3-ol	117.8204	71.2747	77.3128
7.	2-methylpropane-2-ol	132.0219	76.6028	83.0625
8.	Pentane-5-ol	114.7124	69.0861	74.9591
9.	2-methylbutane-4-ol	118.8611	71.5210	77.3650
10.	2-methylbutane-1-ol	124.9558	76.9455	82.8386

Generally speaking, the results from the computing methods follow the same trend in the case of alcohols. Again, one can see that the *CTIs* give always much larger values than the *ab initio* results on both the **3-21G** and the **6-31G** basis set levels. The numerical results from the sophisticated **6-31G** basis set calculations are somewhat larger than these from the **3-21G** basis set. Several factors influence the *CGI* values: the first, as mentioned above, is the size of the molecule; the second is the position of the heteroatom; and the third is the branching of the structure. Actually, many molecular properties depend on the chemical structure branching.

In order to study the influence of the structure branching on the *CMIs*, we compare the *CTI* values with both the *Wiener* index and the *CGI* values, calculated via quantum chemistry methods on *semi-empirical* (**AM1** and **PM3**) and *non-empirical* levels (**6-31G** basis set). These were calculated for a series of isomers of the octane hydrocarbon (C_8H_{18}), having different branching together with their ranking reported by Bertz [7]. By inspecting the different isomers of the same size from **Table 4**, we can figure out that in general the most branched isomers produce higher *CMI* values both for the 2D (*CTI*) and 3D (*CGI*) cases. As expected the *Wiener* index produces values which decrease with the increase of the chemical structure branching.

Although the notion of branching has no strict definition, one can see that in some cases the *CMIs* provide much more reasonable results than the ranking of Bertz. One can see that the *Wiener* index, the *CTIs* of the 2D structures, and the *CGIs* of the 3D structures describe pretty well on *semi-empirical* level the branching of different types of chemical structures, while the *non-empirical* level produce some discrepancies. Thus, unlike the *Wiener* index, and the *CTIs* and *CGIs* on *semi-empirical* level, the most branched structure, the 2,2,3,3-tetramethylbutane, does not produce the highest *CGI* value on the *non-empirical* level, as expected. On the other hand the *Wiener index* has a serious disadvantage, it frequently provides degenerate (the same) values for different structures, as in the case of structures 3,3-dimethylhexane and 2-methyl-3-ethylpentane. They obviously have not only a different constitution but a different branching, too.

The results indicate that both 2D *CTIs* and 3D *CGIs* on *semi-empirical* level are more discriminative concerning branching than the *CGIs*

on *non-empirical* level. The difference between the topological and the geometrical index is certainly in

Table 4. Ranking of octane isomers, compared with the *Wiener*, *CTI*, *CGI* indices (calculated by different quantum chemistry methods on semi- and non-empirical levels). The ranking of the different isomers, according to the branching index of Bertz [7] is given in the brackets.

No	Compound	Wiener index	CTI	CGI (AM1)	CGA (PM3)	CGI (6-31G)
1	octane (1)	84	41.9796	26.5323	28.6211	20.8957
2	2-methylheptane (2)	79	43.6962	27.5524	28.7678	21.3851
3	3-methylheptane (4)	76	45.1788	28.5444	30.7575	22.2655
4	2,5-dimethylhexane (3)	74	45.4882	28.6227	30.9619	21.9044
5	4-methylheptane (5)	75	45.5535	28.8463	31.0634	22.5394
6	2,2-dimethylhexane (12)	71	46.8757	29.2557	31.6989	22.1572
7	3-ethylhexane (7)	72	47.0352	30.1201	32.3656	23.5653
8	2,4-dimethylhexane (6)	71	47.1357	29.8083	32.1435	22.8984
9	2,3-dimethylhexane (8)	70	48.0352	30.2540	32.6000	23.3551
10	2,2,4-trimethylpentane (13)	66	48.9985	30.6053	33.1529	21.9044
11	3,4-dimethylhexane (9)	68	49.3077	31.0533	33.3759	24.0659
12	3,3-dimethylhexane (14)	67	49.4228	30.8739	33.2964	23.1588
13	2-methyl-3-ethylpentane (10)	67	49.6818	31.5014	33.8264	23.5878
14	2,3,4-trimethylpentane (11)	65	50.6825	31.8000	34.2331	24.4201
15	3-ethyl,3-methylpentane (15)	64	51.5943	32.4283	34.8512	24.2955
16	2,2,3-trimethylpentane (16)	63	51.6971	32.1138	34.6474	24.2326
17	2,3,3-trimethylpentane (17)	62	52.5966	32.6185	35.1300	24.6297
18	2,2,3,3-tetramethylbutane (18)	58	54.6152	33.1903	35.8574	24.4034

the charge densities which are influenced by the molecular geometry in the case of quantum chemistry calculations but the main contribution to this difference comes from the inter-atomic distances which are used explicitly. Whereas in the case of the *CTI* these distances account for the number of bonds between the non-bonded atoms, the distances between the non-bonded atoms are through space in the case of the *CGI*. Hence, the *CTI* always prefers the most folded structure, having the shortest topological distances (the number of bonds between different atoms). The latter appears to be the most branched. In the same

time this is not the case with the *CGI* on *non-empirical* level where the distances between the atoms are estimated according to the molecular geometry. Obviously, the semi-empirical calculations produce some borderline results. This gives us a good opportunity to favor the much faster *empirical* and *semi-empirical* approaches.

On the other hand the *CGI* can be used to distinguish between different conformations as shown on **Fig. 2**.

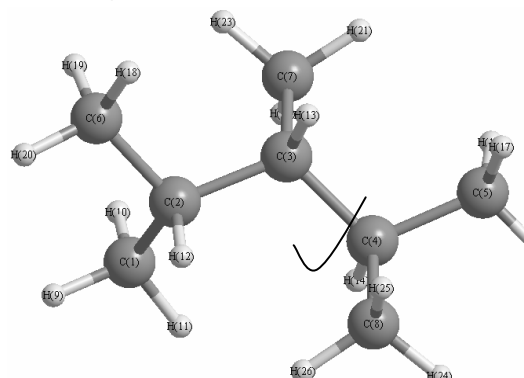


Fig. 2. CGI, total energy values of the lowest 2,3,4-trimethylpentane conformers (rotations at dihedral angle ω (bonds 2–3–4–5)) **a.** $\omega = 163.116$, $E_{total} = -196677.684410672$ kcal, $CGI = 24.29638$; **b.** $\omega = 63.000$, $E_{total} = -196676.354433968$ kcal, $CGI = 24.24072$; **c.** $\omega = -72.700$, $E_{total} = -196676.472099028$ kcal, $CGI = 24.316437$; **d.** $\omega = 96.400$, $E_{total} = -196676.354482224$ kcal, $CGI = 24.24065$

In the previous paper [2] we found a very good correlation between the *CTI* values and the enthalpies of formation ($R = 0.968$) of C_2 – C_3 alkanes and with the octane numbers of some fuels ($R = 0.986$). On the other hand, it was shown that the *CTI* can be used for description of the different environments of the structure atoms, forming

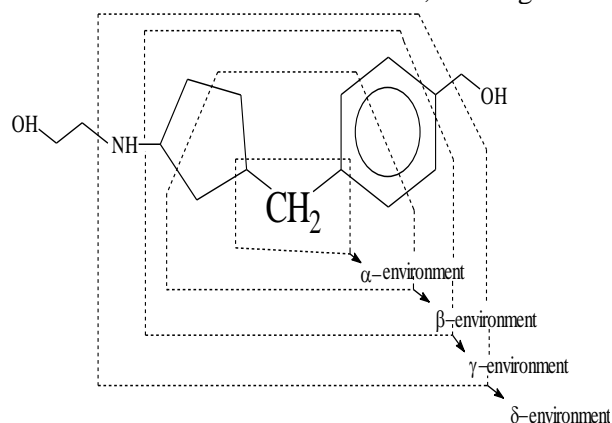


Fig. 3. The picture of the α -, β -, γ -, and δ -environments of a CH_2 carbon atom.

different fragments, hence a procedure similar to that of Bremser [8] for calculation of ^{13}C chemical shifts was reported by one of the authors (Bangov [9]). The method of Bremser was modified in such a way that instead of using Bremser's HOSE code we used the *CTI*. As shown on **Fig. 3**, each carbon atom within a given structure is associated with α , β , γ , and δ environments.

These environments are fragments practically, and we assign a *CTI* value to each of them: α – (CTI_α), β (CTI_β), γ – (CTI_γ), and δ – ($CTI_{\delta\delta}$), and relate these environments (fragments) to their ^{13}C chemical shifts and coupling constants. We can use them either in a relational base or we can form fingerprints similar to these of Daylight [10], and assign to each key in the fingerprint both fragment and spectral characteristics.

CONCLUSIONS

It becomes obvious from our study of the *CTIs* and *CGIs* that they describe not only the connectivity within chemical structures (as the other most popular indices do) but also their multiple bond, heteroatom and polarity density owing to use of charges in their formation. As far as they have the form of an electrostatic potential (1), we can consider them as *molecular potential*.

Since our indices describe well the constitution, the diversity and the structural branching, they have the further potential for deriving efficient *QSAR* and *QSPR* models with *CTIs* and *CGIs*, derived

from both 2D and 3D molecular structures. This might be especially useful for the cases of polar phases. Studies on their usage as basic descriptors for chromatography retention modelling have been carried out [11] and some novel results will be reported in the near future.

REFERENCES

1. I. Bangov, *J. Chem. Inf. Comput. Sci.*, **30**, 277 (1990).
2. P. A. Demirev, A. S. Dyulgerov, I. P. Bangov, *J. Math. Chem.*, **8**, 367 (1991).
3. J. Gasteiger, M. Marsili, *Tetrahedron*, **36**, 3219, (1980).
4. H. Wiener, *J. Am. Chem. Soc.*, **69**(1) 17, (1947).
5. M. Randic, *J. Amer. Chem. Soc.* **97**, 6609, (1975).
6. I. Bangov, *J. Chem. Inf. Comput. Sci.*, **34**, 318, (1994).
7. St. Bertz, *Discr. Appl. Math.* **19**, 65 (1988).
8. W. Bremser, *Anal. Chim. Acta*, **103**, 355 (1978).
9. I. Bangov, *Annuaire Uni. Sofia*, **2001**, 91, 103-113.
10. <http://www.daylight.com/dayhtml/doc/theory/theory.finger.html>
11. M. Moskovkina, *Thesis*, Shumen Univ. Library, 118 (2004).

СВЪРЗАНИЯТ СЪС ЗАРЯДИТЕ МОЛЕКУЛЕН ИНДЕКС (СМИ) – ЕДИН НОВ ДЕСКРИПТОР ЗА МОДЕЛИ НА СТРУКТУРА/СВОЙСТВА КОЛИЧЕСТВЕНИТЕ СЪОТНОШЕНИЯ (QSPR). I. ОБЩИ РАЗГЛЕЖДЕНИЯ.

И.Бангов*, М. Московкина, А.Патлеева

Шуменски университет „Епископ Константин Преславски“, Факултет по природни науки“, ул. Университетска. 115, Шумен, 9712, България,

Постъпила на 7 април, 2010 г.; преработена на 7 юни, 2010 г.

Резюме

Дискутирани са свързаният със зарядите молекулен индекс (*СМИ*), разработен от един от авторите (Бангов) и неговото използване в хемоинформатиката. Проведено е едно сравнение между стойностите на свързания със зарядите топологичен индекс (*СТИ*) и на свързаният със зарядите геометричен индекс (*СГИ*) получени при използването на различни квантово-химични методи. Показано е, че и двата индекса могат успешно да бъдат използвани, както за откриването на изоморфни структури, така за корелация със разклоняването на структурите.

Evaluation of PCB's chromatographic retention indices using multilinear regression method

I. Stanculescu^{1,2*}, G. Mindrila¹, C. Mandravel¹

1- Department of Physical Chemistry, Faculty of Chemistry, University of Bucharest, 4-12 Regina Elisabeta Blvd., District 3, Bucharest, 030018 Romania

2- IRASM Irradiation Technology Center, Horia Hulubei National Institute for Physics and Nuclear Engineering, 407 Atomistilor St, Magurele, Ilfov, 077125 Romania

Received August 6, 2010; Revised September 14, 2010

The multilinear regression method for polychlorinated biphenyls (PCBs) chromatographic retention indices evaluation was applied. Nine reference PCB's chromatographic retention indices (R) were evaluated using 8 calculated molecular properties (descriptors): molecular volume, molecular weight, partition coefficient (logP), van der Waals and solvent accessible surface, dipole moment, and frontier orbital energies. The best equations were selected via the highest value of the F quality index and the most efficient combinations of descriptors. As expected, the van der Waals surface descriptor appears frequently in the best quality equations. In the discussed equations, the logP descriptor, correlated with the lipophilicity and the reactivity indices of ϵ_{HOMO} and ϵ_{LUMO} , has the biggest weight.

Keywords: PCBs; chromatographic retention indices; multilinear regression method; molecular descriptors

INTRODUCTION

Although the production of polychlorobiphenils (PCBs) is forbidden now, the problems of their recurrence in the environmental components are an issue due to the partitioning, biotransformation and bioaccumulation [1–11] of these hazardous chemicals. In these processes, the PCB adsorption in different phases [1–3] is very important.

There are 209 PCB's congeners and their identification is a very difficult task. Such identification is possible through determination of their retention times using the high resolution gas-chromatography [12–14].

The content of PCBs in transformers oil have been evaluated by GC–MS hyphenated method [15]. Now the chromatographic retention indices were evaluated using the multiple linear regression method (MLR).

We adhered to the following equation:

$$R = a_0 + \sum_{i=1}^k a_i x_i \quad (1)$$

MLR attempts to model the correlation between the chromatographic retention index R and the independent variables x_i (descriptors), mediated by $a_0 - a_i$ which are estimated regression parameters. Recently, B. Tiperciuc and C. Sarbu predicted the

chromatographic retention indices (lipophilicity) of some new methyl thiazolil oxadiazoline derivatives using the MLR [16].

CALCULATION DETAILS

Chromatographic retention index values of the PCBs are taken from two literature sources [17, 18]. The molecular weight is considered as a descriptor of a special type because the toxicity and the irreversible absorption increase with the complexity of its structure [12–14]. The molecular properties of the PCBs, the grid (solvent accessible) surface (Sg), the approximate (van der Waals) surface (Sa), the molecular volume (V), the dipole moment (μ), the partition coefficient (logP), the and frontier orbital energies (ϵ_{HOMO} , ϵ_{LUMO}) were calculated for structures, optimized with the AM1 method in the Restricted Hartree Fock (RHF) approximation *in vacuo*, using the HYPERCHEM software [19]. Minimum energy structures were obtained using the Root Mean Square (RMS) gradient of 0.01 kcal/mol·Å. Multilinear regression equations were derived through the MATHCAD 7 software [20].

RESULTS and DISCUSSION

In our study, we considered as descriptors the properties on molecular level such as the molecular volume and weight. We also took into

* To whom all correspondence should be sent:
E-mail: ioana.stanculescu@gmail.com

consideration the properties significant for the energy of the molecular interaction: the partition coefficient, van der Waals and solvent accessible surface, and some properties, related to the nuclear-electronic level such as the dipole moment and frontier orbital energies.

These descriptors can serve as a basis for the development of predictive models with improved accuracy and precision [21].

A set of 9 PCBs are included in this study: **1**(1), **8**(2), **31**(3), **44**(4), **101**(5), **138**(6), **180**(7), **203**(8) and **206**(9). The bold characters indicate the compound in accordance with IUPAC Convention and the number of the chlorine atoms is given in the brackets [13, 14, 17, 22]. In this series, the **PCB1** elutes first, and the **PCB206** elutes last on almost every stationary phase, tested as showed in a 2008

research report of the LECO Corporation [18]. We assumed that these nine PCBs are representative for the multilinear regression study for two reasons: (i) it is considered one PCB of each of the nine classes and (ii) these nine PCB's were proposed as reference compounds because they exhibit linear retention behavior on stationary phases [18]. For example, the regression of the PCB reference series (the retention time versus the chlorine atom number) demonstrates that the behavior is linear for the DB-XLB phase [12–14].

The CAS registry numbers, the retention indices (**RT1** and **RT2**), and the descriptor values, calculated as described in the calculation detail paragraph, are listed in Table 1. This table shows an increase in the property values and the number of the chlorine atoms in the PCB molecules.

Table 1. PCB CAS numbers, calculated molecular properties and chromatographic retention indices.

No.	PCB (Cl position)	CAS number	M (g/mol)	logP	ϵ_{HOMO} (eV)	ϵ_{LUMO} (eV)	Sg(Å ²)	Sa(Å ²)	V(Å ³)	μ (D)	RT 1	RT 2
	1 (2)	2051-60-7	188.66	4.25	9.5023	0.1206	377.27	302.9	589.26	1.160	364.49	2.036
	8 (2,4')	34883-43-7	223.1	4.77	-9.5698	-0.2036	401.05	339.32	631.79	1.402	568.09	2.885
	31 (25,4')	16606-02-3	257.55	5.29	-9.5645	-0.3201	425.68	376.22	675.33	1.043	767.41	4.04
	44 (23,2'5')	41464-39-5	326.44	5.8	-9.5582	-0.3265	438.46	390.02	706.13	1.880	874.29	4.655
	101 (245,2'5')	37680-73-2	291.99	6.32	-9.6378	-0.5953	465.35	428.94	749.93	1.102	1026.68	5.396
	138 (234,2'4'5')	35065-28-2	360.88	6.84	-9.7085	-0.6671	480	458.46	783.3	1.643	1270.29	6.677
	180 (2345,2'4'5')	35065-29-3	395.33	7.36	-9.7703	-0.8302	501.61	492.81	821.63	0.845	1414.49	7.412
	203 (23456,2'4'5')	52663-76-0	429.77	7.88	-9.7548	-0.9909	511.93	510.52	851.71	0.03	1494.29	7.763
	206 (23456,2'3'4'5')	40186-72-9	464.22	8.39	-9.8484	-1.0539	527.61	540.27	884.83	0.820	1669.89	8.642

Taking into account only the combinations with Sa or Sg, 183 equations were derived for each of the retention index series: 27 equations with 2 descriptors, 50 with 3 descriptors, 55 with 4 descriptors, 36 with 5 descriptors, 13 with 6 descriptors, and 2 with 7 descriptors. In tables 2 and 3, according to then F values, the best 10 equations with 2-6 descriptors were selected for each of the index series, and the best 2 equations with 7 descriptors were selected for each of the retention index series.

In practical terms, the MLR equations of Tables 2 and 3, were evaluated by values of correlation coefficient r^2 , F factor, and p value(the equation significance level. The correlation coefficient r^2 is 0.999 for all equations. The F factor which is the measure of the regression relationship, was

calculated with the formula: $F = \frac{MSR}{MSE}$, where MSR

is mean square regression, and MSE is mean square error [24]. An examination of Tables 2 and 3 shows that the same combinations of 6 descriptors (M, logP, ϵ_{LUMO} , Sa, V, μ), 5 descriptors (M, logP, ϵ_{LUMO} , Sa, μ) and 3 descriptors (ϵ_{LUMO} , Sa, μ) give the biggest F value (see lines 12, 22 and 42 in the

tables 2 and 3). The quality of the obtained equations was good, taking into consideration the r^2 and F values. Additionally, the calculated p values (data not shown) are very small for the high quality obtained equations. As expected, M, μ , Sa, and logP descriptors are the most frequently used descriptors in the best equations, with highest F factor. Even equations with 2 descriptors have highest F values when Sa and μ are used as descriptors.

Surely, the weight of a descriptor is determined by the value of the a_i coefficients. Thus, in Table 2, in the equations with 5, 6 and 7 descriptors, logP has the biggest weight almost always and the ϵ_{HOMO} descriptor has the second biggest weight. LogP has the biggest weight 4 times and ϵ_{LUMO} 5 times in the case of 4 descriptor equations. The biggest weight for the equations with 3 descriptors corresponds to ϵ_{LUMO} for half of the equations, and for 3 equations to μ , logP, and ϵ_{HOMO} . The biggest weight varies for the equations with 2 descriptors. We have similar comments about Table 3, and one may see that the M descriptor is never of the biggest weight.

Table 2. Multilinear regression equations, obtained using RT1 ($r^2=0.999$).

No.	Descriptors (X_i)	F	Coefficients (a_i)
7 descriptors			
1	M, logP, E_{HOMO} , E_{LUMO} , Sg, V, μ	6.247E+4	-2.475E+4; -123.183; 7.236E+3; -894.756; 368.737; -23.36; 30.238; 39.314
2	M, logP, E_{HOMO} , E_{LUMO} , Sa, V, μ	1.265E+5	-1.207E+4; -124.437; 8.464E+3; 77.901; 146.13; 5.715; -1.952; 72.107
6 descriptors			
3	logP, E_{HOMO} , E_{LUMO} , Sg, V, μ	1.919E+3	-1.986E+4; -1.932E+3; -1.38E+3; 445.058; -43.617; 53.861; -11.478
4	M, logP, E_{LUMO} , Sg, V, μ	2.057E+3	-1.86E+4; -185.356; 1.29E+4; 84.216; 10.622; -8.514; 85.615
5	M, logP, E_{HOMO} , Sg, V, μ	2.648E+3	-1.853E+4; -141.438; 9.493E+3; -363.543; -0.93; 3.453; 73.595
6	M, E_{HOMO} , E_{LUMO} , Sg, V, μ	3.101E+3	-2.222E+4; -28.453; -1.352E+3; 466.216; -43.289; 53.27; -3.421
7	M, logP, E_{HOMO} , E_{LUMO} , Sg, μ	4.219E+3	-2.09E+4; -165.311; 1.121E+4; -355.324; 169.036; 3.517; 73.036
8	M, logP, E_{HOMO} , E_{LUMO} , Sa, μ	4.372E+4	-1.464E+4; -131.66; 8.889E+3; -74.275; 176.453; 4.164; 69.082
9	M, logP, E_{HOMO} , E_{LUMO} , Sg, V	5.293E+3	-2.524E+4; -68.681; 2.798E+3; -1.283E+3; 522.517; -40.684; 50.528
10	M, logP, E_{HOMO} , E_{LUMO} , V, μ	5.51E+3	-2.143E+4; -158.192; 1.057E+4; -436.346; 206.675; 4.192; 67.217
11	M, logP, E_{HOMO} , Sa, V, μ	1.026E+4	-8.177E+3; -107.624; 7.423E+3; 244.702; 6.936; -4.376; 77.831
12	M, logP, E_{LUMO} , Sa, V, μ	9.087E+4	-1.328E+4; -127.564; 8.65E+3; 156.964; 5.041; -1.163; 71.097
5 Descriptors			
13	M, logP, E_{LUMO} , Sg, μ	1.775E+3	-1.877E+4; -179.604; 1.221E+4; 119.102; 2.709; 78.422
14	logP, E_{HOMO} , E_{LUMO} , Sg, V	1.8E+3	-1.805E+4; -1.672E+3; -1.262E+3; 363.264; -37.918; 47.156
15	logP, E_{HOMO} , Sa, V, μ	1.844E+3	4.146E+3; 211.043; 439.95; 10.58; -6.387; 50.514
16	M, logP, Sg, V, μ	1.92E+3	-1.752E+4; -177.493; 1.244E+4; 11.573; -10.107; 88.477
17	M, logP, E_{HOMO} , Sg, μ	2.61E+3	-1.843E+4; -148.515; 1.01E+4; -308.293; 2.303; 76.921
18	M, logP, E_{HOMO} , V, μ	2.645E+3	-1.849E+4; -143.297; 9.654E+3; -348.053; 2.47; 74.479
19	M, E_{HOMO} , E_{LUMO} , Sg, V	3.063E+3	-2.169E+4; -27.514; -1.324E+3; 441.677; -41.958; 51.661
20	M, logP, E_{HOMO} , Sa, μ	5.033E+3	-1.349E+4; -118.896; 8.054E+3; -110.175; 3.019; 72.287
21	M, logP, Sa, V, μ	7.475E+3	-1.159E+4; -114.647; 7.832E+3; 4.759; -2.097; 75.648
22	M, logP, E_{LUMO} , Sa, μ	2.754E+4	-1.389E+4; -130.726; 8.822E+3; 182.972; 4.374; 68.106
4 descriptors			
23	M, E_{LUMO} , Sa, μ	1.423E+3	-1.559E+3; -0.036; 117.365; 6.207; 32.731
24	logP, E_{LUMO} , Sa, μ	1.423E+3	-1.549E+3; 0.402; 115.411; 6.149; 32.804
25	E_{HOMO} , E_{LUMO} , Sa, μ	1.434E+3	-1.968E+3; -46.539; 112.788; 6.078; 33.181
26	M, logP, V, μ	1.458E+3	-1.743E+4; -168.106; 1.139E+4; 1.702; 81.196
27	E_{LUMO} , Sa, V, μ	1.472E+3	-1.417E+3; 117.902; 7.008; -0.668; 34.308
28	M, Sa, V, μ	1.473E+3	-714.62; 1.296; 6.894; -2.213; 42.352
29	logP, Sa, V, μ	1.5E+3	-808.741; 93.232; 6.9; -2.315; 42.992
30	M, logP, E_{HOMO} , μ	1.526E+3	-2.096E+4; -186.295; 1.27E+4; -250.549; 92.171
31	M, logP, Sg, μ	1.565E+3	-1.716E+4; -165.901; 1.129E+4; 1.898; 80.748
32	M, logP, Sa, μ	4.37E+3	-1.23E+4; -116.773; 7.907E+3; 3.273; 70.992
3 descriptors			
33	E_{HOMO} , E_{LUMO} , Sa	765.695	-1.487E+3; 14.667; 218.625; 6.557
35	E_{LUMO} , Sa, V	765.812	-1.642E+3; 216.891; 6.383; 0.116
35	logP, E_{LUMO} , Sa	771.36	-1.659E+3; -19.33; 229.507; 6.927
36	M, E_{LUMO} , Sa	771.432	-1.686E+3; -0.289; 229.992; 6.927
37	M, logP, μ	1.205E+3	-1.952E+4; -195.322; 1.332E+4; 93.133
38	M, Sa, μ	1.274E+3	-1.348E+3; 0.233; 5.347; 37.097
39	logP, Sa, μ	1.278E+3	-1.367E+3; 18.117; 5.301; 37.173
40	E_{HOMO} , Sa, μ	1.279E+3	-1.978E+3; -65.106; 5.527; 37.5
41	Sa, V, μ	1.295E+3	-1.262E+3; 6.396; -0.618; 38.587
42	E_{LUMO} , Sa, μ	1.423E+3	-1.55E+3; 115.684; 6.157; 32.792
2 descriptors			
43	M, V	396.399	-2.466E+3; -0.699; 5.034
44	E_{HOMO} , Sg	417.698	-7.811E+3; -570.231; 7.312

45	V, μ	467.245	-2.289E+3; 4.451; 25.281
46	E _{HOMO} , V	502.724	-5.92E+3; -420.719; 3.909
47	E _{HOMO} , Sa	599.557	-1.371E+3; -8.739; 5.477
48	logP, Sa	601.981	-1.274E+3; 15.222; 5.223
49	M, Sa	602.332	-1.251E+3; 0.241; 5.209
50	Sa, V	603.079	-1.38E+3; 4.967; 0.418
51	E _{LUMO} , Sa	765.373	-1.619E+3; 218.096; 6.533
52	Sa, μ	1.262E+3	-1.388E+3; 5.618; 37.107

Table 3. Multilinear regression equations, obtained using RT2 ($r^2=0.999$).

No.	Descriptors (X _i)	F	Coefficients (a _i)
7 descriptors			
1	M, logP, E _{HOMO} , E _{LUMO} , Sa, V, μ	4.288E+4	-80.928; -0.727; 48.587; 1.601E-3; 2.202; 0.023; 0.01; 0.327
2	M, logP, E _{HOMO} , E _{LUMO} , Sg, V, μ	1.628E+6	-133.123; -0.704; 41.968; -4.11; 3.173; -0.105; 0.152; 0.182
6 descriptors			
3	M, E _{HOMO} , E _{LUMO} , Sa, V, μ	1.401E+3	9.29; 2.74E-3; 1.763; 1.564; 0.049; -0.011; 0.181
4	logP, E _{HOMO} , E _{LUMO} , Sa, V, μ	1.414E+3	11.499; 0.283; 1.957; 1.519; 0.05; -0.013; 0.189
5	logP, E _{HOMO} , E _{LUMO} , Sg, V, μ	1.604E+3	-105.191; -10.407; -6.882; 3.609; -0.221; 0.287; -0.108
6	M, E _{HOMO} , E _{LUMO} , Sg, V, μ	2.563E+3	-118.467; -0.154; -6.759; 3.738; -0.221; 0.286; -0.066
7	M, logP, E _{LUMO} , Sg, V, μ	2.665E+3	-104.887; -0.989; 67.99; 1.866; 0.051; -0.026; 0.395
8	M, logP, E _{HOMO} , E _{LUMO} , Sg, μ	4.725E+3	-113.808; -0.915; 61.954; -1.398; 2.169; 0.03; 0.351
9	M, logP, E _{HOMO} , E _{LUMO} , Sg, V	7.122E+3	-135.402; -0.452; 21.434; -5.904; 3.884; -0.185; 0.246
10	M, logP, E _{HOMO} , E _{LUMO} , V, μ	7.856E+3	-118.196; -0.861; 56.976; -2.046; 2.443; 0.035; 0.307
11	M, logP, E _{HOMO} , E _{LUMO} , Sa, μ	2.562E+4	-67.387; -0.689; 46.348; 0.804; 2.042; 0.031; 0.343
12	M, logP, E _{LUMO} , Sa, V, μ	4.288E+4	-80.952; -0.727; 48.591; 2.202; 0.023; 0.01; 0.327
5 descriptors			
13	logP, E _{LUMO} , Sa, V, μ	1.265E+3	-11.204; -0.317; 1.742; 0.035; 6.255E-3; 0.144
14	M, E _{LUMO} , Sa, V, μ	1.283E+3	-11.962; -5.351E-3; 1.772; 0.035; 7.057E-3; 0.142
15	logP, E _{HOMO} , E _{LUMO} , Sg, V	1.353E+3	-88.117; -7.953; -5.769; 2.837; -0.167; 0.224
16	logP, E _{HOMO} , E _{LUMO} , Sa, μ	1.358E+3	-1.124; -0.138; 0.942; 1.699; 0.041; 0.156
17	M, E _{HOMO} , E _{LUMO} , Sa, μ	1.366E+3	-1.307; -2.274E-3; 0.949; 1.711; 0.041; 0.156
18	E _{HOMO} , E _{LUMO} , Sa, V, μ	1.392E+3	4.331; 1.393; 1.652; 0.046; -5.583E-3; 0.168
19	M, logP, E _{LUMO} , V, μ	2.033E+3	-106.309; -0.962; 64.299; 2.005; 0.027; 0.359
20	M, E _{HOMO} , E _{LUMO} , Sg, V	2.245E+3	-108.184; -0.136; -6.218; 3.265; -0.195; 0.255
21	M, logP, E _{LUMO} , Sg, μ	2.485E+3	-105.401; -0.972; 65.873; 1.972; 0.027; 0.373
22	M, logP, E _{LUMO} , Sa, μ	1.016E+4	-75.479; -0.699; 47.067; 1.972; 0.029; 0.353
4 descriptors			
23	logP, E _{HOMO} , E _{LUMO} , Sa	812.951	1.334; -0.246; 1.276; 2.26; 0.045
24	M, E _{HOMO} , E _{LUMO} , Sa	813.658	1; -3.679E-3; 1.278; 2.267; 0.045
25	M, logP, Sg, μ	843.345	-78.743; -0.745; 50.74; 0.013; 0.411
26	logP, E _{LUMO} , Sa, V	893.939	-14.44; -0.756; 2.342; 0.032; 0.017
27	M, E _{LUMO} , Sa, V	902.636	-15.695; -0.012; 2.367; 0.031; 0.017
28	M, logP, Sa, μ	1.059E+3	-58.29; -0.549; 37.212; 0.017; 0.385
29	E _{LUMO} , Sa, V, μ	1.21E+3	-9.405; 1.545; 0.035; 5.677E-4; 0.166
30	logP, E _{LUMO} , Sa, μ	1.222E+3	-9.489; -0.094; 1.61; 0.038; 0.165
31	M, E _{LUMO} , Sa, μ	1.227E+3	-9.673; -1.616E-3; 1.622; 0.038; 0.165
32	E _{HOMO} , E _{LUMO} , Sa, μ	1.324E+3	-1.454; 0.873; 1.601; 0.038; 0.16
3 descriptors			
33	M, logP, μ	647.926	-95.341; -0.951; 64.991; 0.498
35	Sa, V, μ	699.133	-7.368; 0.027; 1.217E-3; 0.222
35	M, Sa, μ	708.933	-6.76; 2.104E-3; 0.027; 0.225

36	logP, Sa, μ	710.797	-6.944; 0.153; 0.026; 0.226
37	E _{HOMO} , Sa, μ	715.451	-1.595; 0.609; 0.03; 0.221
38	logP, E _{LUMO} , Sa	722.501	-10.037; -0.193; 2.183; 0.042
39	M, E _{LUMO} , Sa	722.804	-10.316; -2.888E-3; 2.188; 0.042
40	E _{LUMO} , Sa, V	723.541	-10.493; 2.024; 0.032; 4.362E-3
41	E _{HOMO} , E _{LUMO} , Sa	774.729	0.867; 1.168; 2.112; 0.04
42	E _{LUMO} , Sa, μ	1.209E+3	-9.291; 1.546; 0.036; 0.167
2 descriptors			
43	Sg, V	337.821	-12.167; 0.011; 0.017
44	E _{HOMO} , V	349.881	-22.437; -1.267; 0.021
45	logP, Sa	379.717	-6.382; 0.136; 0.026
46	M, Sa	380.153	-6.172; 2.149E-3; 0.026
47	E _{LUMO} , V	387.726	-13.962; 1.174; 0.027
48	E _{HOMO} , Sa	389.388	1.989; 0.942; 0.03
49	Sa, V	393.198	-8.049; 0.019; 7.185E-3
50	V, μ	419.303	-11.779; 0.023; 0.165
51	Sa, μ	697.685	-7.12; 0.029; 0.225
52	E _{LUMO} , Sa	703.095	-9.644; 2.069; 0.038

CONCLUSIONS

Good correlations of chromatographic retention indices for the 9 PCBs with molecular properties using multilinear regression were obtained. The best 10 combinations of 2, 3, 4, 5 and 6 descriptors from the group of 8 considered were determined for each retention index series according the values of the regression quality indices [23, 24].

In the majority of best equations with the biggest F value, the presence of Sa descriptor shows the importance of the molecular surface and stationary phase interaction.

The descriptors with the biggest weight are the logP, correlated with the lipophilicity, and the reactivity indices, ϵ_{HOMO} and ϵ_{LUMO} .

Acknowledgements: The authors would like to thank to Prof. G. Surpateanu from the University of Dunkerque, France for the generous computational resources made available for us. This work was funded by the ANCS, DELCROM and ARCON projects, contract no. 92-086/2008 and 92-083/2008, respectively.

REFERENCES

- 1 R. Fuoco, M. P. Colombini, E. Samcova, *Chromatographia*, **36**, 65 (1993).
- 2 C. von Holst, A. Müller, E. Björklund, E. Anklam, *Eur. Food. Res. Technol.* **213**, 154 (2001)
- 3 F. Krokos, C.S. Creaser, C. Wright, J.R. Startin, *Fresenius J. Anal. Chem.* **357**, 732 (1997)
- 4 H. Steinwandter, *Fresenius J. Anal. Chem.* **343**, 378 (1992)
- 5 E. Sippola, K. Himberg, *Fresenius J. Anal. Chem.*, **339**, 510 (1991)
- 6 A.N. Davies, R. Fobbe, R. Kuckuk, J. Nolte, *Fresenius J. Anal. Chem.* **371**, 855 (2001)
- 7 V. Raverdino, R. Holzer, J.D. Berset, *Fresenius J. Anal. Chem.* **354**, 477 (1996)
- 8 J.L. Martínez Vidal, M. Moreno Frías, A. Garrido Frenich, F. Olea-Serrano, N. Olea, *Anal Bioanal Chem*, **372**, 766 (2002)
- 9 A. Trost, W. Kleiböhmer, K. Cammann, *Fresenius J. Anal. Chem.*, **359**, 249 (1997)
- 10 J. Krupcik, A. Kocan, J. Petrik, P.A. Leclercq, K. Ballschmiter, *Chromatographia*, **35**, 410 (1993)
- 11 S. Pedersen-Bjergaard, S.I. Semb, J. Vedde, E.M. Brevik, T. Greibrokk, *Chromatographia* **43**, 44 (1996)
- 12 J.W. Cochran, G.M. Frame, *J. Chromatogr. A* **843**, 323 (1999)
- 13 S. Chu, X. Miao, X. Xu, *J. Chromatogr. A*, **724**, 392 (1996)
- 14 G. Castello, G. Testini, *J. Chromatogr. A*, **787**, 215 (1997)
- 15 V. Chiosa, G. Mindrila, C. Mandravel, C. Toader, *Proc. 32nd Amer. Rom. Acad. (ARA) Congress*, July 22-27, Boston, MA, USA, 2008, 131-133
- 16 B. Tipericiuc, C. Sarbu, *Liq. Chromat. Rel. Technol.*, **29**, 2257 (2006)
- 17 S.A. Mills III, DI Thal and J Barney, *Chemosphere*, **68**, 1603 (2007)
- 18 http://www.leco.com/resources/application_note_subs/pdf/separation_science/-248.pdf (last accessed September 13, 2010)
- 19 Hyperchem program V. 6.02 for Windows, Hypercube Inc., 2000
- 20 Mathcad 7 professional program, 1986–1997 MathSoft, Inc
- 21 T. Oberg, *Int J Chem*, **5**, 1 (2001)

- 22 R. Done, G. Mindrila, I. Stanculescu, *Anal. Univ. Buc. Chim.*, **XVI**, 45, (2007)
23 Ullmann's Encyclopedia of Industrial Chemistry, 5th edition, Wiley-VCH, Wennheim, Germany, 1997

- 24 A. Beteringhe, A.C. Radutiu, M. Bem, T. Constantinescu, A.T. Balaban, *Int. Electron. J. Mol. Design*, **5**, 237 (2006).

ОПРЕДЕЛЯНЕ НА ИНДЕКСИТЕ НА ЗАДЪРЖАНЕ ПРИ ХРОМАТОГРАФСКИЯ АНАЛИЗ НА ПОЛИ-ХЛОРИРАНИ БИФЕНИЛИ (PCB) С ПОМОЩТА НА МНОЖЕСТВЕНА ЛИНЕЙНА РЕГРЕСИЯ

Й. Станкулеску^{1,2}, Г. Миндрила¹, К. Мандравел¹

Департамент по физикохимия, Химически факултет, Университет на Букурещ, бул. Кралица Елизабет, 4-12 район 3, Букурещ 030018, Румъния

2 – Технологичен център IRASM, Национален институт по физика и чдрено инженерство "Хория Холубеи", ул. Атомистилор, 407, Магуреле, Илфов 077125, Румъния

Постъпила на 6 август, 2010 г.; преработена на 14 септември, 2010 г.

(Резюме)

Приложен е методът на множествената линейна регресия за определяне на времената на задържане при хроматографията на поли-хлорирани бифенили (PCB). Определени са девет референтни хроматографски индекса (R) използвайки 8 изчислени молекулни свойства (дескриптори): моларен обем, молекулна маса, коефициент на разпределение (logP), ван-дер-Ваалс'ова и достъпна повърхност по разтворител, диполен момент, and гранични орбитални енергии. Подбрани са най-подходящите уравнения според най-високия качествен индекс F и най-ефективната комбинация от дескриптори. Както се очаква, дескрипторът "ван-дер-Ваалс'ова повърхност" се явява често в най-добрите уравнения. В обсъжданите уравнения дескрипторът logP, корелиран с липофилността и индекса на реактивност (ε_{НОМО} and ε_{LUMO}) има най-голямо тегло.

AUTHOR INDEX

- Abdel-Sayed N. I., Novel synthesis of new symmetrical bis-heterocyclic compounds: synthesis of bis-thiazolo, bis-pyrazolo-, bis-benzotriazolo, bis-indolo- and bis-pyrazolyl thiazolo-2,6-diamino pyridine derivatives.....20
- Abou El-Nour Kh.M., See Refat M.S., et al.279
- Adinarayana M., See Vijayalakshmi G., et al.246
- Akbari M. T., A. Esmaeili, A. H. Zarea, N. Saad, F. Bagheri, Chemical composition and antibacterial activity of essential oil from leaves, stems and flowers of *Prangos ferulacea* (L.) Lindl. grown in Iran36
- Aher, H. R., See Kokate S. J. et al.107
- Alexandrova A. K., See Uzunova S. A. et al.130
- Andreev A., See Mitov I. et al.180
- Andreev P., See Mitov I. et al.180
- Andreev P., See Uzun D. et al.113
- Ania C., See Petrova B. et al.141
- Ashrafi A. R., See Farhami P. et al.335
- Aydin M., EPR investigation of gamma-irradiated iminodiacetic and amino acid derivatives.....232
- Bagheri F., See Akbari M. T. et al.36
- Balova S., See Uzun D. et al.113
- Bangov I., M. Moskovkina, A. Patleeva, Charge-related molecular index (CMI) – a novel descriptor for quantitative structure/property relationship (QSPR) models. I. General consideration.....338
- Bardarska G., See Petrova B. et al.141
- Beschkov V. N., See Vasileva E. K. et al.174
- Beschkov V.N., See Yankov D.S. et al.327
- Beschkov V., See Krysteva M. et al.46
- Bojinov M. S., See Girginov Chr. A. et al.312
- Boncheva N., See Petrov N. et al.16
- Budinova T., See Petrov N. et al.16
- Budinova T., See Petrova B. et al.141
- Darakchiev R., See Darakchiev S. et al.51
- Darakchiev S., R. Darakchiev, Gas flow maldistribution in ceramic honeycomb packing.....51
- Darakchiev S. R., Gas flow maldistribution in columns packed with HOLPACK packing.....323
- Darakchiev S., See Semkov K. et al.194
- Didamony H. Al., See Refat M.S., et al.279
- Dimitrova Y., Hydrogen-bonded systems of water with dimethyl and diethyl sulfoxides. Theoretical study of structures, stability and vibrational spectra.....3
- Dimitrova Y., Theoretical study of structures, stability and vibrational spectra of the hydrogen - bonded phenoxides containing strong, short hydrogen bonds.....236
- Dimova L., See Lihareva N., et al.305
- Dragieva I. D., See Stoyanova A. E. et al.167
- Elshazly A. H., Batch reactor performance improvement for hexavalent chromium reduction by scrap iron using reciprocating perforated disc.....55
- El-Zayat L., See Refat M.S., et al.279
- Esmaeili A., See Akbari M. T. et al.36
- Farhami P., A. R. Ashrafi, On analyzing DNA sequences.....335
- Gharib A., M. Jahangir, M. Roshani, J. W. Scheeren, Catalytic effective synthesis of substituted flavones and chromones using Preyssler and heteropolyacids (HPAs) as catalyst.....210
- Gharib A., M. Jahangir, M. Roshani, J. (Hans) W. Scheeren, A method of catalytic synthesis of convenient thioxanthone crown ethers using Wells-Dawson $H_6[P_2W_{18}O_{62}]$ and Preyssler $H_{14}[NaP_5W_{30}O_{110}]$ heteropolyacid catalysts.....217
- Girginov A., See Girginov Chr. et al.138
- Girginov Chr. A., Bojinov M. S., Efficiency of formation of nanoporous alumina films in fluoride ion-containing electrolyte.....312
- Girginov Chr., A. Zahariev, A. Girginov, Areas of ionic, electronic and mixed conductivity in Nb/Nb2O5/electrolyte system.....138
- Gopala Krishna A. G., B. R. Lokesh, D. Sugasini, V. D. Kancheva, Evaluation of the antiradical and antioxidant properties of extracts from Indian red chili and black pepper by *in vitro* models.....62
- Grabchev I., See Refat M.S., et al.279
- Grigorova E., Ts. Mandzhukova, M. Khristov, P. Tzvetkov, B. Tsyntsarski, Investigation of hydrogen storage properties of magnesium based composites with addition of activated carbon derived from apricot stones.....70
- Gutzow I., S. Todorova, N. Jordanov, Kinetics of chemical reactions and phase transitions at hanging temperature: General reconsiderations and a new approach – Review.....79
- Iliev P. T., See Stoyanova A. E. et al.167
- Iliev P., See Uzun D. et al.113
- Jahangir M., See Gharib A., et al.210
- Jahangir M., See Gharib A., et al.217
- Jayaprakash Rao P., See Vijayalakshmi G., et al.246
- Jordanov N., See Gutzow I. et al.79
- Kancheva V. D., See Gopala Krishna A. G. et al. ...62
- Kancheva V. D., See Kasaikina O. T. et al.153
- Kartasheva Z. S., See Kasaikina O. T. et al.153
- Kasaikina O. T., Z. S. Kartasheva, V. D. Kancheva, N. V. Yanishlieva, I. R. Totseva, Consumption of quercetin and rutin in reactions with free radicals.....153
- Khristov M., See Grigorova E. et al.70
- Kokate S. J., Y. S. Shelar, H. R. Aher, S. R. Kuchekar, Liquid-liquid extraction and recovery of bismuth(III) from hydrochloric acid media using n-octylaniline in chloroform.....107
- Koseva I.I., V.S. Nikolov, Preparation of aluminium tungstate $Al_2(WO_4)_3$ by sol-gel modified Pechini method.....300

Krastev I., See Valkova T. et al.	317	Patel B. P., See Shah P. J. et al.	274
Krishnamurthy G., Oxidation of lindane in contaminated water under solar irradiation in the presence of photocatalyst and oxidizing agents.....	161	Patel H. S., See Oza K. K. et al.	103
Krysteva M., I. Lalov, V. Beschkov, Acceleration and increase of hydrogen production by simultaneous fermentation of <i>Clostridium butyricum</i> and <i>Rhodobacter sphaeroides</i> on wine-vinasse substrate.....	46	Patel H. S., See Shah P. J. et al.	274
Kuchekar S. R., See Kokate S. J. et al.	107	Patleeva A., See Bangov I. et al.	338
Kuchekar S. R., See Kundlik M. L. et al.	268	Petrova B., See Petrov N. et al.	16
Kundlik M. L., B. H. Zaware, S. R. Kuchekar, A rapid, sensitive and direct quantification of tamosulosin in human plasma by LC-ESI-MS/MS: application to a bioequivalence study.....	268	Petrova B., T. Budinova, B. Tsyntsarski, N. Petrov, G. Bardarska, C. Ania, J. Parra, Phenol adsorption on activated carbons with different structural and surface properties.....	141
Lalov I., See Krysteva M. et al.	46	Petrov K., Iv. Nikolov, T. Vitanov, V. Ognyanov, Pyrolysed Co-phtalocyanine as a catalyst for the oxidation of sulphur dioxide.....	189
Lefterova E. D., See Stoyanova A. E. et al.	167	Petrov K. K., See Vasileva E. K. et al.	174
Lihareva N., L. Dimova, O. Petrov, Y., Tzvetanova Kinetics and equilibrium of ion exchange of Ag ⁺ on Na-clinoptilolite.....	305	Petrov K., See Mitov I. et al.	180
Lokesh B. R., See Gopala Krishna A. G. et al.	62	Petrov K., See Uzun D. et al.	113
Mandravel C., See Stanculescu I. et al.	343	Petrov N., See Petrova B. et al.	141
Mandzhukova Ts., See Grigorova E. et al.	70	Petrov N., T. Budinova, B. Tsyntsarski, B. Petrova, D. Teodosiev, N. Boncheva, Synthesis of nanoporous carbon from plant wastes and coal treatment products.....	16
Midudhula S. S., A. Mundra, Kinetics and mechanism of oxidation of curcumin by sulphate radical anion in aqueous acetonitrile solutions.....	126	Petrov O., See Lihareva N., et al.	305
Mindrilă T., See Stanculescu I. et al.	343	Rai K. M. L., See Umesha K. B. et al.	11
Mitov I., A. Andreev, I. Nikolov, P. Andreev, E. Mladenova, K. Petrov, Sulphide ions heterogeneous catalytic oxidation by electrochemical methods.....	180	Rajendran S., See Nithya A. et al.	119
Mladenova E., See Mitov I. et al.	180	Ramachandran S., See Sathiyam S. et al.	205
Mohana K. N., See Ramdas Bhandarkar P. M et al.	22	Ramdas Bhandarkar P. M., K. N. Mohana, Kinetic and mechanistic study of bromination of sulfanilic acid with N-bromosuccin-imide in alkaline medium.....	222
Mohana K. N., See Ramdas Bhandarkar P. M et al.	222	Ramdas Bhandarkar P. M., K. N. Mohana, Oxidative cleavage of salbutamol with N-bromosuccinimide in acidic and alkaline media: A kinetic and mechanistic study.....	27
Moskovkina M., See Bangov I. et al.	338	Rangarajan M., See Sathiyam S. et al.	205
Mundra A., See Midudhula S. S. et al.	126	Refat M.S., H. Al. Didamony, Kh.M. Abou El-Nour, I. Grabchev, L. El-Zayat, Charge - transfer complexes: synthesis and spectroscopic characterizations on the five fluorescence dyes N-allyl derivatives of 1,8-naphthalimide with different acceptors.....	279
Naik N., H. Vijay Kumar, H. Swetha, Synthesis and evaluation of novel carbazole derivatives as free radical scavengers.....	40	Roshani M., See Gharib A., et al.	210
Nayak S. S., S. Panda, P. M. Panda, S. Padhy, Studies on acridone derivatives with and without inclusion complex formation with β -cyclodextrin.....	147	Roshani M., See Gharib A., et al.	217
Nikolova V. I., See Stoyanova A. E. et al.	167	Saad N., See Akbari M. T. et al.	36
Nikolova V., See Uzun D. et al.	113	Sathiyam S., M. Rangarajan, S. Ramachandran, An experimental study of spiral-plate heat exchanger for nitrobenzene-water two-phase system.....	205
Nikolov I., See Mitov I. et al.	180	Scheeren J. W., See Gharib A., et al.	210
Nikolov Iv., See Petrov K. et al.	189	Scheeren J. (Hans) W., See Gharib A., et al.	210
Nikolov V.S., See Koseva I.I. et al.	300	Semkov K., S. Darakchiev, Influence of small scale maldistribution in the vapor phase on the efficiency of rectification in packed columns	194
Nithya A., S. Rajendran, Synergistic effect of ethylphosphonic acid-Zn ²⁺ system in controlling corrosion of carbon steel in chloride medium	119	Shah P. J., B. P. Patel, H. S. Patel, Synthesis and antibacterial activity of some new azopyrazoles.....	274
Ognyanov V., See Petrov K. et al.	189	Shelar Y. S., See Kokate S. J. et al.	107
Oza K. K., H. S. Patel, Antimicrobial activity of novel 3-substituted 5-(pyridine-4-yl)-3H-1,3,4-oxadiazole-2-thione derivatives.....	103	Slavcheva E. P., See Stoyanova A. E. et al.	167
Padhy S., See Nayak S. S. et al.	147	Sona Bai M., See Krishnamurthy G. et al.	161
Panda P. M., See Nayak S. S. et al.	147	Stanculescu I., T. Mindrilă, C. Mandravel, Evaluation of PCB's chromatographic retention indices by multilinear regression method.....	343
Panda S., See Nayak S. S. et al.	147	Stateva R. P., See Yankov D.S. et al.	327
Parra J., See Petrova B. et al.	141		

Staykov S. G., See Uzunova S. A. et al.	130	Uzunov M., See Uzunova S. A. et al.	130
Stoyanova A. E., E. D. Lefterova, V. I. Nikolova, P. T. Iliev, I. D. Dragieva, E. P. Slavcheva, Water splitting in PEM electrolysis with Ebonex supported catalysts.....	167	Valkova T., I. Krastev A., Zielonka, Influence of D(+)-Glucose on the electrochemical deposition of Ag-Bi alloy from cyanide electrolyte.....	317
Sugasini D., See Gopala Krishna A. G. et al.	62	Vasileva E. K., K. K. Petrov, V. N. Beschkov, Mathematical modelling of biodegradation of monochloroacetic acid by <i>Xanthobacter autotrophicus</i> GJ10 immobilized in polyacrilamide gel.....	174
Swetha H., See Naik N. et al.	40	Vassilev S., See Uzun D. et al.	113
Teodosiev D., See Petrov N. et al.	16	Vassilev S. V., See Uzunova S. A. et al.	130
Totseva I. R., See Kasaikina O. T. et al.	153	Vijayalakshmi G., M. Adinarayana, P. Jayaprakash Rao, Kinetics of oxidation of adenosine by tert-butoxyl radicals – protection and repair by rosmarinic acid.....	246
Tsyntsarski B., See Petrova B. et al.	141	Vijay Kumar H., See Naik N. et al.	40
Tsyntsarski B., See Petrov N. et al.	16	Vitanov T., See Petrov K. et al.	189
Todorova S., See Gutzow I. et al.	79	Vladikova D., See Uzun D. et al.	113
Tsyntsarski B., See Grigorova E. et al.	70	Yanishlieva N. V., See Kasaikina O. T. et al.	153
Tzvetanova Y., See Lihareva N., et al.	305	Yankov D.S., V.N. Beschkov, R. P. Stateva, Influence of acid solutes on the phase behaviour of aqueous two-phase systems, containing poly(ethylene glycol) and poly(ethylene imine).....	327
Tzvetkov P., See Grigorova E. et al.	70	Zahariev A., See Girginov Chr. et al.	138
Umesha K. B., K. M. L. Rai, Synthesis and antimicrobial activity of pyrazole derivatives via 1,3-dipolar cycloaddition of nitrile imines with ethyl acetoacetate.....	11	Zarea A. H., See Akbari M. T. et al.	36
Uzunova S. A., I. M. Uzunov, S. V. Vassilev, A. K. Alexandrova, S. G. Staykov, Preparation of low-ashcontent porous carbonaceous material from rice husks.....	130	Zaware B. H., See Kundlik M. L. et al.	268
Uzun D., P. Iliev, D. Vladikova, P. Andreev, S. Balova, V. Nikolova, S. Vassilev, K. Petrov, Electrocatalytic oxidation-reduction reactions of metal-hydrides alloys with teflon-carbon additives	113	Zielonka A., See Valkova T. et al.	317

SUBJECT INDEX

1-(9H-carbazol-9-yl)-2-chloroethanone.....	40	antioxidants.....	62
1,3,4-oxadiazole-2-thione.....	103	ATPS.....	327
1,3-dipolar cycloaddition,	11	Avrami equation,.....	79
1,8-naphthalimide,.....	279	ball milling.....	70
2,6-diaminopyridine,.....	20	Benzotriazole.....	274
5-Pyrazolinone,.....	274	biodegradation.....	174
<i>ab initio</i> ,.....	3, 236	bis-(hydrazonopyrazolo)pyridine,.....	20
acceptors.....	279	bis-(pyrazolo)pyridine.....	20
acidic and alkaline media.....	27	bis-(thiazolo)pyridine.....	20
Acridone derivatives.....	147	bismuth(III),.....	107
activated carbon,	141	bond energy.....	253
activation.....	130	bromination.....	222
adenosine.....	246	carbamide.....	130
adsorption,	141	carbon steel.....	119
agricultural wastes.....	141	catalyst.....	210, 217
Ag ⁺ sorption.....	305	ceramics.....	300
alkaline medium.....	222	chalcogenide glasses.....	253
alumina films.....	312	charge-related geometrical index (CGI),.....	338
amino acid derivatives.....	232	charge-related molecular index (CMI),.....	338
anodic films.....	312	charge-related topological index (CTI),.....	338
anodic Nb ₂ O ₅ film.....	138	charge-transfer.....	279
antibacterial activity.....	36	chili.....	62
antimicrobial activity.....	274	chromatographic retention indices.....	343
antimicrobial activity.....	103	chromones.....	210
antimicrobial study.....	147	<i>Clostridium butyricum</i> ,.....	46

Co,	167	multilinear regression method,	343
coal,	16	Na-clinoptilolite,	305
COD measurement,	161	nanoporous carbon,	16
corrosion inhibition,	119	nanoporous templates,	312
Crown ether,	217	nanostructured materials,	300
current efficiency,	138	<i>N</i> -bromosuccinimide,	27, 222
D(+)-glucose,	317	nitrile,	11
DESO:H ₂ O complexes,	3	non-isothermal kinetics,	79
DFT,	3, 236	Nusselt number,	205
distillation,	194	oleoresin,	62
DMSO:H ₂ O complexes,	3	optical band gap,	253
DNA sequence matrix,	335	organic acid solutes,	327
DNA sequence,	335	oscillations,	317
Ebonex,	167	oxidation kinetics,	27
efficiency,	194	oxidation of curcumin,	126
electric conductivity,	138	oxidation,	246
electrocatalytic oxidation,	180	oxides,	312
electrodeposition,	317	Ozawa method,	79
EPR,	232	packed columns,	51, 194
equilibrium isotherms,	305	packed-bed columns,	323
essential oil,	36	PCBs,	343
fast screening method,	113	PEM water electrolysis,	167
flavones,	210	penetration depth,	51, 323
free radicals,	153, 232	pepper,	62
F-test,	119	phase solubility,	147
gamma irradiation,	232	phase transitions,	79
gas flow maldistribution,	51, 323	phenol,	141
gas maldistribution,	194	phosphonic acid,	119
heteropolyacid,	210, 217	photocatalyst,	161
hexavalent chromium reduction,	55	photooxidation,	161
HOLPACK packing,	323	physicochemical properties,	253
honeycomb packing,	51	plant,	16
human plasma,	268	poly(ethyleneglycol),	268, 327
hydriding-dehydriding kinetics,	70	poly(ethyleneimine),	327
hydrogen production,	46	polyacrylamide,	174
hydrogen storage,	70	porous carbon,	130
hydrogen-bonding,	3	positive ion electrospray,	268
imines,	11	<i>Prangos ferulacea</i> ,	36
immobilization,	174	Preyssler,	210, 217
<i>in vitro</i> model systems,	62	protection,	246
inclusion complex,	147	Pt,	167
ion exchange capacity,	305	pyrazoles,	11
isoconversional analysis,	79	pyrolyzed Co-phtalocyanine,	189
isonicotinic acid hydrazide,	103	QSPR modelling,	103, 338
lactic acid,	327	quercetin,	153
LC-MS/MS,	268	radical scavengers,	62
linalool,	36	radical scavenging activity,	40
lindane,	161	reciprocation,	55
lipid hydroperoxides,	153	renewable energy resource,	46
liquid-liquid extraction,	107	repair,	246
magnesium-based composites,	70	Reynolds number,	205
maldistribution factor,	51, 323	<i>Rhodobacter sphaeroides</i> ,	46
Mannich base reaction,	103	rice husk,	130
Mannich reaction,	274	rosmarinic acid,	246
mathematical modeling,	174	rutin,	153
metal hydride electrode,	113	salbutamol sulfate,	113, 27
micelles of cetyl trimethylammonium chloride,	153	scrap iron,	55
mixed fermentation,	46	separation,	107
molecular descriptors,	343	silver-bismuth alloys,	317
monochloroacetic acid,	174	single-phase heat transfer coefficients,	205

solar irradiation,.....	161	thioxanthone,.....	217
sol-gel processes,.....	300	topochemical reactions,.....	79
spectral studies,.....	103, 274	transmission electron microscopy,.....	300
spectroscopic studies,.....	279	treatment products,.....	16
spiral plate heat exchanger,.....	205	tungstates,.....	300
SSHB,.....	236	two- phase flow,.....	205
stability,.....	236	two-phase heat transfer coefficients,.....	205
structure,.....	3, 236	umbelliferae,.....	36
sulfanilic acid,.....	222	uniformity limit,.....	51, 323
sulphate radical anion,.....	126	UV spectra,.....	119
sulphate-fluoride electrolyte,.....	312	vibration,.....	55
sulphide ions,.....	180	vibrational spectra,.....	3, 236
sulphur dioxide,.....	189	wastewater,.....	55
surface area,.....	130	Wells-Dawson,.....	217
synergistic effect,.....	119	wine-vinasse,.....	46
synthesis,.....	16	<i>Xanthobacter autotrophicus</i> GJ10,.....	174
tamosulosin,.....	268	X-ray diffraction,.....	300
<i>tert</i> -butoxyl radicals,.....	246	β -cyclodextrin,.....	147
thermodynamic stability,.....	147		

АВТОРСКИ УКАЗАТЕЛ

- Абдел-Сайед Н. И., Нови синтети на нови симетрични бис-хетероциклени съединения: синтез на бис-тиазол-, бис-пиразол-, бис-бензотриазол-, бис-индол- и бис-пиразолил-тиазол-2,6- диаминпиридинови производни26
- Абу Ел-Нур Х.М., Виж Рефат М.С., и др.299
- Адинараяна М., Виж Виджаялакшми Г., и др.252
- Айдън М., Изследване на гама-облъчени имино-диоцетни и аминокиселинни производни чрез електронно-парамагнитен резонанс235
- Акбари М. Т., А. Есмаеили, А. Х. Зареа, Н. Саад, Ф. Багери, Химически състав и анти-бактериална активност на етерични масла от листа, стъбла и цветове от *Prangos ferulacea* (L.) Lindl. растящи в Иран39
- Александрова А. К., Виж Узунова С. А., и др.137
- Ангелова Д. Б., Виж Узунова С. А., и др.137
- Андреев А., Виж Митов И., и др.184
- Андреев П., Виж Митов И., и др.184
- Андреев П., Виж Узун Д., и др.118
- Аня К., Виж Петрова Б., и др.146
- Ахер Х. Р., Виж Кокате С. Дж., и др.112
- Ашрафи А.Р., Виж Фархами П., и др.337
- Багери Ф., Виж Акбари М. Т и др.,.....39
- Балова С., Виж Узун Д., и др.118
- Бангов И., М. Московкина, А.Патлеева, Съвръзаният със зарядите молекулен индекс (СМІ) – един нов дескриптор за модели на структура/свойства количествените съотношения (QSPR). I. Общи разглеждания.....342
- Бардарска Г., Виж Петрова Б., и др.146
- Бешков В., Виж Янков Д., и др.334
- Бешков В. Н., Виж Василева Е. К., и др.179
- Бешков В. Н., Виж Кръстева М., и др.50
- Бончева Н., Виж Петров Н., и др.19
- Божинов , Виж Гиргинов Кр., и др.316
- Будинова Т., Виж Петрова Б., и др.146
- Будинова Т., Виж Петров Н., и др.19
- Василева Е. К., К. К. Петров, В. Н. Бешков, Математично моделиране на био-разграждане на монохлороцетна киселина от клетки на щама *Xanthobacter autotrophicus* GJ10, имобилизирани в полиакриламиден гел..... 179
- Василев С. В., Виж Узунова С. А., и др.137
- Василев С., Виж Узун Д., и др.118
- Виджай Кумар Х., Виж Наик Н., и др.45
- Виджаялакшми Г., М. Адинараяна, П. Джаяпракаш Рао, Кинетика на окислението на аденозин от tert - бутоксилови радикали - защита и възстановяване с розмаринова киселина252
- Витанов Т., Виж Петров К., и др.193
- Владикова Д., Виж Узун Д., и др.118
- Вълкова Т., Ив. Кръстев, А. Циелонка, Влияние на D (+)-глюкозата върху електро-химичното отлагане на сребърно-бисмутови сплави от цианиден електролит.....322
- Гариб А., М. Джахангир, М. Рошани, Й.(Ханс) Схеерен, Ефективна синтеза на субституирани флавонови и хромони чрез Прайслерови аниони и хетеро-поликиселини като катализатори.....216
- Гариб А., М. Джахангир, М. Рошани, Й.(Ханс) Схеерен, Кинетично и механистично изследване на бромането на сулфанилова киселина с N-бромо-сукцинимид в алкална среда221
- Гиргинов А. А., Виж Гиргинов Кр. А., и др.140
- Гиргинов Кр. А., А. С. Захариев, А. А. Гиргинов, Зони на йонна, електронна и смесена проводимост в системата Nb/Nb2O5/ електролит140
- Гиргинов Кр., М. Божинов, Ефективност на образуване на нано-порьозни филми от двуалуминиев триоксид в електролит, съдържащ флуоридни йони.....316
- Гопала Кришна А. Г., Б. Р. Локеш, Д. Сугасини, Кънчева В. Д., Оценка на антирадикаловите и антиоксидантни свойства на екстракти от индийско червено чили и черен пипер чрез „ин витро“ модели 69
- Грабчев И., Виж Рефат М.С., и др.299
- Григорова Е., Цв. Манджукова, М. Христов, П. Цветков, Б. Цинцарски, Изследване на сорбционните характеристики по отношение на водорода на композити на базата на магнезий с добавка от активен въглен получен от кайсиеви костилки74
- Гуцов Ив., С. Тодорова, Н. Йорданов, Кинетика на химични реакции и фазови преходи при изменяща се температура: основно преразглеждане и нов подход – Обзор102
- Даракчиев Р., Виж Даракчиев С., и др.54
- Даракчиев С., Виж Семков К., и др.204
- Даракчиев С., Неравномерност на газовото течение в колони с пълнеж HОLPACK.....326
- Даракчиев С., Р. Даракчиев, Неравномерност на газовото течение в блоков керамичен пълнеж „пчелна пита“.....54
- Джахангир, М. Виж Гариб А., и др.216
- Джахангир, М. Виж Гариб А., и др.221
- Джаяпракаш Рао П., Виж Виджаялакшми Г., и др.252
- Дидамони Х.А., Виж Рефат М.С., и др.299
- Димитрова Й., Водородно-свързани системи на вода с диметил- и диетилсулфоксиди. Теоретично изследване на структури, стабилност и вибрационни спектри10
- Димитрова Й., Теоретично изследване на структури, стабилност и вибрационни спектри на

водородно-свързани феноксида, съдържащи силни, къси водородни връзки	245
Димова Л., Виж Лихарева Н., и др.	311
Драгиева Д., Виж Стоянова А. Е., и др.	173
Ел-Заят Л., Виж Рефат М.С., и др.	299
Елшазли А. Х., Подобряване на действието на реактор с периодично действие за редукция на шествалентен хром чрез железен скрап с използване на възвратно-постъпателен перфориран диск.....	61
Захариев А. С., Виж Гиргинов Кр. А., и др.	140
Есмаейли А., Виж Акбари М. Т., и др.	39
Зареа А. Х., Виж Акбари М. Т., и др.	39
Зауаре Б.Х., Виж Кундлик М.Л., и др.	273
Илиев П. Т., Виж Стоянова А. Е., и др.	173
Илиев П., Виж Узун Д., и др.	118
Йорданов Н., Виж Гуцов Ив., и др.	102
Карташева З. С., Виж Касаикина О. Т., и др.	160
Касаикина О. Т., З. С. Карташева, В. Д. Кънчева, Н. В. Янишлиева, И. Р. Тоцева, Изразходване на кверцетин и рутин в реакции със свободни радикали	160
Кокате С. Дж., Ю. С. Шелар, Х. Р. Ахер, С. Р. Кучекар, Течно-течна екстракция и извличане на бисмут(III) от солнокисела среда с използване на n-октиланилин в хлороформ	112
Косева Й.И., В.С. Николов, Получаване на алуминиев волфрамат $Al_2(WO_4)_3$ по модифицирания зол-гел метод на Печини.....	304
Кришнамурти Г., М. Сона Бай, Окисление на линдан в замърсени води под действие на слънчева светлина в присъствие на фотокатализатор и окислителен агент.....	166
Кръстева М., И. Лалов, В. Бешков, Ускоряване и повишаване на продукцията на водород с едновременна ферментацията на Clostridium butyricum и Rhodobacter sphaeroides върху субстрат от винена винаса.....	50
Кръстев Ив., Виж Вълкова Т., и др.	322
Кундлик М.Л., Б.Х. Зауаре, С.Р. Кучекар, Бързо, чувствително и пряко количествено определяне на тамулозин в човешка плазма чрез LC-ESI-MS/MS при изследването на биеквивалентност.....	273
Кучекар С. Р., Виж Кокате С. Дж., и др.	112
Кучекар С. Р., Виж Кундлик М.Л., и др.	273
Кънчева В. Д., Виж Гопала Кришна А. Г., и др.	69
Кънчева В. Д., Виж Касаикина О. Т., и др.	160
Лалов И., Виж Кръстева М., и др.	50
Лефтерова Е. Д., Виж Стоянова А. Е., и др.	173
Лихарева Н., Л. Димова, О. Петров, Я. Цветанова, Кинетика и равновесие при йонобменното задържане на сребърни йони върху натриево форма на клиноптилолит.....	311
Локеш Б. Р., Виж Гопала Кришна А. Г., и др.	69
Манджукова Цв., Виж Григорова Е., и др.	74
Мандравел К., Виж Станкулеску Й., и др.	348
Мидудхула С. С., А. Мундра, Кинетика и механизъм на окисление на куркумин със сулфатен анион-радикал във водни разтвори на ацетонитрил	129
Миндрила Г., Виж Станкулеску Й., и др.	348
Митов И., А. Андреев, И. Николов, П. Андреев, Е. Младенова, К. Петров, Хетерогенно каталитично окисление на сулфидни йони по електрохимичен път	184
Московкина М., Виж Бангов И., и др.	342
Мохана К.Н., Виж Рамдас Бхаданкар П.М., и др.	231
Мохана К.Н., Виж Рамдас Бхаданкар П.М., и др.	35
Младенова Е., Виж Митов И., и др.	184
Мундра А., Виж Мидудхула С. С., и др.	129
Наик Н., Х. Виджай Кумар, Х. Суита, Синтез и преценка на нови карбазолови производни като антиоксиданти.....	45
Наяк С. С., С. Панда, П. М. Панда, С. Падхи, Изследване на производни на акридон и на комплекси чрез включване на β -циклодекстрин	152
Николова В., Виж Узун Д., и др.	118
Николова В. И., Виж Стоянова А. Е., и др.	173
Николов В.С. Виж Косева Й.И., и др.	304
Николов И., Виж Митов И., и др.	184
Николов Ив., Виж Петров К., и др.	193
Нитя А., С. Раджендран, Синергичен ефект в системата на етилфосфорна киселина- Zn^{2+} за контрол на корозията на въглеродна стомана в среда съдържаща хлориди	125
Огнянов В., Виж Петров К., и др.	193
Оза К. К., Х. С. Пател, Антимикробна активност на нови 3-заместени 5-(пиридин-4-ил)-3Н-1,3,4-оксадиазол-2-тионови производни	106
Падхи С., Виж Наяк С. С., и др.	152
Панда П. М., Виж Наяк С. С., и др.	152
Панда С., Виж Наяк С. С., и др.	152
Пара Х., Виж Петрова Б., и др.	146
Пател Б.П., Х.С. Пател, П.Дж. Шах, Синтеза и анти-бактериална активност на някои нови азо-пиразоли.....	278
Пател Х. С., Виж Оза К. К., и др.	106
Пател Х. С., Виж Пател Б.П., и др.	278
А.Патлеева, Виж Бангов И., и др.	342
Петрова Б., Виж Петров Н., и др.	19
Петрова Б., Т. Будинова, Б. Цинцарски, Н. Петров, Г. Бардарска, К. Аня, Х. Пара, Адсорбция на фенол върху активни въглени с различни структурни и повърхностни характеристики.....	146
Петров К., Виж Митов И., и др.	184
Петров К., Виж Узун Д., и др.	118
Петров К., Ив. Николов, Т. Витанов, Д. Узун, В. Огнянов, Пиролизен Со-фталоцианин като катализатор за окислението на серен диоксид.....	193
Петров К. К., Виж Василева Е. К., и др.	179

Петров Н., Т. Будинова, Б. Цинцарски, Б. Петрова, Д. Теодосиев, Н. Бончева, Синтез на напорорест въглен от продукти на преработка на растителни отпадъци и въглища	19	Стоянова А. Е., Е. Д. Лефтерова, В. И. Николова, П. Т. Илиев, Й. Д. Драгиева, Е. П. Славчева, Разлагане на вода чрез ПЕМ електролиза с катализатори върху носител Ебонекс	173
Петров Н., Виж Петрова Б., и др.	146	Сугасини Д., Виж Гопала Кришна А. Г., и др.	69
Петров О., Виж Лихарева Н., и др.	311	Суита Х., Виж Наик Н., и др.	45
Рай К. М. Л., Виж Умеша К. Б., и др.	15	Схеерен Й. (Ханс), Виж Гариб А., и др.	216
Рамдас Бхаданкар П.М., К.Н Мохана, Кинетично и механистично изследване на бромирането на сулфанилова киселина с N-бромосукцинимид в алкална среда.....	231	Схеерен Й. (Ханс), Виж Гариб А., и др.	221
Рамдас Бхандаркар П. М., К. Н. Мохана, Изследване на кинетиката и механизма на окислително разпадане на салбутамол с N-бромосукцинимид в кисела и алкална среда.....	35	Теодосиев Д., Виж Петров Н., и др.	19
Раджендран С., Виж Нитя А., и др.	125	Тодорова С., Виж Гуцов Ив., и др.	102
Рамачандран С., Виж Сатиян С., и др.	209	Тоцева И. Р., Виж Касаикина О. Т., и др.	160
Рангараджан М., Виж Сатиян С., и др.	209	Умеша К. Б., К. М. Л. Рай, Синтез и антимикробна активност на пиразолови производни получени чрез 1,3-диполярно циклоприсъединяване на нитрилимими и етилацетоацетат.....	15
Рефат М.С., Х.А. Дидамони, Х.М. Абу Ел-Нур, И. Грабчев, Л. Ел-Заят, Синтези и характеризирани на комплекси с пренос на заряда на 1,8-нафталимиди с различни акцептори.....	299	Узун Д., Виж Петров К., и др.	193
Рошани М., Виж Гариб А., и др.	216	Узун Д., П. Илиев, Д. Владикова, П. Андреев, С. Балова, В. Николова, С. Василев, К. Петров, Влияние на въглен-тефлоновата структура върху електрокаталитични окислително-редукционни реакции на метал-хидридни сплави	118
Рошани М., Виж Гариб А., и др.	221	Узунова С. А., И. М. Узунов, С. В. Василев, А. К. Александрова, С. Г. Стайков, Д. Б. Ангелова, Получаване на нископепелен порест въглероден материал от оризови люспи	137
Саад Н., Виж Акбари М. Т и др.....	39	Узунов И. М., Виж Узунова С. А., и др.	137
Сатиян С., М. Рангараджан, С. Рамачандран, Експериментално изследване на работата на топлообменник със спирални пластини при дву-фазната система вода-нитробензен.....	209	Фархами П., А.Р. Ашрафи, Върху анализа на ДНК-секвенции.....	337
Семков К., С. Даракчиев, Отчитане влиянието на дребно-машабната неравномерност в паровата фаза при ректификация с модерни високо-ефективни ненаредени пълнежи.....	204	Христов М., Виж Григорова Е., и др.	74
Славчева Е. П., Виж Стоянова А. Е., и др.	173	Цветанова Я., Виж Лихарева Н., и др.	311
Сона Бай М., Виж Кришнамурти Г., и др.	166	Цветков П., Виж Григорова Е., и др.	74
Стайков С. Г., Виж Узунова С. А., и др.	137	Циелонка А., Виж Вълкова Т., и др.	322
Станкулеску Й., Г. Миндрила, К. Мандравел, Определяне на индексите на задържане при хроматографския анализ на поли-хлорирани бифенили (РСВ) с помощта на множествена линейна регресия.....	348	Цинцарски Б., Виж Григорова Е., и др.	74
Статева Р., Виж Янков Д., и др.	334	Цинцарски Б., Виж Петрова Б., и др.	146
		Цинцарски Б., Виж Петров Н., и др.	19
		П. Дж. Шах, Виж Пател Б.П., и др.	278
		Шелар Ю. С., Виж Кокате С. Дж., и др.	112
		Янишлиева Н. В., Виж Касаикина О. Т., и др.	160
		Янков Д., В. Бешков, Р. Статева, Влияние на киселини върху фазовото поведение на водни двуфазни системи, съдържащи полиетилен гликол и полиетилен имин.....	334

ПРЕДМЕТЕН УКАЗАТЕЛ

1-(9Н-карбазол-9-ил)-2-хлороетанон.....	45	<i>Rhodobacter sphaeroides</i> ,.....	50
1,3,4-оксадиазол-2-тион,.....	103	<i>tert</i> -бутоксидови радикали,.....	252
1,3-диполярно циклоприсъединяване,.....	15	<i>Xanthobacter autotrophicus</i> GJ10,	179
1,8-нафталимид,.....	299	β-Циклодекстрин,	152
2,6-диаминопирин,.....	26	Аденозин,.....	252
5-пиразолинон,.....	278	Акридон, производни,.....	152
<i>ab initio</i> ,.....	10, 245	Активен въглен,.....	146
<i>Clostridium butyricum</i> ,.....	50	Активен въглен, получаване,.....	19
N- бромосукцинимид,	35, 222	Активиране,.....	137
<i>Prangos ferulacea</i> ,	39	Акцептори.....	259, 299

Алкална среда,.....	27, 222	Йонообменен капацитет,.....	311
Аминокиселини, производни,.....	232	Карбамид,.....	137
Аноден филм от Nb ₂ O ₅ ,.....	140	Катализатори,.....	210,221
Антибактериална активност,.....	39, 103, 278	Керамики,.....	304
Антимикробно изследване,.....	153	Кинетика на окисление,.....	35
Антиоксиданти,.....	69	Кинетика на хидриране и дехидриране,.....	74
Антирадикали,.....	69	Кисела и алкална среда,.....	35
Антирадикалова активност,.....	45	Клиноптилолит-натриева форма,.....	311
Бензотиазол,.....	278	Кобалт,.....	173
Биодеградация,.....	179	Кобалто-фталоцианин пиролизиран.....	193
Бис-(пиразоло) пиридин,.....	26	Коефициенти на топлообмен, двуфазни,.....	209
Бис-(тиазоло) пиридин,.....	26	Коефициенти на топлообмен, еднофазни,.....	209
Бис-(хидразоно-пиразоло)пиридин.....	26	Колони с пълнеж,.....	4, 326
Бисмут (III),.....	112	Комплекси на диметисулфоксид и диетилсулфоксид с вода,.....	10
Бромиране,.....	222	Комплекси на включване,.....	152
Вибрационни спектри,.....	10, 245	Композити на база магнезий,.....	74
Вибрация,.....	61	Краун-етери,.....	221
Винаса,.....	50	Критерий на Фишер,.....	125
Водни двуфазни системи,.....	334	Куерцетин,.....	160
Водород, получаване,.....	50	Лимит на равномерност,.....	54, 326
Водород, складиране,.....	74	Линалоол,.....	39
Водородна връзка,.....	10	Линдан,.....	166
Волфрамати,.....	304	Липидо-хидропероксиди,.....	160
Въглеродна стомана,.....	125	Математично моделиране,.....	179
Въглища,.....	19	Матрици на ДНК-секвенции.....	337
Възвратно-постъпателно движение,.....	61	Метод на Ozawa,.....	102
Възобновяем енергиен източник,.....	50	Метод на бърз скрийнинг,.....	118
Възстановяване,.....	252	Мицели на цетил-триметиламониев хлорид,.....	160
Гама-лъчение,.....	232	Млечна киселина,.....	334
Дестилация.....	54, 204	Множествена линейна регресия,.....	348
Дискретна Фуриерова трансформация (ДФТ),.....	10, 245	Моделиране, QSPR,.....	342
ДНК-секвенции,.....	337	Моделни системи <i>in vitro</i> ,.....	69
Добив по ток,.....	140	Молекулни дескриптори,.....	348
Дълбочина на проникване,.....	55, 326	Монохлороцетна киселина,.....	179
Ебонекс,.....	173	Нано-порьозен въглерод,.....	19
Екстракция на бисмут, течно-течна,.....	112	Нанопорьозни образци.....	316
Електрична проводимост,.....	140	Наноструктурирани материали,.....	304
Електрод, метал-хидриден,.....	113	Неизотермична кинетика,.....	102
Електрокаталитично окисление,.....	184	Неравномерност на газово разпределение,.....	54, 204, 326
Електролит, сулфат/флуорид,.....	316	Нитрил имини,.....	15
Електроотлагане,.....	322	Окисление на куркумин,.....	129
Енергия на връзка,.....	259	Окисление, защита от,.....	252
Електронно-парамагнитен резонанс,.....	232	Оксиди,.....	316
Есенциално масло,.....	39	Олеорезин,.....	69
Ефективност,.....	54, 204	Оризиви люспи,.....	137
Железен скрап,.....	61	Осцилации, D(+)-глюкоза,.....	322
Забранена зона, оптична ширина,.....	259	Отпадъчни води,.....	61
Земеделски отпадъци,.....	146	ПЕМ електролиза,.....	173
Зол-гел процеси,.....	304	Пиразоли,.....	15
Изо-конверсиален анализ,.....	102	Плазма човешка,.....	273
Имобилизация,.....	179	Платина, катализатор,.....	173
Индекс, геометричен, свързан с товара (CGI).....	342	Площ на повърхност,.....	137
Индекси на задържане, хроматография,.....	348	Полиакриламид,.....	179
Индекси, молекулни, свързани с товара (CMI),.....	342	Полиетиленгликол,.....	334
Индекс топологичен, свързан с товара (STI),.....	342	Полиетиленимин,.....	224
Инхибиране на корозия,.....	125	Полихлорирани бифенили,.....	348
		Положително йонно разпръскване,.....	273
		Порьозен въглерод,.....	137

Пренос на заряд,.....	259, 299	Сулфидни йони,.....	193
Продукти на третирането, растителни отпадъци.....	19	Тамосулозин,.....	273
Пълнеж “пчелна пита”,.....	54	Течение, двуфазно,.....	209
Пълнеж HОLPACK,.....	326	Течна хроматография/маспектрометрия,	273
Равновесни изотерми,.....	311	Тиоксантон,.....	221
Разтворени органични киселини,.....	334	Топохимични реакции,.....	102
Растения,.....	19	Трансмисионна електронна микроскопия,.....	304
Реакция на Mannich,.....	278	УВ спектри,.....	125
Реакция на бази на Mannich,.....	103	Уравнение на Avrami,.....	102
Редукция на шест-валентен хром,.....	61	Фазова разтворимост,.....	152
Рентгенова дифракция,.....	304	Фазови преходи,.....	102
Розмаринова киселина,.....	252	Фактор на неравномерност,.....	55, 326
Рутин,.....	160	Феноксиди, водородно-свързани, стабилност,.....	245
Салбутанол сулфат,.....	35	Фенол, адсорбция.....	146
Свободни радикали,.....	160, 232	Филми анодни,.....	316
Серен диоксид, електрокатализа,.....	193	Филми от двуалуминиев триоксид,.....	316
Силни-слаби водородни връзки,.....	245	Флавонови,.....	210
Синергичен ефект,.....	125	Фосфонова киселина,.....	125
Слънчево облъчване,.....	161	Фотокатализатор,.....	161
Смесена ферментация, водород,.....	50	Фотоокисление,.....	161
Сорбция на сребърни йони,.....	311	Халкогенидни стъкла,.....	259
Спектрално изследване,.....	3, 278, 259, 299	Хетеро-поликиселини на Preyssler,.....	210, 221
Спирален пластинчат топлообменник,.....	209	Хетеро-поликиселини на Wells-Dawson,.....	221
Сребърно-бисмутови сплави,.....	322	Хидразид на изоникотинова киселина,.....	103
Стъкла от системата Cu-S-Se, физико- химични и оптични свойства.....	259	ХПК-определяне,.....	161
Сульфанилова киселина,.....	222	Хромони,.....	210
Сулфатен анион-радикал,.....	129	Чили пипер,.....	69
		Число на Нуселт,.....	209
		Число на Рейнолдс,.....	2

BULGARIAN CHEMICAL COMMUNICATIONS

Instructions about Preparation of Manuscripts

General remarks: Manuscripts are submitted in English by e-mail or by mail (in duplicate). The text must be typed double-spaced, on A4 format paper using Times New Roman font size 12, normal character spacing. The manuscript should not exceed 15 pages (about 3500 words), including photographs, tables, drawings, formulae, etc. Authors are requested to use margins of 3 cm on all sides. For mail submission hard copies, made by a clearly legible duplication process, are requested. Manuscripts should be subdivided into labelled sections, e.g. **Introduction, Experimental, Results and Discussion, etc.**

The title page comprises headline, author's names and affiliations, abstract and key words.

Attention is drawn to the following:

a) **The title** of the manuscript should reflect concisely the purpose and findings of the work. Abbreviations, symbols, chemical formulas, references and footnotes should be avoided. If indispensable, abbreviations and formulas should be given in parentheses immediately after the respective full form.

b) **The author's** first and middle name initials, and family name in full should be given, followed by the address (or addresses) of the contributing laboratory (laboratories). **The affiliation** of the author(s) should be listed in detail (no abbreviations!). The author to whom correspondence and/or inquiries should be sent should be indicated by asterisk (*).

The abstract should be self-explanatory and intelligible without any references to the text and containing not more than 250 words. It should be followed by key words (not more than six).

References should be numbered sequentially in the order, in which they are cited in the text. The numbers in the text should be enclosed in brackets [2], [5, 6], [9–12], etc., set on the text line. References, typed with double spacing, are to be listed in numerical order on a separate sheet. All references are to be given in Latin letters. The names of the authors are given without inversion. Titles of journals must be abbreviated according to Chemical Abstracts and given in italics, the volume is typed in bold, the initial page is given and the year in parentheses. Attention is drawn to the following conventions:

a) The names of all authors of a certain publications should be given. The use of “*et al.*” in

the list of references is not acceptable.

b) Only the initials of the first and middle names should be given.

In the manuscripts, the reference to author(s) of cited works should be made without giving initials, e.g. “Bush and Smith [7] pioneered...”. If the reference carries the names of three or more authors it should be quoted as “Bush *et al.* [7]”, if Bush is the first author, or as “Bush and co-workers [7]”, if Bush is the senior author.

Footnotes should be reduced to a minimum. Each footnote should be typed double-spaced at the bottom of the page, on which its subject is first mentioned.

Tables are numbered with Arabic numerals on the left-hand top. Each table should be referred to in the text. Column headings should be as short as possible but they must define units unambiguously. The units are to be separated from the preceding symbols by a comma or brackets.

Note: The following format should be used when figures, equations, *etc.* are referred to the text (followed by the respective numbers): Fig., Eqns., Table, Scheme.

Schemes and figures. Each manuscript (hard copy) should contain or be accompanied by the respective illustrative material as well as by the respective figure captions in a separate file (sheet). As far as presentation of units is concerned, SI units are to be used. However, some non-SI units are also acceptable, such as °C, ml, l, etc.

The author(s) name(s), the title of the manuscript, the number of drawings, photographs, diagrams, etc., should be written in black pencil on the back of the illustrative material (hard copies) in accordance with the list enclosed. Avoid using more than 6 (12 for reviews, respectively) figures in the manuscript. Since most of the illustrative materials are to be presented as 8-cm wide pictures, attention should be paid that all axis titles, numerals, legend(s) and texts are legible.

The authors are asked to submit **the final text** (after the manuscript has been accepted for publication) in electronic form either by e-mail or mail on a 3.5” diskette (CD) using a PC Word-processor. The main text, list of references, tables and figure captions should be saved in separate files (as *.rtf or *.doc) with clearly identifiable file names. It is essential that the name and version of

the word-processing program and the format of the text files is clearly indicated. It is recommended that the pictures are presented in *.tif, *.jpg, *.cdr or *.bmp format, the equations are written using "Equation Editor" and chemical reaction schemes

are written using ISIS Draw or ChemDraw programme. The authors are asked to submit the final text with a list of three potential reviewers. The Editorial Board of the journal is not obliged to accept these proposals.

EXAMPLES FOR PRESENTATION OF REFERENCES

REFERENCES

1. D. S. Newsome, *Catal. Rev.–Sci. Eng.*, **21**, 275 (1980).
2. C.-H. Lin, C.-Y. Hsu, *J. Chem. Soc. Chem. Commun.*, 1479 (1992).
3. R. G. Parr, W. Yang, *Density Functional Theory of Atoms and Molecules*, Oxford Univ. Press, New York, 1989.
4. V. Ponec, G. C. Bond, *Catalysis by Metals and Alloys* (Stud. Surf. Sci. Catal., vol. 95), Elsevier, Amsterdam, 1995.
5. G. Kadinov, S. Todorova, A. Palazov, in: *New Frontiers in Catalysis* (Proc. 10th Int. Congr. Catal., Budapest, 1992), L. Guzzi, F. Solymosi, P. Tetenyi (eds.), Akademiai Kiado, Budapest, 1993, Part C, p. 2817.
6. G. L. C. Maire, F. Garin, in: *Catalysis. Science and Technology*, J. R. Anderson, M. Boudart (eds), vol. 6, Springer-Verlag, Berlin, 1984, p. 161.
7. D. Pocknell, *GB Patent 2 207 355* (1949).
8. G. Angelov, PhD Thesis, UCTM, Sofia, 2001.
9. JCPDS International Center for Diffraction Data, *Power Diffraction File*, Swarthmore, PA, 1991.
10. *CA* **127**, 184 762q (1998).
11. P. Hou, H. Wise, *J. Catal.*, in press.
12. M. Sinev, private communication.
13. <http://www.chemweb.com/alchem/articles/1051611477211.html>.

Manuscripts and enclosures should be sent to:

Prof. V. Beschkov
Editor-in-Chief
Bulgarian Chemical Communications
Institute of Chemical Engineering
Bulgarian Academy of Sciences
Acad. G. Bonchev St., Block 103
1113 Sofia,
Bulgaria
E-mail: bioreac@bas.bg or vbeschkov@yahoo.com

or
Assoc. Prof. D. Yankov
Editor
Bulgarian Chemical Communications
Institute of Chemical Engineering,
Bulgarian Academy of Sciences
Acad. G. Bonchev St., Block 103
1113 Sofia,
Bulgaria
E-mail: yanpe@bas.bg

CONTENTS

<i>Announcement: International Year of Chemistry, 2011</i>	265
<i>M. L. Kundlik, B. H. Zaware, S. R. Kuchekar, A rapid, sensitive and direct quantification of tamosulosin in human plasma by LC-ESI-MS/MS: application to a bioequivalence study</i>	268
<i>P. J. Shah, B. P. Patel, H. S. Patel, Synthesis and antibacterial activity of some new azopyrazoles</i>	274
<i>M.S. Refat, H. Al. Didamony, Kh.M. Abou El-Nour, I. Grabchev, L. El-Zayat, Charge-transfer complexes: synthesis and spectroscopic characterizations on the five fluorescence dyes N-allyl derivatives of 1,8-naphthalimide with different acceptors</i>	279
<i>I.I. Koseva, V.S. Nikolov, Preparation of aluminium tungstate Al₂(WO₄)₃ by sol-gel modified Pechini method</i>	300
<i>N. Lihareva, L. Dimova, O. Petrov, Y. Tzvetanova, Kinetics and equilibrium of ion exchange of Ag⁺ on Na-clinoptilolite</i>	305
<i>Chr. A. Girginov, M. S. Bojinov, Efficiency of formation of nanoporous alumina films in fluoride ion-containing electrolyte</i>	312
<i>T. Valkova, I. Krastev, A. Zielonka, Influence of D(+)-Glucose on the electrochemical deposition of Ag-Bi alloy from cyanide electrolyte</i>	317
<i>S. R. Darakchiev, Gas flow maldistribution in columns packed with HOLPACK packing</i>	323
<i>D.S. Yankov, V.N. Beschkov, R. P. Stateva, Influence of acid solutes on the phase behaviour of aqueous two-phase systems, containing poly(ethylene glycol) and poly(ethylene imine)</i>	327
<i>P. Farhami, A. R. Ashrafi, On analyzing DNA sequences</i>	335
<i>I. Bangov, M. Moskovkina, A. Patleeva, Charge-related molecular index (CMI) – a novel descriptor for quantitative structure/property relationship (QSPR) models. I. General consideration</i>	338
<i>I. Stanculescu, T. Mindrilă, C. Mandravel, Evaluation of PCB's chromatographic retention indices by multilinear regression method</i>	343
AUTHOR INDEX	349
SUBJECT INDEX	351
AUTHOR INDEX (In Bulgarian)	354
SUBJECT INDEX(In Bulgarian)	356
Instructions to the authors	359

СЪДЪРЖАНИЕ

<i>Обява: Световна година на химията, 2011</i>	265
<i>М.Л. Кундлик, Б.Х. Зауаре, С.Р. Кучекар, Бързо, чувствително и пряко количествено определяне на тамулозин в човешка плазма чрез LC-ESI-MS/MS при изследването на биоеквивалентност</i>	273
<i>Б.П. Пател, Х.С. Пател, П.Дж. Шах, Синтеза и анти-бактериална активност на някои нови азо-пиразоли</i>	278
<i>М.С. Рефат, Х.А. Дидамони, Х.М. Абу Ел-Нур, И. Грабчев, Л. Ел-Заят, Синтези и характеризирание на комплекси с пренос на заряда на 1,8-нафталимиди с различни акцептори</i>	299
<i>Й.И. Косева, В.С. Николов, Получаване на алуминиев волфрамат $Al_2(WO_4)_3$ по модифицирания зол-гел метод на Печини</i>	304
<i>Н. Лихарева, Л. Димова, О. Петров, Я. Цветанова, Кинетика и равновесие при йонобменното задържане на сребърни йони върху натриева форма на клиноптилолит</i>	311
<i>Кр. Гиргинов, М. Божинев, Ефективност на образуване на нано-порьозни филми от двуалуминиев триоксид в електролит, съдържащ флуоридни йони</i>	316
<i>Т. Вълкова, Ив. Кръстев, А. Циелонка, Влияние на D (+)-глюкозата върху електрохимичното отлагане на сребърно-бисмутови сплави от цианиден електролит</i>	322
<i>С. Даракчиев, Неравномерност на газовото течение в колони с пълнеж HОLPACK</i>	326
<i>Д. Янков, В. Бешков, Р. Статева, Влияние на киселини върху фазовото поведение на водни двуфазни системи, съдържащи полиетилен гликол и полиетилен имин</i>	334
<i>П. Фархами, А.Р. Ашрафи, Върху анализа на ДНК-секвенции</i>	
<i>И. Бангов, М. Московкина, А.Патлеева, Свързаният със зарядите молекулен индекс (СМІ) – един нов дескриптор за модели на структура/свойства количествените съотношения (QSPR). I. Общи разглеждания</i>	?
<i>Й. Станкулеску, Г. Миндрила, К. Мандравел, Определяне на индексите на задържане при хроматографския анализ на поли-хлорирани бифенили (РСВ) с помощта на множествена линейна регресия</i>	348
<i>Авторски указател на английски</i>	349
<i>Прдметен указател на английски</i>	351
<i>Авторски указател на български</i>	354
<i>Предметен указател на български</i>	356
<i>Инструкция за авторите</i>	359